School of Doctoral Studies in Biological Sciences

University of South Bohemia in České Budějovice

Faculty of Science

Interaction of tick-borne encephalitis virus with host and vector cells

Ph.D. Thesis

Mgr. Hana Tykalová

Supervisor: prof. RNDr. Libor Grubhoffer, CSc., Hon. D.Sc., dr. h. c.

Co-supervisor: Prof. Alain Kohl

University of South Bohemia, Faculty of Science

&

Biology Centre of the Academy of Sciences of the Czech Republic, Institute of Parasitology

České Budějovice

2022

ANNOTATION

The proposed thesis deals with the various aspects of tick-borne encephalitis virus infection in the host and the vector on the cellular level. It uncovers transcriptomic and proteomic responses in infected cells in the human neurons and astrocytes, and vector cells. It identifies the subgenomic flaviviral RNA as an important pathogenesis effector that can interfere with the vector RNAi pathway, and at the same time denotes the components of this pathway. It also describes the phenomenon of impairment of host protein and rRNA synthesis upon TBEV infection. Moreover, it uncovers the importance of quasispecies in the adaptation to vector and host cells.

DECLARATION

I hereby declare that I am the author of this dissertation and that I have used only those sources and literature detailed in the list of references.

České Budějovice, 28.6.2022 ....

Hana Tykalová, MSc.

LIST OF PUBLICATIONS AND AUTHOR'S CONTRIBUTION

The thesis is based on the following manuscripts listed in chronological order.

I. Schnettler E., **Tykalová H.**, Watson M., Sharma M., Sterken M.G., Obbard D.J., Lewis S.H., McFarlane M., Bell-Sakyi L., Barry G., Weisheit S., Best S.M., Kuhn R.J., Pijlman G.P., Chase-Topping M.E., Gould E.A., Grubhoffer L., Fazakerley J.K., Kohl A. (2014). Induction and suppression of tick cell antiviral RNAi responses by tick-borne flaviviruses. Nucleic Acids Research 42(14): 9436-46. DOI: 10.1093/nar/gku657

      IF 9.11 (2014)

Hana Tykalová optimized methodology (qPCR), performed RNAi knockdowns of Ago and Dcr genes, and analysed its effect on Langat virus (LGTV) replication and on LGTV replicon luciferase activity, participated on immunofluorescence analysis, prepared samples for miRNAs sequencing and assisted on manuscript drafting.

      Contribution: 25%

II. Weisheit, S., Villar, M., **Tykalová, H.**, Popara, M., Loecherbach, J., Watson, M., Růžek, D., Grubhoffer, L.; de la Fuente, J., Fazakerley, J.K., Bell-Sakyi, L. (2015). *Ixodes scapularis* and *Ixodes ricinus* tick cell lines respond to infection with tick-borne encephalitis virus: transcriptomic and proteomic analysis. Parasites & Vectors 8:599. DOI: 10.1186/s13071-015-1210-x

      IF 3.23 (2015)

Hana Tykalová participated on laboratory-based experimental work.

      Contribution: 5%

III. Selinger M. et **Tykalová H.**; Štěrba J.; Věchtová P.; Vavrušková Z.; Lieskovská J.; Kohl A.; Schnettler E.; Grubhoffer L. (2019). Tick-borne encephalitis virus inhibits rRNA synthesis and host protein production in human cells of neural origin. PLoS Neglected Tropical Diseases 13(9): e0007745. DOI: 10.1371/journal.pntd.0007745

      IF 3.89 (2019)

*Hana Tykalová (**shared first author**), conceptualized the work, participated in experimental procedures, co-wrote original draft, reviewed, and edited the manuscript.*

      Contribution: 45%

IV.   Helmová R., Hönig V., **Tykalová H**., Palus M., Bell-Sakyi L., Grubhoffer L. (2020). Tick-borne encephalitis virus adaptation in different host environments and existence of quasispecies. Viruses 12(8):902. DOI: 10.3390/v12080902

        IF 5.05 (2020)

Hana Tykalová performed and evaluated supplementary experiment, contributed to data analysis and visualisation, and contributed to manuscript major editing.

        Contribution: 25%

V.   Selinger M., Věchtová P., **Tykalová H.**, Ošlejšková P., Rumlová M., Štěrba J., Grubhoffer L., (2022). Integrative RNA profiling of TBEV-infected neurons and astrocytes reveals potential pathogenic effectors. Computational and Structural Biotechnology Journal, 20: 2759-2777. DOI 10.1016/j.csbj.2022.05.052

        IF 7.27 (2022)

Hana Tykalová participated in conceptualization, performed experiments, formal data analysis, participated in original draft writing and reviewed and edited the manuscript.

        Contribution: 20%

AGREEMENT OF THE CO-AUTHORS

The first authors and shared first co-authors of the publications listed in the publication section fully acknowledge the contribution of Hana Tykalová as stated above.

_____

Prof. Dr. Esther Schnettler

_____

Dr. Sabine Weisheit

_____

RNDr. Martin Selinger, Ph.D.

_____

Mgr. Renata Helmová

LIST OF CONTENTS

PREFACE

Tick-borne encephalitis virus (TBEV) infection can cause a severe neurological disease – so-called tick-borne encephalitis (TBE), which worldwide incapacitates 10.000-12.000 patients annually (2). TBEV has long been a poor relative among the other members *Flaviviridae* family, at least with respect to the extent of scientific attention it has captured as illustrated by the number of scientific publications devoted to individual viruses (Figure 1). In the *Flaviviridae* family, hepatitis C virus or dengue virus research received the most attention owing to their vast impact on global health (2). For comparison, West Nile virus which annually causes four times fewer cases than TBEV, was studied in three times higher number of scientific papers than TBEV. This implies that research on TBEV is largely neglected and hopefully this imbalance will equal soon.

Long term, the Czech Republic ranks in the top three countries with the highest incidence of TBE cases in Europe (3). The reason can be found in unsatisfactory protective measures, raising from the underestimation of the risk of the disease and the related low vaccination rate among Czech people, which oscillates around 24 % (4). It is far below the desired protective level of 90 % that would be needed for the reduction of morbidity in endemic areas (5,6). Moreover, under-vaccination is a more general problem in most of the endemic areas (4).

Recently there has been a sudden increase of the incidence of TBE cases in some areas such as Switzerland (7), France (8), or the emergence of TBEV in so far unaffected areas, such as northern parts of Germany (9,10) or Great Britain (11,12). Also, TBEV risk area spread as vector tick distribution extends to higher altitudes (13). There is a tight interconnection among weather variation, tick abundance and activity, and the number of TBE cases. So, the upcoming climate change can be aggravating the TBEV epidemic situation in the future.

The aforementioned facts highlight TBEV as a serious health concern with an outlook to become a more dramatic problem for the healthcare system in the future. Still, the knowledge on TBEV biology and especially interaction with the host cell is far from being complete and specific antiviral treatment is missing. Hopefully, this work can fill in some missing puzzle pieces to the knowledge of TBEV biology.
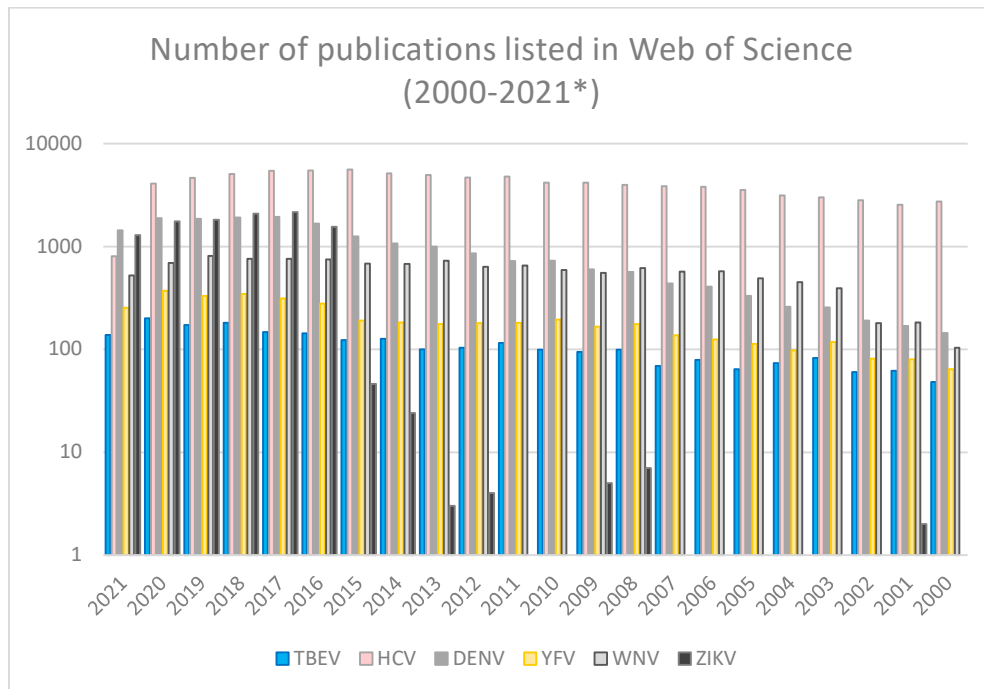
Figure 1. Number of publications listed in the Web of Sciences database for specific representatives of Flaviviridae family in the last two decades (* the year 2021 to the date 15.11.2021). The database was searched for the topic of the specific virus and the counts of retrieved results are recorded on the logarithmic scale. TBEV – tick-borne encephalitis virus, HCV – hepatitis C virus, DENV – dengue virus, YFV – Yellow fever virus, ZIKV – Zika virus.

INTRODUCTION

Tick-borne encephalitis virus (TBEV) belongs to a broad group of flaviviruses (genus *Flavivirus*, family *Flaviviridae*), which was named after the prototype Yellow fever virus (YFV; Latin *flavus* = yellow). Flaviviruses can basically cause three clinical syndromes – fever arthralgia rash, haemorrhagic fevers, and central nervous system infections, which is the case of TBEV (14). The genus *Flavivirus* contains viruses with unknown vector (e.g., Modoc virus or Rio Bravo virus), insect-specific viruses, mosquito-borne viruses, and finally tick-borne viruses. Several mosquito-borne viruses belong to the medically most threatening vector-borne diseases endangering millions of people worldwide, such as Dengue virus (DENV), Zika virus (ZIKV), Japanese encephalitis virus (JEV), Yellow fever virus or West Nile virus (WNV). Tick-borne viruses encompass Omsk haemorrhagic fever virus (OHFV), Louping ill virus (LIV), Langat virus (LGTV), and tick-borne encephalitis virus, which is the most dangerous tick-borne virus representative for humans (15).

The causative agent of encephalitis frequently occurring during summer was uncovered in the years 1937-39 by the expedition launched in the former Soviet Union (16). Later, tick-borne encephalitis (TBE) started to pose a serious health menace in our geographic area as well. There is a significant probability of occurrence of the disease in Bohemia and other European areas before the Second World War even though it was not confirmed (17). Soon, the virus was isolated from human patients (18,19) and its vector, the *Ixodes ricinus* tick (20).

TBE cases are detected in the vast area of Eurasia, ranging from Japan, China, Russia, up to the majority of countries of Eastern, Middle, and Western Europe, including Scandinavia, and scattered cases were noted also in Southern European countries (see Figure 2; (21)). 10.000 - 12.000 TBE clinical cases are recorded annually worldwide, including ca. 400-700 cases being diagnosed in the Czech Republic (22).

EPIDEMIOLOGY

TICK-BORNE ENCEPHALITIS VIRUS

TBEV is transmitted by ticks of the genus *Ixodes* and as such can be classified as an arbovirus, an artificial group clustering viruses transmitted by arthropods. There are two vector species substantially involved in TBEV transmission: *I. ricinus*, the main vector of the European subtype of TBEV; and I. *persulcatus* which is a principal vector of Siberian and Far Eastern subtype of TBEV (23,24). Recently, the introduction of two new TBEV subtypes, Baikalian and Himalayan, was proposed (25,26); however, they were not officially acknowledged by the scientific community yet. The distribution of vector species (Figure 2) correlates with the incidence of the different TBEV subtypes transmitted by them. The European subtype manifests usually mildly with a two-phased course of disease and results in the death in 1-5 %

of cases (the upper limit of the range applies to older patients (70+)). The mortality for the Siberian and Far Eastern subtype reaches 6-8 % and 20-60 %, respectively. The most serious is the infection with Far Eastern subtype that causes severe impairment of meninges and brain with poor prognosis, whereas Siberian subtype displays a tendency to cause chronic infections (3,21,27,28).

Humans are an accidental part of TBEV cycle in the nature and from the perspective of the virus represent a dead-end host. The main TBEV vector in our area, tick *I. ricinus*, needs to feed consecutively on three different hosts to complete its life-cycle (lasts 2-6 years) and all stages, larvae, nymphs, and imagoes, can transmit the infection. Ticks are feeding on broad range of hosts, including rodents, birds, lizards, mammals, deer or reptiles, which comprise natural reservoirs of the virus (5). Ticks can get infected during the blood meal either on a viraemic host, with an acute infection, or non-viraemic host, when a beneficial effect of the so-called co-feeding of infected and uninfected tick on the same host takes place and is sufficient for transmission of virus even on an immune host (29-33). Once infected, tick remains a lifelong vector of TBEV across all stages and rarely can pass the infection on the next generation also transovarially (34).

Besides the classical route of transmission, infection can be acquired also by the consumption of unpasteurized milk and dairy products. Perorally acquired infections tend to be milder with a monophasic manifestation and have an epidemic character reflecting the source of contamination (27,35,36).

LANGAT VIRUS

LGTV is a naturally attenuated flavivirus from the same serogroup as TBEV (37). LGTV was first recovered in the Malayan tick *I. granulatus* (38). Due to a close antigenic relationship to TBEV and the absence of diseases acquired in natural foci, attenuated LGTV strain was contemplated as a vaccine for TBEV (39). However, rare post-vaccination outbreaks of meningoencephalitis provoked vaccine withdrawal (40). Still, LGTV holds for a solid experimental model to study the pathogenesis of tick-transmitted flaviviruses including TBEV, especially because of the feasible maintenance and experimentation under less strict biosafety level practice (41).
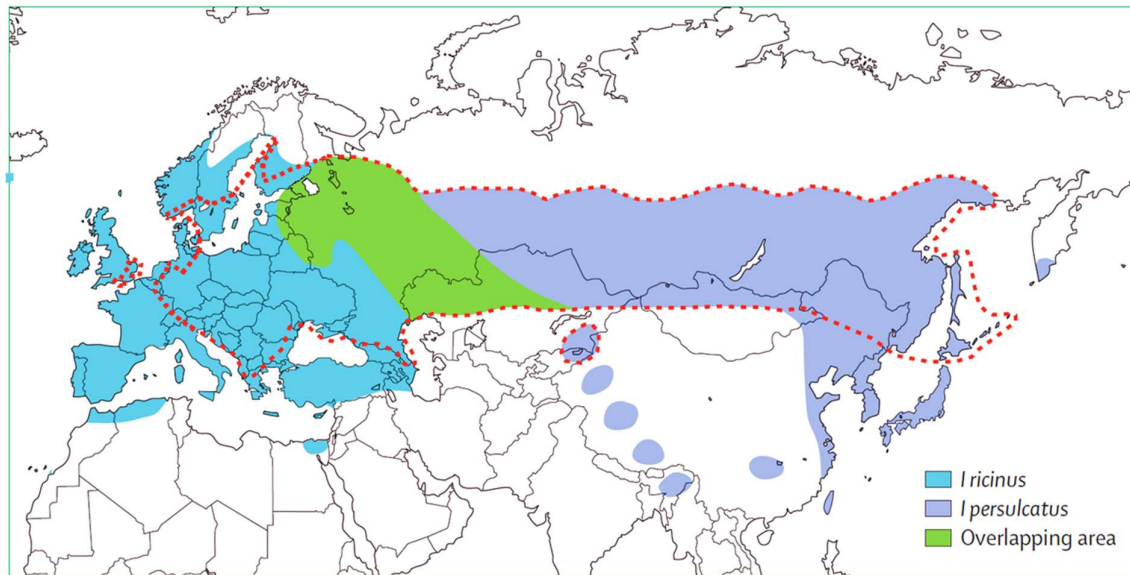
Figure 2. The geographical distribution of TBEV (red dotted line), and distribution of two main TBEV vectors, I. ricinus and I. persulcatus. Adapted from (42) updated on the current epidemiological situation in Europe (2021).

VIRUS, PARTICLE COMPOSITION, VIRAL PROTEINS

A mature TBEV virion is a spherical particle 50 nm in diameter that composes of a nucleocapsid surrounded by a lipid membrane (Figure 3). The membrane is derived from the host cell with incorporated viral glycoprotein E (envelope) and protein M (membrane), which induces a "bumpy ball-like" shape of the membrane (43). The E protein has a principal role in binding to host receptors and mediates entry into the cell. The M protein, or to be more specific the M protein precursor prM, acts during the maturation of viral particle and virion transport. During the maturation process, an asymmetry of immature viral particles was documented. In the acidic environment in the Golgi, reorganization of the proteins is provoked, making prM precursor protein available for the cleavage by host protease furin (43,44). A final building block of the mature virion consists of two E and two M proteins in the form of a heterotetramer (43). The process of maturation might be imperfect with some extent of uncleaved prM retained in the virions. Further, the arrangement state is not passive and can re-shuffle, based on various conditions and based on the proportion of the uncleaved prM retained (45). Membrane envelopes the capsid with icosahedral

Figure 3. Tick-borne encephalitis viral particle structure; modifed from (1).

asymmetry made of C proteins which stashes the 11 kb long single-stranded RNA of positive polarity (genomic RNA – gRNA) (28,43,44).

gRNA is terminated at the 5' end by a 7-methylguanosine cap (7mG) and lacks a poly-(A) tail at the 3' end (46). The coding segment is flanked on both ends by untranslated regions (UTRs). Due to the presence of specific structural motifs in both, 5' and 3' UTRs, these regions attain an important role in genomic RNA cyclization and initiation of genomic RNA replication, polyprotein translation, and they probably also participate in genome packaging (47,48) (49,50). A conserved set of RNA structural elements, often in multiple copies, is a hallmark of flaviviral 3′UTR (51). The flaviviral 3' UTR is commonly organized in a 5' variable region and a 3′conserved core region (49). The TBEV 3′UTR, especially the variable region, differs substantially among the individual TBEV strains. (52,53).

Viral proteins are encoded in a single open reading frame that is translated into one polyprotein. Co- and post-translational processing of the polyprotein by host and viral proteases generates three structural (C, prM, E) and seven non-structural proteins (NS1, NS2A, NS2B, NS3, NS4A, NS4B, NS5) (Figure 4; (28,54)). While the structural proteins pose the main building units of the viral particle, the non-structural proteins are crucial in the TBEV life cycle. They are the essential components of viral replication and also virion assembly process (55). Recently, a role in the suppression of the host antiviral response has been attributed to several of them (detailed further in the text). Functional characteristics of TBEV structural and non-structural proteins are summarized in Table 1.
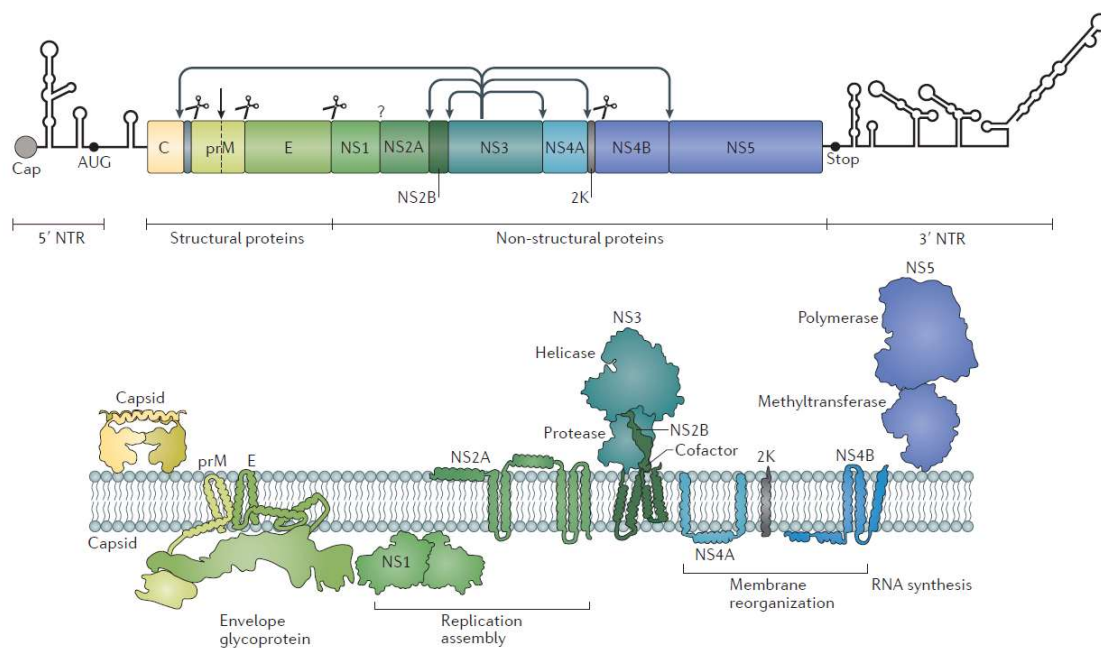
Figure 4. Flaviviridae polyprotein – processing by proteases and putative topologies with respect to the endoplasmic reticulum (ER) membrane. Figure credit (56).

SFRNA

Apart from genetically encoded factors – viral proteins, an additional factor based on the gRNA secondary structure resilience was revealed, the subgenomic flavivirus RNA (sfRNA). sfRNA is a decoy resistant part of 3´UTR produced by inefficient degradation by 5´-3´exonuribonuclease XRN1. The enzyme fails to proceed through complex secondary structures, termed exoribonuclease-resistant RNA element (xrRNA) generating thus short non-translated sfRNAs. The length of these molecules is approximately 500 bases (57,58) but presence of shorter sfRNA species due to an occasional slip through the pseudoknot structure and bumping into the successive xrRNA has been documented in related viruses (59). A unique secondary structure of sfRNA has been elucidated for Murray Valley encephalitis virus and ZIKV. The three-way stem loop structure is folded into a complex ring structure with two important pseudoknot interactions and the 5´end of the RNA being concealed inside the ring (60-62). Production of sfRNA is conserved in and unique for Flavivirus genus members (51,57,63,64). The biological relevance and involvement of sfRNA in the immune response evasion is discussed further (section sfRNA).

Table 1. Functional summary of individual TBEV structural and non-structural proteins. Involvement in the main processes during the viral life cycle is represented by a relative score heatmap. Relative score: 4 – main component, 3 – important cofactor, 2 – cofactor, 1 – involvement with so far unresolved importance. ER = endoplasmic reticulum, ERmem = protein embedded in ER membrane and the rest of the protein facing either luminal or cytoplasmic side of the membrane, MTase = RNA cap methyltransferase, RdRp = RNA-dependent RNA polymerase, TM = transmembrane localization in the ER. Data summarized from (28,43,55,65-70).

	PROTEIN	MW [KDA]	LOCALIZATION	REPLICATION	VIRAL PROTEASE	VIRION ASSEMBLY	MEMBRANE REMODELLING	GLYCOSYLATION	FUNCTION SUMMARY
STRUCTURAL	C	10	cytosol			4			Structural component of the capsid, viral assembly role; C-terminal hydrophobic domain – internal signal of prM translocation into ER lumen where C-prM cleavage occurs
	(pr)M	(10-11)8	(ERmem – lumen) mature virion			4		Yes (Asn32 in prM)	Virion morphogenesis and transport, cleaving off the pr segment is essential for virion maturation
	E	53 (glycosylated 54-55)	ERmem – lumen			4		Yes (Asn154)	Virion assembly, receptor binding and entry into host cell, major viral antigen; association with dsRNA in vesicle packets
NON-STRUCTURAL	NS1	39-40 (glycosylated 46-55)	ER lumen, no TM domain	2			4	Yes (Asn130 and Asn207)	Monomeric or dimeric form is part of the replication complex; hexameric form (requires glycosylation) is secreted out of the infected cells and can induce protective immunity; virulence factor
	NS2A	23-25	TM – cytosol	2		3	3		Involved in gRNA transport from sites of RNA replication across virus-induced membranes to assembly sites; assists in gRNA incorporation into budding virions, essential in virus assembly; biogenesis of virus induced membranes; recruitment of prM/E and NS2B/NS3 to the virion assembly sites via oligomerization of NS2A
	NS2B	13-14	TM	1	3	3			NS3 protease cofactor, anchors it to the membrane, can modulate NS3 helicase activity
	NS3	68-69	cytosol	3	4	3			Viral serine protease in complex with NS2B and cofactor for NS5 (RdRp and helicase); 2 domains, ATPase (nucleoside triphosphatase) activity; needed for virion maturation for cleavage of C anchor in ER membrane; capsid and genome encapsidation assistance
	NS4A	16	TM	2	1		3		NS3 protease cofactor, anchors it to the membrane, replication complex component; can modulate NS3 helicase activity; induction of virus specific membranes
	NS4B	26-28	TM	2			3		Putative RNA replication component involved in RNA accumulation; co-localizes with NS3 in the membrane vesicles at sites of RNA replication; polyprotein orientation
	NS5	103-104	cytosol	4		2			gRNA synthesis – C-terminal RdRp activity, genome capping (N-terminal MTase), regulation and coupling of RNA synthesis and virion morphogenesis – a link that probably depends on physical connections between membranous sites of replication and assembly; possible role in polyprotein orientation

TBEV LIFE CYCLE IN THE CELL

For a successful propagation in the host cell, TBEV needs to pass a sequence of steps (Figure 5). Where the information is incomplete for TBEV, the knowledge will be extrapolated from other flaviviruses. TBEV enters the susceptible cell by binding to a yet undefined receptor through the E protein. Although several receptor molecules have been identified in flaviviruses, for TBEV, none has been characterized satisfactorily (71-73). Involvement of glycosaminoglycans in the virus-cell binding, especially heparan sulfate is likely (74,75). They can serve as virus-accumulation molecules that facilitate interaction with a high-affinity specific receptor (76). Proteins such as DC-SIGN, TIM and TAM family receptor molecules have been implied to play a role in other flaviviruses entry (45,77,78). Broad cell tropism gives us a hint that TBEV either uses a single receptor present on a broad spectrum of cells or exploits multiple molecules (79). Uptake of viral particle is negotiated by receptor-mediated endocytosis (76,80,81). Low pH in the endosome triggers E protein reorganization that enables the fusion of viral and endosomal membrane. After viral gRNA release into the cytoplasm, the first round of translation of viral polyprotein occurs in association with rough ER (65,82). An extensive reorganisation of membranous compartments is a typical feature of TBEV infection and specific membranous structures, that are often located in the vicinity to each other, are being linked to the particular roles in the TBEV life cycle. Convoluted membranes are probable sites of protein synthesis and polyprotein cleavage by the virus NS2B-3 protease and by the host signal peptidase at the cytoplasmic and luminal sites of ER respectively (83,84). Then, viral replication takes place in ER or Golgi apparatus (GA) derived membrane compartments vesicular packets (VP) (69,85-89). Specific microenvironment is created by the flaviviral infection inside the VP and certain host proteins (e.g., RTN3A, DNAJC14) and specific lipids are recruited to aid the replication (90-94). Prior to viral replication, gRNA cyclizes and the 5′stem loop serves as a promotor for NS5 viral polymerase to initiate the gRNA synthesis (47,95,96). Viral NS5 polymerase with the assistance of the remaining viral non-structural proteins and some required host proteins form a replication complex and the negative RNA strand synthesis is initiated. It is promptly followed by the production of surplus gRNA copies (47,91). gRNA replication and assembly of new virions are interconnected processes, the latter requires the former for success (97,98). Replication and assembly sites are located close to each other (83,99) and VP communicate with the cytoplasmic space with a pore-like opening that facilitates gRNA transition between individual stages in the life cycle. No packaging signal was found for the flaviviral gRNA assembly into the virion. Rather sequence-unspecific interaction is needed for the cytoplasmic loop of NS2A interaction with the secondary structures of 3′UTR (100). When new virions assemble, viral structural proteins prM and E dimerize at the membrane of ER and form scaffold inducing local membrane curvature that surrounds the nucleocapsid. The particle buds into the ER lumen and a viral membrane is derived throughout this process (84,101,102). Virions are transported along the host-cell secretory pathway. TBEV matures while being transported, upon cleavage of prM protein in the acid vesicles of trans-GA by the host protease furin. TBEV E protein

glycosylation at a single site (Asn154) aids the secretion of viral progeny particles from the cells; of note, other flaviviral E proteins can contain distinct number of glycosylation sites. Finally, new viral progeny is released out of the cell (43,70,76,103,104).
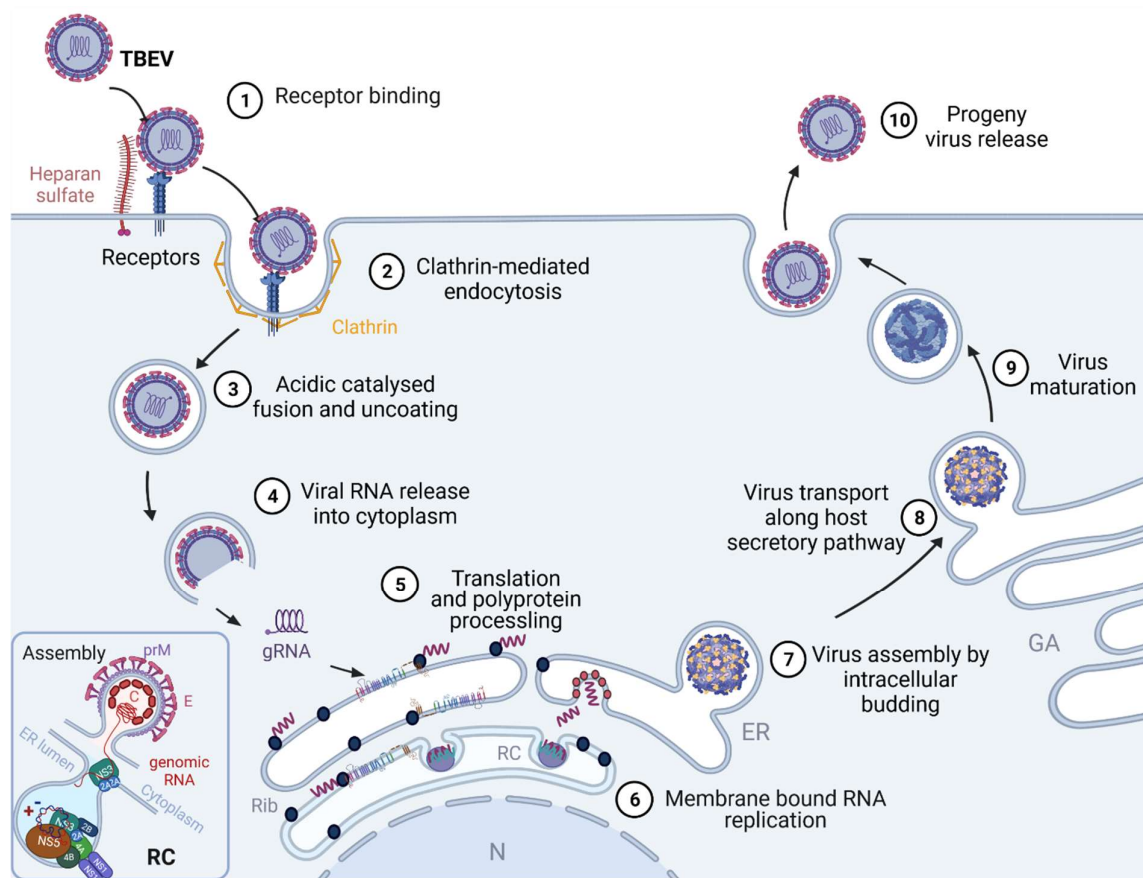
Figure 5. The life cycle of TBEV. Infection is initiated by the virus attachment to a widely specific receptor heparan sulphate and an unknown narrow specific receptor molecule (1), which triggers receptor-mediated endocytosis (2). Uncoating is facilitated by the acidic pH-triggered rearrangement of viral proteins in the late endosome (3) and gRNA is introduced into the cytoplasm (4). gRNA is transported to the endoplasmic reticulum (ER) and translation of a polyprotein at the ER is followed by proteolytic processing by viral and cellular proteases (5). Viral proteins induce an intricate rearrangement of host membranes, and a replication complex is formed (see inset for detail) with the production of negative-RNA strand (-) as a template for further replication and assembly (6). Adjacent to the replication sites are assembly sites (7), where progeny virions are formed. NS2A is involved in gRNA trafficking along and helps to dock gRNA into newly assembled progeny particles at the cytoplasmic site of ER. Viral progeny exits the cell via the host secretory pathway (8) and undergoes maturation while passing through the Golgi apparatus (9), where pr from M is cleaved off and proteins E and M are rearranged finishing the maturation of virions, that are released from the cell (10). Inset: Detail of TBEV replication complex and assembly of progeny particle assisted by NS2A and NS3 proteins. ER – endoplasmic reticulum, GA – Golgi apparatus, N – nucleus, RC – replication complex. Created with BioRender.com.

Pathogenetic processes related to TBEV infection start with the bite of an infected tick and the virus is introduced into the skin of vertebrate hosts with tick saliva (82,105). However, tick saliva is not just a passive medium for delivery. It is a mixture of bioactive molecules, whose composition is cleverly tailored and changing on-demand during feeding. Successful tick feeding relies on inhibition of homeostasis, and anticoagulatory, vasodilatory, and immunomodulatory properties of tick salivary proteins (105-110). On top of that, bioactive tick salivary proteins augment the development and spread of the infection, and they promote pathogen transmission (30,111). At the tick feeding site, TBEV infection as early as three hours after the tick attachment can be detected. Initially, virus infects epidermal fibroblasts, epidermal Langerhans cells (specialized dendritic cells – DCs) and mononuclear cells, that are attracted to the site of intrusion (112,113). DCs also function as a shuttle that spreads the infection into the body after migration to draining lymph nodes (113,114). In the presence of flaviviral infection (WNV), epidermal Langerhans cells exhibit an activated phenotype and migrate to the draining lymph nodes, upon the signal of IL1β (114). Tick feeding site has substantially more cellular infiltrates, comprising mainly of neutrophils and monocytes, when we compare infected tick (POWV) versus non-infected tick (115). Exposure to tick saliva results in a higher percentage of TBEV infected DCs, probably by virtue of tick saliva halting the cells at the feeding site for a longer time, attenuating the inflammatory response they elicit, and by prolonging DCs survival at the same time (116,117). Also, an immune response is reshaped towards the activation of the inflammatory responses when TBEV infected ticks feed. Other inflammatory cells, namely neutrophils, are attracted to the feeding site as well (112).

After inoculation, the virus rapidly disappears from the inoculation site and re-emerges in the draining lymph nodes (118). TBEV can be detected there 6-12 hours post-infection (119). Once lymph nodes are infected, the virus resides in them long-term and amplifies. The node infection is accompanied by inflammatory changes and by their enlargement. Infection from the lymph nodes disseminates further (118-121). Replication in the body tissues leads to systemic infection and viremia. In vertebrate hosts not naturally exposed to infection, the virus invades the CNS and elicits its neuropathogenic effects. Two main neuropathogenic variables are the capacity of the virus to enter the CNS, called neuroinvasiveness, and neurovirulence, which is the ability to replicate and cause damage within the CNS (76,122). The mechanism by which the virus can cross the blood-brain barrier (BBB) and invade CNS is not completely clear; however, several routes have been outlined. The virus can be smuggled into the brain by infiltrating infected immune cells that pass into the brain by transcytosis (the so-called Trojan horse strategy). There is also a hematogenous mode of infiltration when free virus particles slip through disassembled tight junctions of the BBB. The next possibility is that endothelial cells get directly infected and either transfer the virus upon replication in them to the other side of the barrier by transcytosis, or the virus

induces modulation of tight-junction integrity during infection of endothelial cells. The last option is a retrograde transport of the virus along the olfactory nerve from the rostral to the caudal part of the brain (79). No unambiguous data have been published to declare the route by which TBEV enters the brain, most probably multiple gates are hijacked by TBEV. A temporary increase in BBB permeability was described in animal models for WNV and TBEV (123-126). In TBEV patients, an increased blood-brain barrier permeability was demonstrated by the elevated serum level of matrix metalloproteinase-9 (MMP-9), a chemokine capable of loosening the tight junctions of BBB (127). Palus and colleagues showed an increased production of MMP-9 by TBEV infected astrocytes (128). On the other hand, TBEV antigen was found disseminated in CNS already in early disease stages supporting a hematogenous route for CNS infestation (129). Infection of microvascular endothelial cells by TBEV and WNV does not cause cytopathic effect, facilitates the entry of the cell-free virus into the CNS without BBB disruption and without increasing adhesion molecules expression (130,131). Recently, exosomes were revealed as an alternative to virus dissemination among neural cells with the potential to serve as a shuttle to overcome the BBB (132). Regardless of the gate of virus entry, a key prerequisite for neuroinvasiveness seems to be the presence of high viremia (133), since it is necessary for WNV invasion of the CNS and correlates with its entry into the CNS (134).

When a virus infiltrates the brain, neurons are a primary target for its multiplication (129,135). However, infection of glial cells of the brain was also noted, namely astrocytes, microglia/macrophages, and oligodendrocytes (81,135-138). Infection of the CNS is accompanied by histopathologic and inflammatory changes, especially perivascular cellular infiltrates, necroses, neuronal loss by neurophagy or nodule formation from glial cells at the site of degenerating lesions are detected (14). The brain is infiltrated by numerous immune cells in the advanced stages of infection (138). The predominance of T cells and macrophages/microglia was demonstrated and only a few B cells were present. Some cytotoxic T cells were in direct contact with TBEV-infected neurons; however, the most prominent infiltrates were concentrated in the areas with the absence of TBEV antigen. Conversely, intact neurons with only scarce inflammatory infiltrates in the immediate surroundings were usually heavily infected. While examining the brains of patients who deceased due to TBEV infection, TBEV antigen was most prominently linked to large neurons of anterior horns, medulla oblongata, pons, dentate nucleus, Purkinje cells, and striatum. Immunoreactivity was also detected in neurons of other brainstem nuclei, isocortex, and basal ganglia (129). Ultrastructural and morphological changes in human neural cells upon TBEV infection have been described as well. The structure of tubulin filaments was impaired and vast rearrangement of membranous structures was discovered together with altered morphology of GA or mitochondria (139).

Neuronal damage can be caused by viral replication itself, by virus-induced inflammatory reaction or by a combination of both possibilities (82). Immunopathologic aspects

substantially contribute to CNS pathology severity (138). There is contradictory evidence on the role of CD8+ T cells in immunopathology. According to King and colleagues (79), they contribute to the severity of CNS pathology. CD8+ T cell infiltrates in the brain have also a detrimental effect on the survival times of TBEV infected mice, thus having an immunopathologic function (140). However, Wang *et al.* showed that after sub-cutaneous infection with WNV, CD8+ T cells play a dual role – protective and immunopathological (141). Moreover, the presence of both CD8+ and CD4+ T cells is essential to clear WNV from infected neurons in the CNS (134).

TBEV infection in neurons triggers major structural changes. Neuronal membranes proliferate and the ER is rearranged into whorls. Also, tubule-like structures, replication sites in dendrites, and the formation of autophagosomes were described. Autophagy was shown to have a beneficial effect on TBEV progeny production (142). A discrete feature of TBEV infection of neurons was antigen accumulation (E, NS3) and virus replication (dsRNA) in neuronal dendrites associated with laminar membrane structures, and neurite membranes with altered ultrastructure in a specific way (143). The transport of viral RNA along the dendrites was mediated by the cis-acting element of stem-loop 2 (SL-2) in the gRNA 5´UTR and interfered with the transport of host mRNAs. Loss of the transport function did not affect the lethality of infection, however, it correlated with the reduction of symptoms severity (144). In a related flavivirus (WNV), a spread of virions across the synapses was observed both in the direction and against the direction of the synaptic signal transfer (145).

Astrocytes are a glial cell type that provides all the necessary support to the neurons to function properly. They maintain homeostasis, regulate the blood flow in the brain or the function of the BBB, support the synaptic function of neurons, assist them with the energetic metabolism and last but not least support them during infection (146,147). During TBEV infection, astrocytes are less susceptible, and virus is less pathogenic for them than for neurons (81,128,137,142). Astrocytes can also sustain productive TBEV infection without being substantially affected on viability, even though the infection is accompanied by astrocyte activation and dramatic ultrastructural changes in the ER (128). Astrocytes can have a protective role towards neurons, in their underrepresentation, neurons were more vulnerable to TBEV infection (137,148). Astrocytes are more potent producers of proinflammatory cytokines and chemokines in the brain and by the production of these they contribute to the protective function (148). Still, the overall picture is not clear yet. For example, infected neurons were described as the main producers of IFNα and β by Delhaye et al. (149); on the other hand, astrocytes were described as the major IFNβ producers and as minor producers presented microglia and neurons by Ghita et al. (150). Overall, different cell types in the CNS have a different share of the defence against viral infection. The factors determining the differences in the outcome of the infection in different neural cell types, neurons and astrocytes, are yet to be determined. The topic was researched in the paper Chapter 2, Publication 4.

The lower permissivity of certain neuronal types to flavivirus infection can be linked to the state of preparedness, such as a higher basal expression of certain immune response related genes and their higher upregulation when infection of flavivirus strikes. Antiviral genes capable of such antiviral alertness are *Ifi27*, *Irg1*, *rsad2*, *Irf1* in WNV infection. Moreover, miRNA-132 has been shown as a negative regulator of such antiviral response at least in part (151). This might explain the presence of separate infection loci (sometimes even on the level of individual cells) throughout the brain described for various flaviviruses such as TBEV or WNV (129,151,152).

INFECTION OF HUMAN

Most people infected with TBEV do not show any symptoms. Manifestative disease develops in 0.5-5 % of cases (14) and has usually two phases. An incubation period before the onset of symptoms ranges from 7 to 14 days (max. range 4-28 days). The first viraemic phase of the disease, lasting about 4 days, correlates with the onset of the first, rather unspecific flu-like symptoms, comprising of fever, muscle pain, fatigue, headache, and dizziness (153). After a short prodromal period of approximately 8 days (range 1-33 days), the disease advances into the second phase with neurologic symptoms in 20-30 % of patients (154,155). Characteristic, although not disease-specific, neuropathologic changes include meningitis and multinodular to patchy polioencephalomyelitis accentuated in the spinal cord, brainstem, and cerebellum (129). Depending on the affected brain areas, meningitis, meningoencephalitis, meningoencephalomyelitis or meningoencephaloradiculitis lead to neurological symptoms and the outcome of the disease reflects also the TBEV subtype that caused the disease (21,28). Major symptoms are fever, headache, meningeal signs, ataxia, cognitive dysfunctions such as impaired concentration and memory, dysphasia, altered consciousness, confusion, irritability, tremor, and cranial nerve paralysis. Lesions in the CNS are widespread and involve predominantly grey matter and leptomeninges, with the medulla oblongata, nuclei, brainstem, cerebellum, and spinal cord being particularly affected (154). TBE patients are usually admitted to hospital in the second phase of the disease when neurological symptoms manifest. At this time point, virus has already been cleared from the blood and the cerebrospinal fluid and specific IgM and IgG antibodies have been produced. Thus, their detection by the ELISA method is of choice for TBE diagnosis. In case of possible cross-reactivity of antibodies (e.g., after vaccination against a related virus), a virus-neutralizing assay is an alternative diagnostic method (156). Leukocytes in CSF and increased CSF:serum ratio of albumin are the key features of TBE in patients. Another TBE-specific marker is the occurrence of granulocytes in a substantial portion of patients and the presence of intrathecal IgM antibodies (157).

Up to 46 % of patients are left with permanent sequelae at long-time follow-up. The only tool available to prevent disease outbreaks currently is vaccination (158). As a prevention, it is recommended for all individuals aged 1 year or older to undergo vaccination in highly endemic

areas (≥5 cases/100 000/year) and for individuals at risk in areas with a lower incidence (e.g., forest workers) (159). Protective level of immunity in the majority of population, such as seen in Austria due to a complex immunization program running in recent decades, can yield a substantial decrease in morbidity of TBE (5). Currently, there is no specific treatment for TBE (159), the disease symptoms in patients are alleviated at least partially by supportive treatment (160). Thus, there is a pending need for a development of specific therapy against TBE; specific immunotherapeutic approaches and specific anti-TBEV drug candidates are reviewed recently (160).

Tick as TBEV vector

Ixodes ricinus tick (Acari: *Ixodida*, Family *Ixodidae*) (161) accounts for the main transmission vector of the European subtype of TBEV and *I. persulcatus* for Siberian and Far Eastern subtype of TBEV. They also serve as a main reservoir of TBEV in nature (162). Other tick species, such as *I. trianguliceps*, *I. hexagonus*, *I. arboricola*, *Haemaphysalis inermis, H. punctata, D. reticulatus*, or *D. marginatus* can support the infection (5,27,163,164). However, their role in the TBEV transmission to humans and circulation in the natural foci is minimal (165). Human becomes only an accidental host of the main tick vectors (5). As a three-host ectoparasite, *I. ricinus* needs to feed consecutively on three different hosts to complete its life-cycle, which lasts 2-6 years depending on the wide range of biotic and abiotic factors, and all stages, larvae, nymphs, and imagoes can transmit the infection. Ticks are feeding on a broad range of hosts, including rodents, birds, lizards, mammals, deer, or reptiles, which comprise natural reservoirs of the virus (5,166). A range of hosts is similar in all life stages, however, larger body size hosts are preferred by the more advanced life stages (167).

There are several ways how tick can become infected. TBEV transmission during *I. ricinus* life cycle is depicted in Figure 6. During blood-feeding, tick can ingest a virus with the viraemic blood of the host that currently undergoes acute TBEV infection (168). This route has long been considered the main way of transmission. Nevertheless, most of the natural hosts undergo asymptomatic infection with only a short period of viremia and thus the "window" enabling infection by viraemic blood is relatively narrow (105). The second alternative is transmission during co-feeding of infected and uninfected ticks on the same host without the need for viremia to occur (29-32,169). With the advancement of knowledge, this route has proven effective in the laboratory (30,32) as well as in nature (31,33), even indispensable for the maintenance of the infection in natural foci (170,171). Interestingly, infection via co-feeding is possible also on an immune host (33). Larval aggregation on small rodents may lead to amplification of the virus and infiltration of co-feeding larvae and consequently could heighten the nymphal infection rate (172). The final option of conveying TBEV is through transstadial and transovarial transmission. The chance of trans-stadial passing of TBEV infection from larvae to nymphs and nymphs to adults infected during co-feeding was estimated at 0.8 % and 14 %, respectively. The efficiency of transovarial transmission

to the new tick generation is very low, only about 0.5 % (173,174). Still, such a low efficiency can have a substantial role in the TBEV natural circulation and maintenance of the natural foci. In laboratory, yet another possibility by various ways of artificial infection exists, with up to 92 % trans-stadial transmission rate to adults (175).
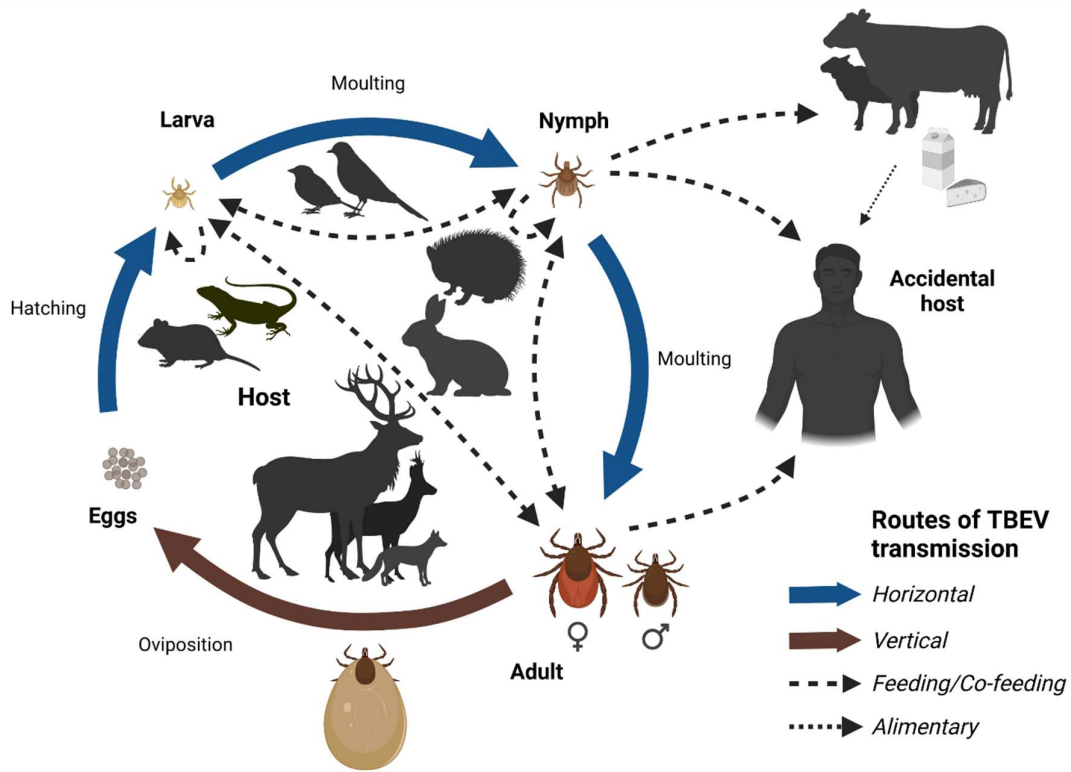
Figure 6. Tick-borne encephalitis virus transmission cycle. In the vector tick I. ricinus or I. persulcatus, TBEV is maintained during the vector life cycle either by the horizontal transmission when the infection is passed to the following life stage (blue arrow) or vertical transmission when the infection is passed on the next tick generation (brown arrow). Various tick life stages – larvae, nymphs, and adult females feed with different preferences on the various host species, with the less mature stages preferring the smaller hosts. Main route of TBEV transmission to the new vector individual is by co-feeding of the infected and uninfected ticks on the same host or by feeding on the host undergoing acute TBEV infection (dashed arrow). Infection of human, an accidental host, is most often mediated by infestation with infected nymphs or adult females or rarely via alimentary route by consumption of unpasteurized milk or dairy products (dotted arrow). Inspired by (176). Created with BioRender.com.

TBEV prevalence in infected ticks in nature ranges usually between 0.1-1 % (172,177,178) and in endemic areas up to 5 % (173). Several studies have documented a boost in viral load retrieved from ticks upon the onset of feeding (179-181).

Transmission of TBEV in the ecosystem relies upon a complex web of interactions that comprise the density of available hosts, tick-host preferences, aggregation of ticks on the host individuals and coincidence of the tick and host populations, all of which are dependent on the climate/natural conditions as reviewed in (27,176). Special importance in the TBEV maintenance and amplification in hosts is attributed to rodents, especially to the genera *Apodemus* and *Clethrionomys*, which serve as a natural reservoir. Their population explosions

are followed by an upsurge in tick populations within a year or two (5). Then, tick activity is, with a certain prolapse, reflected in the TBE incidence in human patients. Two main peaks of tick seasonal activity can be discerned during the year (182) and span from April/May to June and September to October (27,28). Maintenance of an active TBE focus relies on the tick survival, pathogen survival and the chance of human exposure (183).

INFECTION OF TICK

After ingestion of infected blood, midgut epithelial cells are believed to serve as a primal harbour for the virus to survive and replicate in (184). The development of these cells starts during the blood-feeding, as the intracellular digestion starts, and lasts during the metamorphosis period. In the *I. ricinus,* salivary glands and epidermal cells were found positive for the virus antigen 36 hours post-infection (105,184,185). Also, transit through the oesophagus to the suboesophageal ganglion was documented. Further the virus could be detected in the lumen of Malpighian tubules of TBEV infected *D. marginatus* and in a few gut cells (184,186). The virus then spreads to the midgut and via hemocoel reaches the salivary glands. The saliva is the shuttle that delivers TBEV into the host (105). Salivary glands serve as a long-term reservoir of the virus for successive transmission. Initiation of the blood meal increases the virus load in the salivary glands markedly (by three orders of magnitude) and the effect lasts for successive three months. However, it takes more than three days until the virus reaches the salivary glands (175).

The amount of the virus detected in the infected ticks varies on a particular life stage. Viral load in adults is one to three orders of magnitude higher than in nymphs, most probably due to the higher volume of blood ingested during feeding (187). After metamorphosis and fasting the infection rate of ticks decreases and only 33 % of nymphs and 61 % of adults retain a detectable level of infection (187). Conflicting results on the TBEV prevalence in questing ticks and ticks removed from host are being reported (188). Virus load detected in ticks can increase upon partial or full engorgement (175,179,180). This can be one of the reasons for discrepancies in the rate of infections in TBEV endemic areas and low TBEV prevalence in ticks. Another explanation can be the skewed behaviour of infected ticks towards higher activity and aggressiveness (180).

Although life-long persistence of tick infection is often referred (5,28), some studies assess the persistence of the virus in ticks as limited (175,189). Under natural conditions, TBEV persistence in ticks was prolonged when compared to the same batch of ticks kept under laboratory conditions (approx. 260 days and 120 days, respectively) (189). Infectious viral particles can no longer be detected in ticks fasting for more than a year (187).

In comparison to the mammalian cells, infection of tick cells with TBEV exhibits some substantially different features. There is a slower take off in the infection growth kinetics, viability of infected cells is not affected, and no cytopathic effect is visible in *in vitro* infections. This applies also to the tick cells persistently infected by LGTV (190,191). Immunolabelling of TBEV E surface glycoprotein revealed a general cytoplasmic signal in *I. ricinus* derived cell lines with a slight concentration in the perikaryal region. In non-vector tick cells, a slower rate of replication, lower virus yield, and a tendency of antigen to form specific cytoplasmic foci were found (191). In LGTV-infected tick cell culture, viral markers (NS3, NS5, E, and dsRNA) associated prominently with ER but not GA. There were no morphological differences between acutely and persistently infected tick cells, only an increase in the amount of ER structures increased due to the infection and these structures co-localized/were associated with viral proteins. Electron microscopy and 3D electron tomography however determined substantial ultrastructural differences. The ER structures proliferation and reorganization were in tick cells less prominent than in the mammalian cells, however, accentuated with the transition to the persistent infection. In a chronic infection bundles of tubules containing vesicles were induced and were wrapped in a single membrane layer (190).

Only until recently the protein interactions of TBEV with host proteins were missing (192) so we sought to identify the transcriptomic and proteomic response of tick cells infected with TBEV (Chapter 1, Publication 2).

TICK IMMUNE RESPONSE

Contrasting the vertebrates, which can use a finely tuned adaptive immune response against invading microbes, arthropods can rely on innate immunity only. Even though the innate immune system is not narrowly specific and rather than individual pathogen recognizes general infection-associated markers, it is still a highly effective first line of defence (193). As ticks are phylogenetically grouped among the basal arthropods, tick immunity exhibits all the general features of arthropod immunity. Cellular immunity reliant on haemocytes is capable of phagocytosis, nodulation, and encapsulation. Ticks are also armed with antimicrobial peptides, lectins, complement-like system, pattern recognition receptors (PRRs), reactive oxygen species, and reactive nitrogen species which are mainly involved in the defence against pathogenic bacteria or fungi. Tick immune response is characterized with few own specifics. Active melanisation cascade (pro-phenoloxidase system) and common coagulation cascade (coagulogen, crustacean clotting protein) appear to be missing in hard ticks. However, a stand-in by some alternative proteins working on the same principle is likely (194-196). Also, Sonenshine and colleagues suggested absence of the activity of defensins and lysozymes in the midgut lumen on *D. variabilis* (197); however, defensins are expressed in the tick tissues, but their activity needs to be proved in hard ticks (194). For the blood-transmitted disease, such is the TBEV, the midgut is the main gate for the virus

entry. The intracellular digestion in ticks with the slow resorption by the gut epithelium provides invading agents with ample time to invade the vector (193). However, during the tick infection, TBEV still needs to overcome several barriers (193,198). It needs to withstand attacks of immune effector molecules mentioned earlier (199), cross the peritrophic membrane into haemocoel, and lastly cross into the salivary glands for both the successful infection transmission to the host and carrying the infection to the next tick life stage (200,201). Evidence for such constraint limiting the spread of TBEV infection from the ingested bloodmeal into the midgut and/or salivary glands and a subsequent failure of TBEV infection was documented by Slovák and colleagues (175).

Three major signalling pathways are involved in the antimicrobial response in ticks. These are the Toll pathway, Immune deficiency (Imd) pathway, and Janus kinase/signal transducer and activator of transcription (Jak/STAT) pathway and their activation triggers the production of antimicrobial peptides (202). They correspond to TLR, TNFα, and Jak-STAT pathways in mammals respectively (193,203,204). Immune response pathways of arthropods on the example of *Drosophila* are summarized in the Figure 7. Distinct pathogen associated molecular patterns (PAMPs) are sensed and coupled by specific receptors targeting their recognition. For the Toll pathway, Spaetzle is recognized by the Toll receptor and the signalling proceeds via Dorsal; for IMD pathway, the signalling is mediated by Relish; and in JAK-STAT pathway, by Stat homodimer upon recognition of UPD molecule (205). There are indications that certain level of interconnection among the pathways takes place (206). In ticks, several components of all three pathways have been found (195,207,208), still, adaptor molecules responsible for signal transduction in Imd pathway and signalling molecule capable of binding to Domeless receptor are yet to be identified (193,207).

Antiviral innate immune system of ticks remains largely enigmatic, and we can only assume that ticks have common features with the more studied arthropod relatives, such as *Drosophila* or mosquitoes. Against viruses, the major defensive role is attributed to the RNAi pathway (RNA interference, also termed siRNA pathway) (209,210) (summarized in Figure 8). Based on the lengths and nature of interfering RNAs, we discern Piwi-interacting RNA (piRNA) pathway microRNA (miRNA) interacting pathway and small interfering RNA (siRNA) pathway. Piwi pathway relies on 24-30 nucleotides long RNAs and on the function of Argonaute-3 protein (Ago-3) and deals mainly with defence against transposons (211,212). miRNA pathway functions in post-transcriptional gene regulation and is mediated via Dicer-1 (Dcr-1) and Argonaute-1 (Ago-1) proteins and 20-25 nucleotide-long miRNA (213). In the exogenous siRNA pathway long dsRNA molecules produced by viral infection – either dsRNA replication intermediates or RNA secondary structures – are recognized by Dicer-2 (Dcr-2) (213-215). Dcr-2 is closely associated with the R2D2 protein, and both are needed to bind the RNA and form the RISC loading complex. The RNase III domain of Dcr-2 cleaves out the short double-stranded segments, typically 21 nucleotides long siRNAs (216-218). They are then transferred to Argonaute-2 (Ago-2), which associates with other proteins to give rise

to RNA-induced silencing complex (RISC). Only a guide RNA strand is kept in RISC and serves as a base-pairing key for Ago-2 nuclease activity to target and degrade specific viral RNAs (209,219).
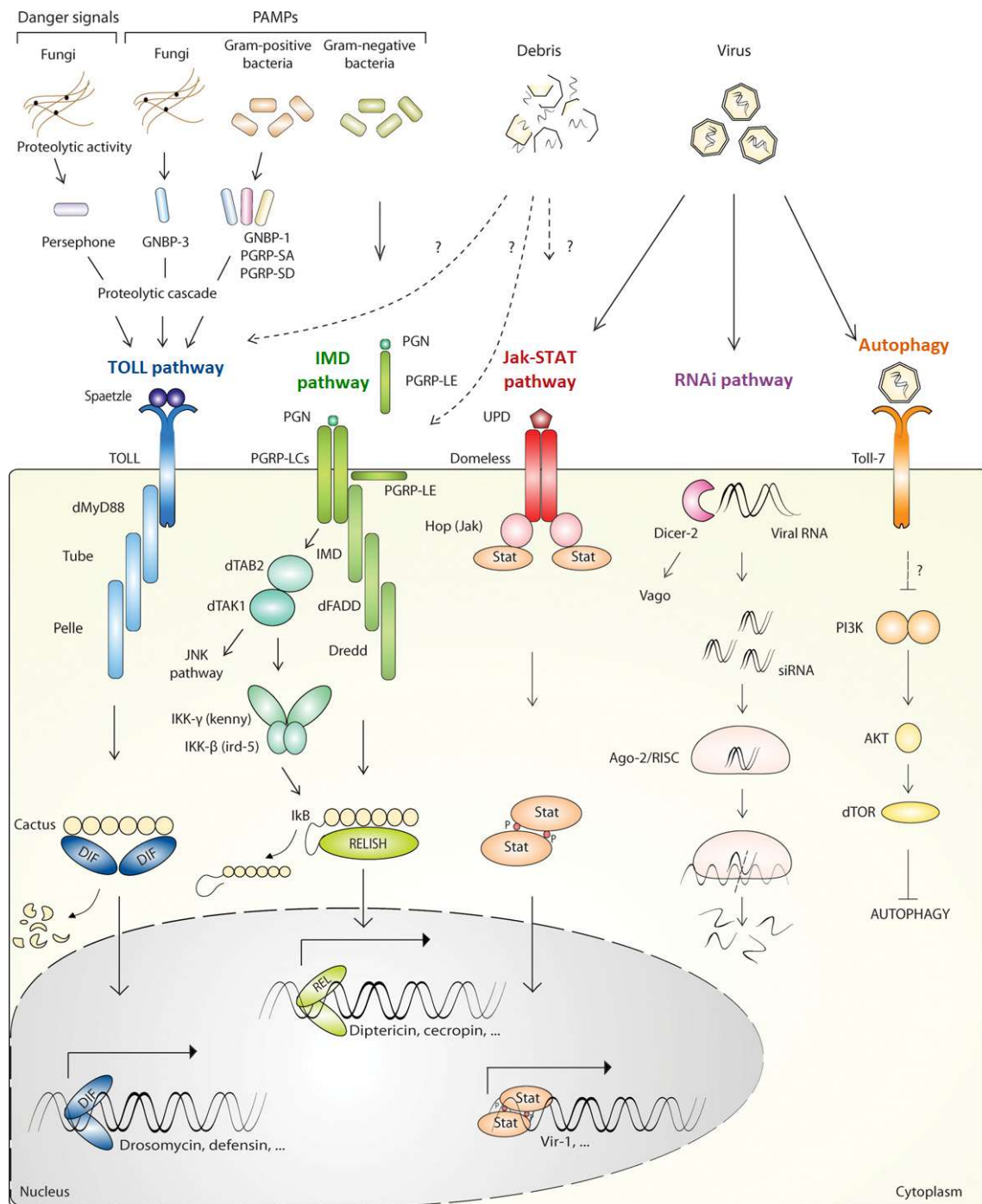
Figure 7. A general overview of inducible immune signalling cascades in Drosophila. Toll pathway (blue), Imd pathway (green), Jak-STAT pathway (red), RNAi pathway (purple), Autophagy pathway (orange). Edited from (208).
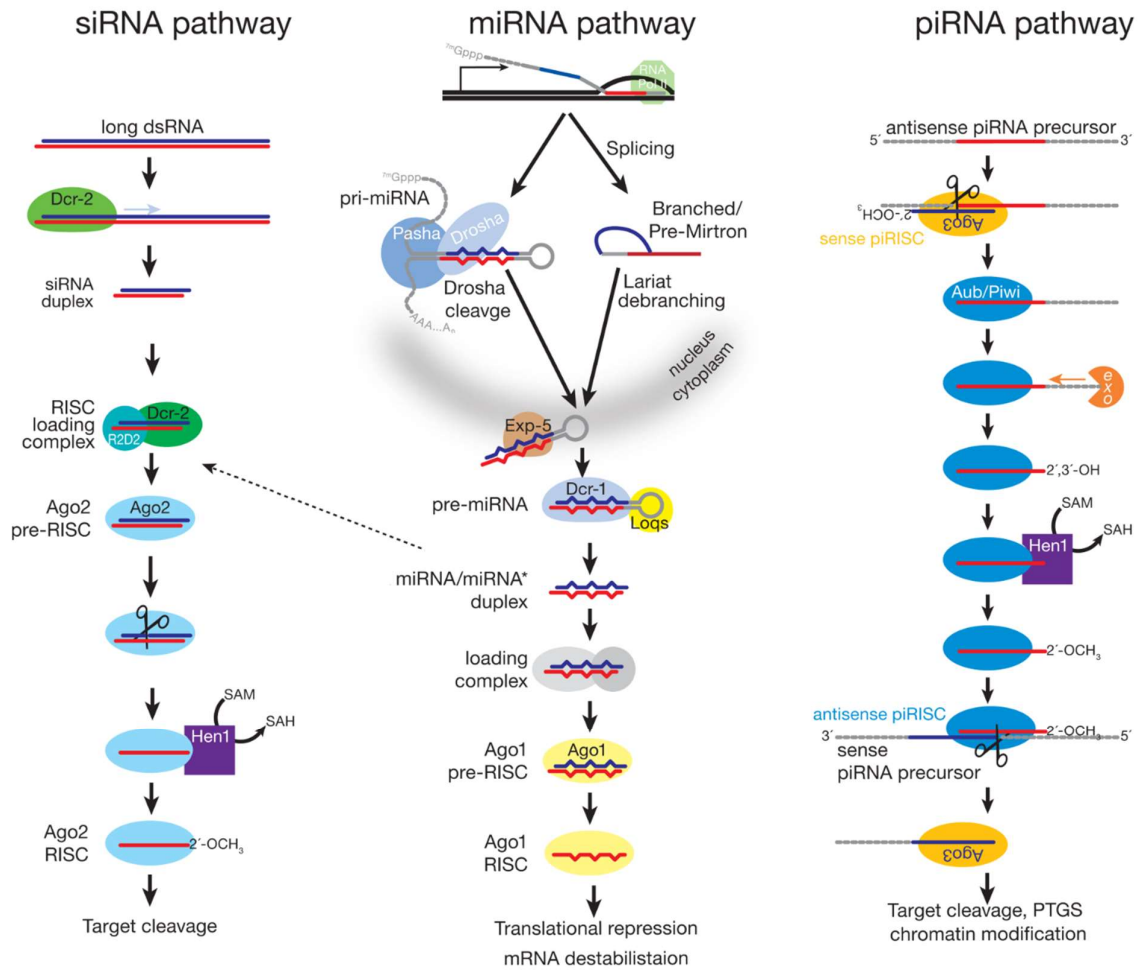
Figure 8. A general overview of RNAi pathways in Drosophila. siRNA pathway (left) is activated by dsRNA replication intermediates. Dicer-2 (Dcr-2) produces small interfering RNA (siRNA) molecules. The complex then associates with Argonaute-2 (Ago-2), one of the strands Is eliminated and RNA-induced silencing complex (RISC) complex is formed, that is able to degrade specific target. miRNA pathway (middle) employs Dicer-1 (Dcr-1) and gives rise to a miRNA specific RISC complex where target cleavage is performed by Ago-1 nuclease, piRNA pathway (right) forms piRISC and uses different sets of Piwi proteins and Ago-3 for the cleavage. Adapted from (213).

Despite the intensive research on extrinsic RNAi in insect, understanding of this pathway in ticks was missing. However, evidence for active RNAi has been shown in *ex-vivo* tick tissues (220). An involvement of particular structural components in the efficient extrinsic RNAi signalling in ticks and elucidation of their antiviral potential of against LGTV and TBEV was researched in Chapter 1, Publication1.

Quasispecies and host switch

A virus should not be perceived as a uniform entity stable in place and time. In the host or vector, the viral variants population composition oscillates and the various viral sequences co-exist, even though the ratio of these variants can change; this provides the resulting variant mixture with the cooperative power to contribute to the fitness of the virus in the host. Such

a group of viral variants is termed quasispecies. According to Lauring et Andino a quasispecies can be defined as a pool of genetically diverse variants of the virus that together embody characteristics of the population (221) or alternatively "non-identical but related genomes subjected to a continuous process of genetic variation, competition, and the selection and which act as a unit of selection" as defined by Domingo and colleagues (222). The diversity of the quasispecies may condition the virulence of the virus (221,223).

Variation in the virus population arises from the multiple cycles of virus replication. The TBEV RdRp lacks the proofreading activity (221,224) giving rise to a dynamic population of viral variants. Analysis of the mutation rate in the coding sequence assessed an evolutionary rate for TBEV to be 3.97×10^{-5} nucleotide substitutions per site per year (225). That is higher genetical stability than for positive ssRNA viruses on average (226). Most of the newly generated viral variants have lower fitness and low potential to prevail in the population. These variants, however, may be favoured when the environment changes dramatically, like in the case of a sudden immune pressure (221). A similar situation can happen during a vector-host switch when the virus needs to adapt to the new host environment. Host alternations frequently cause declines in the population size (227). Such decreases occur during the initial establishment of the infection, spread through the host body as well as during the bottleneck of tick feeding when only a small fraction of variants trespasses from the host to the vector (227). For the WNV, there is a higher genetic variability of quasispecies in the mosquito (invertebrate vector) than in the vertebrate host and the immune system was proposed to play a role in this phenomenon (228). In research on DENV horizontal transmission, the viral quasispecies diversity is quickly restored even when the population is reduced by 90 % and a new quasispecies pool originates *de novo* in the new host or tissue (227).

For TBEV, quasispecies have been described in field studies (229,230) as well as in laboratory experiments (191,231-233). An important landmark was the retrieval of TBEV quasispecies from the natural virus isolates (feeding tick and tick pool) that had no history of artificial passage (229,230). They exhibited variability in the lengths of the polyA region in the 3´UTR or several single nucleotide polymorphisms (SNPs) (230). Interestingly, 40 % of single nucleotide polymorphisms (SNPs) were shared by two distinct TBEV strains (JP-296 and JP-554) originating from the same natural focus area revealing the shared pool of quasispecies in one population (229). Under-represented viral variants (below 1 %) can be drawn and restored from the "molecular memory" in the conditions convenient for its growth when the virus adapts to specific cells (233). To gain a deeper insight into the adaptation of TBEV to either host or vector environment, we performed a long-term adaptation to either cell type, and the result is presented in Chapter 3, Publication 5.

In the host, the first line of defence fighting viral infection is the innate immune response, an essential non-specific immune reaction that can postpone the spreading of viral invasion until the adaptive immune response manages to activate or even deter the infection completely (234,235). The overall antiviral processes that are triggered in the host cell during acute virus infection are complex and highly integrated (236). Hereafter I will focus on the intrinsic immune response elicited in the (flavi)virus-infected non-immune cells, with a special focus on TBEV.

SENSING THE VIRAL INFECTION

There are two major receptor systems that cells possess to detect viral infection. Both utilize recognition of molecular structures characteristic for pathogens of various origins so-called (PAMPs) by pattern recognition receptors (PRRs) (237), summarized in Figure 9. First category are Toll-like receptors (TLRs). TLR 3, 7, 8, and 9 are located in endosomal membranes and recognize distinct types of virally derived nucleic acids. TLR7/8 recognize ssRNA while TLR3 recognizes viral dsRNA (238,239). Upon activation, TLRs bind to their adaptor molecules and activate transcription factors interferon regulatory factor (IRF) 3, IRF7, and NF-κB (nuclear factor kappa-light-chain-enhancer of activated B cells), which trigger pro-inflammatory cytokines production and especially type I IFN induction (240). Another receptor group are the cytosolic RIG-I like receptors (RLRs) that are specialized in the recognition of intracellular viral dsRNA by three proteins: (i) retinoic acid inducible gene I (RIG-I), (ii) melanoma differentiation-associated protein 5 (MDA5) and (iii) LGP2 (Laboratory of Genetics and Physiology 2). RIG-I and MDA5 are RNA helicases similar in function and structure and induce IFN response independently on TLRs (241). LGP2 is also an RNA helicase, however, it lacks the CARD domain and acts as a negative regulator of the RLR signalling (242). RIG-I and MDA5 recognize unique structures and sequence motifs of viral RNA (243,244). RNA containing a 5'-triphosphate, short dsRNA with blunt ends, and uridine- or adenosine-rich viral RNA motifs have been identified as RIG-I ligands (245-247). MDA5 is believed to recognize long dsRNA (> 5 kb) (243,248). RLRs bind to a common adaptor molecule MAVS (mitochondrial antiviral signalling; also known as IPS-1) upon recognition of their ligand (249) and activation of signalling cascade proceeds through mobilization of IRF3, IRF7, AP-1, and NFκB transcription factors that launch production of IFN-I (236,250).

With regard to the defence pathways that are involved in the TBEV infection sensing in infected cells, activation of RIG-I has been documented several times (150,251,252) and only marginal involvement of the MDA5 pathway was shown (251). RIG-I activation indicates that the replication step of TBEV is most probably recognized by the infected cell. The importance of signalling via MAVS in anti-flavivirus response has been shown in knockout mice. It was necessary for controlling the infection in the brains of infected mice and lack of MAVS led to

a boosted viral growth and worsened neuropathogenesis (253). In infected astrocytes, two-stage IFN signalling has been shown with RIG-I being involved at first and TRIM (Tripartite motif-containing, antiviral protein) /Myd88 being engaged later (150).

Interferons are multifunctional secreted proteins that have different antigenic structures and various cell types produce them under divergent conditions (254). Up to day, three IFN classes have been identified that are grouped according to the receptor complex they signal through (255); as summarized in Figure 9.

Type I IFNs, which in humans comprise 13 IFNα subtypes, IFNβ, IFNκ, IFNε, IFNω, engage the ubiquitously expressed IFNα receptor (IFNAR) complex that is composed of two components – IFNAR1 and IFNAR2. The function of type I IFNs is well characterized, and they are known to be essential for mounting a robust host response against viral infection (234,235,255,256). IFNα/β are produced by most cell types following virus infection and induce a so-called "antiviral state" by up-regulating genes with direct and indirect antiviral functions (134). IFNα/β binding to IFNAR triggers activation of Jak1 and Tyk-2 kinases from the Janus kinase family. Then they phosphorylate STAT1 and STAT2 proteins (signal transducer and activator of transcription) transcription factors, that further associate with IRF9 forming together ISGF3 (IFN-stimulated gene factor 3). ISGF3 complex translocates into the nucleus and upon binding to interferon-stimulated response elements (ISRE) promotor initiates the transcription and activation of hundreds of interferon-stimulated genes (ISGs) (239,257). Products of these genes involve proteins with direct antiviral effects (e.g., PKR, MX1, OAS, etc., in detail later). There are also further effects, such as inhibition of cell proliferation, anti-tumour responses, stimulation of NK cells activity, increasing antigen presentation with MHC I molecules, and priming adaptive immune response (258).

Type II IFN consists of a single IFNγ gene product that binds the IFNGR receptor complex. Major producers are T-lymphocytes and NK cells, and it launches different signalling cascades than the other IFN types involving STAT1 homodimer designated as GAF (gamma-activated factor) (235,254). IFNγ mediates broad immune responses to pathogens, and mainly regulates the functions of macrophages, NK cells and T-lymphocytes (255). Apart from immunomodulatory functions, they have also a pro-inflammatory role (259).

The more recently described type III IFNs include four IFNλ gene products in human (IFNλ1-3 also called IL-29, IL-28A, IL-28B; and IFNλ4) that signal via the combined IFNLR1 and interleukin-10 receptor 2 (IL-10R2) receptors. They regulate the antiviral response and have been proposed to be the ancestral type I IFNs (255,260,261). They serve as a bumper – the first line of the immune response, that is triggered on the epithelial barriers. The onset of their action is more gradual and less pungent yet less harmful (258). Most of the cells

express both types I and type III interferons after TLR stimulation or virus infection, whereas the ability of cells to respond to IFNλ is restricted to a narrow subset of cells, including epithelial cells, hematopoietic cells, and neutrophils (258). Mice lacking IFNLR1 molecule were indistinguishable from wild-type mice with respect to clearance of different viruses, whereas mice lacking type I IFN receptor were significantly impaired. Type I IFNs mediate positive feedback on type III IFNs but not contrariwise, so that type III IFN target a specific subset of cells and contribute to the antiviral response evoked by TLRs (262).
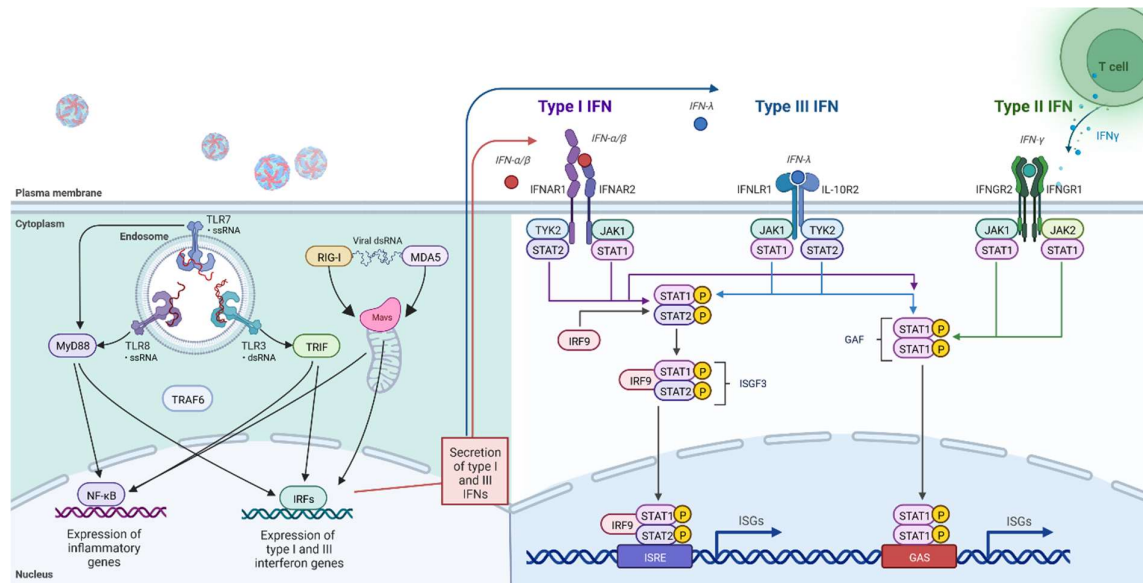
Figure 9. An overview of antiviral innate immune signalling pathways in human. Flaviviral infection is recognized (left) either by endosomal TLRs (TLR 3, 7, 8) or by cytoplasmic RLRs (RIG-I, MDA5). Their activation leads through adaptor molecules to downstream activation of NF-κB and IRFs transcription factors and production of type I (IFNα/β) or type III (IFNλ) interferons. Type I and III IFNs in autocrine and paracrine manner stimulate interferon signalling cascades (right). Type II interferon signalling is induced by IFNγ produced by activated immune cells, such as T-lymphocytes or natural killer cells. Activation of IFN receptors leads to activation of adaptor Janus kinase family proteins (Tyk2, Jak1, Jak2) that phosphorylate STAT transcription factors, which translocated into the nucleus trigger production of interferon stimulated genes (ISGs). Created with BioRender.com.

ANTIVIRAL PROTEINS

As mentioned above, activation of IFN response induces expression of several hundred genes (ISGs), whose combination specifies the antiviral state of the cell. Only some of the ISGs can exert a direct antiviral effect. For a given virus, a subset of ISGs is probably required to limit the viral replication more likely than the overpowering activity of a single gene (263,264). Antiviral ISGs with the power to limit TBEV will be mentioned further, some in more and some in less detail.

TRIM

Tick-borne flaviviruses specifically have been shown prone to the restriction by Tripartite motif-containing proteins (TRIM) which share E-3ubiquitin ligase activity (265). TRIM5α was shown to hamper replication of TBEV and mediate proteasomal degradation of the NS2B/NS3 viral protease (266). Another family member, TRIM79α targets viral polymerase NS5, but its degradation is facilitated by the lysosome-mediated degradation pathway (267). Other flaviviruses are restricted also by different TRIM family members, which demonstrates the importance of these factors in fighting flaviviral infections (268-270).

IFITM

IFITM family proteins (Interferon-inducible transmembrane) share a strong homology and reside at either plasma membrane (predominantly IFITM1), early endosomes (predominantly IFITM1), and late endosomes and lysosomes (IFITM2, IFITM3 prevail) (271). Apart from having immune, developmental, and cell cycle-related functions, they are involved in antiviral defence (271). They are believed to exert their antiviral function in the step of flavivirus entry but conjointly they affect virus replication (272). Recently, they were described to act as enhancers of viral particles trafficking to lysosomes, favouring thus virion degradation over the uncoating (273). IFITM1, IFITM2, and IFITM3 exert antiviral function in TBEV infected cells, from which IFITM3 was the most potent. However, different IFITM proteins complement each other in their functions, that is reducing the spread of the virus, especially at a greater distance (274). *In vivo*, the lack of the *Ifitm3* gene conferred mice vulnerable to a lethal course of WNV encephalitis. More virus accumulated in extra neural organs as well as in CNS, but the major effect of IFITM3 flaviviral restriction was noted in extra neural tissues (275).

IFI6

IFI6 (IFN-α-inducible protein 6) is a potent antiviral factor against several flaviviruses (WNV, ZIKV, YFV, DENV) (276,277). As an ER-resident protein, IFI6 impairs the formation of virus replication organelles (VP) and reduces thus the flavivirus replication level (277). It was proposed that direct contact of IFI6 and viral proteins might not be necessary to accomplish this effect (265).

PKR

PKR (protein kinase R) is activated to its dimeric autophosphorylated state by recognition of dsRNA sourced either directly from viral genomes or from replication intermediates. PKR has a dual function, it is an ISG and type I IFN inducer at the same time, especially during viral infections (278). PKR phosphorylates eIF2α (eukaryotic translation initiation factor 2 subunit alpha), which is a critical cofactor required for translation initiation – recruitment of initiator methionine-tRNA to a ribosome. PKR phosphorylation of eIF2α enables it to irreversibly bind to the nucleotide exchange factor eIF2B, a key molecule that regulates protein synthesis rate. This 'freezes' eIF2α in the complex and hinders eIF2B from initiating future translational

events. This prevents the ribosomal translation of cellular and viral proteins, ultimately blocking viral replication in the cell (278-280). Överby and colleagues researched the involvement of PKR in the stimulation of the immune response in TBEV infected cells. Even though PKR together with RLRs was the mediator of the IFN signalling, it had an inferior role in triggering IFN response and was not even localized to the replication sites (281).

2´-5´ oligoadenylate synthetase (OAS) is self-activated by binding to viral dsRNA and synthesize adenosine oligomers that are linked by an unusual phosphodiester bond in a 2´ to 5´ configuration (2-5A) (282). RNaseL is activated by interaction with those adenosine oligomers and instigates the degradation of viral and cellular mRNA to prevent viral protein synthesis (283). This mechanism operates using a positive feedback loop, whereby increasing amounts of viral dsRNA consequently activate additional RNaseL. Viral overload results in the degradation of cellular RNA to such an extent that apoptotic pathways are activated to avert widespread viral dissemination (284).

Resistance or susceptibility to flavivirus infection can have a genetic background. An identified flavivirus resistant allele was characterized and linked to gene *oas1b* for tick-borne as well as mosquito-borne flaviviruses. Susceptible mouse strains have an isoform of the *oas* gene that is truncated due to nonsense mutation in the gene and 30 % of proteins lack the C-terminal sequence (285-287). On the contrary, expression of the full-length *oas* gene in susceptible cells conferred partial resistance to WNV infection (288). The role of OAS in human susceptibility has been researched on a small scale with WNV-infected patients. Yakub and colleagues found no deletion or insertion linked to the severity of the disease. They however showed that certain SNPs occurred at higher frequencies in case-patients (289).

The OASL protein belongs to the same family as OAS, however, it lacks the capacity to synthesise 2-5A due to several mutations in the active site (290). OASL gene encodes a two-domain protein. The N-terminal OASL domain is surprisingly similar to the structure of activated OAS and has a binding groove for the dsRNA. The C-terminal domain shares a weak sequence similarity (30 %) to ubiquitin (291,292).

OASL has an antiviral effect against a wide range of viruses (reviewed in (293)), which is dependent on the ubiquitin-like C-terminal domain (291). It binds also to RIG-I and enhances RIG-I signalling. Against HCV, however, both OASL domains attain inhibitory activity. The N-terminal domain is inhibitory for cell growth as well as HCV replication, whereas the C-terminal domain is inhibitory only for HCV replication (294). OASL also exerts a function conflicting to the antiviral ISG, that is a negative regulation of the antiviral function of OAS (293).

Two decades ago, a gene with antiviral function termed RSAD2 (former vig-1, cig-5) was discovered. It codes for a protein viperin (virus-inducible endoplasmic reticulum associated) that belongs to the group of proteins with antiviral properties and was originally identified thanks to markedly pronounced expression in fibroblasts infected with human cytomegalovirus (295). Since then, viperin has revealed to be a potent antiviral protein acting in defence of cells against a wide spectrum of DNA and RNA viruses, likewise, several members of the family *Flaviviridae* (reviewed in (296)). Viperin is a highly evolutionarily conserved protein that executes its role of an antiviral effector in fish, rodent, and primate species (295,297-299). It belongs to the superfamily of radical S-adenosyl-L-methionine (SAM) enzymes and contains a conserved CX_3CX_2C motif in its central domain, that binds a [4Fe-4S] cluster which engages SAM as a substrate. During the enzymatic reaction, SAM is cleaved to methionine and a highly reactive radical, the 5´-deoxyadenosyl (5´dA) (300-302). Alternative substrates generating 5´dA have also been identified (302). The N-terminal variable amphipathic α-helix is responsible for protein embedding in the cytoplasmic face of the ER membrane, or under viral infection circumstances for relocation to lipid droplets or GA (299,303,304). The C-terminal part of the protein is conserved and seems to be important for viperin antiviral activity and interaction with other proteins ad recognition of a substrate (302,305,306).

Viperin expression is mostly induced by the IFN type I signalling pathway and leads to activation of ISGF3 transcription complex (299,307-309). However, in certain cases, such as JEV infection, an interferon independent signalling pathway depending on TLRs or RLRs signalling and IRF3, MAVS, and NF-κB mediation are involved (297,307,308,310).

Viperin's mode of action against such a diverse range of viruses has for long pondered scientists. Several mechanistic explanations on how viperin is mediating the antiviral effect have emerged recently. Some of them are dependent, some independent of the SAM enzymatic activity. Viperin is able to produce a unique nucleotide analogue 3´-deoxy-3´,4´-didehydro-CTP (ddhCTP) that acts as an end-chain terminator of genome synthesis by some viral RNA polymerases (311). Viperin companion molecule, cytidylate monophosphate kinase 2 (CMPK2), provides a substrate (CTP) for viperin and boosts its activity. Both genes are usually jointly regulated, and they also share a controller, a long non-coding RNA (lncRNA-CMPK2) (311,312). Also, viperin is a component of the TLR7/9 signalling pathway eventually leading to the production of interferon. It is bound to IRAK1 (interleukin-1 receptor-associated kinase) in a complex with TRAF6 (TNF receptor-associated factor 6), an E3 ubiquitin ligase. This interaction enables activating ubiquitylation of IRAK1, which transduces the signal further to the transcription factors, such as NF-κB or IRF7 and eventually leads to type I IFN production (313,314). The presence of TRAF6 and IRAK1 enhances the enzymatic activity of viperin and it in return promotes the process of IRAK1 ubiquitylation, which is directly linked to the viperin enzymatic activity and the production

of ddhCTP (313). A distinct mechanism of viperin action was described for influenza virus infection. Viperin impaired the formation of lipid rafts at the surface of the host cell which are necessary for proper influenza virus budding. The mechanism of this viperin action was indirect, mediated by FPPS (farnesyl diphosphate synthase), a protein important in isoprenoid biosynthesis (315,316).

A viral countermeasure against the antiviral action of viperin was exemplified in the case of JEV infection. Even though a transcription of viperin was induced intensively, the protein itself was not expressed, because it was targeted for proteasome-dependent degradation (307).

Our previous results suggested, that viperin could be one of the key antiviral effectors in TBEV infected neural cells since its mRNA was one of the most markedly increased upon TBEV infection in neural cells (317). Soon the importance of viperin in fighting flaviviral infection was more than prominent (307,318,319). Several research groups revealed specific points of TBEV-viperin interaction and described its effect in further detail. Viperin can impair gRNA synthesis (306) and interacts with several structural and non-structural proteins of TBEV (prM, E, NS2A, NS2B, NS3). Via interaction with the NS3 protein, viperin targets those viral proteins for proteasomal mediated degradation (320). Also, it can intervene with the proper viral particle assembly and release somehow indirectly involving GBF1, a Golgi brefeldin A-resistant guanine exchange factor 1, a protein involved in the COPI dependent and trans-Golgi vesicle budding (306,321). Viperin was also responsible for cell-type-specific control of TBEV infection in diverse brain areas (olfactory bulb, cerebrum), but failed to curb the infection in the cerebellum, similarly to other neurotropic flaviviruses (LGTV, WNV). The absence of viperin boosted the replication of TBEV and LGTV mainly in astrocytes and cortical neurons (322,323). While most of the TBEV-related studies are using gene-engineered viperin stably expressed in target cells, data on viperin function under more natural conditions, in virus-infected cells, are scarce. The possibility of viperin protein interfering with TBEV pathogenesis was investigated in Chapter 2, Publication 3.

VIRAL HOST CELL ADAPTATION AND COUNTERMEASURES

EMPLOYING AND ADAPTING OF HOST MACHINERY

Successful invasion of the host cell is conditioned by the adaptation of the host-cell environment to suit the needs of the virus. Each specific virus thus recruits some general and some unique host factors that help it reach the needed microenvironment and serve the viral purposes. Such host factors, that virus employs for its own needs, have just started to be revealed for TBEV or related flaviviruses. TBEV NS3 protease interacts with the host E3-ubiquitin ligase TRAF6 (TNF receptor associated factor 6). TRAF6 is, under general conditions, involved in immune signalling. Interaction with TRAF6 advances viral replication ten times, however, the sequestration did not affect type-I IFN levels (324). Another example

is TMEM41B protein (325). This enzyme is a putative autophagy factor, that is recruited to the viral replication organelle during flaviviral infection where co-localizes with flaviviral NS4A and NS4B proteins. TMEM41B takes part in forming membrane curvature. That specific replication niche is essential for effective viral replication. An absence of TMEM41B results in increased immune response, probably via making viral PAMPs more accessible to the host defence system. VMP1 gene from the same pathway worked in a similar way and was able to compensate low abundance of TMEM41B in certain cell types (325). A wide array of other factors that contribute to the virus-induced membrane structures and replication complex are reviewed in detail by Aktepe and Mackenzie (90). Another factor, Adenosine deaminase acting on RNA 1 (ADAR1) supports DENV replication and progeny production. It is a nice example of how flavivirus infection is causing underrepresentation of a specific negative regulator, that is miR-3614-5p which has ADAR1 as one of its targets and enables ADAR1 assistance in the virus life cycle (67).

Immune evasion

Another aspect of host cell exploitation is the counteraction of the host immune response aimed at the virus. A very effective and unique strategy of immune response evasion by flaviviruses is hiding the replication in the complex ER membranous structures reorganized by pathogenesis. This way, viral recognition is more difficult for cellular defending machinery and the IFN response is delayed. That lag enables the virus to well establish replication and progeny production (281,326).

A family of antiviral ISGs IFIT proteins (IFN-induced proteins with tetra-tricopeptide repeats) are induced by flaviviral and other viral infections and can limit the translation of viral RNA. Flaviviruses have been conferred the resistance to IFIT 2 recognition by 2´-O-methylation of their 7mG cap, which is the way IFITs are able to recognize self from non-self RNA and limit the intruder in the cell (327).

A common feature for flaviviruses is to impair type I IFN signalling by the inhibition of Jak-STAT signal transduction. TBEV NS5 protein inhibits STAT1 phosphorylation, which is an essential component of the type I and II signalling pathway (Figure 9). It is done in cooperation with the cellular protein hScrib. As a result, the capacity of STAT1 to translocate to the nucleus is impeded and it also affects the launch of expression initiation of ISRE-dependent genes (328,329). The closely related LGTV NS5 protein also blocks the phosphorylation of STAT1 and further of STAT2, Tyk2 and Jak1 signalling molecules while interacting with the IFN receptor molecule itself (IFNAR1, IFNAR2) (330). TBEV NS5 can also diminish the expression of a receptor component IFNAR1 on the surface of infected cells by association with prolidase, the enzyme involved in the surface expression of IFNAR1 (331). The ability to inhibit the IFN-mediated signal transduction is a common strategy among flaviviruses, but the specific type of interaction or a viral protein involved seems to be unique for each specific virus (234,329,332-337). In addition to a comprehensive block of phosphorylation of STAT

factors, the WNV and ZIKV impair not only all three IFN signalling pathways but also distinct immune pathways that employ STAT factors as messenger molecules, such as inflammatory IL-6 (interleukin) pathway or immune response regulating IL-4 and IL-10 pathways. Interestingly the NF-κB pathway remained unaffected. NS5 was identified as the major viral effector involved with the participation of other non-structural proteins (NS2A, NS2B, NS2B/NS3). The mechanism relied on detaining the chaperone HSP 90 (heat shock protein 90) at the virus replication site (338).

sfRNA

Preservation of sfRNA presence in the various flaviviruses argues for the beneficial biological relevance of this molecule for flavivirus life cycle. Indeed, several functions affecting the infectious process in the host have been linked to sfRNA. The presence of sfRNA promotes flaviviral replication, virion formation and advances cytopathic effect in vector as well as in host cells by facilitation of host cell dying (57). sfRNA is substantial also for pathogenesis and the outcome of infection *in vivo*, in infected mice (57,339). Further, sfRNA is engaged in the evasion of the immune response. It is involved in interfering with host RNAi and miRNA pathways in both, the vector and the host. In part possibly owing to the impeded Dicer capacity to cleave dsRNA caused by the sfRNA (58). On top of that, its counteracting host antiviral response, especially type I IFN response, was shown (339-341), with the span to the signalling (342,343), inhibition of antiviral proteins translation by their mRNA sponging (340) or targeting a function of certain antiviral proteins, such as RNase L (339). A higher sfRNA to gRNA ratio is associated with increased viral fitness and can increase its epidemiological success (342). sfRNA attracts host proteins, XRN1 included couples with them long-term and makes them unavailable for regular cellular processes. In this way, mRNA turnover, RNA decay, splicing, and editing processes are disrupted (344,345).

sfRNA is also involved in increased infectivity of flaviviruses for the vector, for instance in WNV, ZIKV or DENV infection (346-348). For DENV infection, viral fitness in a vector is positively correlated with the sfRNA amount (346). Production of different sfRNA species in DENV vector and mammalian host infections due to distinct selective pressure plays a role in vector-host switch and highlights the importance of duplication of xrRNA motifs. However, the same sfRNA species were noted in ZIKV vector and host, arguing for virus-specific regulation in sfRNA species production (59,349).

Most of our knowledge on sfRNA function and roles in successful infection has been gained from mosquito-borne flaviviruses (MBFVs). Tick-borne flaviviruses sfRNA shows different structural features and shares a low sequence homology with MBFVs sfRNAs, thus, simple extrapolations of knowledge coming from MBFVs can lead to incorrect conclusions. A production of sfRNA in TBEV and LGTV infected cells and the relevance for vector cells defence against flavivirus infection will be dealt with in the chapter Chapter 1, Publication 1.

Extensive reorganization of ER membrane structures due to viral infection and abundance of viral RNA and viral proteins being produced leads to the accumulation of unfolded host proteins, ER stress, and a subsequent trigger of the unfolded protein response (UPR). Activation of UPR should lead to the re-establishment of the lost balance in the ER. The initial sensor of UPR is the BiP protein (immunoglobulin heavy chain-binding protein) that interacts with either of three ER-located mediators. That is, i) IRE1 (inositol requiring ring enzyme 1) that signals through XBP1 transcription factor (X box-binding protein 1) leading to increased protein folding and ER biogenesis or protein degradation, ii) PERK (protein kinase R-like endoplasmic reticulum kinase) that phosphorylates eIF2α (eukaryotic translation initiation factor 2-α), a key checkpoint of translation initiation, causing thus the attenuation of translation or iii) ATF6 (activating transcription factor 6), a transcription factor itself that, when translocated to the nucleus, stimulates transcription of UPR regulated genes (including XBP1) and promotes protein folding via chaperone (56,350). In case this palette of responses fails to restore the skewed balance in the ER of the infected cell, UPR drives the cell to apoptosis (56,350).

During TBEV infection, stimulation of all three effectors of UPR (i.e., IRE1, PERK, and ATF6) was recognized (351-353). However, only the IRE1 branch effectively restricted viral replication, PERK and ATF were dispensable for the observed phenomenon (353). Slight differences in UPR regarding the pathway triggered and transcriptional factors used can be seen for different cell types and TBEV strains used (352). Even though IRE1 activation promoted XBP1 splicing (352,353), it was dispensable for TBEV infection promotion and so far unrevealed way of signalling was possibly activated (353). Moreover, UPR activation was a way, how infected cells could activate antiviral response sooner through the involvement of immune signalling molecules IRF3 and RIG-I. In such a way, UPR co-operates with the otherwise delayed antiviral immune response (281,353).

Activation of UPR by TBEV is a hint of deeper manipulation of host transcription and/or translation machinery. Decreasing the host translation would benefit the virus by recruiting more working capacity of the cell translation machinery for its purposes. The strategies that viruses use to interfere with host translation have been summarized in detail by Walsh, Mathews and Mohr (354). There are three main checkpoints, where translation can be targeted: i) mRNA transcription, ii) pre-mRNA processing, and iii) the translation itself (354). Except for HCV, *Flaviviridae* family members were not considered to interfere with host translation machinery (354) until recently. In neural cells, ZIKV caused ribosomal stress that disrupted the structural integrity of the nucleolus and caused apoptosis (355). Roth and colleagues discovered translation shut-off caused by DENV and ZIKV infection. Specifically, a reduced portion of host mRNAs was coupled to actively translating polyribosomes. The step of translation initiation was affected but none of the classical checkpoints of translation complex association was identified (eIF2α and eIF4E

phosphorylation was excluded) as a culprit of the phenomenon, thus the authors inferred the inhibition occurred further in the assembly of the pre-initiation complex (356). We were interested in researching host translation manipulation by TBEV Chapter 2, Publication 3.

AIMS

The thesis objective is to bring more insight into the specific interaction of the tick-borne encephalitis virus or a closely related Langat virus and the infected cell of either vector or host origin. Special emphasis is put on the immune response elicited by the host cell and virus immune evasion strategies.

Specific aims:

I.   Analyse vector cell response to TBEV and/or LGTV infection on the level of gene and protein expression, characterize the major pathways altered and identify the factors involved in the innate immune response. Characterize the tick antiviral RNAi pathway and its factors and investigate virus countermeasures.

II.   Analyse the host neural cell response to TBEV infection on transcriptomic level, characterize the major pathways altered, identify the factors involved in the innate immune response and investigate countermeasures of the virus. Identify common and unique features of the response for human astrocytes and neurons.

III.   Evaluate the adaptation of TBEV to the vector and host cell environment with respect to biological properties and pathogenesis and in newly derived variants define genetic changes underlying the altered biological properties.

CHAPTER 1 CHARACTERIZATION OF VECTOR CELLS RESPONSE TO TBEV INFECTION

MANUSCRIPT 1

Schnettler E., **Tykalová H.**, Watson M., Sharma M., Sterken M.G., Obbard D.J., Lewis S.H., McFarlane M., Bell-Sakyi L., Barry G., Weisheit S., Best S.M., Kuhn R.J., Pijlman G.P., Chase-Topping M.E., Gould E.A., Grubhoffer L., Fazakerley J.K., Kohl A. (2014). Induction and suppression of tick cell antiviral RNAi responses by tick-borne flaviviruses. Nucleic Acids Research 42(14): 9436-46. DOI: 10.1093/nar/gku657

Induction and suppression of tick cell antiviral RNAi responses by tick-borne flaviviruses

Esther Schnettler[1,2,*], Hana Tykalová[3], Mick Watson[2], Mayuri Sharma[4], Mark G. Sterken[5], Darren J. Obbard[6], Samuel H. Lewis[6], Melanie McFarlane[1], Lesley Bell-Sakyi[2], Gerald Barry[2], Sabine Weisheit[2], Sonja M. Best[7], Richard J. Kuhn[4], Gorben P. Pijlman[5], Margo E. Chase-Topping[8], Ernest A. Gould[9,10], Libor Grubhoffer[3], John K. Fazakerley[2] and Alain Kohl[1,2,*]

[1]MRC - University of Glasgow Centre for Virus Research, Glasgow G11 5JR, UK, [2]The Roslin Institute and Royal (Dick) School of Veterinary Studies, University of Edinburgh, Easter Bush, Midlothian EH25 9RG, UK, [3]Faculty of Science, University of South Bohemia and Biology Centre, Institute of Parasitology, Czech Academy of Sciences, 37005 České Budějovice (Budweis), Czech Republic, [4]Markey Centre for Structural Biology, Department of Biological Sciences, Purdue University, West Lafayette IN 47907, USA, [5]Laboratory of Virology, Wageningen University, 6708 PB Wageningen, The Netherlands, [6]Institute of Evolutionary Biology and Centre for Infection Immunity and Evolution, University of Edinburgh, EH9 3JT, UK, [7]Innate Immunity and Pathogenesis Unit, Laboratory of Virology, Rocky Mountain Laboratories, Division of Intramural Research, National Institute of Allergy and Infectious Diseases, National Institutes of Health, Hamilton, MT 59840, USA, [8]Centre for Immunity, Infection and Evolution, University of Edinburgh, EH9 3JT, UK, [9]Unité des Virus Emergents, Faculté de Médecine Timone, 13385 Marseille Cedex 05, France and [10]Centre for Hydrology and Ecology, Maclean Building, Oxon OX10 8BB, UK

ABSTRACT

Arboviruses are transmitted by distantly related arthropod vectors such as mosquitoes (class *Insecta*) and ticks (class *Arachnida*). RNA interference (RNAi) is the major antiviral mechanism in arthropods against arboviruses. Unlike in mosquitoes, tick antiviral RNAi is not understood, although this information is important to compare arbovirus/host interactions in different classes of arbovirus vectos. Using an *Ixodes scapularis*-derived cell line, key Argonaute proteins involved in RNAi and the response against tick-borne Langat virus (*Flaviviridae*) replication were identified and phylogenetic relationships characterized. Analysis of small RNAs in infected cells showed the production of virus-derived small interfering RNAs (viRNAs), which are key molecules of the antiviral RNAi response. Importantly, viRNAs were longer (22 nucleotides) than those from other arbovirus vectors and mapped at highest frequency to the termini of the viral genome, as opposed to mosquito-borne flaviviruses. Moreover, tick-borne flaviviruses expressed subgenomic flavivirus RNAs that interfere with tick RNAi. Our results characterize the antiviral RNAi response in tick cells including phylogenetic analysis of genes encoding antiviral proteins, and viral interference with this pathway. This shows important differences in antiviral RNAi between the two major classes of arbovirus vectors, and our data broadens our understanding of arthropod antiviral RNAi.

INTRODUCTION

Tick-borne arboviruses of the *Flaviviridae* family are highly relevant to public health (1). Much work on tick-borne arboviruses has been carried out with Langat virus (LGTV), isolated from *Ixodes granulatus* and *Haemaphysalis* ssp.

36

ticks in Malaysia and Thailand and related to tick-borne encephalitis virus (TBEV) (1–4). Flaviviruses are positive-stranded RNA viruses. Viral proteins are encoded in a single open reading frame. The untranslated RNA regions (UTRs) at the genome termini regulate replication and translation (5–8).

Arbovirus infection of arthropod cells is characterized by little or no cytopathic effects (9). Studies of vector/arbovirus interactions suggests that this may be at least partly due to regulation of arbovirus replication by innate immune responses (10). Research on vector immune responses to arboviruses has focused on mosquitoes (11,12) despite the fact that many European/Asian arboviruses are tick-borne (13). Antiviral responses in mosquitoes rely on a small RNA-based mechanism called RNA interference (RNAi) (10,11). The exogenous small interfering (si)RNA pathway is especially important and can be induced by virus-derived long double-stranded (ds)RNA molecules generated during infection (either replication intermediates or secondary RNA structures) or dsRNA viral genome (10). In insects, dsRNA is targeted by the Dicer enzyme (Dcr-2) and cleaved into 21 nucleotide (nt) siRNAs, also known as viRNAs (10,11). In *Drosophila*, viRNAs are integrated into the Argonaute-2 protein (Ago-2) containing RNA-induced silencing complex, unwound and one strand of the viRNA is retained by Ago-2 to guide degradation of complementary (viral) RNA (14). Other Ago and Dcr proteins, i.e. Dcr-1 and Ago-1, are involved in the microRNA (miRNA) pathway (10–11,14).

Following treatment with gene-specific dsRNA or siRNAs, ticks and tick cell cultures can induce sequence-specific RNAi of endogenous genes (15) and restrict viral infections (16–18). Sequence analysis has also identified putative Ago and Dcr genes in the *I. scapularis* genome (19). However, it is not known if these are transcribed and involved in tick antiviral RNAi responses. All studied insect specific viruses and plant-infecting viruses have been shown to express RNA silencing suppressor (RSS) proteins which interfere with the RNAi response (20). No RSS proteins have been identified for arboviruses although evasion strategies have been suggested for the alphavirus Semliki Forest virus (SFV) (21), and the production of a subgenomic flavivirus RNA (sfRNA) interfering with the RNAi response was reported for mosquito-borne flaviviruses (22).

In this study, we identify and characterize key RNAi players of the Ago family that interfere with LGTV replication and describe characteristics of viRNAs in tick vector cells, which are different to viRNAs in mosquitoes. We also demonstrate that the recently described RSS activity of mosquito-borne flavivirus sfRNA can be broadened to tick-borne LGTV and TBEV sfRNA. The results imply that the antiviral RNAi system in ticks is more complex and has important differences to that of mosquitoes.

MATERIALS AND METHODS

Viruses and plasmids

The LGTV replicon (E5repRluc2B/3) was derived from the infectious cDNA of LGTV E5 (4). Modifications in the LGTV replicon were based on the previously described replicon construct for TBEV Neudoerfl strain (23). This construct encodes the first 17 residues of capsid, followed by the Rluc gene, the last 27 residues of the envelope and all non-structural proteins, as described in Supplementary Data. For infections of tick cells, LGTV strain TP21 was used.

Invertebrate expression vectors, pIZ-Fluc, pAcIE1-Rluc and pIB-MBP-HDVr have been described previously (22). The 3′UTRs of LGTV and TBEV were amplified by polymerase chain reaction (PCR) using, respectively, E5repRluc2B/3 or pTNd/ΔME (24) as templates. Invertebrate expression plasmids were obtained by fusing the 3′ terminus to the HDVr sequence from a WNV 3′UTR expression construct (22) using PCR. The resulting products were cloned into pDonor207 and pIB-GW plasmids (Invitrogen) using Gateway technology.

Luciferase assays

Luciferase activities were determined using a Dual Luciferase assay kit (Promega) in a GloMax multi-luminometer following cell lysis in Passive Lysis Buffer.

Cell culture, transfection and infection

BHK-21 cells were grown in GMEM at 37°C as previously described (25). Cells (3×10^5/well) were seeded in a 6-well plate prior to transfection with Lipofectamine2000 (Invitrogen) according to the manufacture's protocol. The *I. scapularis*-derived IDE8 cells were grown in L-15B medium (26) at 32°C in ambient air as previously described (27). Cells (6.5×10^5/well) were seeded in 24-well plates prior to transfection. Transient RNAi suppression assays were performed by transfecting 200 ng pIZ-Fluc, 300 ng pAcIE1-Rluc and 500 ng pIB-MBP-HDVr, TBEV 3′UTR or LGTV 3′UTR into IDE8 cells using Genejammer (Agilent) following the manufacturer's instructions. Silencing of reporter genes was induced at 24 h post-transfection (hpt) through addition of 280 ng dsRNA to the cell culture medium; luciferase was measured 48 hpt.

In case of studies involving replicon, putative RNAi genes were silenced by the addition of 300 ng dsRNA to cell culture medium at 6 and 30 h post-seeding (hps). Then, capped *in vitro*-transcribed E5repRluc2B/3 was transfected 48 hps using Lipofectamine2000 according to the manufacturer's instructions. Luciferase expression was measured 24 hpt.

For infection assays, target genes were first silenced by transfection of 100 ng dsRNA using Lipofectamine2000, followed by LGTV TP21 infection at 24 hpt at a multiplicity of infection (MOI) of 0.1. RNA was isolated at 48 h post infection (hpi) by Trizol.

Statistical analysis

The relative luciferase expression (RL) was calculated as:

$$RL_i = I_{Fluc,i}/I_{Rluc,i}$$

Where I is the measured intensity and *i* is the sample. To cancel out construct specific effects, values under treatment (for example co-transfected with dsFFluc) were normalized

against the same construct that was treated with a negative control (in this example dseGFP). Thus:

$$NRL_x = RL_{i,\text{treated}} / RL_{i,\text{neg.control}}$$

Experiments were performed in duplicate or in triplicate and repeated independently at least three times. The independent experiments were averaged:

$$\overline{NRL} = \sum_{x}^{n} \frac{NRL_x}{n}$$

Where x is the xth experiment and n is the total number of experiments.

The significances were calculated using custom-written scripts in R (www.r-project.org). In case of pairwise testing a two-sample independent t-test was performed, as provided by R.

Multiple testing was done by applying Tukey's HSD (also known as Tukey's range test), the q-value was calculated and compared to the indexed q in the studentized range distribution available in R. Significant differences ($P \leq 0.05$) are indicated in the graphs with an *.

Small RNA isolation and deep sequencing analysis

1.5×10^6 cells per tube were either transfected with 1 µg of eGFP-derived dsRNA, capped *in vitro*-transcribed E5repRluc2B/3 RNA, infected with LGTV TP21 (MOI 10) or untreated. At 48 hpt or 72 hpi, RNA was isolated using 1 ml Trizol (Invitrogen) per tube, small RNAs of 18–30 nt were sequenced and analyzed using viRome as previously described (28,29). Small RNA data was submitted to the European Nucleotide Archive (accession number ERP006219).

Reverse transcription and PCR

RNA was isolated by Trizol, following the manufacturer's protocol. Total RNA (500 ng for untreated/dsRNA-treated cells as well as knockdowns followed by LGTV infection or 5 µg LGTV antigenome detection) was reverse transcribed with Superscript III (Invitrogen) and using either oligo dT primers (knockdowns), an antigenome specific primer (LGTV antigenome detection) or random hexamers (LGTV infection) following the manufacturer's instructions. For the detection and amplification of Ago and Dcr transcripts, PCR was carried out using 2 µl of the cDNA reaction with corresponding primers (Table 1). The eGFP-derived PCR product was produced using eGFP-C1 (Clontech) as template. In case of LGTV antigenome detection, two rounds of PCR were performed using LGTV specific primers. PCR products were gel-purified, cloned into the pJet blunt1.2 vector (Fermentas) and sequenced.

LGTV RNA was determined by QRT-PCR with NS5 specific primers using the Fast SYBR Green PCR Master Mix (Life Technologies) according to manufacturer's instructions. Previously described actin primers were used as housekeeping genes (16).
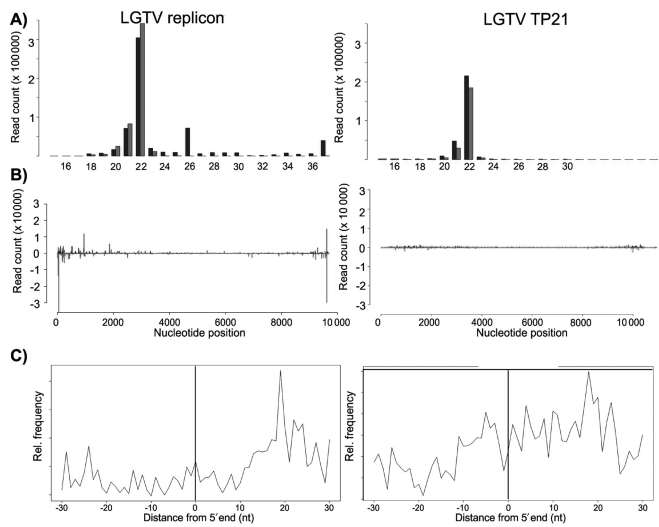
Figure 1. Characterization of exogenous-derived small RNAs in IDE8 cells. (**A**) Size distribution of small RNA molecules mapping either to LGTV E5repRluc2B/3 replicon (left panel) at 48 hpt or LGTV TP21 (right panel) at 72 hpi in IDE8 cells. (**B**) Frequency distribution of 22 nt small RNA molecules mapped to the E5repRluc 2B/3 replicon (5′UTR to 3′UTR) (left panel) or LGTV TP21 (right panel). The y-axis shows the frequency of the 22 nt siRNAs mapping to the corresponding nucleotide position in the x-axis. Positive numbers and dark gray peaks represent the frequency of siRNAs mapping to the genome (in 5′-3′ orientation) and light gray peaks/negative numbers to the antigenome (in 3′-5′ orientation). See also Supplementary Figure S2. (**C**) Frequency map of 22 nt small RNAs mapping to the opposite strand of the LGTV replicon (left panel) or LGTV TP21 (right panel).

In vitro transcription and dsRNA production

E5repRluc2B/3 was linearized by EcoRV and *in vitro*-transcribed using a SP6 Megascript kit (Ambion) in the presence of cap analogue according to the manufacturer's protocol. dsRNA was produced with the RNAi Megascript kit (Ambion) from PCR products flanked by T7 promoter sequences.

Phylogenetic analysis

To place the *Ixodes* sequences within gene trees, representative sequences were downloaded from Genbank (see Supplementary Figure S5 for sequence identifiers) for selected arthropods (waterfleas, copepods, lice, ticks, centipedes, flies, butterflies, beetles and wasps) and deuterostomes (sea squirt, human, chicken and zebrafish) that have sufficient complete genomes and/or transcriptomes. Ago and Piwi were aligned with translational MAFFT (30) and poorly-aligned regions were removed manually, resulting in an aligned matrix of 2349 positions for Ago and 2241 positions for Piwi. Due to a higher level of sequence divergence and higher proporation of incomplete orthologus sequences, Dicer was aligned under a codon model using PRANK (31), and then GBLOCKs (32) was used to exclude regions of poor alignment, resulting in an aligned matrix of 810 positions. Gene trees were inferred with Mr-Bayes (33) using unlinked General Time Reversible models with Gamma-distributed rate variation for each of the three codon positions. Two parallel MCMC chains of >25 mil-

38

Table 1. List of primer sequences used

Gene	Upstream/downstream primer sequences (5′-3′)
Ago-68	*gtaatacgactcactataggg*CGAGACTTTCAGAGCGTG/ *gtaatacgactcactataggg* GTTGGTGTACTTCGCCAT
Ago-30	*gtaatacgactcactataggg*ACATACGAGCACTGACGG/ *gtaatacgactcactataggg*TGGTGCAACATTTTATCGA
Ago-30–2	*gtaatacgactcactataggg*GAACGCCAAAAAGATCCCA/ *gtaatacgactcactataggg*CCGGTACCATCCTCATTTCT
Ago-16	*gtaatacgactcactataggg*AAGATCACGAGGGTATCGGTAGT/ *gtaatacgactcactataggg*ACTTTTCTGCACCACGTCTTG
Ago-16-2 (RT-PCR detection)	*gtaatacgactcactataggg*CGTTATGAAGGGTGATCAGAAG/ *gtaatacgactcactataggg*GACTGGTACTGATTCTCCCA
Ago-96	*gtaatacgactcactataggg*ATGCCTGCTCGGACATCTAC/ *gtaata cgactcactataggg*TCGAGTGAACGTCCAAATTCT
Ago-78	*gtaatacgactcactataggg*GAGGTGAAGCGTGTGGGG/ *gtaatacga ctcactataggg*GATGGAAGGCTTCTTGTTGTC
Dcr-90	*gtaatacgactcactataggg*ATCCTCAAGGAGTACAAGCC/ *gtaata cgactcactataggg*ACAGAGCATTAGGGTCGTC
Dcr-98	*gtaatacgactcactataggg*ATCCCGTCTTTCCCGATCTT/ *gtaatacgactcactataggg* TGCATCACAGGTGCCAGG
eGFP	*gtaatacgactcactataggg*GGCGTGCAGTGCTTCAGCCGC/ *gtaatacgactcactataggg* GTGGTTGTCGGGCAGCAGCAC
Firefly luciferase	*gtaatacgactcactataggg*ATGGAAGCAGCCAAAAAC/ *gtaatacgactcactataggg* TTACACGGCGATCTTTCC
LGTV antigenome RT-PCR	aattccacccatgaaatgtac
LGTV NS5 (QT-PCR)	acccaagactgctacgtgtggaaa/tgaggaagtaaagggccttgctga

T7 promoter region is indicated in italics.
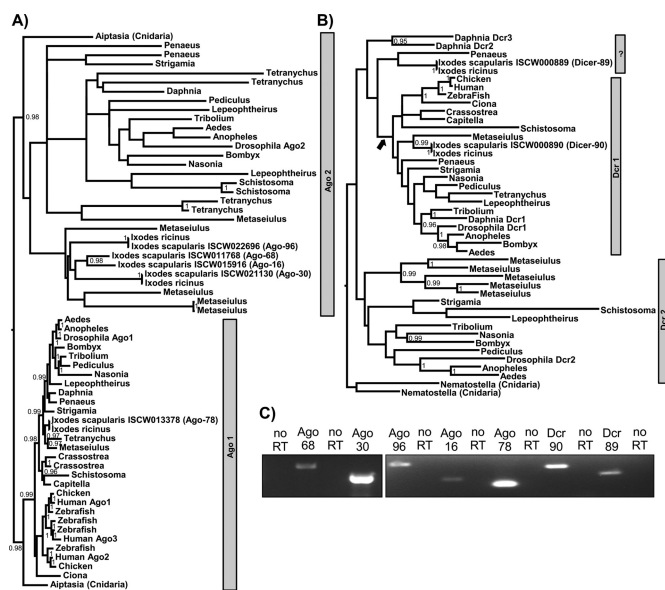
Figure 2. Analysis of Ago and Dcr protein-encoding genes in the *Ixodes scapularis* genome. (**A**) and (**B**) are gene trees for metazoan Ago-subfamily genes (**A**) and Dcr genes (**B**) respectively, constructed using a Bayesian approach under a GTR model (nodes are labeled if they receive >90% support; see Materials and Methods). Trees are unrooted, but presented as if the root fell between the two Cnidarian homologs. (**C**) Detection of transcripts encoding Ago and Dcr proteins in IDE8 cells by RT-PCR. RNA not treated with reverse transcriptase was used as control during the PCR reaction (no RT). See also Supplementary Figure S5.

lion steps were run for each tree (sampling every 1000 steps) and the first 25% of steps were discarded as burn-in. Stationarity was inferred by comparing parallel runs and inspection of the chains for each parameter: Potential Scale Reduction Factors approached 1.000, the variation in split frequencies was <0.01, and effective sample sizes were >1000 for all parameters. The trees presented in Figure 2 and Supplementary Figure S5 are maximum clade credibility trees, with branch lengths proportional to the number of substitutions. Only partitions with >90% Bayesian Posterior support are labeled.

RNA structure predictions

Consensus RNA structures were predicted using the LocARNA web server (Vienna RNA web server 1.8.2) (34) with standard settings. Pseudoknots were identified manually. Thermodynamic stability was calculated by folding an individual sequence with RNAfold (Vienna RNA web server 1.8.2), using a secondary structure constraint and standard settings.

Northern blot analysis

Northern blot analysis was performed by loading 4.5 µg or 3 µg of total RNA of BHK-21 or tick cells, respectively, on a 1.5% agarose-2% formaldehyde MOPS gel and transferred to a nitrocellulose (Hybond-N+, GE Healthcare) membrane using 'top down' blotting with 20xSSC as transfer buffer. Transferred RNA was UV-crosslinked for 2 min. Hybridization was performed for 2 h in HybPerfect buffer (Sigma) at 63°C using DIG-labeled PCR product as probe (TBEV 3′UTR or LGTV 3′ UTR). Membranes were washed twice with 2xSSC + 0.1% SDS for 5 min, twice with 0.2xSSC + 0.1% SDS for 20 min at 63°C and DIG was detected using an anti-DIG antibody as described previously (35).

39

RESULTS

scapularis-derived-IDE8 cells mount RNAi responses against LGTV and TBEV

An uncharacterized RNAi response was shown to restrict mosquito-borne arbovirus infections in *I. scapularis*-derived ISE6 and IDE8 cells (16–18). It is not known if RNAi is induced in tick cells following infection with tickborne arboviruses. Production of viRNAs is an indicator of an antiviral RNAi response. An LGTV E5 strain replicon encoding the *Renilla* luciferase (Rluc) gene as a reporter (E5repRluc2B/3) was constructed to investigate antiviral RNAi in IDE8 cells (Supplementary Figure S1A). The ability to successfully transfect E5repRluc2B/3 RNA into IDE8 cells (77%) was determined, using either fluorescently labeled replicon RNA or immune-fluorescence detection of NS3, respectively (Supplementary Figure S6A). Following transfection with E5repRluc2B/3 RNA, IDE8 cells were lysed and Rluc expression determined at 24, 48, 72, 96 and 120 hpt. Expression was observed 24 hpt then decreased (Supplementary Figure S1C). Replication was verified by detection of LGTV antigenome (Supplementary Figure S1B). These results suggest that the LGTV replicon is inhibited by an induced antiviral response in IDE8 cells.

Previous work has documented the production of viRNAs in ISE6 cells; however, the sequences and their distribution on the virus genome are not known (17,18). The production of LGTV-specific viRNAs in IDE8 cells was therefore analyzed. At 48 hpt, total RNA was isolated and small RNAs sequenced; frequencies and LGTV genome location of small RNAs were determined (Table 2). 7.1% of the small RNA sequences mapped to the LGTV replicon sequence. viRNAs were predominantly 22 nt in length (59.6%) and mapped with similar frequency to the genome and antigenome (Figure 1A, left panel). viRNAs were scattered along the LGTV replicon genome/antigenome with variable frequency into hot spots/cold spots (21) (Figure 1B, left panel). The 5′ and 3′UTRs generated the highest viRNA frequencies (Figure 1B, left panel). Comparing the base composition of 22 nt viRNAs of hot spots versus cold spots showed a substantial bias away from G toward A at the 5′ end ($P < 0.0001$, Fishers exact test [FET]) and a bias away from A at the 3′ end ($P < 0.0001$, FET). Bias at other positions was found but none was particularly striking (Supplementary Figure S2A). The 5′ ends of the complementary LGTV specific 22 nt RNAs were most frequently separated by 20 nt (Figure 1C, left panel) suggesting generation from dsRNA of 20 nt with 2 nt overhangs. Experiments performed with a previously described TBEV replicon (23) (Supplementary Figure S2C) showed similar results regarding the predominance of 22 nt viRNAs and 5.9% of total small RNAs mapping to the TBEV replicon (Table 2), with similar frequency to the genome and antigenome. The 22 nt small RNAs mapping to TBEV, are scattered along the genome/-antigenome. Again the highest frequency of viRNAs was generated from the 5′ and 3′ UTRs (Supplementary Figure S2D). Experiments with IDE8 cells infected with LGTV TP21 showed the production of virus specific small RNAs sharing several of the characteristics of LGTV replicon-derived viRNAs, although at a lower overall frequency (0.27% for virus and 7.12% for replicon (Table 2)). The majority of viRNAs were 22 nts in length, most frequently separated by 20 nts and the highest viRNA frequencies were generated from and around the 5′ and 3′ ends of the viral genome/antigenome (Figure 1, right panels and Table 2).

The length of small RNAs in IDE8 cells is a host property

Recent studies have shown that insect viRNAs are generally 21 nt in length, in contrast to nematode *Caenorhabditis elegans* viRNAs of predominantly 22 or 23 nt depending on the virus (21,28,36–47). To determine whether generation of 22 nt as the dominant viRNA length was a property of the cells or the virus, an eGFP-derived dsRNA was transfected into IDE8 cells and small RNAs analyzed. Again, 22 nt was the dominant length (Supplementary Figure S2E) and small RNAs mapped in hot/cold spots along the whole eGFP sequence and its complement (Supplementary Figure S2E).

We also analyzed viRNAs targeting the dsRNA orbivirus St. Croix River virus (SCRV) (48,49), which persistently infects IDE8 cells (Table 2). Again, the majority of SCRV viRNAs were 22 nt, with similar frequencies being detected on the (+) and the (–) strand (Supplementary Figure S3).

To determine the properties of endogenous small RNA molecules such as miRNAs, endogenous siRNAs and PIWI-interacting (pi)RNAs (10) in IDE8 cells, the small RNA profiles from uninfected and treated (eGFP dsRNA and LGTV replicon) IDE8 cells were analyzed. Small RNAs mapping to the *I. scapularis* genome (https://www.vectorbase.org) had a predominant length of 22 nt (44.4%) in all samples, with slightly higher frequencies for the sense orientation. Moreover, a class of small RNA molecules of 27 to 29 nt was identified with a peak at 28 nt (27 nt: 6.7%, 28 nt: 10.1% and 29 nt: 5%) as strongly represented as 21 nt small RNAs (12.5%) (Supplementary Figure S4). This indicates that 22 nt is the dominant length of small RNAs (endogenous or viral) in IDE8 cells.

Identification of Dcr and Ago proteins involved in antiviral RNAi in tick cells

Ago-2 and Dcr-2 proteins are key effectors in the insect antiviral RNAi pathway (10,50). Dcr-1 and Ago-1 are known to be important for the insect miRNA pathway (10,14). Previous sequence analysis has shown that the *I. scapularis* genome contains at least one putative Dcr gene, Dcr-89 (ISCW000889) and two putative Ago subfamily genes; Ago-68 (ISCW011768), Ago-30 (ISCW0021130) (19). In the present study, Basic Local Alignment Search Tool (BLAST) similarity searches with Dcr (Dcr-1 and Dcr-2) and Ago subfamily genes (Ago-1 and Ago-2) of *Drosophila melanogaster* and *Aedes aegypti* were performed to identify further putative homologs in the *I. scapularis* genome. Three additional putative Ago subfamily genes; Ago-96 (ISCW022696), Ago-16 (ISCW015916), Ago-78 (ISCW013378) and another putative Dcr gene, Dcr-90 (ISCW0008890) were identified.

To understand the function of *Ixodes* Ago and Dcr proteins within the wider context of their evolution, gene trees were constructed using a Bayesian approach (Figure 2A and

40

Table 2. Number of small RNA reads

	Langat virus replicon	St. Croix River virus	Langat virus TP21	TBEV replicon	TBEV NS5 GAA replicon
Genome/coding strand reads	719782	1462846	294390	3906753	3153338
Anti-genome/coding strand reads	553286	1242195	227753	3606509	2921677
Total viral reads	1273068	2705041	522143	7513262	6075015
Reads in total	17875799	18806256	190908946	127799016	127066875

Indicated are read numbers of small RNAs mapping to the genomes and antigenomes of St. Croix River virus, Langat virus replicon, Langat virus TP21 and TBEV replicons.

B; Supplementary Figure S5). The last common ancestor of each of these gene families probably pre-dates the origin of the animals (51), so that saturation and long-branch artifacts make reliable tree inference extremely challenging. Rooting the Ago tree between the two cnidarian paralogs identified two well-supported clades: the slowly evolving clade homologous to drosophila Ago-1 (miRNA pathway) and the rapidly evolving clade homologous to drosophila Ago-2 (siRNA pathway). The Ago-1 clade exactly mirrors the known phylogeny of the species, and clearly identifies *Ixodes* Ago-78 as an ortholog of drosophila Ago-1. The other four *Ixodes* Ago (-96, -68, -16, -30) then appear as more recent Ago-2 paralogs that have evolved since the last common ancestor of *Arachnida* and Pancrustacea, although a lack of support within this clade makes it hard to draw conclusions beyond this. The Dcr gene-tree also lacks support, and when similarly rooted using the cnidarian paralogs results in a pattern that is hard to interpret. With this rooting, *Ixodes* Dcr-90 clusters with other arachnid Dicers basal to an arthropod clade that includes drosophila Dcr-1, suggesting that Dcr-90 is a Dcr-1 homologue. However, the basal position of *Ixodes* Dcr-89 and the remaining crustacean Dicers is difficult to reconcile with the known organismal phylogeny. If the divergent Cnidarian outgroup is excluded, then an alternative rooting immediately basal to the deuterostome/arthropod Dcr-1 clade (marked by a black arrow in Figure 2B) would place Dcr-89 and the remaining Crustacean Dcrs as the most basally-branching arthropod Dcr-2, consistent with the species phylogeny and suggesting it is homologous to drosophila Dcr-2. Transcription of putative Ago and Dcr genes was verified in IDE8 cells (Figure 2C).

In order to investigate mediators of antiviral activity in IDE8 cells, transcripts of individual Dcr or Ago genes were knocked down by RNAi as previously described (16) and the effect on the LGTV replicon determined. Efficiency of knockdown/silencing of cells treated with dsRNA specific for Ago (Ago-68, Ago-30, Ago-16, Ago-96 and Ago-78) and Dcr (Dcr-90 and Dcr-89) genes was determined by semi-quantitative RT-PCR and quantified in relation to control dsRNA using 16S as loading control (Figure 3). Cells treated with dsRNA against Ago-68, Ago-30, Ago-96, Ago-16, Ago-78 or Dcr-90 showed reduction in target transcript levels (9–40%). No significant reduction of Dcr-89 transcript was observed, due to a high variability between samples (Figure 3).

Following successful individual knockdowns of most putative RNAi genes, the experiment was repeated, LGTV
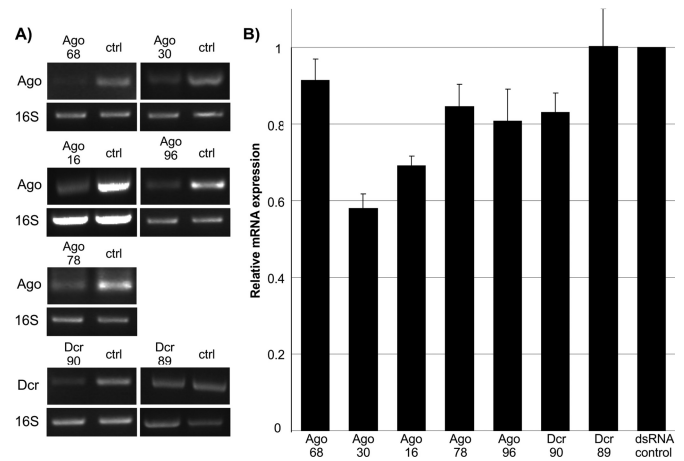
Figure 3. Knockdown of transcripts encoding Ago or Dcr proteins. (**A**) dsRNA-based silencing of Ago and Dcr encoding transcripts in IDE8 cells. Transcripts were detected by RT-PCR using gene-specific primers. A PCR product of 16S ribosomal RNA was used as housekeeping gene and eGFP specific dsRNA treated cells as control (crtl). (**B**) mRNA knockdowns quantification by Image J software, using 16S as control. The relative mean (normalized to eGFP-dsRNA controls) with standard error is shown for at least 10 repeats.

replicon RNA was transfected into silenced IDE8 cells and replicon-mediated Rluc activities determined. Significant increases in replicon Rluc activity were observed in IDE8 cells treated with dsRNA specific for Ago-30, Ago-16 and Dcr-90, compared to control dsRNA (Figure 4A). No significant increase of Rluc was observed following Ago-68, -78, -96 and Dcr-89 knockdowns. To ensure that the observed effect was not due to off target effects, the Ago-30 knockdown was repeated with an additional Ago-30 specific dsRNA molecule (Ago30–2); this resulted in a similar increase of luciferase activity thus confirming previous results (Supplementary Figure S6B). Similar experiments were also performed with silenced IDE8 cells and the effect on LGTV infection (MOI 0.1) at 48 hpi was determined by QRT-PCR. Significant increases in LGTV RNA levels were observed in cells treated with dsRNA specific for Ago-68, -30, -16 and Dcr-89, although Dcr-89 resulted only in a small increase (Figure 4B).

Targeting of the same cells by dsRNA and LGTV replicon or LGTV infection was established, using fluorescently labeled dsRNA and immunostaining of LGTV NS3 or E protein (Supplementary Figure S6A). In summary, tick

41
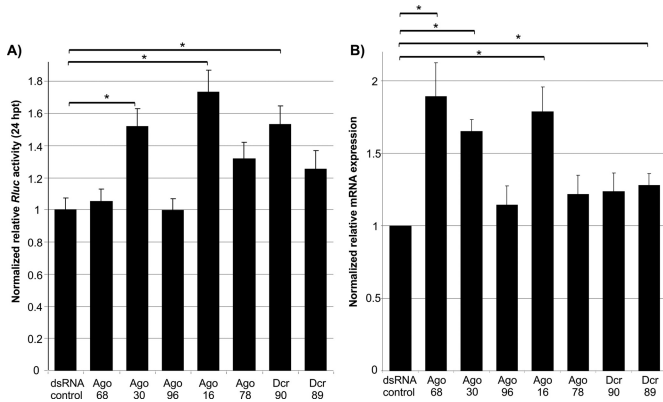
Figure 4. Effects of Ago and Dcr knockdowns on LGTV replication. (**A**) Ago or Dcr silenced cells were transfected with capped *in vitro-* transcribed LGTV E5repRluc2B/3 replicon RNA, and Rluc activity was determined at 24 hpt. The mean with standard error is shown for three independent experiments performed in duplicate (two experiments)/triplicate (one experiment). The data were normalized to cells treated with eGFP-specific control dsRNA. * indicate significance by Tukey's HSD ($P \leq 0.05$). (**B**) Silenced cells were infected with Langat virus (MOI 0.1) and viral RNA was determined by QRT-PCR at 48 hpi, using actin as housekeeping gene internal standard. The mean with standard error is shown for three independent experiments performed in triplicate. The data were normalized to cells treated with eGFP-specific control dsRNA. * indicate significance by Student *t*-test ($P \leq 0.05$).

Ago-30 and Ago-16 mediate antiviral activity against both LGTV and its replicon.

Tick-borne subgenomic flavivirus (sf)RNA interferes with antiviral RNAi

sfRNA is derived from the flavivirus 3′UTR, produced in vertebrate and invertebrate cells by mosquito and tick borne-flaviviruses and contains a complex RNA structure (52–54). West Nile virus (WNV) and dengue virus (DENV) sfRNAs both interfere with RNAi (22).

Production of sfRNA and suppression of RNAi by both LGTV and TBEV was investigated. The 3′UTRs of flaviviruses share common characteristics in their RNA architecture (55). It has been demonstrated that mosquito-borne flaviviruses share an RNA stem loop structure (called SL II) toward the 5′ end of the 3′UTR which has similarities to SL IV of the 3′UTR and is important for sfRNA production (52–54). RNA folding predictions of the 3′UTR of tick-borne flaviviruses showed RNA structures with folds highly similar to SL II and SL IV (respectively named SL 2 and SL 1 in the tick-borne viruses) for most tick-borne flaviviruses, despite sequence differences to mosquito-borne flavivirus 3′UTRs (Supplementary Figure S7).

To determine if the predicted LGTV and TBEV RNA stem loop structures (Figure 5A and Supplementary Figure S7) give rise to sfRNAs, vertebrate and tick cells were infected with LGTV (56) or transfected with TBEV replicon (24). Northern blot analysis detected TBEV and LGTV RNA at the expected size of ∼0.4 kb (predicted SL 2, LGTV: −447 nt; TBEV: −453 nt) (Figure 5A and B). In addition, similar to WNV a lower band was observed. This may be due to the presence and characteristics of two SL
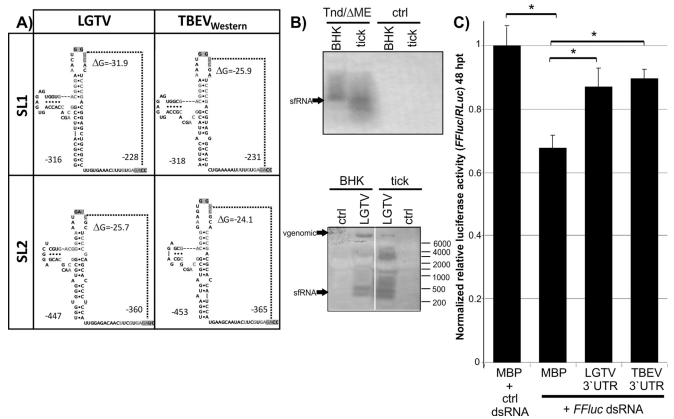
Figure 5. Analysis of subgenomic flavivirus (sf)RNA in the 3′UTR of tick-borne flaviviruses. (**A**) Structure model of SL 2 and SL 1 RNA stem loop structures of TBEV and LGTV. (**B**) Expression of TBEV (TND/ΔME) (top) and LGTV (bottom) sfRNA in replicon (top), non-transfected (control CTRL) or infected cells (bottom) was detected by northern blot analysis with 3′UTR specific DIG-PCR probes. (**C**) The effect of sfRNA on RNAi in IDE8 cells was determined by co-transfection of *FFluc*, Rluc and expression constructs for MBP-HdVr (MBP), LGTV 3′UTR or TBEV 3′UTR. Silencing was induced 24 hpt following addition of dsRNA to the culture medium. At 48 hpt, relative luciferase activity (*FFluc*/Rluc) was determined and normalized to cells treated with eGFP specific (ctrl) dsRNA. The luciferase expression level measured with MBP-HdVr was set at 1.0. The mean with standard error is shown for three independent experiments performed in duplicate (one experiment)/triplicate (two experiments). ∗ indicate significance by Tukey's HSD ($P \leq 0.05$). See also Supplementary Figure S7.

structures [SL 1 and 2]. Moreover, there are differences between arthropod and vertebrate cells (Figure 5B) (52,53).

The RSS activity of these sfRNAs was investigated next, after establishing successful plasmid transfections in IDE8 cells (Supplementary Figure S6A). IDE8 cells were co-transfected with plasmids encoding Firefly luciferase (*FFluc*; reporter gene), Rluc (internal control), and plasmids expressing LGTV or TBEV 3′UTRs. Maltose binding protein (MBP) sequence fused to the hepatitis delta virus ribozyme (HDVr) was used as negative control RNA as the 3′UTRs plasmids also contain an HDVr. Subsequently, silencing was induced by either *FFluc*-specific (ds*FFluc*) or control (eGFP) dsRNA and luciferase activity determined. Reduced silencing was observed in cells expressing 3′UTR constructs compared to MBP-HDVr (Figure 5C). These results indicate that the 3′UTRs of LGTV and TBEV are able to interfere with the tick siRNA pathway.

DISCUSSION

RNAi is known to be a major defense mechanism against arboviruses in mosquitoes (10,11). Much less is known about ticks. Here, we investigated the antiviral RNAi response in *I. scapularis*-derived cells and viral counter-defense strategies. Our analysis reveals tick Ago and Dcr genes additional to those previously described (19). A significant gene expansion in the Ago subfamily has occurred in arachnids, compared to insects such as *D. melanogaster* and *A. aegypti*. Our results characterize key differences between *Ixodes* and mosquito RNAi responses. The antiviral activity of Ago-30, Ago-16 and Ago-68 (in case of vi-

ral infection) is in line with previous reports showing that mosquito/fly Ago-2 is involved in the antiviral RNAi response and phylogenetic analysis indicates that *Ixodes* Ago-30, Ago16 and Ago-68 are homologous to Ago-2 of insects (57,58). The expansion of putative Ago-2 paralogs in arachnids is different from other arthropods, which generally have one, or at most two, Ago-2 homologs. In contrast to Ago-16 and Ago-30, Ago-68 only shows antiviral activity in case of virus infection, which may suggests its involvement in limiting virus spread by pre-priming yet uninfected cells using systemic RNA silencing. Like mosquitoes, ticks appear to have undergone an expansion of the Piwi clade (Supplementary Figure S5C), though the expansion is smaller and occurred independently, in addition to a possible loss of Ago-3. We show that Dcr-90 is involved in antiviral RNAi against replicon in contrast to Dcr-89 showing significant antiviral activity in case of virus. However, failure of consistent/ efficient knockdown of Dcr-89 between experimental approaches and the borderline increase/significance of Dcr knockdowns on virus infection leaves it open whether or not a second Dcr protein is involved and if there are differences between effects of Dcr knockdowns on replicon and virus. Phylogenetic analysis, dependent on the rooting, maps Dcr-89 in a cluster with Dcr-2 proteins in insects. Dcr-2 is critical for the exogenous antiviral siRNA pathway in *Drosophila*, and presents a limiting factor for sufficient knockdown involving exogenous RNAi (using dsRNA) in this organism (14). Dcr-89 could act in a similar way in ticks, which may explain the lack of consistent knockdown. Dcr-90 showed an antiviral effect in IDE8 cells despite clustering with Dcr-1 proteins which have not yet been reported as antiviral in flies or mosquitoes. It cannot be excluded that potential antiviral functions of some Ago/Dcr proteins we describe here may have been missed due to inefficient knockdown of the transcript; however our results already show that mechanisms in ticks may differ in detail from those present in insects.

A key feature of antiviral RNAi in mosquitoes is the production of 21 nt viRNA molecules (10,11). The majority of viRNAs in IDE8 cells are 22 nt in length [as reported for viRNAs of the positive strand nodavirus in *C. elegans* (45,46)]. The same observation was made if an RNAi response was artificially induced by dsRNA. As the length of the siRNAs or viRNAs is mostly dependent on the Dcr enzyme, this indicates a key difference between *I. scapularis* and insect Dcr proteins. In insects, miRNA molecules differ from siRNA molecules (22 versus 21 nt) as they are mostly produced by Dcr-1. The antiviral effect of Dcr-90, which clusters with insect Dcr-1 proteins, and the production of 22 nt viRNAs points to differences between the antiviral RNAi pathways in *I. scapularis* and insects. Small RNAs of 22 nt were also found to be the major class of small RNA molecules that map to the genome of *I. scapularis*.

Little is known about the dsRNA substrate for Dcr-2 and the origin of viRNAs. Findings by us and others suggest that dsRNA replicative intermediates are Dcr-2 substrates in mosquitoes and derived cell lines and show that hot and cold spots of viRNAs are present along arbovirus genomes/antigenomes (21,38,40–43). This is in agreement with our results for SCRV and transfected dsRNA. In contrast, LGTV viRNAs map at highest frequencies to or

around the 5′ and 3′ termini. In contrast, similar regions present in DENV and WNV are not particularly targeted by the RNAi machinery in mosquitoes (41–43). It has to be mentioned that recent work has shown that certain hot and cold spot observations are due to cloning bias of the small RNAs (59,60). The presence of small RNAs mapping to the non-coding strand of SCRV with a similar frequency as to the coding strand, supports the dsRNA genome as inducer molecule even with cloning bias. The same dsRNA-mediated induction may explain the bias of targeting the 5′ and 3′ genome termini of LGTV in IDE8 cells. A previously described replication-incompetent TBEV replicon (C17Fluc NS5 GAA) (23) behaved similar as the corresponding wild-type replicon in IDE8 cells with regards to luciferase production over time [in contrast to BHK where it shows reduction of luciferase production overtime as previously reported (23)] and production/ mapping of TBEV-specific small RNAs (Supplementary Figure S8 and Table 2). This suggests replication of the GAA mutant either by the viral replicase or other enzymes with complementing or replicative activity present in the IDE8 cells. Therefore such a mutant can unfortunately not be used to determine whether the observed TBEV-specific small RNAs are produced from incoming single stranded RNA, dsRNA replication intermediates or partial dsRNA.

Differences in the number of cells targeted by replicon or virus and the amount of virus/replicon RNA per cell could explain the difference in production of overall LGTV-specific small RNAs for replicon versus virus-infected IDE8 cells. Infection by full-length virus may also hide and limit the antiviral RNAi response in IDE8 cells more efficiently than replicon RNA which misses the coding sequences for structural proteins. Besides, the presence of structural proteins and nucleotide sequence (and thus changes in overall length of the viral RNA) may explain the observation that distribution of replicon viRNA versus virus shows some difference. Despite these differences though, LGTV viRNAs share common characteristics (bias for 22 nts viRNAs and targeting areas around the 5′ and 3′ genome termini) which are different to flavivirus-specific viRNAs reported in mosquitoes (41–43).

The detection of LGTV-specific viRNAs indicates the ability of the RNAi response to target the virus, raising the question: how can the virus still replicate in tick cells? Plant and 'true insect' viruses encode RSS proteins that interfere with the antiviral RNAi to allow successful viral infection (14,61). No arbovirus RSS protein is known, but an evasion strategy has been suggested for the alphavirus SFV (21) and the sfRNA molecules of mosquito-borne viruses interfere with RNAi responses (22). The 3′UTRs of tick- and mosquito-borne flaviviruses do not share high similarity at the nucleotide level and exchanging these sequences mostly leads to replication-deficient viruses (62–64). Despite this, bioinformatic modeling suggested a highly similar secondary RNA structure profile in the 3′ UTR of arthropod-borne flaviviruses, production and interference with the RNAi response was shown of TBEV and LGTV. WNV sfRNA is believed to mediate RSS activity by acting as a competitive substrate for Dcr (22). In contrast to WNV and DENV UTRs that do not appear to be specif-

ically targeted by Dcr (41–43), the 3′ UTR of the LGTV and TBEV replicon in IDE8 cells appears to be a target for Dcr activities; along with the 5′ UTR it generates the highest frequency of viRNAs. The sfRNA RSS activity probably results in less powerful activity than the known protein-based RSS of insect viruses. Expression of an RSS protein by alphaviruses results in reduced mosquito survival (40,65). Using a weak suppressor such as sfRNA may allow for sufficient levels of replication needed for successful transmission.

Taken together, our findings define details of the tick antiviral RNAi response and its interference by tick-borne arboviruses. They show several important differences in antiviral RNAi between different classes of arbovirus vectors (*Arachnida* versus *Insecta*) and broaden our knowledge about arthropod antiviral RNAi.

ACCESSION NUMBERS

ERP006219.

SUPPLEMENTARY DATA

Supplementary Data are available at NAR Online.

ACKNOWLEDGMENT

FUNDING

REFERENCES

1. Gritsun,T.S., Nuttall,P.A. and Gould,E.A. (2003) Tick-borne flaviviruses. *Adv. Virus Res.*, **61**, 317–371.
2. Best,S.M., Morris,K.L., Shannon,J.G., Robertson,S.J., Mitzel,D.N., Park,G.S., Boer,E., Wolfinbarger,J.B. and Bloom,M.E. (2005) Inhibition of interferon-stimulated JAK-STAT signaling by a tick-borne flavivirus and identification of NS5 as an interferon antagonist. *J. Virol.*, **79**, 12828–12839.
3. Park,G.S., Morris,K.L., Hallett,R.G., Bloom,M.E. and Best,S.M. (2007) Identification of residues critical for the interferon antagonist function of Langat virus NS5 reveals a role for the RNA-dependent RNA polymerase domain. *J. Virol.*, **81**, 6936–6946.
4. Pletnev,A.G. (2001) Infectious cDNA clone of attenuated Langat tick-borne flavivirus (strain E5) and a 3′ deletion mutant constructed from it exhibit decreased neuroinvasiveness in immunodeficient mice. *Virology*, **282**, 288–300.
5. Lindenbach,B.D. and Rice,C.M. (2003) Molecular biology of flaviviruses. *Adv. Virus Res.*, **59**, 23–61.
6. Villordo,S.M. and Gamarnik,A.V. (2009) Genome cyclization as strategy for flavivirus RNA replication. *Virus Res.*, **139**, 230–239.
7. Gritsun,T.S. and Gould,E.A. (2007) Origin and evolution of flaviviruses 5′UTRs and panhandles: trans-terminal duplications? *Virology*, **366**, 8–15.
8. Gritsun,T.S. and Gould,E.A. (2007) Origin and evolution of 3′UTR of flaviviruses: long direct repeats as a basis for the formation of secondary structures and their significance for virus transmission. *Adv. Virus Res.*, **69**, 203–248.
9. Bell-Sakyi,L., Kohl,A., Bente,D.A. and Fazakerley,J.K. (2011) Tick cell lines for study of crimean-congo hemorrhagic fever virus and other arboviruses. Vector Borne Zoonotic Dis, **12**, 769–781.
10. Donald,C.L., Kohl,A. and Schnettler,E. (2012) New insights into control of arbovirus replication and spread by insect RNA interference pathways. *Insects*, **3**, 511–531.
11. Blair,C.D. (2011) Mosquito RNAi is the major innate immune pathway controlling arbovirus infection and transmission. *Future Microbiol.*, **6**, 265–277.
12. Fragkoudis,R., Attarzadeh-Yazdi,G., Nash,A.A., Fazakerley,J.K. and Kohl,A. (2009) Advances in dissecting mosquito innate immune responses to arbovirus infection. *J. Gen. Virol.*, **90**, 2061–2072.
13. Charrel,R.N., Attoui,H., Butenko,A.M., Clegg,J.C., Deubel,V., Frolova,T.V., Gould,E.A., Gritsun,T.S., Heinz,F.X., Labuda,M. *et al.* (2004) Tick-borne virus diseases of human interest in Europe. *Clin. Microbiol. Infect.*, **10**, 1040–1055.
14. Kemp,C. and Imler,J.L. (2009) Antiviral immunity in drosophila. *Curr. Opin. Immunol.*, **21**, 3–9.
15. de la Fuente,J., Kocan,K.M., Almazan,C. and Blouin,E.F. (2007) RNA interference for the study and genetic manipulation of ticks. *Trends Parasitol.*, **23**, 427–433.
16. Barry,G., Alberdi,P., Schnettler,E., Weisheit,S., Kohl,A., Fazakerley,J.K. and Bell-Sakyi,L. (2013) Gene silencing in tick cell lines using small interfering or long double-stranded RNA. *Exp. Appl. Acarol.*, **59**, 319–338.
17. Garcia,S., Billecocq,A., Crance,J.M., Munderloh,U., Garin,D. and Bouloy,M. (2005) Nairovirus RNA sequences expressed by a Semliki Forest virus replicon induce RNA interference in tick cells. *J. Virol.*, **79**, 8942–8947.
18. Garcia,S., Billecocq,A., Crance,J.M., Prins,M., Garin,D. and Bouloy,M. (2006) Viral suppressors of RNA interference impair RNA silencing induced by a Semliki Forest virus replicon in tick cells. *J. Gen. Virol.*, **87**, 1985–1989.
19. Kurscheid,S., Lew-Tabor,A.E., Rodriguez Valle,M., Bruyeres,A.G., Doogan,V.J., Munderloh,U.G., Guerrero,F.D., Barrero,R.A. and Bellgard,M.I. (2009) Evidence of a tick RNAi pathway by comparative genomics and reverse genetics screen of targets with known loss-of-function phenotypes in Drosophila. *BMC Mol. Biol.*, **10**, 26.
20. Ding,S.W. (2010) RNA-based antiviral immunity. *Nat. Rev. Immunol.*, **10**, 632–644.
21. Siu,R.W., Fragkoudis,R., Simmonds,P., Donald,C.L., Chase-Topping,M.E., Barry,G., Attarzadeh-Yazdi,G., Rodriguez-Andres,J., Nash,A.A., Merits,A. *et al.* (2011) Antiviral RNA interference responses induced by Semliki Forest virus infection of mosquito cells: characterization, origin, and frequency-dependent functions of virus-derived small interfering RNAs. *J. Virol.*, **85**, 2907–2917.
22. Schnettler,E., Sterken,M.G., Leung,J.Y., Metz,S.W., Geertsema,C., Goldbach,R.W., Vlak,J.M., Kohl,A., Khromykh,A.A. and Pijlman,G.P. (2012) Noncoding flavivirus RNA displays RNA interference suppressor activity in insect and Mammalian cells. *J. Virol.*, **86**, 13486–13500.
23. Hoenninger,V.M., Rouha,H., Orlinger,K.K., Miorin,L., Marcello,A., Kofler,R.M. and Mandl,C.W. (2008) Analysis of the effects of

alterations in the tick-borne encephalitis virus 3′-noncoding region on translation and RNA replication using reporter replicons. *Virology*, **377**, 419–430.

24. Gehrke,R., Ecker,M., Aberle,S.W., Allison,S.L., Heinz,F.X. and Mandl,C.W. (2003) Incorporation of tick-borne encephalitis virus replicons into virus-like particles by a packaging cell line. *J. Virol.*, **77**, 8924–8933.

25. Varela,M., Schnettler,E., Caporale,M., Murgia,C., Barry,G., McFarlane,M., McGregor,E., Piras,I.M., Shaw,A., Lamm,C. *et al.* (2013) Schmallenberg virus pathogenesis, tropism and interaction with the innate immune system of the host. *PLoS Pathog.*, **9**, e1003133.

26. Munderloh,U.G. and Kurtti,T.J. (1989) Formulation of medium for tick cell culture. *Exp. Appl. Acarol.*, **7**, 219–229.

27. Bell-Sakyi,L. (2004) Ehrlichia ruminantium grows in cell lines from four ixodid tick genera. *J. Comp. Pathol.*, **130**, 285–293.

28. Schnettler,E., Ratinier,M., Watson,M., Shaw,A.E., McFarlane,M., Varela,M., Elliott,R.M., Palmarini,M. and Kohl,A. (2013) RNA interference targets arbovirus replication in culicoides cells. *J. Virol.*, **87**, 2441–2454.

29. Watson,M., Schnettler,E. and Kohl,A. (2013) viRome: an R package for the visualization and analysis of viral small RNA sequence datasets. *Bioinformatics*, **29**, 1902–1903.

30. Katoh,K., Misawa,K., Kuma,K. and Miyata,T. (2002) MAFFT: a novel method for rapid multiple sequence alignment based on fast Fourier transform. *Nucleic Acids Res.*, **30**, 3059–3066.

31. Loytynoja,A. and Goldman,N. (2010) webPRANK: a phylogeny-aware multiple sequence aligner with interactive alignment browser. *BMC Bioinformatics*, **11**, 579.

32. Talavera,G. and Castresana,J. (2007) Improvement of phylogenies after removing divergent and ambiguously aligned blocks from protein sequence alignments. *Syst. Biol.*, **56**, 564–577.

33. Ronquist,F., Teslenko,M., van der Mark,P., Ayres,D.L., Darling,A., Hohna,S., Larget,B., Liu,L., Suchard,M.A. and Huelsenbeck,J.P. (2012) MrBayes 3.2: efficient Bayesian phylogenetic inference and model choice across a large model space. *Syst. Biol.*, **61**, 539–542.

34. Will,S., Reiche,K., Hofacker,I.L., Stadler,P.F. and Backofen,R. (2007) Inferring noncoding RNA families and classes by means of genome-scale structure-based clustering. *PLoS Comput. Biol.*, **3**, e65.

35. Hemmes,H., Kaaij,L., Lohuis,D., Prins,M., Goldbach,R. and Schnettler,E. (2009) Binding of small interfering RNA molecules is crucial for RNA interference suppressor activity of rice hoja blanca virus NS3 in plants. *J. Gen. Virol.*, **90**, 1762–1766.

36. Campbell,C.L., Keene,K.M., Brackney,D.E., Olson,K.E., Blair,C.D., Wilusz,J. and Foy,B.D. (2008) Aedes aegypti uses RNA interference in defense against Sindbis virus infection. *BMC Microbiol.*, **8**, 47.

37. Flynt,A., Liu,N., Martin,R. and Lai,E.C. (2009) Dicing of viral replication intermediates during silencing of latent Drosophila viruses. *Proc. Natl. Acad. Sci. U.S.A.*, **106**, 5270–5275.

38. Morazzani,E.M., Wiley,M.R., Murreddu,M.G., Adelman,Z.N. and Myles,K.M. (2012) Production of virus-derived ping-pong-dependent piRNA-like small RNAs in the mosquito soma. *PLoS Pathog.*, **8**, e1002470.

39. Myles,K.M., Morazzani,E.M. and Adelman,Z.N. (2009) Origins of alphavirus-derived small RNAs in mosquitoes. *RNA Biol.*, **6**, 387–391.

40. Myles,K.M., Wiley,M.R., Morazzani,E.M. and Adelman,Z.N. (2008) Alphavirus-derived small RNAs modulate pathogenesis in disease vector mosquitoes. *Proc. Natl. Acad. Sci. U.S.A.*, **105**, 19938–19943.

41. Scott,J.C., Brackney,D.E., Campbell,C.L., Bondu-Hawkins,V., Hjelle,B., Ebel,G.D., Olson,K.E. and Blair,C.D. (2010) Comparison of dengue virus type 2-specific small RNAs from RNA interference-competent and -incompetent mosquito cells. *PLoS Negl. Trop. Dis.*, **4**, e848.

42. Brackney,D.E., Beane,J.E. and Ebel,G.D. (2009) RNAi targeting of West Nile virus in mosquito midguts promotes virus diversification. *PLoS Pathog.*, **5**, e1000502.

43. Brackney,D.E., Scott,J.C., Sagawa,F., Woodward,J.E., Miller,N.A., Schilkey,F.D., Mudge,J., Wilusz,J., Olson,K.E., Blair,C.D. *et al.* (2010) C6/36 Aedes albopictus cells have a dysfunctional antiviral RNA interference response. *PLoS. Negl. Trop. Dis.*, **4**, e856.

44. Ding,S.W. and Lu,R. (2011) Virus-derived siRNAs and piRNAs in immunity and pathogenesis. *Curr. Opin. Virol.*, **1**, 533–544.

45. Felix,M.A., Ashe,A., Piffaretti,J., Wu,G., Nuez,I., Belicard,T., Jiang,Y., Zhao,G., Franz,C.J., Goldstein,L.D. *et al.* (2011) Natural and experimental infection of Caenorhabditis nematodes by novel viruses related to nodaviruses. *PLoS Biol.*, **9**, e1000586.

46. Wu,Q., Luo,Y., Lu,R., Lau,N., Lai,E.C., Li,W.X. and Ding,S.W. (2010) Virus discovery by deep sequencing and assembly of virus-derived small silencing RNAs. *Proc. Natl. Acad. Sci. U.S.A*, **107**, 1606–1611.

47. Aliyari,R., Wu,Q., Li,H.W., Wang,X.H., Li,F., Green,L.D., Han,C.S., Li,W.X. and Ding,S.W. (2008) Mechanism of induction and suppression of antiviral immunity directed by virus-derived small RNAs in Drosophila. *Cell Host Microbe*, **4**, 387–397.

48. Alberdi,M.P., Dalby,M.J., Rodriguez-Andres,J., Fazakerley,J.K., Kohl,A. and Bell-Sakyi,L. (2012) Detection and identification of putative bacterial endosymbionts and endogenous viruses in tick cell lines. *Ticks Tick Borne Dis.*, **3**, 137–146.

49. Attoui,H., Stirling,J.M., Munderloh,U.G., Billoir,F., Brookes,S.M., Burroughs,J.N., de Micco,P., Mertens,P.P. and de Lamballerie,X. (2001) Complete sequence characterization of the genome of the St Croix River virus, a new orbivirus isolated from cells of Ixodes scapularis. *J. Gen. Virol.*, **82**, 795–804.

50. Aliyari,R. and Ding,S.W. (2009) RNA-based viral immunity initiated by the Dicer family of host immune receptors. *Immunol. Rev.*, **227**, 176–188.

51. Cerutti,H. and Casas-Mollano,J.A. (2006) On the origin and functions of RNA-mediated silencing: from protists to man. *Curr. Genet.*, **50**, 81–99.

52. Funk,A., Truong,K., Nagasaki,T., Torres,S., Floden,N., Balmori Melian,E., Edmonds,J., Dong,H., Shi,P.Y. and Khromykh,A.A. (2010) RNA structures required for production of subgenomic flavivirus RNA. *J. Virol.*, **84**, 11407–11417.

53. Pijlman,G.P., Funk,A., Kondratieva,N., Leung,J., Torres,S., van der Aa,L., Liu,W.J., Palmenberg,A.C., Shi,P.Y., Hall,R.A. *et al.* (2008) A highly structured, nuclease-resistant, noncoding RNA produced by flaviviruses is required for pathogenicity. *Cell Host Microbe*, **4**, 579–591.

54. Silva,P.A., Pereira,C.F., Dalebout,T.J., Spaan,W.J. and Bredenbeek,P.J. (2010) An RNA pseudoknot is required for production of yellow fever virus subgenomic RNA by the host nuclease XRN1. *J. Virol.*, **84**, 11395–11406.

55. Markoff,L. (2003) 5′- and 3′-noncoding regions in flavivirus RNA. *Adv. Virus Res.*, **59**, 177–228.

56. Mitzel,D.N., Best,S.M., Masnick,M.F., Porcella,S.F., Wolfinbarger,J.B. and Bloom,M.E. (2008) Identification of genetic determinants of a tick-borne flavivirus associated with host-specific adaptation and pathogenicity. *Virology*, **381**, 268–276.

57. Keene,K.M., Foy,B.D., Sanchez-Vargas,I., Beaty,B.J., Blair,C.D. and Olson,K.E. (2004) RNA interference acts as a natural antiviral response to O'nyong-nyong virus (Alphavirus; Togaviridae) infection of Anopheles gambiae. *Proc. Natl. Acad. Sci. U.S.A.*, **101**, 17240–17245.

58. van Rij,R.P., Saleh,M.C., Berry,B., Foo,C., Houk,A., Antoniewski,C. and Andino,R. (2006) The RNA silencing endonuclease Argonaute 2 mediates specific antiviral immunity in Drosophila melanogaster. *Genes Dev.*, **20**, 2985–2995.

59. Sorefan,K., Pais,H., Hall,A.E., Kozomara,A., Griffiths-Jones,S., Moulton,V. and Dalmay,T. (2012) Reducing ligation bias of small RNAs in libraries for next generation sequencing. *Silence*, **3**, 4.

60. Zhuang,F., Fuchs,R.T., Sun,Z., Zheng,Y. and Robb,G.B. (2012) Structural bias in T4 RNA ligase-mediated 3′-adapter ligation. *Nucleic Acids Res.*, **40**, e54.

61. Li,F. and Ding,S.W. (2006) Virus counterdefense: diverse strategies for evading the RNA-silencing immunity. *Annu. Rev. Microbiol.*, **60**, 503–531.

62. Friebe,P., Shi,P.Y. and Harris,E. (2011) The 5′ and 3′ downstream AUG region elements are required for mosquito-borne flavivirus RNA replication. *J. Virol.*, **85**, 1900–1905.

63. Romero,T.A., Tumban,E., Jun,J., Lott,W.B. and Hanley,K.A. (2006) Secondary structure of dengue virus type 4 3′ untranslated region: impact of deletion and substitution mutations. *J. Gen. Virol.*, **87**, 3291–3296.

64. Tumban,E., Mitzel,D.N., Maes,N.E., Hanson,C.T., Whitehead,S.S. and Hanley,K.A. (2011) Replacement of the 3′ untranslated variable

45

region of mosquito-borne dengue virus with that of tick-borne Langat virus does not alter vector specificity. *J. Gen. Virol.*, **92**, 841–848.

65. Cirimotich,C.M., Scott,J.C., Phillips,A.T., Geiss,B.J. and Olson,K.E. (2009) Suppression of RNA interference increases alphavirus replication and virus-associated mortality in Aedes aegypti mosquitoes. *BMC Microbiol.*, **9**, 49.

MANUSCRIPT 2

Weisheit, S., Villar, M., **Tykalová, H.**, Popara, M., Loecherbach, J., Watson, M., Růžek, D., Grubhoffer, L.; de la Fuente, J., Fazakerley, J.K., Bell-Sakyi, L. (2015). *Ixodes scapularis* and *Ixodes ricinus* tick cell lines respond to infection with tick-borne encephalitis virus: transcriptomic and proteomic analysis. Parasites & Vectors 8:599. DOI: 10.1186/s13071-015-1210-x

Parasites &Vectors

CrossMark

Ixodes scapularis and *Ixodes ricinus* tick cell lines respond to infection with tick-borne encephalitis virus: transcriptomic and proteomic analysis

Sabine Weisheit[1,2,7], Margarita Villar[3], Hana Tykalová[4], Marina Popara[3], Julia Loecherbach[1], Mick Watson[1], Daniel Růžek[4,5], Libor Grubhoffer[4], José de la Fuente[3,6], John K. Fazakerley[1,2] and Lesley Bell-Sakyi[2*]

Abstract

Background: Ixodid ticks are important vectors of a wide variety of viral, bacterial and protozoan pathogens of medical and veterinary importance. Although several studies have elucidated tick responses to bacteria, little is known about the tick response to viruses. To gain insight into the response of tick cells to flavivirus infection, the transcriptomes and proteomes of two *Ixodes* spp cell lines infected with the flavivirus tick-borne encephalitis virus (TBEV) were analysed.

Methods: RNA and proteins were isolated from the *Ixodes scapularis*-derived cell line IDE8 and the *Ixodes ricinus*-derived cell line IRE/CTVM19, mock-infected or infected with TBEV, on day 2 post-infection (p.i.) when virus production was increasing, and on day 6 p.i. when virus production was decreasing. RNA-Seq and mass spectrometric technologies were used to identify changes in abundance of, respectively, transcripts and proteins. Functional analyses were conducted on selected transcripts using RNA interference (RNAi) for gene knockdown in tick cells infected with the closely-related but less pathogenic flavivirus Langat virus (LGTV).

Results: Differential expression analysis using DESeq resulted in totals of 43 and 83 statistically significantly differentially-expressed transcripts in IDE8 and IRE/CTVM19 cells, respectively. Mass spectrometry detected 76 and 129 statistically significantly differentially-represented proteins in IDE8 and IRE/CTVM19 cells, respectively. Differentially-expressed transcripts and differentially-represented proteins included some that may be involved in innate immune and cell stress responses. Knockdown of the heat-shock proteins HSP90, HSP70 and gp96, the complement-associated protein Factor H and the protease trypsin resulted in increased LGTV replication and production in at least one tick cell line, indicating a possible antiviral role for these proteins. Knockdown of RNAi-associated proteins Argonaute and Dicer, which were included as positive controls, also resulted in increased LGTV replication and production in both cell lines, confirming their role in the antiviral RNAi pathway.

Conclusions: This systems biology approach identified several molecules that may be involved in the tick cell innate immune response against flaviviruses and highlighted that ticks, in common with other invertebrate species, have other antiviral responses in addition to RNAi.

Keywords: Tick, *Ixodes*, Flavivirus, Tick-borne encephalitis virus, Tick cell line, Innate immunity, Antiviral response

* Correspondence: lesley.sakyi@pirbright.ac.uk
[2]The Pirbright Institute, Ash Road, Pirbright, Surrey GU24 0NF, UK
Full list of author information is available at the end of the article

BioMed Central

Weisheit *et al. Parasites & Vectors* (2015) 8:599

Page 2 of 26

Background

Ticks are hematophagous ectoparasites that are second only to mosquitoes in their importance as vectors of viral, bacterial and protozoan pathogens that cause human disease, and they are probably the most important vectors of livestock disease worldwide [1].

Tick-borne encephalitis virus (TBEV), a member of the family *Flaviviridae*, is a medically-important virus transmitted by ticks. TBEV is one of the most important tick-borne viruses in Europe, Russia and many parts of Asia, causing tick-borne encephalitis in humans with an estimated annual number of disease cases >10,000 [2, 3]. The Western European subtype of TBEV is transmitted by *Ixodes ricinus* ticks in Central, Eastern and Northern Europe, whereas the Siberian and Far-Eastern subtypes are transmitted by *Ixodes persulcatus* ticks in Siberia, parts of Russia, Latvia and Finland and the latter subtype additionally in Central and Eastern Asia including China and Japan [4, 5]. Other tick species may also transmit TBEV under certain ecological conditions [5]; however it is not known if *Ixodes scapularis* ticks found in the United States, where TBEV does not occur, are capable of transmitting the virus.

Langat virus (LGTV), a close relative of TBEV, was isolated from *Ixodes granulatus* ticks in Malaysia [6]. Although the virus is antigenically closely related to TBEV, there are no reports of naturally-acquired cases of human disease caused by LGTV. The attenuated LGTV strain E5 was tested as a candidate live vaccine against TBEV in animals and human volunteers. It resulted in high levels of neutralising antibodies which cross-reacted with TBEV, Powassan virus and Kyasanur Forest disease virus [7, 8]. Due to its close antigenic relationship with TBEV, low pathogenicity and lack of naturally-occurring cases of disease in humans and animals, LGTV is a useful experimental model for more virulent tick-borne flavivirus infections.

Most knowledge of the response of arthropods to microorganisms has been obtained from studies in insects. These have revealed the involvement in the antiviral response of several signaling pathways including RNA interference (RNAi) [9, 10], Toll, Immune deficiency (IMD), and Janus kinase-signal transducers and activators of transcription (JAK/STAT), as well as melanisation, autophagy and possibly heat shock proteins (HSPs) (reviewed by [11–14]). RNAi, Toll, IMD and JAK/STAT pathway components have been identified in the genome of the tick *I. scapularis* [15, 16], but in comparison to insects there is only limited knowledge on tick innate immune responses to pathogen infection [15, 17–19]. A recent study reported a role for the JAK/STAT pathway in *I. scapularis* ticks during *Anaplasma phagocytophilum* infection [20]. This study showed that silencing of STAT or JAK, but not Toll-1, TAK1 or TAB1, which are

components of the Toll and IMD pathways, resulted in an increase in *A. phagocytophilum* in infected ticks and that the JAK/STAT pathway controls bacterial infection by regulating the expression of antimicrobial peptides of the 5.3 kD gene family. Other important regulatory molecules with a possible role in tick innate immune responses include RNA-dependent RNA polymerase, subolesin and ubiquitin-related molecules [21–24].

The only antiviral innate immune response described to date in ticks is RNAi [25, 26]. RNAi has been efficiently used for gene knockdown in ticks and tick cell lines [27–29]. Tick cell lines have been used as tools to understand LGTV and TBEV interactions with their vectors [30–38]. Recently, Dicer (Dcr) and several orthologues of Argonaute (Ago) 2, a key member of the exogenous siRNA pathway in insects, were identified in ticks and Dcr 90, Ago 16 and Ago 30 were shown to mediate an antiviral response [38].

The present study was carried out with the aim of identifying transcripts and proteins with a possible role in tick innate antiviral responses. We first characterised TBEV infection in the tick cell lines IDE8 derived from the only tick species with a sequenced genome, *I. scapularis*, and IRE/CTVM19 derived from *I. ricinus*, a natural vector of TBEV. We then investigated differences in transcript and protein abundance between TBEV-infected and mock-infected tick cells using the Illumina HiSeq2000 platform and LC-MS/MS, respectively. Statistically significantly differentially-expressed transcripts and differentially-represented proteins were identified, annotated and grouped according to their biological function. Finally, using LGTV which could be handled at a lower level of biosafety containment than TBEV, we silenced selected transcripts and proteins by RNAi, to elucidate their effect on virus replication and production.

Methods

Ethics statement

This study was carried out in strict accordance with the Czech national law and guidelines on the use of experimental animals and protection of animals against cruelty (the Animal Welfare Act Number 246/1992 Coll.). The protocol was approved by the Committee on the Ethics of Animal Experiments of the Institute of Parasitology and of the Departmental Expert Committee for the Approval of Projects of Experiments on Animals of the Czech Academy of Sciences (Permit Number: 165/2010).

Tick and mammalian cell lines

The *I. scapularis*-derived cell line IDE8 [39] was maintained in ambient air at 32 °C in L-15B medium [40] supplemented with 10 % tryptose phosphate broth (TPB), 5 % fetal calf serum (FCS), 0.1 % bovine

Weisheit *et al. Parasites & Vectors* (2015) 8:599

Page 3 of 26

lipoprotein (MP Biomedicals), 2 mM L-glutamine and 100 units/ml penicillin and 100 µg/ml streptomycin (pen/strep). The *I. ricinus*-derived cell line IRE/CTVM19 [41] was maintained in ambient air at 28 °C in L-15 (Leibovitz) medium supplemented with 10 % TPB, 20 % FCS, 2 mM L-glutamine and pen/strep [42]. Baby hamster kidney (BHK-21) cells (C-13, ATCC, cat: CCL-10) and African green monkey kidney epithelial (Vero) cells (ECACC, cat: 84113001) were grown at 37 °C in a humidified atmosphere of 5 % CO_2 in air. Porcine kidney stable (PS) cells were grown at 37 °C in ambient air [43]. BHK-21 cells were maintained in Glasgow Minimal Essential Medium (GMEM) supplemented with 5 % newborn calf serum (NBCS), 10 % TPB, 2 mM L-glutamine and pen/strep (GMEM/5 % NBCS). Vero cells were grown in Dulbecco's Minimal Essential Medium containing 10 % FCS and pen/strep. PS cells were maintained in L-15 (Leibovitz) medium supplemented with 3 % NBCS, 2 mM L-glutamine, pen/strep and 0.25 µg/ml amphotericin B (L-15/3 % NBCS).

Virus strains, propagation and virus titration

The TBEV strain Neudoerfl was kindly provided by Professor F.X. Heinz, Institute of Virology, Medical University of Vienna, Austria, and had been passaged five times by intracranial infection of suckling mice before use in the present study. Suckling CD1 mice were intracranially infected with 1 µl of TBEV-infected mouse brain suspension corresponding to 100 plaque-forming units (PFU) per mouse, or mock-infected with the same volume of uninfected mouse brain suspension. After the onset of symptoms, 4 to 5 days post infection (p.i.), the TBEV-infected mice were euthanised and the brains removed. The mock-infected mice were euthanised 2 days later, to prevent any possibility of cross contamination while handling the samples. The brains were homogenised in L-15/3 % NBCS to obtain a 20 % mouse brain suspension (w/v) using a Tissue Lyser II (Retsch) at 30 Hz (30/s) for 2 min. The homogenate was then centrifuged for 10 min at 16,000 x g at 4 °C and the clarified supernatant was used for infection of tick cell lines.

The LGTV strain TP-21 was kindly provided by Dr Sonja Best, Laboratory of Virology, Rocky Mountain Laboratories, NIAID, NIH, Hamilton, Montana, USA and was propagated in Vero cells prior to being used for infection. TBEV was titrated on PS cells as described previously [44, 45]; the titre of the stock used in the experiments was $6x10^7$ PFU/ml. LGTV was titrated on BHK-21 cells in 12-well plates using Avicel (RC-581, FMC Biopolymer) as an overlay. In brief, cells were seeded at a density of $1.5x10^5$ cells per well in GMEM/5 % NBCS and incubated overnight. When the cells were 80 % confluent, medium was removed and replaced with supernatant of test samples which had been 10-fold

serially diluted in GMEM/2 % NBCS. After incubation on a shaker for 1 h, cells were overlaid with 1 ml of Avicel suspension (1.2 g Avicel in 100 ml PBS) mixed in a 1:1 ratio with 2x Minimal Essential Medium (Gibco) supplemented with 5 % FCS. Cells were incubated for 4 days, fixed in 10 % neutral buffered formaldehyde (Leica), stained with 0.1 % aqueous toluidine blue for 30 min and plaques were counted. The titre of the LGTV stock used in the experiments was $2x10^6$ PFU/ml.

Infection of tick cell lines

For establishing a TBEV growth curve, both tick cell lines were seeded at a density of $5x10^5$ cells per ml in 2 ml total medium volume in flat-sided tubes (Nunc) and 24 h later were infected with TBEV diluted in the respective tick cell growth medium to a multiplicity of infection (MOI) of 5. After infection, supernatant was collected over a 10 day time-period for virus titration. Tick cells used for transcriptomic and proteomic analysis were seeded at a density of $1.5x10^6$ (IDE8) or $1x10^6$ (IRE/CTVM19) cells per ml in flat-sided tubes and were infected 24 h later with TBEV at MOI 5. Preliminary experiments (data not shown) revealed that RNA and protein yields from equivalent numbers of cells were higher from IRE/CTVM19 cells than from IDE8 cells, presumably because IRE/CTVM19 cells are larger than IDE8 cells (authors' observations), and established that the cell densities used were the minimum required to produce acceptable RNA and protein yields. After incubation for the required time cells were harvested by pipetting for analysis as indicated below. To validate differential expression of transcripts in IDE8 and IRE/CTVM19 cells upon LGTV infection, cells were seeded at a density of $5x10^5$ per ml in flat-sided tubes, mock-infected or infected 24 h later with LGTV at MOI 5 and the medium was changed 2 h p.i.. At 2 and 6 days p.i., cells were harvested and RNA was isolated for qRT-PCR analysis as described below.

Immunostaining

Tick cells were seeded at a density of $5x10^5$ cells per ml on 12 mm diameter glass coverslips in 24-well plates, incubated overnight and two replicate wells were infected with TBEV at each of MOI 0.1, 1 and 5. The immunostaining procedure was carried out in the 24-well plates. At day 2 p.i. the cells on the coverslips were washed in PBS, fixed in 10 % neutral buffered formaldehyde for 1 h and washed for 5 min in PBS. The cells were then permeabilised with 300 µl of 0.3 % TritonX-100 for 30 min and subsequently with 0.1 % SDS for 10 min. After permeabilisation, the cells were washed in PBS and then blocked with 300 µl of 1 % bovine serum albumin (BSA) in PBS for 60 min. The blocking solution was removed and the primary antibody, Anti-Flavivirus Group antigen

Weisheit *et al. Parasites & Vectors* (2015) 8:599

Page 4 of 26

antibody (clone D1-4G2-4-15, Millipore, recognising the E protein of flaviviruses) diluted 1:100 in 1 % BSA, was added and incubated for 2 h at room temperature. The cells were washed three times for 5–10 min in PBS and the secondary antibody, Goat anti-Mouse IgG (H + L) DyLight 488 conjugate (Pierce Thermo Scientific) diluted 1:1000 in 1 % BSA, was added and incubated for 1 h. After three washes of 5 min each in PBS, the coverslips were mounted on glass microscope slides with Vectashield HardSet mounting medium containing DAPI (Vector Laboratories). Images were taken of randomly-selected fields using an Olympus Fluoview FV10 confocal microscope and the percentage of green cells determined by visual counting of DyLight 488-positive and negative cells.

RNA and protein isolation

IDE8 and IRE/CTVM19 cells were seeded at densities of, respectively, $1x10^6$ and $1.5x10^6$ cells per ml into 24 tubes per cell line and, 24 h later, 12 tubes per cell line were infected with TBEV at MOI 5 and 12 tubes were mock-infected with the same volume (300 µl) of diluted uninfected mouse brain suspension. On each of days 2 and 6 p.i., cells from six tubes per treatment were harvested by pipetting and the cell suspension from each replicate tube was split into two aliquots of 1 ml, which were both centrifuged at 500 x g for 5 min and the supernatants discarded. One aliquot from each replicate tube was used for RNA isolation using 1 ml of TriReagent (Sigma) according to the manufacturer's instructions. To improve RNA purity, RNA samples were further purified using the RNeasy Mini kit (Qiagen) according to the manufacturer's instructions. RNA samples were stored at –80 °C. The second aliquot from each replicate tube was used for protein isolation as follows. The cell pellet was washed twice with ice-cold PBS and resuspended in 350 µl ice-cold PBS supplemented with 1 % Triton X-100, 50 µl cOmplete, Mini, EDTA-free Protease Inhibitor Cocktail (Roche) and 3.5 µl Halt Phosphatase Inhibitor Cocktail (Thermo Scientific Pierce). After incubation for 1 h on ice, the cell suspension was homogenised at 4 °C using a micro pestle and centrifuged at 200 x g for 5 min to remove cell debris. Supernatants were collected and protein concentration was determined with the BCA protein assay kit (Thermo Scientific Pierce) using BSA as standard. Samples were stored at –80 °C until use.

Protein quality was tested by SDS-PAGE with subsequent Coomassie staining as follows. Protein samples were mixed 1:1 (v/v) with 2x Laemmli buffer (Biorad) supplemented with 5 % β-mercaptoethanol (Sigma), heated at 96 °C for 10 min and then loaded onto discontinuous SDS-PAGE (0.75 mm thick, 4 % stacking and 12 % resolving) gels. The gels were run at 40 V for 30 min followed by 120 V for 30 min. For staining gels, a solution consisting of 0.25 g Coomassie Brilliant Blue R-250 (Thermo Scientific Pierce) dissolved in 40 % water, 50 % methanol and 10 % glacial acetic acid was prepared. The gels containing protein were immersed in staining solution for 3 h prior to de-staining in a solution containing 50 % methanol, 40 % water and 10 % glacial acetic acid. The de-staining solution was changed several times until the protein bands were clearly visible. Samples showing good protein quality with clear, distinct bands and widely-distributed molecular masses were considered suitable for proteomic analysis.

RNA sequencing and assembly

RNA integrity was assessed using the RNA 6000 Nano Kit (Agilent) according to the manufacturer's instructions and tested for RNA integrity using a 2100 Bioanalyser (Agilent) according to the manufacturer's instructions. Before sequencing, infection levels were measured by qRT-PCR using primers targeting the TBEV NS5 protein (Additional file 1). Aliquots of only those samples showing satisfactory RNA quality, and presence or absence of TBEV infection in the case of infected cells and mock-infected controls respectively, were pooled according to time-point, cell line and condition. The pooled RNA samples containing total RNA were processed by ARK-Genomics (http://www.ark-genomics.org/) according to the Truseq RNA sample guide 1500813 (Illumina Inc). In brief, mRNA molecules containing poly(A) tails were purified from total RNA using poly-T oligo-attached magnetic beads. The resulting mRNA was fragmented, first and second strand cDNAs were synthesised, ends repaired and adapters ligated. After PCR amplification, the cDNA library was quantified, multiplexed and sequenced on the HiSeq2000 platform, generating paired end reads of approximately 2 x 100 bp in length. The reads were sorted into samples according to cell line, time-point and treatment using the software CASAVA 1.8 (Illumina, https://support.illumina.com/sequencing/sequencing_software/casava.ilmn).

Reads obtained from the *I. scapularis*-derived cell line IDE8 were mapped with TopHat 2.0.3 [46] against the *I. scapularis* reference genome (iscapularis.SUPERCONTIGS-Wikel.IscaW1.fa). Counts of reads mapping to the genome were generated with HTSeq count 0.5.3p9 (http://www.huber.embl.de/users/anders/HTSeq/doc/count.html). The unmapped reads were *de novo* assembled with CLC genomic workbench 5.1 (http://www.clcbio.com/products/clc-genomics-workbench/) and mapped with BWA 0.6.1 [47] against the mapped, filtered (5x 400b) reads for generating counts using a Perl script. The reads obtained from the *I. ricinus* cell line IRE/CTVM19 were *de novo* assembled as described for the unmapped reads from IDE8. Only reads mapping unambiguously to contigs were counted.

Weisheit *et al. Parasites & Vectors* (2015) 8:599

Page 5 of 26

Differential gene expression analysis and annotation

Each assembled contig was assumed to represent a transcript and, since the majority of reads generated during sequencing mapped unambiguously, it was assumed that the count data reflected the expression of each transcript. As reported in previous studies [48–51], we did not use biological replicates for RNA-seq but used pooled RNA isolated from replicate samples; the algorithm used to quantitate transcriptomics data allows the use of non-replicated samples [52, 53]. Differential gene expression was analysed using DESeq in R following the script for working without replicates [52]. DESeq uses a very conservative approach in calling statistical significance in samples without biological replicates. This results in fewer transcripts being called statistically significant; thus some important transcripts might have been missed, whereas the transcripts that were included were strongly supported. Transcripts that were greater than $\log_2$ 2-fold differentially expressed, and those statistically significantly differentially expressed, were annotated first using Blast2GO [54] with a Blastx algorithm against the NCBI nr database using a threshold of E-value $< 10^{-6}$ as cut-off. Those sequences which did not result in any blast hits with Blast2GO were blasted manually using Blastx and Blastn algorithms against the nr and nt NCBI databases and were included when they showed more than 50 % coverage and more than 25 % sequence similarity. All sequences obtained by either of the two approaches were additionally blasted against the UniProt/Swiss-Prot and VectorBase databases to retrieve ontology information, including ontology information for conserved domains provided by NCBI and UniProt. For the statistically significantly differentially-expressed transcripts, literature research was performed in addition to database information retrieval to assign biological process groups.

Proteomic analysis

For those samples which passed both the RNA and protein quality checks in each experimental group, protein extracts equivalent to 100 μg for each group, obtained by pooling equal aliquots from the replicates, were suspended in 100 μl of Laemmli buffer supplemented with 5 % β-mercaptoethanol and applied to 1.2 cm-wide wells of a conventional discontinuous SDS-PAGE gel (0.75 mm thick, 4 % stacking, and 12 % resolving). The electrophoretic run was stopped as soon as the dye front entered 3 mm into the resolving gel. The whole proteome, concentrated within the stacking/resolving gel interface, was visualised using Bio-Safe Coomassie Stain G-250 (BioRad), excised and cut into cubes of 2 x 2 mm. The gel pieces were destained in a 1:1 mixture of acetonitrile and water and digested overnight at 37 °C with 60 ng/ml sequencing grade trypsin (Promega, Madison, WI) as described previously [55]. Trifluoroacetic acid was added to a final concentration of 1 % to stop digestion, and peptides were desalted onto OMIX Pipette tips C18 (Agilent Technologies, Santa Clara, CA, USA) as described previously [56], dried down and stored at −20 °C until required for mass spectrometry analysis. The desalted protein digests were resuspended in 0.1 % formic acid and analysed by reversed phase liquid chromatography coupled to mass spectrometry (RP-LC-MS/MS) using an Easy-nLC II system coupled to an ion trap LTQ-Orbitrap-Velos-Pro mass spectrometer (Thermo Scientific, San Jose, CA, USA). The peptides were concentrated (on-line) by reverse phase chromatography using a 0.1 mm × 20 mm C18 RP precolumn (Thermo Scientific), and separated using a 0.075 mm x 100 mm C18 RP column (Thermo Scientific) operating at 0.3 μl/min. Peptides were eluted using a 180-min gradient from 5 % to 40 % solvent B in solvent A (Solvent A: 0.1 % formic acid in water, solvent B: 0.1 % formic acid, 80 % acetonitrile in water). ESI ionisation was carried out using a nano-bore emitters stainless steel ID 30 μm (Thermo Scientific) interface. Peptides were detected in survey scans from 400 to 1600 atomic mass units (amu, 1 μscan), followed by fifteen data-dependent MS/MS scans (Top 15), using an isolation width of 2 mass-to-charge ratio units, normalised collision energy of 35 %, and dynamic exclusion applied during 30 s periods.

Proteomic data analysis and annotation

Peptide identification from the MS/MS raw data was carried out using the SEQUEST algorithm (Proteome Discoverer 1.3, Thermo Scientific). Database searches were performed against UniProt-Arthropoda.fasta and UniProt-Flaviviridae.fasta. The following constraints were used for the searches: tryptic cleavage after Arg and Lys, up to two missed cleavage sites, and tolerances of 10 ppm for precursor ions and 0.8 Da for MS/MS fragment ions, and the searches were performed allowing optional methionine oxidation and cysteine carbamidomethylation. Searches were performed against a decoy database in an integrated decoy approach. A false discovery rate (FDR) < 0.01 was considered as a condition for successful peptide assignments and at least 2 peptides per protein in at least one of the samples analysed was the condition for subsequent protein identification (Additional file 2). The total number of peptide assignments for each protein were normalised against the total number of peptide assignments in each sample (control and infected tick cell lines at days 2 and 6 p.i.) and differential representation of individual proteins between different samples was determined using Chi-square test statistics with Bonferroni correction in the IDEG6 software (http://telethon.bio.unipd.it/bioinfo/IDEG6 form/) ($p < 0.05$) as published [56]. Samples with

Weisheit *et al. Parasites & Vectors* (2015) 8:599

Page 6 of 26

a p-value equal to or lower than 0.05 were considered statistically significant. Statistically significantly differentially-represented proteins were allocated to biological process groups using ontology information available on the UniProt/Swiss-Prot and Panther databases, including information for conserved domains. Information was curated manually through literature search.

Reverse transcription

For verification of infection status of TBEV-infected and mock-infected cells, 1 μg of total RNA was reverse-transcribed using Superscript III (Invitrogen) and random hexamers according to the manufacturer's instructions. For verification of RNA-Seq data and knockdowns followed by LGTV infection, 1 μg of total RNA was reverse-transcribed using the High-Capacity cDNA Reverse Transcription kit (Applied Biosystems) according to the manufacturer's instructions.

Verification of TBEV infection and RNA-Seq data by qRT-PCR

TBEV RNA levels were measured by qRT-PCR with TBEV NS5-specific primers (Additional file 1) using FastStart SYBR Green Master Mix (Roche) according to the manufacturer's instructions with a final reaction volume of 20 μl and a temperature profile of 95 °C for 5 min, 95 °C for 20s, 55 °C for 20s, 72 °C for 15 s and 95 °C for 20s. For calculating the TBEV infection levels of transcriptomic samples, TBEV NS5 copy numbers were calculated using a linearised plasmid encoding the TBEV NS5 protein as standard in a standard curve method as follows. The linearised plasmid was 9 x 10-fold serially diluted starting with 2 ng and the corresponding copy numbers were entered into the Rotor-GENE software which generated the standard curve and calculated the copy numbers for each unknown sample automatically. The number of copies of the linearised plasmid was calculated using the following formula [57]:

$$\text{Number of copies} = \frac{amount\ of\ plasmid\ (ng)\ \times\ 6.022\ x\ 10^{23}\ \left(\frac{molecules}{mol}\right)}{length\ (bp)\ \times\ 1\ x\ 10^{9}\ \left(\frac{ng}{g}\right)\ \times\ 660\ \left(\frac{g}{mol\ of\ bp}\right)}$$

The gene coding for TBEV NS5 protein was cloned into the pJET vector using the CloneJET PCR Cloning Kit (Fermentas) according to the manufacturer's instructions. In brief, the plasmid pTND/ΔME [58] was linearised, purified and used as DNA template for amplification of TBEV NS5 using KOD polymerase (Novagen). An aliquot of the 187 bp PCR product was visualised by gel electrophoresis and, since only one band with the correct size was visible, the non-purified product was directly used for ligation. For ligation, 10 μl 2x reaction buffer, 2 μl non-purified PCR product, 1 μl

pJET1.2 blunt cloning vector, 6 μl nuclease-free water and 1 μl T4 DNA ligase were mixed by vortexing. The ligation mixture was incubated for 5 min at room temperature before using directly for transformation of DH5α. To check if the correct insert was cloned into the vector, the plasmid was linearised and sent for sequencing to GATC Biotech (London, UK).

For verification of RNA-Seq data, primers for 12 transcripts (Additional file 1) were designed, using as template species-specific sequences or identical regions from sequences common to both *I. scapularis* and *I. ricinus* obtained by HiSeq2000. The same samples from which aliquots had been pooled for the transcriptome profiling were used individually for qRT-PCR analysis. Beta actin and ribosomal protein L13A were used as housekeeping genes for normalisation. Primer efficiencies were calculated for each primer and the quantity of gene transcripts in infected samples relative to controls was calculated using the $2^{-\Delta\Delta CT}$ method [59, 60].

dsRNA production and silencing of tick transcripts

Long dsRNA transcripts (407 - 615 bp in length) specific to genes from each cell line were produced from PCR products flanked by T7 promoter sequences using the MegaScript RNAi kit (Ambion). In brief, cDNA generated by reverse transcription from total RNA of tick cells or from the plasmid pIRES2-eGFP (Clontech) was used as template to generate specific PCR products using T7 primers (Additional file 1) by PCR. PCR products were gel-purified and sequenced. The gel-purified PCR products were subjected to an additional PCR amplification and were then transcribed using the MegaScript kit according to the manufacturer's instructions.

For knockdown experiments, LGTV was used at a low MOI to ensure that not all cells would be infected initially, thereby allowing virus to spread from cell to cell which might enhance detection of any effect of transcript knockdown on virus replication and/or production. Cell lines IDE8 and IRE/CTVM19 were seeded at a density of $5x10^5$ cells per ml in 24-well plates and were incubated in humidified self-sealing polythene bags. For IDE8 cells, 300 ng of dsRNA was added to the supernatant twice, at 8 h and 48 h post-seeding. Approximately 72 h post-seeding, cells were infected with LGTV at MOI 0.01; 48 h later supernatant was collected for plaque assay and cells were harvested for RNA extraction. To achieve a good knockdown in IRE/CTVM19 cells, cells were transfected 24 h post-seeding with 400 ng of dsRNA using Lipofectamine® 2000 (Invitrogen) as previously described [29] and, after incubation for a further 48 h, were infected with LGTV at MOI 0.5. At 24 h p.i supernatant was collected for plaque assay and RNA was extracted using TriReagent as above. Non-specific dsRNA encoding eGFP was used as a negative

Weisheit *et al. Parasites & Vectors* (2015) 8:599

Page 7 of 26

control, to provide a baseline level of activation above which the effect of the specific exogenous dsRNA was measured. Additional controls, in which samples were not treated with dsRNA prior to infection, were included to test whether or not addition of any non-specific dsRNA triggers an innate immune response in tick cells and to provide a baseline for virus replication and virus titres in untreated cells. For the detection of Ago and Dcr knockdowns, PCR was carried out (95 °C for 2 min, 95 °C for 30 s, primer set specific annealing temperature (Additional file 1) for 30s, 72 °C for 50 s, 72 °C for 7 min) using GoTaq reaction mix (Promega), according to the manufacturer's instructions, together with 2 μl of the cDNA reaction and the corresponding primers (Additional file 1).

PCR products were run on a 1 % agarose gel and gel images were taken and used to quantify mRNA knockdown with Image Lab software (BioRad) normalised to beta actin. Gene knockdowns and LGTV RNA levels were measured by qRT-PCR with, respectively, target gene-specific primers or LGTV NS5-specific primers (Additional file 1), using FastStart Universal SYBR Green Master (Rox) (Roche) with a temperature profile of 95 °C for 10 min, 95 °C for 15 or 20s, specific annealing temperature for 20 or 30s, 72 °C for 15 or 30s and 95 °C for 15 s. All qRT-PCR reactions were followed by melting curve generation (60-95 °C) to confirm amplification specificity. Primer efficiencies were calculated for each primer and the quantity of gene transcripts in infected samples relative to controls was calculated using the $2^{-\Delta\Delta CT}$ method [59, 60].

Statistical analysis of gene knockdown experiments

Gene knockdowns were done in quadruplicate in three independent experiments. Only those samples in which a knockdown occurred were included in subsequent statistical analysis. Analysis was done in GraphPad Prism (http://www.graphpad.com/scientific-software/prism/). Statistical significance of the three independent experiments was analysed using the two-way Analysis of Variance Fisher's LSD test ($P = 0.05$).

Results and discussion

Characterisation of TBEV growth in tick cells

Tick cells are able to support infection with a variety of different viruses; as expected, the dynamics of infection vary according to the virus and the cell line [61–63]. To date only two studies have been published on TBEV using cell lines derived from its natural vector *I. ricinus* [34, 35]. To establish the appropriate MOI and time-points for transcriptomic and proteomic analysis, it was first necessary to determine the MOI at which most of the cells would be infected, thereby preventing uninfected cells from masking the transcriptomic

and proteomic changes occurring upon TBEV infection. Two cell lines were studied: IRE/CTVM19 derived from *I. ricinus* and IDE8 derived from *I. scapularis*. To determine the appropriate MOI, tick cells were grown on coverslips in 24-well plates and infected with TBEV at MOI 0.1, 1 or 5. Cells were fixed at day 2 p.i., immunostained for TBEV E protein and the percentage of positive cells calculated (Fig. 1a). MOIs of 0.1 and 1 resulted in approximately 40 % of E protein-positive IRE/CTVM19 cells in comparison to 70 % at MOI 5. In IDE8 cells, however, less than 10 % of cells were E protein-positive when infected with MOI 0.1, 25 % with MOI 1 and 55 % with MOI 5. All currently-available tick cell lines are phenotypically and genotypically heterogeneous [41] and relatively uncharacterised; some cell types within the two cell lines used might not support virus infection or the amount of E protein in some infected cells might be below the detection limit of the assay. The observation that not all tick cells are positive for TBEV upon TBEV infection and that the percentage of infected cells varies according to the cell line is consistent with a previous report on TBEV infection in tick cell lines [34]. Since both tick cell lines showed the highest percentage of TBEV-positive cells with MOI 5, the course of infection at this MOI was determined in greater detail.

To measure newly-produced virus within defined time-periods, tick cells were infected with TBEV at MOI 5. The cells were then washed and fresh medium was added at 2 h p.i. for time-points 12, 18 and 24 h, and at 24 h prior to each sampling for the subsequent daily time-points up to day 10 p.i. (Fig. 1b). Supernatants were collected at each time-point and the virus titre measured by plaque assay on PS cells. The pattern of TBEV infection was similar in both cell lines with the highest level of virus production between 2 and 4 days p.i. (Fig. 1b). Interestingly, the maximum titre in the cell line IRE/CTVM19 derived from a known TBEV vector was approximately 2 $\log_{10}$ higher than in the IDE8 cell line. The higher level of virus production in the *I. ricinus* cell line compared to the cell line derived from *I. scapularis*, which is not known to be a natural vector of TBEV, confirms previous studies [31, 34]. The lower virus titres in IDE8 cells might be an indicator of reduced vector capacity of *I. scapularis* for this virus, which could be due to cells being less efficiently infectable or having a more rapid and efficient antiviral response.

In order to examine how these two cell lines react to virus infection, two time-points were chosen for transcriptomic and proteomic analysis: one early in infection at day 2 when virus production was increasing, and one later in infection at day 6 when virus production was decreasing.

Weisheit *et al. Parasites & Vectors* (2015) 8:599

Page 8 of 26
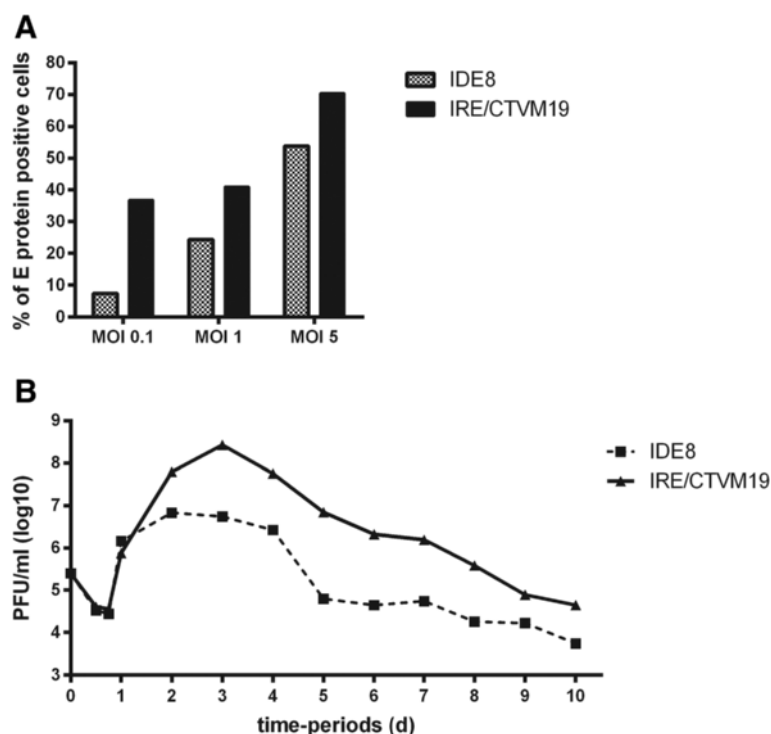
Fig. 1 Characterisation of TBEV infection in IDE8 and IRE/CTVM19 cells. **a** Percentage of E protein-positive tick cells following TBEV infection. IDE8 and IRE/CTVM19 cells were infected with TBEV at MOI 0.1, 1.0 and 5.0 and cells were fixed and immunostained at day 2 p.i. The percentage of E protein-positive cells was calculated. The mean of duplicate cultures is shown. **b** TBEV production over a 10-day time course in tick cell lines. IDE8 and IRE/CTVM19 cells were infected with TBEV at MOI 5 and virus was titrated by plaque assay on PS cells. The mean PFU/ml of duplicate cultures is shown. The limit of detection was 56 PFU/ml in a 10^{-1} dilution

Generation of samples for transcriptomic and proteomic analysis

Six replicate tubes per time-point per cell line were either infected with TBEV at MOI 5 or mock-infected. At days 2 and 6 p.i., both RNA and protein were isolated from each tube by dividing the cell suspension in half, thus ensuring that both transcriptomic and proteomic analyses were carried out on samples derived from each tube. Because of the biosafety restrictions on handling TBEV, it was only possible to generate a single set of samples, which yielded sufficient material for a single sequencing run and proteomic analysis for each treatment. Therefore the results will be considered in this context as a baseline for future studies.

Prior to RNA sequencing, RNA samples were tested for the presence of TBEV by qRT-PCR (Additional file 3). Only mock-infected samples negative for TBEV with NS5 RNA levels below the detection limit of the assay, and infected samples positive for TBEV with NS5 levels above 10,000 copies, were included in the subsequent analysis. Furthermore, only high quality samples showing no signs of RNA degradation were used. The soluble proteins extracted from mock-infected and TBEV-infected IDE8 and IRE/CTVM19 cells at days 2 and 6 p.i. were tested for protein quality prior to pooling. Only those RNA samples and protein samples which passed both the RNA and protein quality checks (Additional file 3) were pooled, guaranteeing that pooled RNA samples and protein samples contained RNA and protein, respectively, from the same original samples.

Table 1 Sequencing depth, assembly of RNA-Seq data and total number of proteins identified by MS from TBEV-infected and mock-infected (control) IDE8 and IRE/CTVM19 cells on days 2 (2d) and 6 (6d) p.i

Sample	Mean reads per lane	Total no. of contigs assembled	Mean contig length	Total no. of proteins identified by RP-LC-MS/MS
IDE8 control 2d	3.71E + 07	44562	938	907
IDE8 infected 2d	3.25E + 07	44907	937	770
IDE8 control 6d	3.18E + 07	44684	938	824
IDE8 infected 6d	2.96E + 07	44474	939	725
IRE/CTVM19 control 2d	3.03E + 07	70701	1087	835
IRE/CTVM19 infected 2d	2.70E + 07	70067	1092	762
IRE/CTVM19 control 6d	4.44E + 07	70842	1086	1133
IRE/CTVM19 infected 6d	2.61E + 07	70273	1091	1032

Weisheit *et al. Parasites & Vectors* (2015) 8:599

Page 9 of 26

Illumina sequencing, assembly and differential gene expression analysis

Aliquots of RNA from two or three replicate samples per time-point per cell line (Additional file 3) were pooled and sequenced on the Illumina HiSeq2000 platform. Totals of 29–37 million and 26–44 million raw reads of 100 bp in length were sequenced for IDE8 and IRE/CTVM19 cells, respectively (Table 1). The raw reads from IDE8 were assembled into 44,474 - 44,907 contigs with a mean length of 938 bp and those of IRE/CTVM19 were assembled into 70,067 - 70,842 contigs with a mean length of 1089 bp (Table 1). The difference in contig numbers between the two cell lines is not unexpected since the former were assembled against the sequenced *I. scapularis* genome while the latter were, in the absence of a genome, *de novo* assembled. From the sequencing data for each cell line almost the complete TBEV genome was *de novo* assembled. Of the total number of reads generated, approximately 3.0 % and 2.8 % aligned to TBEV in infected IDE8 cells at days 2 and 6 p.i. respectively, whereas 4.0 % and 7.7 % aligned to TBEV in infected IRE/CTVM19 cells on days 2 and 6 p.i. respectively. The higher level of viral RNA present within IRE/CTVM19 cells compared to IDE8 cells is in agreement with the greater number of infected cells (Fig. 1a) and the higher infectious virus titre (Fig. 1b) in IRE/CTVM19 cultures. The almost completely-assembled virus genome obtained from the two cell lines was identical at each time-point and in each cell line (data not shown). The assembled virus showed 99 % coverage and 99 % similarity to the TBEV Neudoerfl sequence on NCBI (U27495.1). Although TBEV does not have a poly(A) tail, the Neudoerfl strain of TBEV contains a poly(A) sequence within the variable region of the 3' non-coding region [64] which might explain its presence in the poly(A)-selected RNA pool used for sequencing.

Only raw reads that mapped unambiguously to assembled contigs were counted, and it was assumed that the counts for each contig represented the expression level of each transcript. While the majority of reads mapped unambiguously, this approach could lead to an underestimation of transcript expression; however, this would affect both TBEV-infected and mock-infected samples in a similar way. This approach could create problems if there was a true shift of splice isoforms, with one isoform only present in the infected and the other only in the mock-infected samples. It was not possible to determine whether this phenomenon occurred in the present study. The raw count data was used to determine differential gene expression between each of the infected IDE8 and IRE/CTVM19 samples and their respective mock-infected controls using DESeq [52] in R. This allows for calling significance in samples without replicates [65]. It also uses a very conservative estimation of variance, reducing the number of transcripts called as statistically significant. This focus on statistically significantly differentially-expressed transcripts is a stringent filter which may miss some transcripts. In IDE8 cells at days 2 and 6 p.i., totals of 23 and 21 transcripts respectively were statistically significantly differentially expressed with a majority of genes down-regulated on both days (Table 2). In contrast, in IRE/CTVM19 cells totals of 40 and 43 transcripts were statistically significantly differentially expressed on days 2 and 6 p.i. respectively, with the majority of transcripts being up-regulated on both days (Table 2).

Protein identification and differential protein representation

Proteins in pooled samples from 2–3 replicates (Additional file 3) were analysed by RP-LC-MS/MS and identified by searching against the arthropod and *Flaviviridae* Uniprot databases. For IDE8 cells, 725–907 proteins were identified in mock-infected and TBEV-infected samples at days 2 and 6 p.i., with slightly fewer proteins being identified at day 6 p.i. than at day 2 p.i. (Table 1 and Additional file 2). For IRE/CTVM19 cells, 762–1133 proteins were identified in mock-infected and TBEV-infected tick cells, with more proteins being identified at day 6 p.i. than at day 2 p.i. (Table 1 and Additional file 2). In both cell lines, slightly higher numbers of proteins were identified in control cells than in TBEV-infected cells, suggesting that TBEV might have an inhibitory effect on protein representation. The higher number of *I. scapularis* protein sequences present

Table 2 Number of statistically significantly differentially expressed transcripts that were up- or down-regulated upon TBEV infection of IDE8 and IRE/CTVM19 cells on days 2 (2d) and 6 (6d) p.i

Transcript status	IDE8		IRE/CTVM19	
	2d	6d	2d	6d
Up-regulated	8	7	24	43
Down-regulated	15	14	16	0
TOTAL	23	21	40	43

Table 3 Number of statistically significantly differentially-represented proteins upon TBEV infection of IDE8 and IRE/CTVM19 cells on days 2 (2d) and 6 (6d) p.i

Protein status	IDE8		IRE/CTVM19	
	2d	6d	2d	6d
Over-represented	20	14	10	24
Under-represented	32	10	10	85
TOTAL	52	24	20	109

Weisheit *et al. Parasites & Vectors* (2015) 8:599

Page 10 of 26

in the arthropod database compared to *I. ricinus* sequences did not influence peptide/protein identification. In addition to the arthropod database, MS spectra were used to search against the *Flaviviridae* database. Considering only those peptides with more than one peptide match (FDR <0.01) against the database, only TBEV-infected samples were positive for TBEV and mock-infected cells were negative (Additional file 2). The presence of TBEV proteins was in accordance with detection of TBEV sequences by RNA-seq and confirmed that infected samples, but not mock-infected samples, were infected and that the level of infection was greater in IRE/CTVM19 cells than in IDE8 cells (Additional file 2). Totals of 52 and 24 proteins were differentially represented in IDE8 cells on days 2 and 6 p.i. respectively, while 20 and 109 proteins were differentially represented in IRE/CTVM19 cells on days 2 and 6 p.i. respectively (Table 3). Overall, more proteins were differentially represented in IRE/CTVM19 cells than in IDE8 cells, reflecting the difference observed in gene expression between the two cell lines.

Annotation and ontology of tick cell transcripts and proteins
The majority of blast hits obtained for both transcripts and proteins of IDE8 and IRE/CTVM19 cells corresponded to *I. scapularis* (Fig. 2), which is not surprising since the majority of tick sequences deposited in databases to date were derived from *I. scapularis*, which is the only tick species with a sequenced genome.

In IDE8 cells, all 42 statistically significantly differentially-expressed tick cell transcripts (Fig. 2a) were annotated; 32 were most closely related to transcripts from *I. scapularis,* 2 to transcripts from other *Ixodes* spp, and 8 to transcripts from rodent species. In IRE/CTVM19 cells (Fig. 2b), only 56 of the 81 statistically significantly differentially-expressed tick cell transcripts could be annotated; 54 corresponded to *I. scapularis* and one each to *Rattus norvegicus* and *Harpegnathos saltator*. The other 25 transcripts did not return any blast hits and were excluded from further analysis. This lack of homology has been reported in other tick studies [66–68] and might be attributed to factors such as low sequence and/or
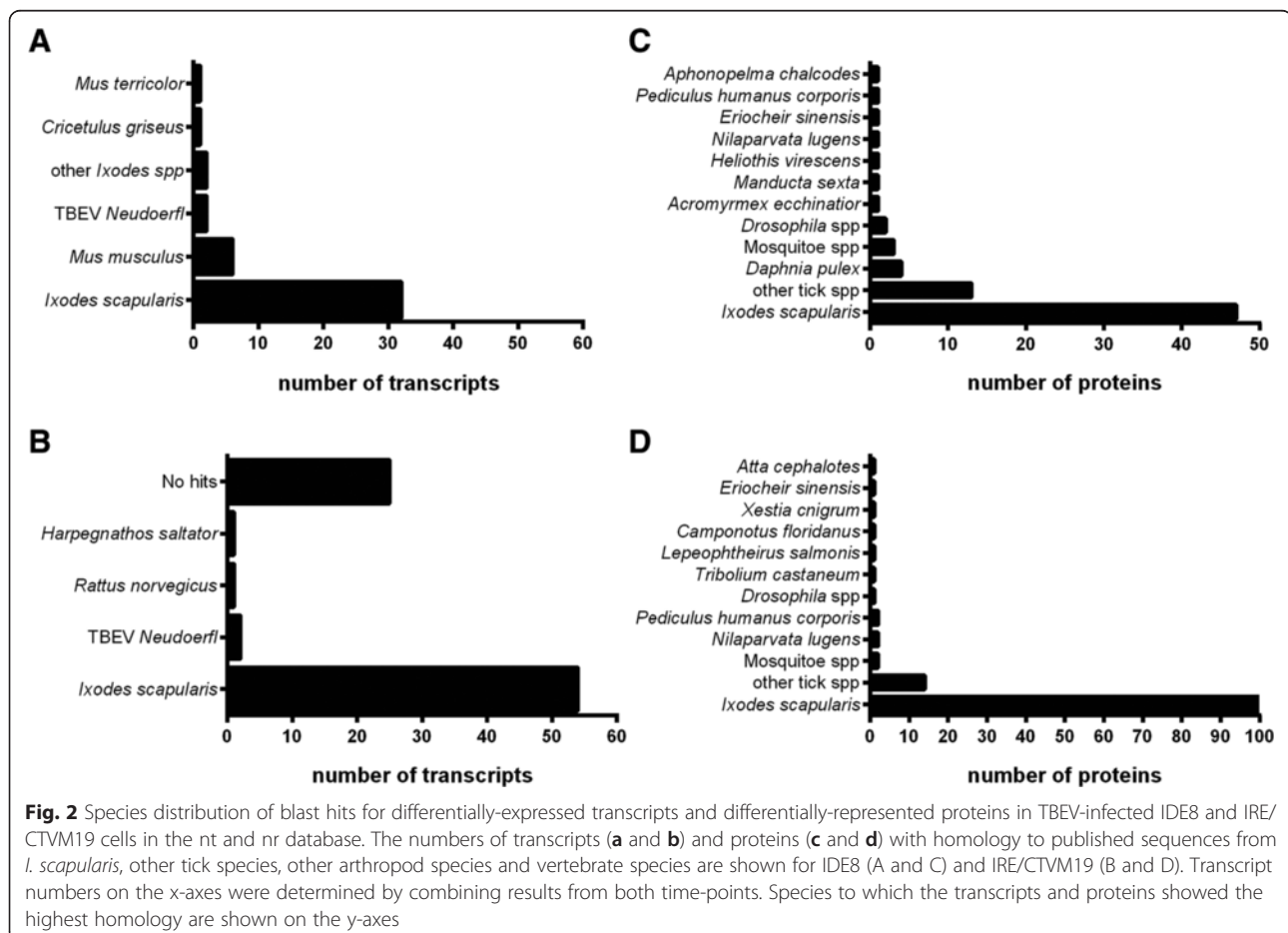
Fig. 2 Species distribution of blast hits for differentially-expressed transcripts and differentially-represented proteins in TBEV-infected IDE8 and IRE/CTVM19 cells in the nt and nr database. The numbers of transcripts (**a** and **b**) and proteins (**c** and **d**) with homology to published sequences from *I. scapularis*, other tick species, other arthropod species and vertebrate species are shown for IDE8 (A and C) and IRE/CTVM19 (B and D). Transcript numbers on the x-axes were determined by combining results from both time-points. Species to which the transcripts and proteins showed the highest homology are shown on the y-axes

Weisheit *et al. Parasites & Vectors* (2015) 8:599

Page 11 of 26

assembly quality, lack of homology to the *I. scapularis* genome due to its fragmented state or that these sequences represent novel species-specific transcripts [68].

With respect to the statistically significantly differentially-represented proteins, the majority in both IDE8 (Fig. 2c) and IRE/CTVM19 (Fig. 2d) corresponded to *I. scapularis* followed by other tick species including *Amblyomma* spp., *Hyalomma marginatum rufipes* and *Haemaphysalis qinghaiensis*.

The *I. scapularis* genome is currently not fully annotated, and annotation of transcripts or proteins, including the inference of their functional role, relies in the majority of cases on sequence similarity to evolutionarily quite distant species, including mammals and insects with well-annotated genomes. Thus although homology is observed for a specific transcript or protein, it might have evolved functions within the tick different from those within other species. This comparative approach might therefore be misleading and makes it difficult to infer true biological role by sequence similarity, conserved domains and/or literature search. Currently the only method to identify possible target genes within large datasets of ticks is to infer biological function from other better-annotated organisms or from sequence similarity to other model or non-model organisms.

To allocate annotated differentially-expressed transcripts and differentially-represented proteins to biological process groups, ontology information, including information for conserved domains, was retrieved from the UniProt/Swiss-Prot and Panther databases. Ontology information was manually augmented and/or curated using literature search. Some of the transcripts and proteins were grouped into more than one biological process. In IDE8 the most abundant subcategories within biological processes were nucleic acid processing (23 %), metabolism (23 %) and cell stress (21 %) at the transcript level (Fig. 3a), and nucleic acid processing (30 %), transport (22 %) and cell cycle (20 %) at the protein level (Fig. 4a). In IRE/CTVM19, ignoring those transcripts with no blast hits (30 %), the majority of transcripts were of unknown ontology (26 %) followed by those involved in immunity (10 %), transport (10 %) and cell stress (8 %) (Fig. 3b). At the protein level the majority were classed into nucleic acid processing (25 %), transport (22 %) and cell stress (15 %) (Fig. 4b).

In both cell lines, high levels of virus (Fig. 1b) were associated with up-regulation of transcripts annotated as immunity or metabolism and down-regulation of transcripts annotated as cell stress and protein folding. At the protein level, proteins annotated as cell stress or protein folding were, as with transcripts, amongst those consistently down-regulated. Equivalent biological process groups, as well as specific transcripts and proteins, have been observed to be differentially expressed in studies of mosquitoes and mosquito cells upon virus infection [65, 69, 70]. Although some of these studies showed different directions of representation, this might be attributed to different sampling times, different host and/or virus species and/or *in vivo* versus cell line usage. When comparing the transcript and protein profiles for each cell line at each time-point individually, there is little correlation at the biological process group level (Fig. 3a and b compared to Fig. 4a and b) between transcripts and proteins, apart from those involved in protein folding and cell stress, both of which are generally down-regulated in both TBEV-infected cell lines at both time-points. This lack of correlation between statistically significantly differentially-expressed transcripts and differentially-represented proteins was also observed in studies on tick cell responses to infection with intracellular bacteria [67, 71, 72], and probably reflects the different half-lives of mRNA and proteins and differential regulation of systems at the transcriptional, post-transcriptional, translational or post-translational levels. Novel approaches could increase the correlation between these datasets, for example proteomics informed by transcriptomics [73] which has recently been applied to ticks *in vivo* [51, 74].

Comparing the response to TBEV infection of IDE8 cells with that of IRE/CTVM19 cells, it is apparent that the two cell lines respond differently. Both the actual differentially-expressed transcripts (Fig. 3c) and differentially-represented proteins (Fig. 5), and their expression/representation levels, were different. The differential response at the transcript level might be, at least in part, an artefact resulting from the necessity for using different assembly approaches for the two cell lines, with *de novo* assembly for IRE/CTVM19 and mapping against a reference genome for IDE8; however, a recent study investigating the effect of these two different approaches on differential gene expression found that they usually agree well with each other [75]. Furthermore, the same method of protein identification and statistical analysis was used for both cell lines, and thus the different response is more likely to be due to cell line-specific differences.

To validate the differential gene expression observed during RNA-Seq, twelve transcripts differentially expressed in the transcriptomics data, and/or coding for differentially represented proteins in the proteomics data, were selected for qRT-PCR analysis. Preference was given to those putatively involved in immunity or cell stress, and transcripts/proteins with a range of different expression levels were chosen. Transcripts for the housekeeping genes ribosomal protein L13A and beta actin were used for normalisation since neither was differentially expressed in either of the cell lines at either time-point in the transcriptomic data. Most of the twelve

Fig. 3 Gene ontology and expression profiles of differentially-expressed transcripts in TBEV-infected IDE8 and IRE/CTVM19 cells. Each individual transcript of IDE8 (**a**) and IRE/CTVM19 (**b**) differentially expressed on days 2 (2d) and 6 (6d) p.i. was assigned to a biological process group according to its regulation status (up or down). Biological process (ontology) groups were assigned using information available on UniProt/Swiss-Prot databases, and were then manually curated according to gene function published in the literature. **c** Differentially-expressed transcripts in IDE8 and IRE/CTVM19 and their levels of differential expression on days 2 (2d) and 6 (6d) p.i. are depicted in the heatmap. Green = up-regulation; red = down-regulation; black = no change. Numbers on the colour key indicate the log$_2$-fold change in differential expression

transcripts showed similar fold changes by qRT-PCR and RNA-Seq, or at least confirmed the trend seen in the sequencing data (Additional file 4). The differences

observed between the two techniques qRT-PCR and RNA-Seq for complement factor H in both cell lines and coagulation factor in IDE8 cells at day 6 p.i.

Weisheit *et al. Parasites & Vectors* (2015) 8:599

Page 13 of 26
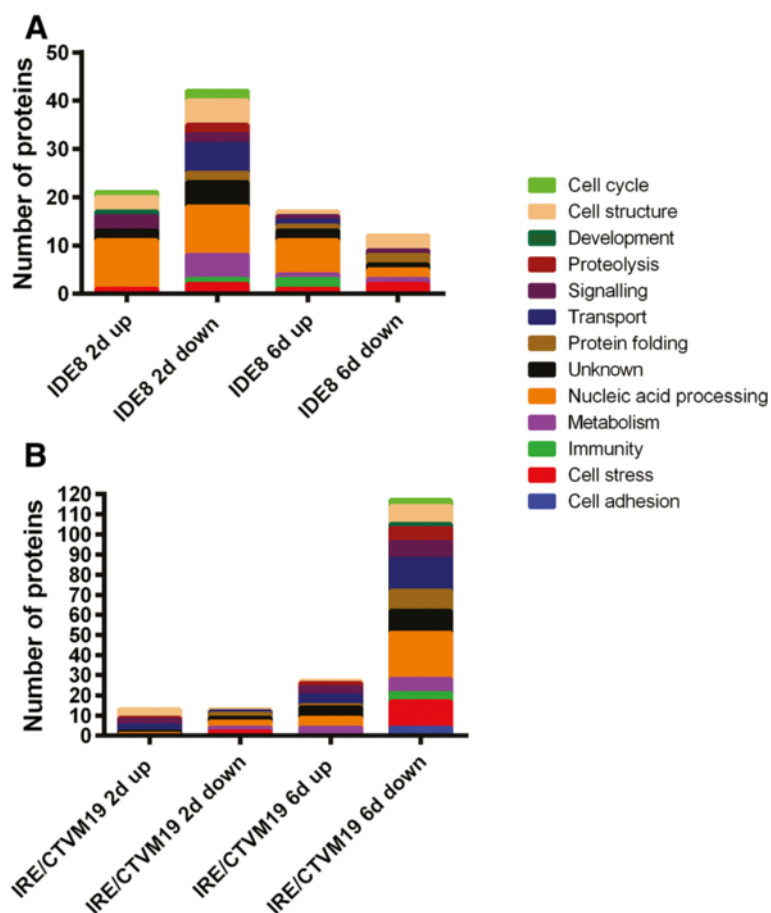
Fig. 4 Ontology of differentially-represented proteins in TBEV-infected IDE8 and IRE/CTVM19 cells. Each individual protein of IDE8 (**a**) and IRE/CTVM19 (**b**) differentially represented on days 2 (2d) and 6 (6d) p.i. was assigned to a biological process group according to its regulation status. Ontology groups were assigned using information available on UniProt/Swiss-Prot databases, and were then manually curated according to gene function published in the literature

(Additional file 4, A) might result from splice variants of these transcripts, different RNA processing techniques, primer design, the choice of reference genes and/or the different normalisation methods – normalisation across the whole transcriptome for sequencing depth with RNA-Seq versus normalisation against specific transcripts with qRT-PCR [76]. Similar observations, in which the differential gene expression data by RNA-Seq was, for most transcripts, in good agreement with qRT-PCR data in showing at least a similar trend in differential expression, have also been reported in other transcriptomic studies [77–79].

Functional role of selected cell stress and immunity genes and proteins in tick cells during LGTV infection

The main aim of this study was to identify transcripts and proteins which might have an antiviral role in tick cells. Therefore further analysis was undertaken on differentially-expressed transcripts and differentially-represented proteins with a possible role in innate immunity or cell stress (Fig. 6). For these experiments we used LGTV because it can be used at biosafety level 2, in comparison to TBEV which in many countries has to be handled at a higher level of containment. As it cross-protects against the more pathogenic virus [80], LGTV is likely to be affected by the same cellular responses as TBEV. To test this hypothesis, IDE8 and IRE/CTVM19 cells were infected with LGTV at MOI 5 or mock-infected with the same culture medium as that used to grow LGTV in Vero cells. At days 2 and 6 p.i., RNA was extracted and transcribed into cDNA. The cDNA was used for qPCR analysis using the same primers that were used for validating differential expression in TBEV-infected cells. Transcript expression in LGTV-infected cells (Additional file 5) revealed a similar trend in differential expression to that of TBEV-infected cells (Additional file 4). However, for some transcripts there was a difference in the level and/or timing of transcript expression. With the exception of complement factor H and coagulation factor, which

Weisheit *et al. Parasites & Vectors* (2015) 8:599

Page 14 of 26

Fig. 5 Representation profiles of differentially-represented proteins in TBEV-infected IDE8 and IRE/CTVM19 cells. Differentially-represented proteins in IDE8 and IRE/CTVM19 and their levels of differential representation on days 2 (2d) and 6 (6d) p.i. are depicted in the heatmap. Green = over-represented; red = under-represented; black = no change. Numbers on the colour key indicate the log₂-fold change in differential representation

were both up-regulated in TBEV-infected cells (Additional file 4) and down-regulated in LGTV-infected cells (Additional file 5), the trend in differential expression of all other transcripts was the same in LGTV- and TBEV-infected cells.

Selected transcripts were then silenced using sequence-specific dsRNA in IDE8 and/or IRE/CTVM19 cells, the cells were then infected with LGTV and virus replication and infectious virus production were measured by qRT-PCR and plaque assay respectively. Genes possibly involved in immunity such as those encoding complement factor H or trypsin or those possibly involved in cell stress such as those encoding calreticulin, HSP90, gp96 and HSP70 were silenced in both tick cell lines. Transcripts encoding Argonaute (Ago 30) and Dicer (Dcr 90) were included as positive controls [38], while cells treated with non-specific dsRNA against eGFP were used as baseline controls. Three independent

experiments with quadruplicate samples were conducted per cell line; thus 12 samples were analysed in total per cell line. Only those replicates in which silencing was confirmed were included in the statistical analysis.

In IDE8 cells, silencing was confirmed in all 12 replicate samples treated with dsRNA against Ago 30, trypsin, HSP90, HSP902 and gp96 with 44-98 % efficiency, 11/12 replicates for calreticulin and HSP70 with 31-85 % efficiency and 9/12 replicates for Dcr 90 and complement factor H with 7-100 % efficiency; silencing efficiencies are shown in Fig. 7a, b and c. Variability in knockdown efficiency and consistency for individual transcripts has also been observed in other studies on tick cells [67] as well as studies on other arthropods [81–83]. Variability could be due to tick cells counteracting the RNAi response by increasing transcription, transcripts being differentially protected from RNases, particular dsRNAs being efficiently
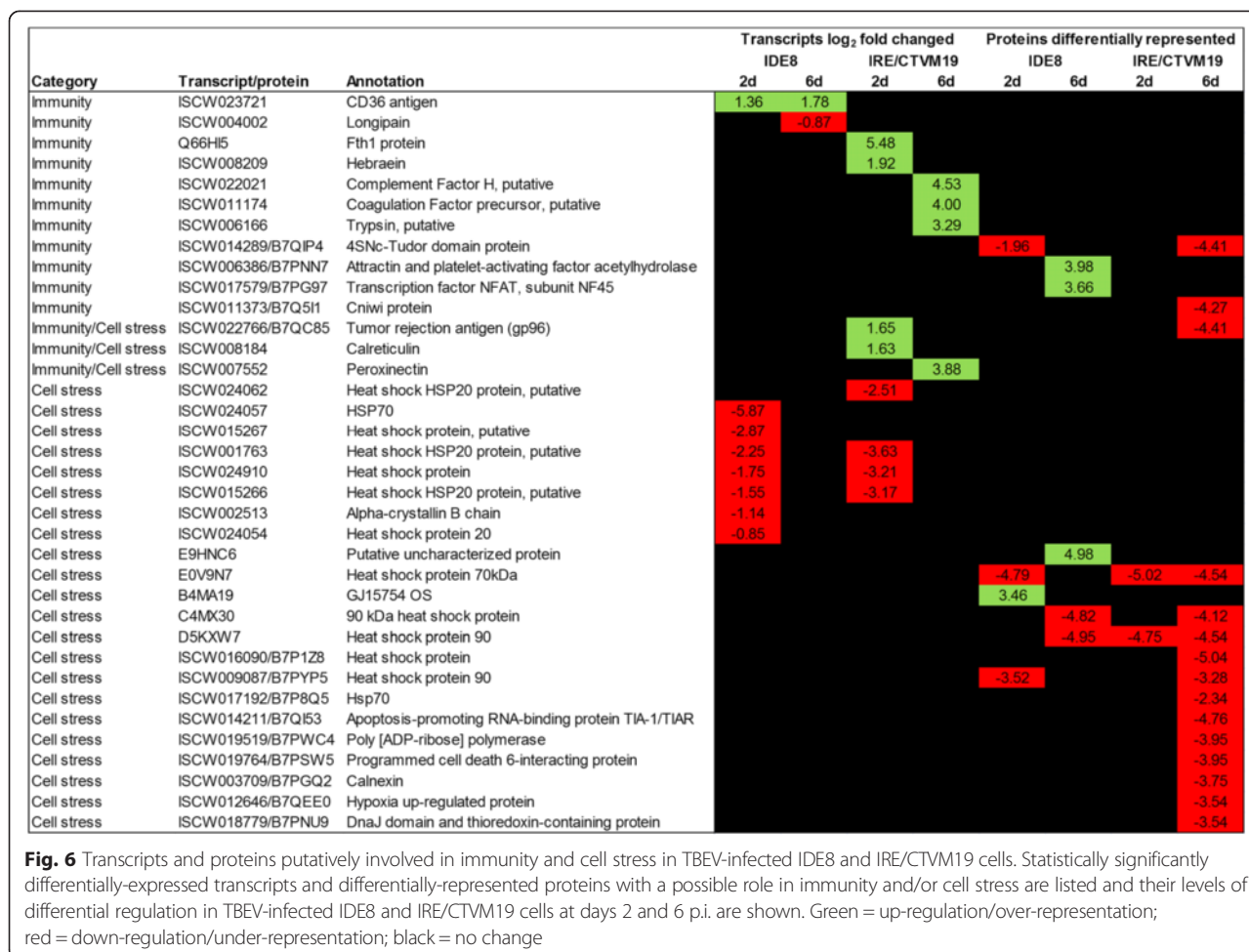
Weisheit *et al. Parasites & Vectors* (2015) 8:599

Page 15 of 26

Category	Transcript/protein	Annotation	Transcripts log₂ fold changed IDE8 2d	IDE8 6d	IRE/CTVM19 2d	IRE/CTVM19 6d	Proteins differentially represented IDE8 2d	IDE8 6d	IRE/CTVM19 2d	IRE/CTVM19 6d
Immunity	ISCW023721	CD36 antigen	1.36	1.78						
Immunity	ISCW004002	Longipain		-0.87						
Immunity	Q66HI5	Fth1 protein			5.48					
Immunity	ISCW008209	Hebraein			1.92					
Immunity	ISCW022021	Complement Factor H, putative				4.53				
Immunity	ISCW011174	Coagulation Factor precursor, putative				4.00				
Immunity	ISCW006166	Trypsin, putative				3.29				
Immunity	ISCW014289/B7QIP4	4SNc-Tudor domain protein					-1.96			-4.41
Immunity	ISCW006386/B7PNN7	Attractin and platelet-activating factor acetylhydrolase						3.98		
Immunity	ISCW017579/B7PG97	Transcription factor NFAT, subunit NF45						3.66		
Immunity	ISCW011373/B7Q5I1	Cniwi protein								-4.27
Immunity/Cell stress	ISCW022766/B7QC85	Tumor rejection antigen (gp96)			1.65					-4.41
Immunity/Cell stress	ISCW008184	Calreticulin			1.63					
Immunity/Cell stress	ISCW007552	Peroxinectin				3.88				
Cell stress	ISCW024062	Heat shock HSP20 protein, putative			-2.51					
Cell stress	ISCW024057	HSP70	-5.87							
Cell stress	ISCW015267	Heat shock protein, putative	-2.87							
Cell stress	ISCW001763	Heat shock HSP20 protein, putative	-2.25		-3.63					
Cell stress	ISCW024910	Heat shock protein	-1.75		-3.21					
Cell stress	ISCW015266	Heat shock HSP20 protein, putative	-1.55		-3.17					
Cell stress	ISCW002513	Alpha-crystallin B chain	-1.14							
Cell stress	ISCW024054	Heat shock protein 20	-0.85							
Cell stress	E9HNC6	Putative uncharacterized protein						4.98		
Cell stress	E0V9N7	Heat shock protein 70kDa					-4.79		-5.02	-4.54
Cell stress	B4MA19	GJ15754 OS					3.46			
Cell stress	C4MX30	90 kDa heat shock protein						-4.82		-4.12
Cell stress	D5KXW7	Heat shock protein 90						-4.95	-4.75	-4.54
Cell stress	ISCW016090/B7P1Z8	Heat shock protein								-5.04
Cell stress	ISCW009087/B7PYP5	Heat shock protein 90					-3.52			-3.28
Cell stress	ISCW017192/B7P8Q5	Hsp70								-2.34
Cell stress	ISCW014211/B7QI53	Apoptosis-promoting RNA-binding protein TIA-1/TIAR								-4.76
Cell stress	ISCW019519/B7PWC4	Poly [ADP-ribose] polymerase								-3.95
Cell stress	ISCW019764/B7PSW5	Programmed cell death 6-interacting protein								-3.95
Cell stress	ISCW003709/B7PGQ2	Calnexin								-3.75
Cell stress	ISCW012646/B7QEE0	Hypoxia up-regulated protein								-3.54
Cell stress	ISCW018779/B7PNU9	DnaJ domain and thioredoxin-containing protein								-3.54

Fig. 6 Transcripts and proteins putatively involved in immunity and cell stress in TBEV-infected IDE8 and IRE/CTVM19 cells. Statistically significantly differentially-expressed transcripts and differentially-represented proteins with a possible role in immunity and/or cell stress are listed and their levels of differential regulation in TBEV-infected IDE8 and IRE/CTVM19 cells at days 2 and 6 p.i. are shown. Green = up-regulation/over-representation; red = down-regulation/under-representation; black = no change

degraded before achieving a knockdown or target mRNAs being too transient [81]. In IRE/CTVM19 cells, knockdown of transcripts was generally less efficient and consistent than in IDE8 cells, ranging from 5-85 % silencing efficiency and between 6 and 12 replicates showing silencing, depending on the target transcript, over three independent experiments; silencing efficiencies are shown in Fig. 8a, b and c.

RNAi is probably the most important antiviral response in insects [9]. The importance of the RNAi response in the antiviral defence response in tick cells was recently confirmed by detecting specific viRNAs in tick cells infected with LGTV and observing a proviral effect upon silencing of orthologues of key members of the RNAi pathway (Ago 30 and Dcr 90) [38]. Although Ago 30 and Dcr 90 were not differentially expressed upon TBEV infection in the present study, they were included as positive controls. Both proteins are known to be involved in RNAi [38] and knockdown would be expected to result in an increase in levels of viral RNA as well as infectious virus. In IDE8 cells, silencing of Dcr 90 resulted in a significant increase in LGTV RNA levels and

silencing of Ago 30 resulted in a significant increase in levels of both LGTV RNA and infectious virus (Fig. 7d and e). In IRE/CTVM19 cells, significant increases in both LGTV RNA levels (Fig. 8d) and infectious virus (Fig. 8e) were observed following knockdown of both Ago 30 and Dcr 90. This confirms the role of RNAi as an antiviral response in tick cells.

Knockdown of ISCW022021, annotated as complement factor H, resulted in an increase in LGTV RNA and infectious virus in IDE8 cells (Fig. 7) but not in IRE/CTVM19 cells (Fig. 8). Complement Factor H, up-regulated on day 6 p.i. in IRE/CTVM19 cells (Fig. 6), functions in vertebrates as a negative regulator of the alternative pathway of the complement system and as a pattern recognition molecule binding with high efficiency to host-specific molecular signatures, such as heparin and sialic acid, thereby protecting uninfected cells from the complement system [84]. In vertebrates, the complement system is an important innate immune response against different families of viruses [85–87]. However some viruses, such as West Nile virus (WNV), are able to evade the complement system by binding
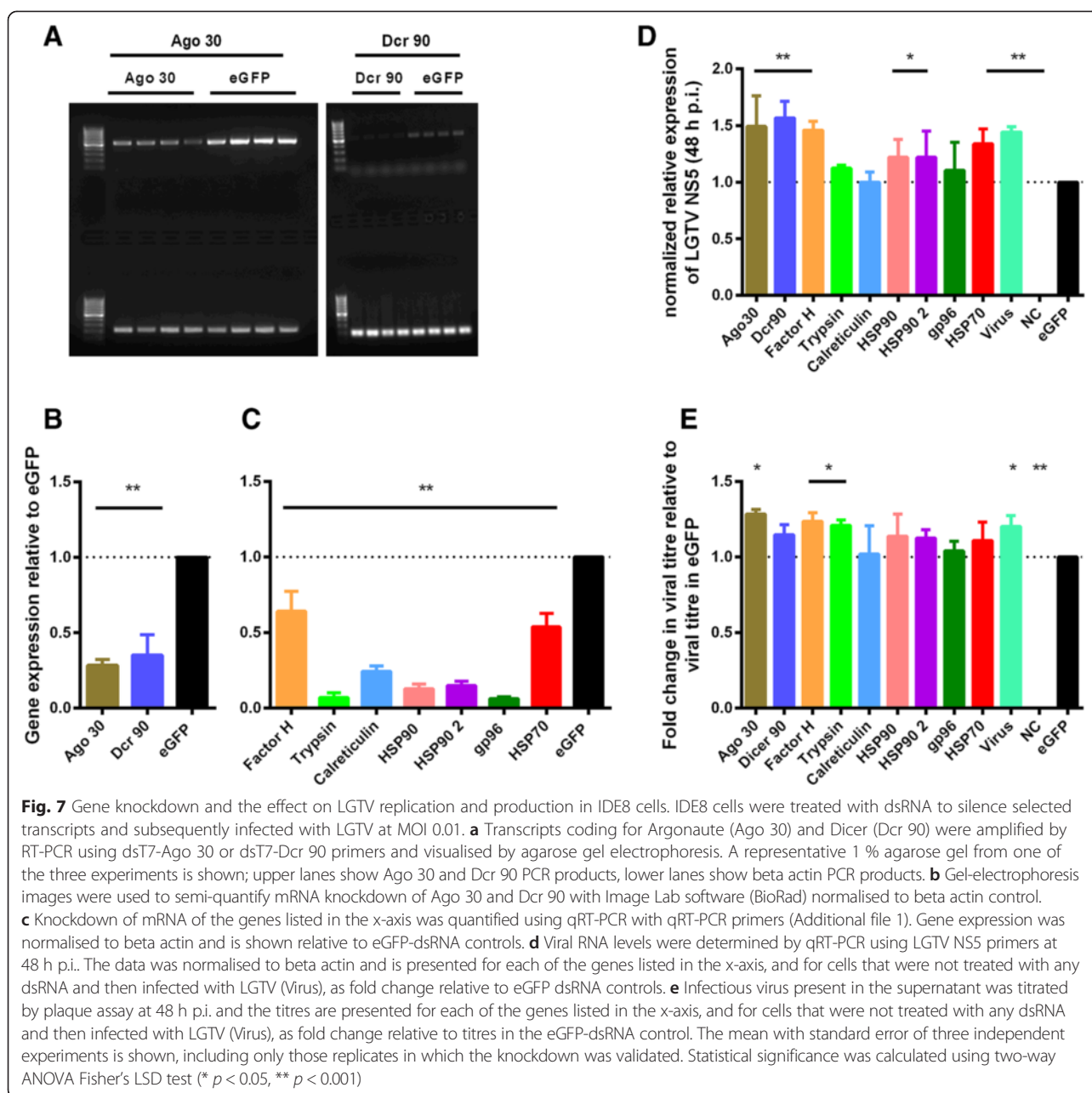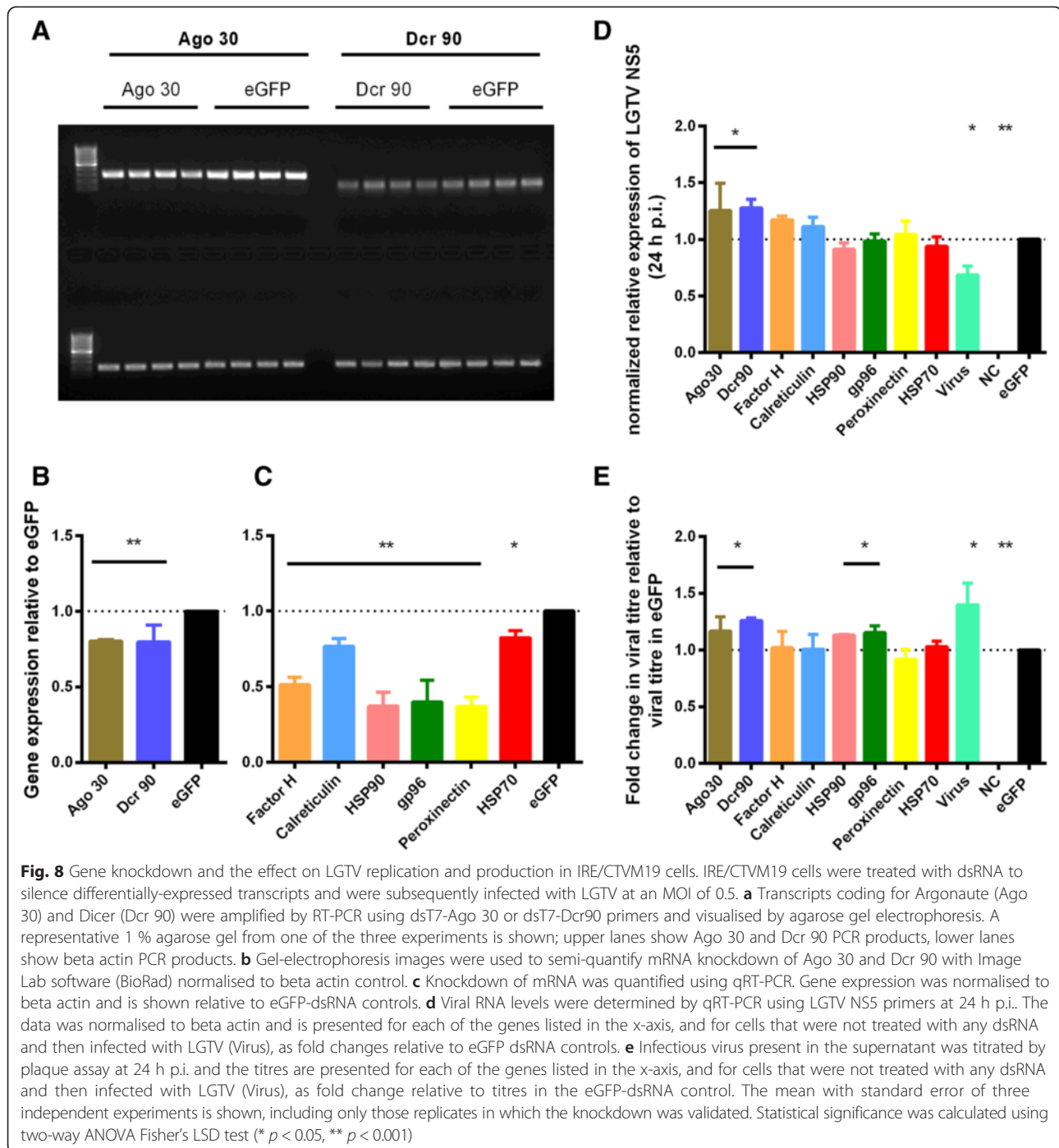
Weisheit *et al. Parasites & Vectors* (2015) 8:599

Page 16 of 26

Fig. 7 Gene knockdown and the effect on LGTV replication and production in IDE8 cells. IDE8 cells were treated with dsRNA to silence selected transcripts and subsequently infected with LGTV at MOI 0.01. **a** Transcripts coding for Argonaute (Ago 30) and Dicer (Dcr 90) were amplified by RT-PCR using dsT7-Ago 30 or dsT7-Dcr 90 primers and visualised by agarose gel electrophoresis. A representative 1 % agarose gel from one of the three experiments is shown; upper lanes show Ago 30 and Dcr 90 PCR products, lower lanes show beta actin PCR products. **b** Gel-electrophoresis images were used to semi-quantify mRNA knockdown of Ago 30 and Dcr 90 with Image Lab software (BioRad) normalised to beta actin control. **c** Knockdown of mRNA of the genes listed in the x-axis was quantified using qRT-PCR with qRT-PCR primers (Additional file 1). Gene expression was normalised to beta actin and is shown relative to eGFP-dsRNA controls. **d** Viral RNA levels were determined by qRT-PCR using LGTV NS5 primers at 48 h p.i.. The data was normalised to beta actin and is presented for each of the genes listed in the x-axis, and for cells that were not treated with any dsRNA and then infected with LGTV (Virus), as fold change relative to eGFP dsRNA controls. **e** Infectious virus present in the supernatant was titrated by plaque assay at 48 h p.i. and the titres are presented for each of the genes listed in the x-axis, and for cells that were not treated with any dsRNA and then infected with LGTV (Virus), as fold change relative to titres in the eGFP-dsRNA control. The mean with standard error of three independent experiments is shown, including only those replicates in which the knockdown was validated. Statistical significance was calculated using two-way ANOVA Fisher's LSD test (* $p < 0.05$, ** $p < 0.001$)

and recruiting Factor H, resulting in decreased complement activation and reduced targeting of virus-infected cells [88]. Although ticks have been shown to have a complement system, with all $\alpha 2$-macroglobulin family proteins, insect thioester-containing and macroglobulin-related proteins [89, 90], that functions against different types of bacteria [89, 91], nothing is known about the antiviral effect of the tick complement system.

If complement factor H interacts with LGTV in tick cells similarly to WNV in mammalian cells, a decrease in virus replication and/or production would be expected but the opposite was seen in the present study. The increase in viral RNA levels and infectious

virus in tick cells upon silencing of complement factor H might have resulted in exhaustion of the complement system and lack of any complement antiviral-activity. The fact that complement factor H was up-regulated in response to virus infection suggests an antiviral role, supported by the observed increase in viral RNA levels and infectious virus upon silencing of complement factor H. The designation of ISCW022021 as complement Factor H by the *Ixodes scapularis* Genome Project [92] might be misleading and, instead of being involved in the complement system, it might be involved in another antiviral innate immune response. Further sequence and functional analyses are required

Weisheit *et al. Parasites & Vectors* (2015) 8:599

Page 17 of 26

Fig. 8 Gene knockdown and the effect on LGTV replication and production in IRE/CTVM19 cells. IRE/CTVM19 cells were treated with dsRNA to silence differentially-expressed transcripts and were subsequently infected with LGTV at an MOI of 0.5. **a** Transcripts coding for Argonaute (Ago 30) and Dicer (Dcr 90) were amplified by RT-PCR using dsT7-Ago 30 or dsT7-Dcr90 primers and visualised by agarose gel electrophoresis. A representative 1 % agarose gel from one of the three experiments is shown; upper lanes show Ago 30 and Dcr 90 PCR products, lower lanes show beta actin PCR products. **b** Gel-electrophoresis images were used to semi-quantify mRNA knockdown of Ago 30 and Dcr 90 with Image Lab software (BioRad) normalised to beta actin control. **c** Knockdown of mRNA was quantified using qRT-PCR. Gene expression was normalised to beta actin and is shown relative to eGFP-dsRNA controls. **d** Viral RNA levels were determined by qRT-PCR using LGTV NS5 primers at 24 h p.i.. The data was normalised to beta actin and is presented for each of the genes listed in the x-axis, and for cells that were not treated with any dsRNA and then infected with LGTV (Virus), as fold changes relative to eGFP dsRNA controls. **e** Infectious virus present in the supernatant was titrated by plaque assay at 24 h p.i. and the titres are presented for each of the genes listed in the x-axis, and for cells that were not treated with any dsRNA and then infected with LGTV (Virus), as fold change relative to titres in the eGFP-dsRNA control. The mean with standard error of three independent experiments is shown, including only those replicates in which the knockdown was validated. Statistical significance was calculated using two-way ANOVA Fisher's LSD test (* $p < 0.05$, ** $p < 0.001$)

to determine the role of ISCW022021 within the tick cell innate immune response.

Silencing of HSP90 and HSP70 resulted in an increase in LGTV RNA levels in IDE8 cells (Fig. 7). This suggests that HSP90 and HSP70 might be involved in loading of siRNA duplexes into Ago 2, as observed in *Drosophila* [93]; thus knockdown of either protein would lead to an impairment of RNAi, which would result in reduction of degradation of viral RNA, as suggested by the higher viral RNA levels seen in the present study in cultures in which HSP90 and HSP70 were silenced, compared to unsilenced controls. It would be interesting to test whether simultaneous knockdown of both HSP70 and HSP90 would augment the increase in viral RNA levels. Knockdown of trypsin also resulted in a significant increase in LGTV production accompanied by a slight non-significant increase in viral RNA levels. The putative antiviral effect of trypsin might be due to its serine

Weisheit *et al. Parasites & Vectors* (2015) 8:599

Page 18 of 26

protease activity, since serine proteases are involved in the modulation of several immune signaling pathways [94–96] and, of these, one or more might mediate an antiviral role in tick cells.

In contrast to the results with IDE8 cells, in IRE/CTVM19 cells only silencing of Ago 30 and Dcr 90 resulted in significantly increased virus replication and production (Fig. 8). Silencing of HSP90 and gp96 in IRE/CTVM19 cells resulted in a significant increase in virus production without affecting LGTV RNA levels, suggesting an antiviral role for these proteins at the post-transcriptional level in this cell line. HSP90 and gp96 are both heat-shock proteins which are involved in folding of different client proteins. Inhibition of HSP90 in mammalian cells has been shown to block viral replication [97, 98] and this protein has been proposed to be an important factor in the replication of a wide spectrum of RNA viruses [98]. In the present study in tick cells, however, HSP90 seemed to be involved in the antiviral response with an inhibitory influence on virus RNA levels in IDE8 and at the post-translational level in IRE/CTVM19. The ER-based heat-shock protein gp96 is important for the folding of Toll-like receptors (TLRs) and integrins in mammals and *Drosophila* [99]. The putative antiviral role of gp96 observed in the present study might be due to its capacity for folding TLRs or other client proteins involved in the antiviral response, which upon silencing would cause an increase in virus production.

Silencing of complement factor H, which resulted in increased LGTV replication and production in IDE8 cells, did not show any effect in IRE/CTVM19 cells. This could be due to the less efficient and more variable silencing in the latter cell line, compared to IDE8 cells. Additionally the different responses of the two cell lines to LGTV infection could represent a cell line-specific response towards flavivirus infection; however most of the transcripts tested in silencing experiments were differentially expressed upon TBEV infection in IRE/CTVM19 but not in IDE8. The different responses could indicate a species-specific response since the two cell lines were derived from different tick species, or could be due to the heterogeneity of the cell lines [41] or presence of endogenous viruses. Both IDE8 and IRE/CTVM19 cells are persistently infected with endogenous viruses, St Croix River virus and unidentified reovirus-like particles respectively [100, 101], which could affect the innate immune response towards infection with another virus. The presence of an endogenous virus could either suppress or persistently activate certain immune responses thereby affecting silencing of genes and the effect on virus replication and production. Furthermore, each cell line might have a different timing in the response to virus infection, with IDE8 cells possibly activating a response faster than IRE/CTVM19, which could explain

the higher virus titres observed for IRE/CTVM19 in the TBEV growth curve experiment.

Interestingly, LGTV production in samples of both cell lines not treated with dsRNA prior to LGTV infection was significantly higher in comparison to samples treated with control dsRNA against eGFP, suggesting that dsRNA treatment alone triggers an antiviral immune response. This is in contrast to studies on mosquitoes and *Drosophila* in which an antiviral response, possibly RNAi, was shown to be triggered by virus-specific dsRNA but not by non-specific dsRNA [102, 103]. A possible explanation for this difference could be the presence of RNA-dependent RNA polymerase in ticks [21] that could be involved in boosting the non-specific antiviral immune response seen in tick cells against non-specific dsRNA. However, studies in other arthropod systems including sandfly cells [104], shrimp [105] and honey bees [106] also showed that non-specific dsRNA can trigger an antiviral state affecting virus infection. Interestingly, dsRNA encoding eGFP resulted in an increase in Dcr 2 levels in *Bombyx mori* [107], suggesting that Dcr 2 recognises dsRNA as a pathogen-associated molecular pattern, which might result in the expression of Vago, an interferon-like molecule inducing an antiviral state in neighbouring cells, as described in *Drosophila* and mosquitoes [108, 109]. Possible homologues of insect Dicers were recently identified in the *I. scapularis* genome and phylogenetic analysis suggests that Dcr 89 is a possible homologue of insect Dcr 2, whereas Dcr 90 is a possible homologue of Dcr 1 [38]. If Dcr 2 and Vago are also induced in tick cells upon addition of non-specific dsRNA, thereby causing an antiviral state in neighbouring uninfected cells and resulting in reduced virus infection levels in the culture overall as observed in the present study, this could suggest a non-specific antiviral response which recognises dsRNA as foreign in tick cells. Vago has been shown to be present within the *I. scapularis* genome [110]; it would therefore be interesting to investigate whether it has a similar function in ticks as it has in insects.

The observation that, in both tick cell lines, silencing of Ago 30, Dcr 90 and HSP90 resulted in increased LGTV NS5 expression and/or virus production strengthens the hypothesis that these proteins are involved in the antiviral response in tick cells. Additionally, the finding that silencing of complement factor H, trypsin and HSP70 in IDE8 and gp96 in IRE/CTVM19 resulted in a proviral effect is encouraging and warrants further experiments to elucidate their roles in the antiviral response in tick cells.

Other transcripts and proteins that may be involved in innate immunity

In addition to complement factor H and trypsin, which were grouped into the biological process group innate

Weisheit *et al. Parasites & Vectors* (2015) 8:599

Page 19 of 26

immunity and were functionally analysed in the previous section, several other transcripts and proteins with a possible role in the innate immune response of tick cells to virus infection were differentially expressed/represented. Those most likely to be involved in innate immunity are discussed below; others are discussed in Additional file 6.

Of the differentially-expressed transcripts in IDE8 cells, two were inferred by GO ontology descriptors to be involved in innate immunity: the class B scavenger receptor CD36 and the cysteine protease longipain (Fig. 6). CD36 is a surface receptor on tick haemocytes that is up-regulated upon bacterial infection in *H. longicornis*, where it is involved in granulocyte-mediated phagocytosis of *Escherichia coli* [111]. CD36 has also been suggested to be involved in the RNAi pathway [112]. RNAi is currently the only antiviral pathway known to be effective in ticks [38]. Up-regulation of CD36 in IDE8 cells upon TBEV infection is therefore intriguing and could be an indicator of up-regulation of the RNAi response. Longipain is present in and on the surface of lysosomes in the midgut of the tick *Haemaphysalis longicornis* and, in addition to playing a role in blood digestion, is involved in dose-dependent killing of *Babesia* parasites [113]. Longipain has a high homology to cathepsin B [113], which in mosquitoes is indirectly involved in defence responses against viruses by triggering apoptosis as observed during dengue virus (DENV) infection [83]. It is not known whether longipain has a similar function in ticks.

In IRE/CTVM19 cells, more transcripts with a potential link to an antiviral response were up-regulated than in IDE8 (Fig. 6). One of these, peroxinectin, up-regulated on day 6 p.i. (Fig. 6), is a cell adhesive peroxidase which is stored in haemocyte granules in crustaceans. Upon an immune stimulus, peroxinectin is released from cells by degranulation and is activated by serine proteases to stimulate cell adhesion, encapsulation, phagocytosis and peroxidase activity [114–117]. In the mud crab, white spot syndrome virus (WSSV) infection results in increased expression of peroxinectin within the first 48 h; this increase is associated with a latent period of WSSV infection, suggesting that peroxinectin is involved in the early defence response against this virus [118]. Furthermore, peroxinectin in crustaceans is associated with the prophenoloxidase (proPO) system, as both require the same activating enzyme, a trypsin-like serine protease [119, 120]. However in contrast to other arthropods, ticks are assumed to lack the proPO system, since no proPO-related gene has so far been identified [15, 18], although controversial reports of the existence of this innate immune response in ticks exist [121–123]. Interestingly, the serine protease trypsin was also up-regulated on day 6 in IRE/CTVM19 cells (Fig. 6).

At the protein level, in IDE8 on day 2 and IRE/CTVM19 on day 6, the 4SNc-Tudor (Tudor-SN) domain protein was under-represented. Tudor-SN is part of the RISC complex in *Drosophila*, *Caenorhabditis elegans* and mammals [124] and is involved in binding and possibly cleaving hyper-edited dsRNAs and miRNAs in *Xenopus laevis* and humans respectively [125, 126]. Tudor-SN is expressed, and suspected to be part of the RISC complex, in ticks [21]; it plays a role in tick feeding and the RNAi pathway but does not appear to be involved in innate responses to TBEV or LGTV [127].

In IRE/CTVM19 at day 6 p.i., Cniwi, a PIWI 1 protein, was under-represented. PIWI proteins are part of the piRNA pathway which was initially thought to protect germline cells from transposable elements in *Drosophila*. However, virus-specific piRNA molecules were found to be expressed for a variety of different viruses in *Drosophila* [128] and mosquitoes [129–132], suggesting a possible antiviral role for the piRNA pathway. In a recent study, the antiviral role of PIWI proteins was confirmed when knockdown of PIWI proteins resulted in an increase in Semliki Forest virus replication and production in mosquito cells [132]. It would be tempting to speculate that this pathway might also be important for the antiviral response against TBEV in tick cells. Under-representation of these two proteins in infected cells would be consistent with suppression of RNAi or perhaps customisation of the RNAi system to virus infection.

Other transcripts and proteins that may be involved in cell stress

In addition to HSP70, HSP90, gp96 and calreticulin, which were grouped into the biological process group cell stress and were functionally analysed above, several other transcripts and proteins involved in cell stress (Fig. 6) might also have an important role in the response of tick cells to virus infection. Those most likely to be involved in cell stress are discussed below; others are discussed in Additional file 6.

Heat-shock proteins are the most abundant and ubiquitous soluble proteins in all forms of life and are involved in a multitude of housekeeping functions essential for cell survival [133]. Studies on tick cell responses to bacterial infection revealed pathogen- and species-specific differences in the expression of HSPs [71, 134]. HSP20 and the small HSP alpha-crystallin B chain were under-represented in both IDE8 and IRE/CTVM19 cells on day 2 p.i. at the transcript level (Fig. 6). In vertebrate cells the generation of large amounts of viral proteins leads, through the unfolded protein response of the endoplasmic reticulum (ER), to cell stress and an increase in HSPs [135, 136]. However, there is evidence that in vertebrates some HSPs may be controlled to disrupt virus replication.

Weisheit *et al. Parasites & Vectors* (2015) 8:599

Page 20 of 26

Other proteins involved in cell stress include the three ER chaperones calreticulin, calnexin and gp96. In mammalian cells, calreticulin, a soluble lectin-like chaperone, is involved in Ca^{2+} homeostasis and is important for the processing and maturation of viral glycoproteins [137, 138]. Knockdown of calreticulin in Vero cells reduces the yield of infectious DENV particles [139]. Similarly, knockdown of calreticulin in *Babesia bigemina*-infected *Rhipicephalus microplus* ticks reduced the level of this protozoan parasite [140]. Calnexin, a membrane-bound chaperone of the ER similar to calreticulin, that was up-regulated at the transcript level in IRE/CTVM19 at day 2 p.i., has been shown to be important for viral glycoprotein processing and maturation [138]. In Vero cells, both calnexin and calreticulin have been shown to be important for the production of infectious DENV particles by interacting with the glycosylated DENV E protein, facilitating proper folding and assembly of DENV proteins [139]. Under-representation of calnexin in IRE/CTVM19 cells at day 6 could be interpreted as an antiviral response selected to curtail virus production.

The tumour-rejection antigen gp96 which was up-regulated in IRE/CTVM19 cells on day 2 p.i. and under-represented at the protein level on day 6 p.i. (Fig. 6), is important in mammalian cells for chaperoning TLRs and integrins. Up-regulation of ER chaperones such as gp96 and calreticulin upon virus infection could be a sign of ER stress, which in mammals can lead to triggering of apoptosis or the unfolded protein response leading to inhibition of translation or apoptosis [141]. There is currently no published information on translational inhibition or regulation of the unfolded protein response in ticks.

Transcripts and proteins that may be involved in nucleic acid processing

Several transcripts and proteins involved in nucleic acid processing functions, such as replication, transcription, processing of nucleic acid or translation, were differently expressed upon TBEV infection in tick cells. This is not surprising since viruses require the nucleic acid processing machinery of the host to amplify their genome and many viruses perturb these processes in cells or manipulate them for their own advantage. Differential regulation of this group of transcripts and proteins was also observed in several other transcriptomic and proteomic studies of arthropods upon virus infection (e.g. [65, 66, 70, 83, 142]). Many of these transcripts and proteins might be involved in replication and translation of TBEV in tick cells and might be interesting targets for future research to understand virus infections in tick cells and ticks. Histones and elongation factor (EF)-1 alpha

were differentially represented at both the transcript and protein levels. Several viral proteins have been shown to target histone proteins and host chromatin to interfere with host gene expression by various mechanisms and for different purposes [143]. The C protein of DENV for example targets core histones during infection to disrupt the host cell genetic machinery in favour of viral replication [144]. EF-1 alpha was up-regulated and shown to be important for virus replication in mammalian and mosquito cells during DENV and WNV infection [145–147]. Interestingly, the eukaryotic translation initiation factor eIF3 was under-represented at the protein level in IDE8 cells at day 6 p.i. and in IRE/CTVM19 cells at day 2 p.i. as observed during WNV infection in Vero cells [148]. This is surprising since eIF3 together with the 40S ribosomal subunit, also under-represented in the present study, have been shown to be important during the initial phase of protein synthesis, and flaviviruses are thought to prevent host cell protein shutoff, at least in mammalian cells [149]. However, a recent study using yellow fever virus (YFV) in mammalian cells found that NS5 interacts with eIF3L, a subunit of eIF3, and that overexpression of this subunit facilitates YFV translation but does not affect global protein synthesis [150]. This suggests that eIF3 is also important in tick cells for replication of flaviviruses but that down-regulation of this initiation factor might have an antiviral effect. Furthermore EF-2, t-RNA synthetasen and several other participants in the translation of RNA were also under-represented in the present study.

Another interesting observation is that in both cell lines at both time-points DEAD-box RNA helicase was up-regulated at the protein level which was also seen at the transcriptional level for DENV in *Aedes aegypti* cells [69]. This is interesting, since Dcr 2, a DExD/H-box helicase, was shown to be capable of sensing viral dsRNA in *Drosophila* leading to the production of possibly antiviral molecules [108].

Conclusions

This is the first study that combines transcriptomic and proteomic analysis to investigate the response of tick cells to infection with a medically important virus. Despite the limitations imposed on the study by biosafety considerations, the findings represent a valuable baseline for future research. Tick cells responded to TBEV infection by changing the expression and/or representation of cellular genes and proteins involved in a variety of biological processes, including metabolism, transport, protein folding, nucleic acid processing, signaling, cell stress and immunity, revealing a complex response of tick cells to virus infection at both the transcriptome and proteome levels, as observed in other arthropods upon virus

Weisheit *et al. Parasites & Vectors* (2015) 8:599

Page 21 of 26

infection [65, 66, 69, 70, 83, 142, 148, 151–153]. Some of these transcripts and/or proteins, such as those involved in nucleic acid processing, transport, metabolism, protein folding and cell stress, have also been identified in other species as important host cell factors exploited by viruses to support their life cycle in processes including endocytosis, trafficking, viral RNA transcription and translation and virus maturation. Further analyses of these transcripts/proteins using techniques such as Western blotting, although limited by the lack of specific antibodies to tick proteins, might reveal specific factors required for successful infection, replication and production of viruses in ticks and tick cell lines. The dataset created in the present study represents an important starting point for elucidating the viral life cycle and virus-vector relationships.

Several of the identified transcripts and/or proteins have a possible role in immune-related pathways such as the ubiquitin-proteasome pathway, phagocytosis, the complement system, the piRNA pathway and the unfolded protein response. It is obvious from the present study that RNAi is not the only mechanism involved in the antiviral defence response of ticks and that further research is required to elucidate the cellular mechanisms behind virus infection in tick cell lines and ticks. While some of the changes observed upon virus infection could be a response to any microorganism or to cell stress, others appear to be more specific to virus infection, including a Cniwi protein and the 4SNc Tudor domain protein, which are components of the RNAi pathway. Therefore tick cells seem to be able to respond differently to viral and bacterial infection. This is not surprising since tick cells have been shown to be able to raise a specific response against certain bacterial infections [89, 91].

An unexpected but interesting observation was the down-regulation/under-representation of the heat-shock proteins upon TBEV infection in both tick cell lines. This is surprising since vertebrate and invertebrate HSPs are usually up-regulated upon virus infection and some viruses exploit the presence of HSPs to support virus infection [135, 136]. However, HSPs might also have an antiviral effect due to their implication in loading siRNAs into the RISC complex in *Drosophila*. Thus the down-regulation of HSPs might either be a cellular innate immune response protecting the cell by possibly preventing correct folding of the large number of viral proteins, thereby reducing the production of viral particles, or a response induced by the virus to prevent an efficient RNAi response. Knockdown of the RNAi components Ago 30, Dcr 90, the putative complement component complement factor H, the serine protease trypsin and the HSPs HSP90, HSP70 and gp96, suggests a role for these in the antiviral response of tick cells.

Overall the two cell lines showed a complex expression pattern upon TBEV infection, with differences in expression when compared to each other at both the transcript and protein levels (Fig. 6). These differences could be caused by the necessity of using different methods used to assemble the transcriptomic data, or could represent cell line-specific responses to TBEV infection. One cell line might react more slowly in response to virus infection than the other. Alternatively the response might be species-specific, since the two cell lines are derived from different tick species. Furthermore, both cell lines are heterogeneous, with a range of different cell types present within each culture which could be responding differently to virus infection.

This study enhances the understanding of viral infection of tick cells by identifying transcripts and proteins which may have a role in the innate antiviral defence response of ticks by augmenting or limiting virus production. This preliminary knowledge can be used in future studies to identify important host cell factors required for viral infection, as well as elucidating the innate immune response of tick cells to virus infection.

Additional files

Additional file 1: List of primers used in the quantification of TBEV infection, for validation of differential transcript expression and for preparation of dsRNA for gene knockdown. (DOCX 22 kb)

Additional file 2: Protein identification after proteomics analysis. (XLS 461 kb)

Additional file 3: TBEV infection levels in mock-infected and TBEV-infected tick cells. Numbers of copies of TBEV NS5 were determined by qRT-PCR using NS5 primers and the linearised plasmid pJET-NS5 to create a standard curve. Copy numbers were normalised to 1 μg of total RNA. The limit of detection was derived from the number of NS5 copies in the highest dilution which was still detectable with a variance less than one Ct and was normalised to 1 μg of total RNA. (A) IDE8 infected and mock-infected (control) at days 2 (2d) and 6 (6d) p.i. (B) IRE/CTVM19 infected and mock-infected (control) at days 2 and 6 p.i.. Error bars are standard deviations. Samples marked with + passed both RNA and protein quality checks and were used in transcriptomic and proteomic analyses.

Additional file 4: Validation by qRT-PCR of RNA-Seq data for TBEV-infected IDE8 and IRE/CTVM19 cells. The fold changes in transcript expression in pooled IDE8 (A) and IRE/CTVM19 (B) samples from RNA-Seq data calculated by DESeq in R at days 2 (2d) and 6 (6d) p.i. were compared to the average fold change obtained by qRT-PCR in 2–3 individual biological replicate samples. The dotted line at fold change 1 represents the cut-off for differential expression. Error bars are standard error of the mean.

Additional file 5: Differential expression levels of transcripts in LGTV-infected IDE8 and IRE/CTVM19 cells. The fold changes in transcript expression in IDE8 (A) and IRE/CTVM19 (B) samples infected with LGTV at MOI 5 at days 2 and 6 p.i. were determined by qRT-PCR. The mean of three individual biological replicate samples at days 2 (2d) and 6 (6d) p.i. is depicted. The dotted line at fold change 1 represents the cut-off for differential expression. Error bars are standard error of the mean.

Additional file 6: Discussion of additional transcripts and proteins that may be involved in innate immunity and cell stress [154-181]. (DOCX 16 kb)

Weisheit *et al. Parasites & Vectors* (2015) 8:599

Page 22 of 26

Author details
[1]The Roslin Institute and Royal (Dick) School of Veterinary Studies, University of Edinburgh, Easter Bush, Midlothian, Scotland EH25 9RG, UK. [2]The Pirbright Institute, Ash Road, Pirbright, Surrey GU24 0NF, UK. [3]SaBio. Instituto de Investigación en Recursos Cinegéticos IREC-CSIC-UCLM-JCCM, Ronda de Toledo s/n, Ciudad Real 13005, Spain. [4]Faculty of Science, University of South Bohemia and Biology Centre, Institute of Parasitology, Czech Academy of Sciences, Branisovska 31, České Budějovice (Budweis) 37005, Czech Republic. [5]Veterinary Research Institute, Hudcova 70, Brno 62100, Czech Republic. [6]Department of Veterinary Pathobiology, Center for Veterinary Health Sciences, Oklahoma State University, Stillwater, OK 74078, USA. [7]Institute for Cancer Research, The Norwegian Radium Hospital, Oslo University Hospital, Oslo 0377, Norway.

References
1. Jongejan F, Uilenberg G. The global importance of ticks. Parasitology. 2004; 129:S3–14.
2. Vaccines against tick-borne encephalitis. WHO position paper – recommendations. Vaccine. 2011;29:8769–70.
3. Süss J. Tick-borne encephalitis 2010: Epidemiology, risk areas, and virus strains in Europe and Asia — An overview. Ticks Tick Borne Dis. 2011;2:2–15.
4. Lindquist L, Vapalahti O. Tick-borne encephalitis. Lancet. 2008;371:1861–71.
5. Dobler G, Gniel D, Petermann R, Pfeffer M. Epidemiology and distribution of tick-borne encephalitis. Wien Med Wochenschr. 2012;162:230–8.
6. Smith CE. A virus resembling Russian spring–summer encephalitis virus from an Ixodid tick in Malaya. Nature. 1956;178:581–2.
7. Price WH, Thind IS, Teasdall RD, O'Leary W. Vaccination of human volunteers against Russian spring-summer (RSS) virus complex with attenuated Langat E5 virus. Bull World Hlth Org. 1970;42:89–94.
8. Price WH, Thind IS. Immunization of mice against Russian spring-summer virus complex and monkeys against Powassan virus with attenuated Langat E5 virus. Am J Trop Med Hyg. 1973;22:100–8.
9. Blair CD. Mosquito RNAi is the major innate immune pathway controlling arbovirus infection and transmission. Future Microbiol. 2011;6:265–77.
10. Donald CL, Kohl A, Schnettler E. New insights into control of arbovirus replication and spread by insect RNA interference pathways. Insects. 2012;3:511–31.
11. Fragkoudis R, Attarzadeh-Yazdi G, Nash AA, Fazakerley JK, Kohl A. Advances in dissecting mosquito innate immune responses to arbovirus infection. J Gen Virol. 2009;90:2061–72.
12. Kingsolver MB, Huang Z, Hardy RW. Insect antiviral innate immunity: pathways, effectors, and connections. J Mol Biol. 2013;425:4921–36.
13. Merkling SH, van Rij RP. Beyond RNAi: antiviral defense strategies in *Drosophila* and mosquito. J Insect Physiol. 2013;59:159–70.
14. Rückert C, Bell-Sakyi L, Fazakerley J, Fragkoudis R. Antiviral responses of arthropod vectors: an update on recent advances. VirusDisease. 2014;25:249–60.
15. Kopáček P, Hajdusek O, Buresová V, Daffre S. Tick innate immunity. Adv Exp Med Biol. 2010;708:137–62.
16. Smith AA, Pal U. Immunity-related genes in *Ixodes scapularis* – perspectives from genome information. Front Cell Infect Microbiol. 2014;4:116. doi:10.3389/fcimb.2014.00116.
17. Taylor D. Innate immunity in ticks : a review. Acarol Soc Japan. 2006;15:109–27.
18. Hajdušek O, Šíma R, Ayllón N, Jalovecká M, Perner J, de la Fuente J, et al. Interaction of the tick immune system with transmitted pathogens. Front Cell Infect Microbiol. 2013;3:26. doi:10.3389/fcimb.2013.00026.
19. Ayllón N, Villar M, Galindo RC, Kocan KM, Šíma R, López JA, et al. Systems biology of tissue-specific response to *Anaplasma phagocytophilum* reveals differentiated apoptosis in the tick vector *Ixodes scapularis*. PLoS Genet. 2015;11, e1005120. Available: http://dx. plos.org/10.1371/journal.pgen.1005120.
20. Liu L, Dai J, Zhao YO, Narasimhan S, Yang Y, Zhang L, et al. *Ixodes scapularis* JAK-STAT pathway regulates tick antimicrobial peptides, thereby controlling the agent of human granulocytic anaplasmosis. J Infect Dis. 2012;206:1233–41.
21. Kurscheid S, Lew-Tabor AE, Rodriguez Valle M, Bruyeres AG, Doogan VJ, Munderloh UG, et al. Evidence of a tick RNAi pathway by comparative genomics and reverse genetics screen of targets with known loss-of-function phenotypes in *Drosophila*. BMC Mol Biol. 2009;10:1–21.
22. Zivkovic Z, Torina A, Mitra R, Alongi A, Scimeca S, Kocan KM, et al. Subolesin expression in response to pathogen infection in ticks. BMC Immunol. 2010; 11:7. doi:10.1186/1471-2172-11-7.
23. De la Fuente J, Kocan KM, Blouin EF, Zivkovic Z, Naranjo V, Almazán C, et al. Functional genomics and evolution of tick-*Anaplasma* interactions and vaccine development. Vet Parasitol. 2010;167:175–86.
24. Severo MS, Choy A, Stephens KD, Sakhon OS, Chen G, Chung D-WD, et al. The E3 ubiquitin ligase XIAP restricts *Anaplasma phagocytophilum* colonization of *Ixodes scapularis* ticks. J Infect Dis. 2013;208:1830–40.
25. Garcia S, Billecocq A, Crance J-M, Munderloh UG, Garin D, Bouloy M. Nairovirus RNA sequences expressed by a Semliki Forest virus replicon induce RNA interference in tick cells. J Virol. 2005;79:8942–7.
26. Garcia S, Billecocq A, Crance J-M, Prins M, Garin D, Bouloy M. Viral suppressors of RNA interference impair RNA silencing induced by a Semliki Forest virus replicon in tick cells. J Gen Virol. 2006;87:1985–9.
27. Blouin EF, Manzano-Roman R, de la Fuente J, Kocan KM. Defining the role of subolesin in tick cell culture by use of RNA interference. Ann N Y Acad Sci. 2008;1149:41–4.
28. De la Fuente J, Kocan KM, Almazán C, Blouin EF. RNA interference for the study and genetic manipulation of ticks. Trends Parasitol. 2007;23:427–33.
29. Barry G, Alberdi P, Schnettler E, Weisheit S, Kohl A, Fazakerley JK, et al. Gene silencing in tick cell lines using small interfering or long double-stranded RNA. Exp Appl Acarol. 2013;59:319–38.
30. Kopecký J, Stanková I. Interaction of virulent and attenuated tick-borne encephalitis virus strains in ticks and a tick cell line. Folia Parasitol (Praha). 1998;45:245–50.
31. Lawrie CH, Uzcátegui NY, Armesto M, Bell-Sakyi L, Gould EA. Susceptibility of mosquito and tick cell lines to infection with various flaviviruses. Med Vet Entomol. 2004;18:268–74.
32. Senigl F, Kopecký J, Grubhoffer L. Distribution of E and NS1 proteins of TBE virus in mammalian and tick cells. Folia Microbiol (Praha). 2004;49:213–6.

69

Weisheit *et al. Parasites & Vectors* (2015) 8:599

Page 23 of 26

33. Senigl F, Grubhoffer L, Kopecký J. Differences in maturation of tick-borne encephalitis virus in mammalian and tick cell line. Intervirology. 2006;49:239–48.

34. Růzek D, Bell-Sakyi L, Kopecký J, Grubhoffer L. Growth of tick-borne encephalitis virus (European subtype) in cell lines from vector and non-vector ticks. Virus Res. 2008;137:142–6.

35. Schrauf S, Mandl CW, Bell-Sakyi L, Skern T. Extension of flavivirus protein C differentially affects early RNA synthesis and growth in mammalian and arthropod host cells. J Virol. 2009;83:11201–10.

36. Offerdahl DK, Dorward DW, Hansen BT, Bloom ME. A three-dimensional comparison of tick-borne flavivirus infection in mammalian and tick cell lines. PLoS One. 2012;7, e47912. doi:10.1371/journal.pone.0047912.

37. Yoshii K, Yanagihara N, Ishizuka M, Sakai M, Kariwa H. N-linked glycan in tick-borne encephalitis virus envelope protein affects viral secretion in mammalian cells, but not in tick cells. J Gen Virol. 2013;94:2249–58. Available from: http://www.ncbi.nlm.nih.gov/pubmed/23824303.

38. Schnettler E, Tykalová H, Watson M, Sharma M, Sterken MG, Obbard DJ, et al. Induction and suppression of tick cell antiviral RNAi responses by tick-borne flaviviruses. Nucleic Acids Res. 2014;42:9436–46.

39. Munderloh UG, Liu Y, Wang M, Chen C, Kurtti TJ. Establishment, maintenance and description of cell lines from the tick *Ixodes scapularis*. J Parasitol. 1994;80:533–43.

40. Munderloh UG, Kurtti TJ. Formulation of medium for tick cell culture. Exp Appl Acarol. 1989;7:219–29.

41. Bell-Sakyi L, Zweygarth E, Blouin EF, Gould EA, Jongejan F. Tick cell lines: tools for tick and tick-borne disease research. Trends Parasitol. 2007;230:450–7.

42. Bell-Sakyi L. *Ehrlichia ruminantium* grows in cell lines from four ixodid tick genera. J Comp Pathol. 2004;130:285–93.

43. Kozuch O, Mayer V. Pig kidney epithelial (PS) cells: a perfect tool for the study of flaviviruses and some other arboviruses. Acta Virol. 1975;19:498.

44. De Madrid AT, Porterfield JS. A simple micro-culture method for the study of group B arboviruses. Bull World Hlth Org. 1969;40:113–21.

45. Růzek D, Vancová M, Tesarová M, Ahantarig A, Kopecký J, Grubhoffer L. Morphological changes in human neural cells following tick-borne encephalitis virus infection. J Gen Virol. 2009;90:1649–58.

46. Kim D, Pertea G, Trapnell C, Pimentel H, Kelley R, Salzberg SL. TopHat2: accurate alignment of transcriptomes in the presence of insertions, deletions and gene fusions. Genome Biol. 2013;14:R36. doi:10.1186/gb-2013-14-4-r36.

47. Li H, Durbin R. Fast and accurate short read alignment with Burrows-Wheeler transform. Bioinformatics. 2009;25:1754–60.

48. Sonenshine DE, Bissinger BW, Egekwu N, Donohue KV, Khalil SM, Roe RM. First transcriptome of the testis-vas deferens-male accessory gland and proteome of the spermatophore from *Dermacentor variabilis* (Acari: Ixodidae). PLoS One. 2011;6, e24711. doi:10.1371/journal.pone.0024711.

49. Francischetti IM, Anderson JM, Manoukis N, Pham VM, Ribeiro JM. An insight into the sialotranscriptome and proteome of the coarse bontlegged tick, *Hyalomma marginatum rufipes*. J Proteomics. 2011;74:2892–908.

50. Schicht S, Qi W, Poveda L, Strube C. Whole transcriptome analysis of the poultry red mite *Dermanyssus gallinae* (De Geer, 1778). Parasitology. 2014; 141:336–46.

51. Villar M, Popara M, Ayllón N, de Mera IG F, Mateos-Hernández L, Galindo RC, et al. A systems biology approach to the characterization of stress response in *Dermacentor reticulatus* tick unfed larvae. PLoS One. 2014;9, e89564. doi: 10.1371/journal.pone.0089564.

52. Anders S, Huber W. Differential expression analysis for sequence count data. Genome Biol. 2010;11:R106. doi:10.1186/gb-2010-11-10-r106.

53. Anders S, Pyl PT, Huber W. HTSeq - A Python framework to work with high-throughput sequencing data. Bioinformatics. 2015;31:166–9.

54. Conesa A, Götz S, García-Gómez JM, Terol J, Talón M, Robles M. Blast2GO: a universal tool for annotation, visualization and analysis in functional genomics research. Bioinformatics. 2005;21:3674–6.

55. Shevchenko A, Tomas H, Havlis J, Olsen JV, Mann M. In-gel digestion for mass spectrometric characterization of proteins and proteomes. Nat Protoc. 2006;1:2856–60.

56. Popara M, Villar M, Mateos-Hernández L, de Mera IGF, Marina A, del Valle M, et al. Lesser protein degradation machinery correlates with higher BM86 tick vaccine efficacy in *Rhipicephalus annulatus* when compared to *Rhipicephalus microplus*. Vaccine. 2013;31:4728–35.

57. Whelan JA, Russel NB, Whelan MA. A method for the absolute quantification of cDNA using real-time PCR. J Immunol Methods. 2003;278:261–9.

58. Gehrke R, Ecker M, Aberle SW, Allison SL, Heinz FX, Mandl CW. Incorporation of tick-borne encephalitis virus replicons into virus-like particles by a packaging cell line. J Virol. 2003;77:8924–33.

59. Livak KJ, Schmittgen TD. Analysis of relative gene expression data using real-time quantitative PCR and the 2(−Delta Delta C(T)) Method. Methods. 2001;25:402–8.

60. Schmittgen TD, Livak KJ. Analyzing real-time PCR data by the comparative CT method. Nat Protoc. 2008;3:1101–8.

61. Bhat BKM, Yunker CE. Susceptibility of a tick cell line (*Dermacentor parumapertus* Neumann) to infection with arboviruses. In: Kurstak E, editor. Arctic and Tropical arboviruses. New York, NY: Academic Press; 1979. p. 263–75.

62. Leake CJ, Pudney M, Varma M. Studies on arboviruses in established tick cell lines. In: Kurstak E, Maramorosch K, Dubendorfer A, editors. Invertebrate systems *in vitro*. Amsterdam: Elsevier/North Holland Biomedical Press; 1980. p. 327–35.

63. Rehacek J. Arthropod cell cultures in studies of tick-borne togaviruses and orbiviruses in Central Europe. In: Yunker CE, editor. Arboviruses in arthropod cells *in vitro*, vol. I. Boca Raton: CRC Press; 1987. p. 115–32.

64. Wallner G, Mandl CW, Kunz C, Heinz FX. The flavivirus 3'-noncoding region: extensive size heterogeneity independent of evolutionary relationships among strains of tick-borne encephalitis virus. Virology. 1995;213:169–78.

65. Bonizzoni M, Dunn WA, Campbell CL, Olson KE, Marinotti O, James AA. Complex modulation of the *Aedes aegypti* transcriptome in response to dengue virus infection. PLoS One. 2012;7, e50512. doi:10.1371/journal.pone.0050512.

66. McNally KL, Mitzel DN, Anderson JM, Ribeiro JMC, Valenzuela JG, Myers TG, et al. Differential salivary gland transcript expression profile in *Ixodes scapularis* nymphs upon feeding or flavivirus infection. Ticks Tick Borne Dis. 2012;3:18–26.

67. De La Fuente J, Blouin EF, Manzano-Roman R, Naranjo V, Almazán C, Pérez de la Lastra JM, et al. Functional genomic studies of tick cells in response to infection with the cattle pathogen, *Anaplasma marginale*. Genomics. 2007; 90:712–22.

68. Gibson AK, Smith Z, Fuqua C, Clay K, Colbourne JK. Why so many unknown genes? Partitioning orphans from a representative transcriptome of the lone star tick *Amblyomma americanum*. BMC Genomics. 2013;14:135. doi:10.1186/1471-2164-14-135.

69. Sim S, Dimopoulos G. Dengue virus inhibits immune responses in *Aedes aegypti* cells. PLoS One. 2010;5, e10678. doi:10.1371/journal.pone.0010678.

70. Zhang M, Zheng X, Wu Y, Gan M, He A, Li Z, et al. Differential proteomics of *Aedes albopictus* salivary gland, midgut and C6/36 cell induced by dengue virus infection. Virology. 2013;444:109–18.

71. Villar M, Ayllón N, Busby AT, Galindo RC, Blouin EF, Kocan KM, et al. Expression of heat shock and other stress response proteins in ticks and cultured tick cells in response to *Anaplasma* spp. infection and heat shock. Int J Proteomics. 2010;2010:657261. doi:10.1155/2010/657261.

72. Villar M, Torina A, Nuñez Y, Zivkovic Z, Marina A, Alongi A, et al. Application of highly sensitive saturation labeling to the analysis of differential protein expression in infected ticks from limited samples. Proteome Sci. 2010;8:43. doi:10.1186/1477-5956-8-43.

73. Evans V, Barker G, Heesom K, Fan J, Bessant C, Matthews D. *De novo* derivation of proteomes from transcriptomes for transcript and protein identification. Nat Methods. 2012;9:1207–11.

74. Mudenda L, Pierlé SA, Turse JE, Scoles GA, Purvine SO, Nicora CD, et al. Proteomics informed by transcriptomics identifies novel secreted proteins in *Dermacentor andersoni* saliva. Int J Parasitol. 2014;44:1029–37.

75. Nookaew I, Papini M, Pornputtapong N, Scalcinati G, Fagerberg L, Uhlén M, et al. A comprehensive comparison of RNA-Seq-based transcriptome analysis from reads to differential gene expression and cross-comparison with microarrays: a case study in *Saccharomyces cerevisiae*. Nucleic Acids Res. 2012;40:10084–97.

76. Devonshire AS, Sanders R, Wilkes TM, Taylor MS, Foy CA, Huggett JF. Application of next generation qPCR and sequencing platforms to mRNA biomarker analysis. Methods. 2013;59:89–100.

77. Hegedus Z, Zakrzewska A, Agoston VC, Ordas A, Rácz P, Mink M, et al. Deep sequencing of the zebrafish transcriptome response to mycobacterium infection. Mol Immunol. 2009;46:2918–30.

78. Zeng D, Chen X, Xie D, Zhao Y, Yang C, Li Y, et al. Transcriptome analysis of Pacific white shrimp (*Litopenaeus vannamei*) hepatopancreas in response to Taura syndrome Virus (TSV) experimental infection. PLoS One. 2013;8, e57515. doi:10.1371/journal.pone.0057515.

79. Zhu J-Y, Yang P, Zhang Z, Wu G-X, Yang B. Transcriptomic immune response of *Tenebrio molitor* pupae to parasitization by *Scleroderma guani*. PLoS One. 2013;8, e54411. doi:10.1371/journal.pone.0054411.

80. Price WH, Parks JJ, Ganaway J, O'Leary W, Lee R. The ability of an attenuated isolate of Langat virus to protect primates and mice against other members of the Russian spring-summer virus complex. Am J Trop Med Hyg. 1963;12:787–99.

81. Bellés X. Beyond *Drosophila*: RNAi *in vivo* and functional genomics in insects. Annu Rev Entomol. 2010;55:111–28.

82. Terenius O, Papanicolaou A, Garbutt JS, Eleftherianos I, Huvenne H, Kanginakudru S, et al. RNA interference in Lepidoptera: an overview of successful and unsuccessful studies and implications for experimental design. J Insect Physiol. 2011;57:231–45.

83. Sim S, Ramirez JL, Dimopoulos G. Dengue virus infection of the *Aedes aegypti* salivary gland and chemosensory apparatus induces genes that modulate infection and blood-feeding behavior. PLoS Pathog. 2012;8, e1002631. doi:10.1371/journal.ppat.1002631.

84. Makou E, Herbert AP, Barlow PN. Functional anatomy of complement factor H. Biochemistry. 2013;52:3949–62.

85. Blue CE, Spiller OB, Blackbourn DJ. The relevance of complement to virus biology. Virology. 2004;319:176–84.

86. Favoreel HW. Virus complement evasion strategies. J Gen Virol. 2003;84:1–15.

87. Lachmann PJ, Davies A. Complement and immunity to viruses. Immunol Rev. 1997;159:69–77.

88. Chung KM, Liszewski MK, Nybakken G, Davis AE, Townsend RR, Fremont DH, et al. West Nile virus nonstructural protein NS1 inhibits complement activation by binding the regulatory protein factor H. Proc Natl Acad Sci U S A. 2006;103:19111–6.

89. Buresova V, Hajdusek O, Franta Z, Loosova G, Grunclova L, Levashina EA, et al. Functional genomics of tick thioester-containing proteins reveal the ancient origin of the complement system. J Innate Immun. 2011;3:623–30.

90. Kopacek P, Hajdusek O, Buresova V. Tick as a model for the study of a primitive complement system. In: Mylonakis E, Ausubel FM, Gilmore M, Casadevall A, editors. Recent advances on model hosts. New York, NY: Springer New York; 2012. p. 83–93.

91. Buresova V, Hajdusek O, Franta Z, Sojka D, Kopacek P. IrAM—An alpha2-macroglobulin from the hard tick *Ixodes ricinus*: characterization and function in phagocytosis of a potential pathogen *Chryseobacterium indologenes*. Dev Comp Immunol. 2009;33:489–98.

92. Hill CA, Wikel SK. The *Ixodes scapularis* Genome Project: an opportunity for advancing tick research. Trends Parasitol. 2005;21:151–3.

93. Iwasaki S, Kobayashi M, Yoda M, Sakaguchi Y, Katsuma S, Suzuki T, et al. Hsc70/Hsp90 chaperone machinery mediates ATP-dependent RISC loading of small RNA duplexes. Mol Cell. 2010;39:292–9.

94. De Gregorio E, Spellman PT, Rubin GM, Lemaitre B. Genome-wide analysis of the *Drosophila* immune response by using oligonucleotide microarrays. Proc Natl Acad Sci U S A. 2001;98:12590–5.

95. De Gregorio E, Han S-J, Lee W-J, Baek M-J, Osaki T, Kawabata S-I, et al. An immune-responsive Serpin regulates the melanization cascade in *Drosophila*. Dev Cell. 2002;3:581–92.

96. Ligoxygakis P, Pelte N, Hoffmann JA, Reichhart J-M. Activation of *Drosophila* Toll during fungal infection by a blood serine protease. Science. 2002;297:114–6.

97. Hung J-J, Chung C-S, Chang W. Molecular chaperone Hsp90 is important for vaccinia virus growth in cells. J Virol. 2002;76:1379–90.

98. Connor JH, McKenzie MO, Parks GD, Lyles DS. Antiviral activity and RNA polymerase degradation following Hsp90 inhibition in a range of negative strand viruses. Virology. 2007;362:109–19.

99. Morales C, Wu S, Yang Y, Hao B, Li Z. *Drosophila* glycoprotein 93 is an ortholog of mammalian heat shock protein gp96 (grp94, HSP90b1, HSPC4) and retains disulfide bond-independent chaperone function for TLRs and integrins. J Immunol. 2009;183:5121–8.

100. Attoui H, Stirling JM, Munderloh UG, Billoir F, Brookes SM, Burroughs JN, et al. Complete sequence characterization of the genome of the St Croix River virus, a new orbivirus isolated from cells of *Ixodes scapularis*. J Gen Virol. 2001;82:795–804.

101. Alberdi MP, Dalby MJ, Rodriguez-Andres J, Fazakerley JK, Kohl A, Bell-Sakyi L. Detection and identification of putative bacterial endosymbionts and endogenous viruses in tick cell lines. Ticks Tick Borne Dis. 2012;3:137–46.

102. Keene KM, Foy BD, Sanchez-Vargas I, Beaty BJ, Blair CD, Olson KE. RNA interference acts as a natural antiviral response to O'nyong-nyong virus (Alphavirus; Togaviridae) infection of *Anopheles gambiae*. Proc Natl Acad Sci U S A. 2004;101:17240–5.

103. Saleh M-C, Tassetto M, van Rij RP, Goic B, Gausson V, Berry B, et al. Antiviral immunity in *Drosophila* requires systemic RNA interference spread. Nature. 2009;458:346–50.

104. Pitaluga AN, Mason PW, Traub-Cseko YM. Non-specific antiviral response detected in RNA-treated cultured cells of the sandfly, *Lutzomyia longipalpis*. Dev Comp Immunol. 2008;32:191–7.

105. Robalino J, Bartlett TC, Chapman RW, Gross PS, Browdy CL, Warr GW. Double-stranded RNA and antiviral immunity in marine shrimp: inducible host mechanisms and evidence for the evolution of viral counter-responses. Dev Comp Immunol. 2007;31:539–47.

106. Flenniken ML, Andino R. Non-specific dsRNA-mediated antiviral response in the honey bee. PLoS One. 2013;8, e77263. doi:10.1371/journal.pone.0077263.

107. Liu J, Smagghe G, Swevers L. Transcriptional response of BmToll9-1 and RNAi machinery genes to exogenous dsRNA in the midgut of *Bombyx mori*. J Insect Physiol. 2013;59:646–54.

108. Deddouche S, Matt N, Budd A, Mueller S, Kemp C, Galiana-Arnoux D, et al. The DExD/H-box helicase Dicer-2 mediates the induction of antiviral activity in *Drosophila*. Nat Immunol. 2008;9:1425–32.

109. Paradkar PN, Trinidad L, Voysey R, Duchemin J-B, Walker PJ. Secreted Vago restricts West Nile virus infection in *Culex* mosquito cells by activating the Jak-STAT pathway. Proc Natl Acad Sci U S A. 2012;109:18915–20.

110. Rückert C. Alphavirus and flavivirus infection of *Ixodes* tick cell lines: an insight into tick antiviral immunity. PhD thesis, University of Edinburgh. 2014. Available: http://hdl.handle.net/1842/10063

111. Aung KM, Boldbaatar D, Umemiya-Shirafuji R, Liao M, Tsuji N, Xuenan X, et al. HlSRB, a Class B scavenger receptor, is key to the granulocyte-mediated microbial phagocytosis in ticks. PLoS One. 2012;7, e33504. doi:10.1371/journal.pone.0033504.

112. Aung KM, Boldbaatar D, Umemiya-Shirafuji R, Liao M, Xuenan X, Suzuki H, et al. Scavenger receptor mediates systemic RNA interference in ticks. PLoS One. 2011;6, e28407. doi:10.1371/journal.pone.0028407.

113. Tsuji N, Miyoshi T, Battsetseg B, Matsuo T, Xuan X, Fujisaki K. A cysteine protease is critical for *Babesia* spp. transmission in *Haemaphysalis* ticks. PLoS Pathog. 2008;4, e1000062. doi:10.1371/journal.ppat.1000062.

114. Johansson MW, Söderhäll K. Isolation and purification of a cell adhesion factor from crayfish blood cells. J Cell Biol. 1988;106:1795–803.

115. Kobayashi M, Johansson M, Söderhäll K. The 76 kDa cell-adhesion factor from crayfish haemocytes promotes encapsulation *in vitro*. Cell Tissue Res. 1990;260:113–8.

116. Thörnqvist P, Johansson MW, Söderhäll K. Opsonic activity of cell adhesion proteins and β-1,3-glucan binding proteins from two crustaceans. Dev Comp Immunol. 1994;18:3–12.

117. Johansson MW, Lind MI, Holmblad T, Thörnqvist P-O, Söderhäll K. Peroxinectin, a novel cell adhesion protein from crayfish blood. Biochem Biophys Res Commun. 1995;216:1079–89.

118. Du Z-Q, Ren Q, Huang A-M, Fang W-H, Zhou J-F, Gao L-J, et al. A novel peroxinectin involved in antiviral and antibacterial immunity of mud crab, *Scylla paramamosain*. Mol Biol Rep. 2013;40:6873–81.

119. Lin X, Cerenius L, Lee BL, Söderhäll K. Purification of properoxinectin, a myeloperoxidase homologue and its activation to a cell adhesion molecule. Biochim Biophys Acta. 2007;1770:87–93.

120. Sritunyalucksana K, Wongsuebsantati K, Johansson MW, Söderhäll K. Peroxinectin, a cell adhesive protein associated with the proPO system from the black tiger shrimp, *Penaeus monodon*. Dev Comp Immunol. 2001;25:353–63.

121. Zhioua E, Yeh MT, LeBrun A. Assay for phenoloxidase activity in *Amblyomma americanum*, *Dermacentor variabilis*, and *Ixodes scapularis*. J Parasitol. 1997;83:553–4.

122. Kadota K, Satoh E, Ochiai M, Inoue N, Tsuji N, Igarashi I, et al. Existence of phenol oxidase in the argasid tick *Ornithodoros moubata*. Parasitol Res. 2002;88:781–4.

123. Simser JA, Mulenga A, Macaluso KR, Azad AF. An immune responsive factor D-like serine proteinase homologue identified from the American dog tick, *Dermacentor variabilis*. Insect Mol Biol. 2004;13:25–35.

124. Caudy AA, Ketting RF, Hammond SM, Denli AM, Bathoorn AMP, Tops BBJ, et al. A micrococcal nuclease homologue in RNAi effector complexes. Nature. 2003;425:411–4.

125. Scadden ADJ. The RISC subunit Tudor-SN binds to hyper-edited double-stranded RNA and promotes its cleavage. Nat Struct Mol Biol. 2005;12:489–96.

126. Yang W, Chendrimada TP, Wang Q, Higuchi M, Seeburg PH, Shiekhattar R, et al. Modulation of microRNA processing and expression through RNA editing by ADAR deaminases. Nat Struct Mol Biol. 2006;13:13–21.

127. Ayllón N, Naranjo V, Hajdušek O, Villar M, Galindo RC, Kocan KM, et al. Nuclease Tudor-SN is involved in tick dsRNA-mediated RNA interference and feeding but not in defense against flaviviral or *Anaplasma phagocytophilum* rickettsial infection. PLoS One. 2015;10, e0133038. doi:10.1371/journal.pone.0133038.

128. Wu Q, Luo Y, Lu R, Lau N, Lai EC, Li W-X, et al. Virus discovery by deep sequencing and assembly of virus-derived small silencing RNAs. Proc Natl Acad Sci U S A. 2010;107:1606–11.

129. Vodovar N, Bronkhorst AW, van Cleef KWR, Miesen P, Blanc H, van Rij RP, et al. Arbovirus-derived piRNAs exhibit a ping-pong signature in mosquito cells. PLoS One. 2012;7, e30861. doi:10.1371/journal.pone.0030861.

130. Morazzani EM, Wiley MR, Murreddu MG, Adelman ZN, Myles KM. Production of virus-derived ping-pong-dependent piRNA-like small RNAs in the mosquito soma. PLoS Pathog. 2012;8, e1002470. doi:10.1371/journal.ppat.1002470.

131. Léger P, Lara E, Jagla B, Sismeiro O, Mansuroglu Z, Coppée JY, et al. Dicer-2- and Piwi-mediated RNA interference in Rift Valley fever virus-infected mosquito cells. J Virol. 2013;87:1631–48.

132. Schnettler E, Donald CL, Human S, Watson M, Siu RWC, McFarlane M, et al. Knockdown of piRNA pathway proteins results in enhanced Semliki Forest virus production in mosquito cells. J Gen Virol. 2013;94:1680–9.

133. Srivastava P. Roles of heat-shock proteins in innate and adaptive immunity. Nat Rev Immunol. 2002;2:185–94.

134. Busby AT, Ayllón N, Kocan KM, Blouin EF, de la Fuente G, Galindo RC, et al. Expression of heat shock proteins and subolesin affects stress responses, *Anaplasma phagocytophilum* infection and questing behaviour in the tick, *Ixodes scapularis*. Med Vet Entomol. 2012;26:92–102.

135. Nagy PD, Wang RY, Pogany J, Hafren A, Makinen K. Emerging picture of host chaperone and cyclophilin roles in RNA virus replication. Virology. 2011;411:374–82.

136. Zhao L, Jones W. Expression of heat shock protein genes in insect stress responses. Invertebr Surviv J. 2012;9:93–101.

137. Michalak M, Corbett EF, Mesaeli N, Nakamura K, Opas M. Calreticulin: one protein, one gene, many functions. Biochem J. 1999;344:281–92.

138. Pieren M, Galli C, Denzel A, Molinari M. The use of calnexin and calreticulin by cellular and viral glycoproteins. J Biol Chem. 2005;280:28265–71.

139. Limjindaporn T, Wongwiwat W, Noisakran S, Srisawat C, Netsawang J, Puttikhunt C, et al. Interaction of dengue virus envelope protein with endoplasmic reticulum-resident chaperones facilitates dengue virus production. Biochem Biophys Res Commun. 2009;379:196–200.

140. Antunes S, Galindo RC, Almazán C, Rudenko N, Golovchenko M, Grubhoffer L, et al. Functional genomics studies of *Rhipicephalus* (*Boophilus*) *annulatus* ticks in response to infection with the cattle protozoan parasite, *Babesia bigemina*. Int J Parasitol. 2012;42:187–95.

141. Pastorino B, Nougairède A, Wurtz N, Gould E, de Lamballerie X. Role of host cell factors in flavivirus infection: Implications for pathogenesis and development of antiviral drugs. Antiviral Res. 2010;87:281–94.

142. Colpitts TM, Cox J, Vanlandingham DL, Feitosa FM, Cheng G, Kurscheid S, et al. Alterations in the *Aedes aegypti* transcriptome during infection with West Nile, dengue and yellow fever viruses. PLoS Pathog. 2011;7, e1002189. doi: 10.1371/journal.ppat.1002189.

143. Wei H, Zhou M-M. Viral-encoded enzymes that target host chromatin functions. Biochim Biophys Acta. 2010;1799:296–301.

144. Colpitts TM, Barthel S, Wang P, Fikrig E. Dengue virus capsid protein binds core histones and inhibits nucleosome formation in human liver cells. PLoS One. 2011;6, e24365. doi:10.1371/journal.pone.0024365.

145. Blackwell J, Brinton M. Translation elongation factor-1 alpha interacts with the 3'stem-loop region of West Nile virus genomic RNA. J Virol. 1997;71:6433–44.

146. Davis WG, Blackwell JL, Shi P-Y, Brinton MA. Interaction between the cellular protein eEF1A and the 3'-terminal stem-loop of West Nile virus genomic RNA facilitates viral minus-strand RNA synthesis. J Virol. 2007;81:10172–87.

147. Pattanakitsakul S, Rungrojcharoenkit K, Kanlaya R, Sinchaikul S, Noisakran S, Chen S-T, et al. Proteomic analysis of host responses in HepG2 cells during dengue virus infection. J Proteome Res. 2007;6:4592–600.

148. Pastorino B, Boucomont-Chapeaublanc E, Peyrefitte CN, Belghazi M, Fusaï T, Rogier C, et al. Identification of cellular proteome modifications in response to West Nile virus infection. Mol Cell Proteomics. 2009;8:1623–37.

149. Emara MM, Brinton MA. Interaction of TIA-1/TIAR with West Nile and dengue virus products in infected cells interferes with stress granule formation and processing body assembly. Proc Natl Acad Sci U S A. 2007; 104:9041–6.

150. Morais AT, Terzian AC, Duarte DV, Bronzoni RV, Madrid MC, Gavioli AF, et al. The eukaryotic translation initiation factor 3 subunit L protein interacts with Flavivirus NS5 and may modulate yellow fever virus replication. Virol J. 2013; 10:205. doi:10.1186/1743-422X-10-205.

151. Bartholomay L, Cho W, Rocheleau T, Boyle JP, Beck ET, Fuchs JF, et al. Description of the transcriptomes of immune response-activated hemocytes from the mosquito vectors *Aedes aegypti* and *Armigeres subalbatus*. Infect Immun. 2004;72:4114–26.

152. Waldock J, Olson KE, Christophides GK. *Anopheles gambiae* antiviral immune response to systemic O'nyong-nyong infection. PLoS Negl Trop Dis. 2012;6, e1565. doi:10.1371/journal.pntd.0001565.

153. Xi Z, Ramirez JL, Dimopoulos G. The *Aedes aegypti* toll pathway controls dengue virus infection. PLoS Pathog. 2008;4, e1000098. doi:10.1371/journal. ppat.1000098.

154. Lai R, Takeuchi H, Lomas LO, Jonczy J, Rigden DJ, Rees HH, et al. A new type of antimicrobial protein with multiple histidines from the hard tick, *Amblyomma hebraeum*. FASEB J. 2004;18:1447–9.

155. Silva FD, Rezende CA, Rossi DCP, Esteves E, Dyszy FH, Schreier S, et al. Structure and mode of action of microplusin, a copper II-chelating antimicrobial peptide from the cattle tick *Rhipicephalus* (*Boophilus*) *microplus*. J Biol Chem. 2009;284:34735–46.

156. Mulenga A, Macaluso KR, Simser JA, Azad AF. Dynamics of *Rickettsia*-tick interactions: identification and characterization of differentially expressed mRNAs in uninfected and infected *Dermacentor variabilis*. Insect Mol Biol. 2003;12:185–93.

157. Mulenga A, Simser JA, Macaluso KR, Azad A. Stress and transcriptional regulation of tick ferritin HC. Insect Mol Biol. 2004;13:423–33.

158. Ong ST, Ho JZS, Ho B, Ding JL. Iron-withholding strategy in innate immunity. Immunobiology. 2006;211:295–314.

159. Fric J, Zelante T, Wong AYW, Mertes A, Yu H-B, Ricciardi-Castagnoli P. NFAT control of innate immunity. Blood. 2012;120:1380–9.

160. Rao A, Luo C, Hogan PG. Transcription factors of the NFAT family: regulation and function. Annu Rev Immunol. 1997;15:707–47.

161. Wu H, Peisley A, Graef IA, Crabtree GR. NFAT signaling and the invention of vertebrates. Trends Cell Biol. 2007;17:251–60.

162. Zanoni I, Granucci F. Regulation and dysregulation of innate immunity by NFAT signaling downstream of pattern recognition receptors (PRRs). Eur J Immunol. 2012;42:1924–31.

163. Keyser P, Borge-Renberg K, Hultmark D. The *Drosophila* NFAT homolog is involved in salt stress tolerance. Insect Biochem Mol Biol. 2007;37:356–62.

164. Song X, Hu J, Jin P, Chen L, Ma F. Identification and evolution of an NFAT gene involving *Branchiostoma belcheri* innate immunity. Genomics. 2013; 102:355–62.

165. Stafforini DM, McIntyre TM, Zimmerman GA, Prescott SM. Platelet-activating factor acetylhydrolases. J Biol Chem. 1997;272(29):17895–8.

166. McIntyre TM, Prescott SM, Stafforini DM. The emerging roles of PAF acetylhydrolase. J Lipid Res. 2009;50(Suppl):S255–9. doi:10.1194/jlr.R800024-JLR200.

167. Prescott SM, Zimmerman GA, Stafforini DM, McIntyre TM. Platelet-activating factor and related lipid mediators. Annu Rev Bio. 2000;69:419–45.

168. Cheeseman MT, Bates PA, Crampton JM. Preliminary characterisation of esterase and platelet-activating factor (PAF)-acetylhydrolase activities from cat flea (*Ctenocephalides felis*) salivary glands. Insect Biochem Mol Biol. 2001; 31:157–64.

169. Figueiredo MB, Genta FA, Garcia ES, Azambuja P. Lipid mediators and vector infection: *Trypanosoma rangeli* inhibits *Rhodnius prolixus* hemocyte phagocytosis by modulation of phospholipase A2 and PAF-acetylhydrolase activities. J Insect Physiol. 2008;54:1528–37.

170. Garcia ES, Castro DP, Figueiredo MB, Genta FA, Azambuja P. *Trypanosoma rangeli*: a new perspective for studying the modulation of immune reactions of *Rhodnius prolixus*. Parasit Vectors. 2009;2:33. doi:10.1186/1756-3305-2-33.

171. Rachinsky A, Guerrero FD, Scoles GA. Differential protein expression in ovaries of uninfected and *Babesia*-infected southern cattle ticks, *Rhipicephalus* (*Boophilus*) *microplus*. Insect Biochem Mol Biol. 2007;37:1291–308.

Weisheit *et al. Parasites & Vectors* (2015) 8:599

Page 26 of 26

172. Behnke J, Hendershot LM. The large Hsp70 Grp170 binds to unfolded protein substrates *in vivo* with a regulation distinct from conventional Hsp70s. J Biol Chem. 2013;289:2899–907.

173. Yu S-W, Wang H, Poitras MF, Coombs C, Bowers WJ, Federoff HJ, et al. Mediation of poly(ADP-ribose) polymerase-1-dependent cell death by apoptosis-inducing factor. Science. 2002;297:259–63.

174. Odorizzi G. The multiple personalities of Alix. J Cell Sci. 2006;119:3025–32.

175. Le Blanc I, Luyet P-P, Pons V, Ferguson C, Emans N, Petiot A, et al. Endosome-to-cytosol transport of viral nucleocapsids. Nat Cell Biol. 2005;7:653–64.

176. Sangsuriya P, Rojtinnakorn J, Senapin S, Flegel TW. Identification and characterization of Alix/AIP1 interacting proteins from the black tiger shrimp, *Penaeus monodon*. J Fish Dis. 2010;33:571–81.

177. Anderson P, Kedersha N. RNA granules. J Cell Biol. 2006;172:803–8.

178. Anderson P, Kedersha N. Stress granules: the Tao of RNA triage. Trends Biochem Sci. 2008;33:141–50.

179. Valiente-Echeverría F, Melnychuk L, Mouland AJ. Viral modulation of stress granules. Virus Res. 2012;169:430–7.

180. Lloyd RE. Regulation of stress granules and P-bodies during RNA virus infection. WIREs RNA. 2013;4:317–31.

181. Li W, Li Y, Kedersha N, Anderson P, Emara M, Swiderek KMK, et al. Cell proteins TIA-1 and TIAR interact with the 3' stem-loop of the West Nile virus complementary minus-strand RNA and facilitate virus replication. J Virol. 2002;76:11989–2000.

MANUSCRIPT 3

Selinger M. et **Tykalová H.**; Štěrba J.; Věchtová P.; Vavrušková Z.; Lieskovská J.; Kohl A.; Schnettler E.; Grubhoffer L. (2019). Tick-borne encephalitis virus inhibits rRNA synthesis and host protein production in human cells of neural origin. PLoS Neglected Tropical Diseases 13(9): e0007745. DOI: 10.1371/journal.pntd.0007745

RESEARCH ARTICLE

Tick-borne encephalitis virus inhibits rRNA synthesis and host protein production in human cells of neural origin

Martin Selinger[1,2☯], Hana Tykalová[1,2☯], Ján Štěrba[1,2], Pavlína Věchtová[1,2], Zuzana Vavrušková[1], Jaroslava Lieskovská[2], Alain Kohl[3], Esther Schnettler[4,5]*, Libor Grubhoffer[1,2]*

1 Institute of Parasitology, Biology Centre of the Czech Academy of Sciences, Branišovská 31, České Budějovice, Czech Republic, **2** Faculty of Science, University of South Bohemia in České Budějovice, Branišovská, České Budějovice, Czech Republic, **3** MRC-University of Glasgow Centre for Virus Research, Glasgow, Scotland, United Kingdom, **4** Bernhard-Nocht-Institute for Tropical Medicine, Bernhard-Nocht-Str. 74, Hamburg, Germany, **5** German Centre for Infection Research (DZIF), partner site Hamburg-Luebeck-Borstel-Riems, Hamburg, Germany

☯ These authors contributed equally to this work.
* schnettler@bnitm.de (ES); liborex@paru.cas.cz (LG)

Abstract

Tick-borne encephalitis virus (TBEV), a member of the genus *Flavivirus* (*Flaviviridae*), is a causative agent of a severe neuroinfection. Recently, several flaviviruses have been shown to interact with host protein synthesis. In order to determine whether TBEV interacts with this host process in its natural target cells, we analysed *de novo* protein synthesis in a human cell line derived from cerebellar medulloblastoma (DAOY HTB-186). We observed a significant decrease in the rate of host protein synthesis, including the housekeeping genes HPRT1 and GAPDH and the known interferon-stimulated gene viperin. In addition, TBEV infection resulted in a specific decrease of RNA polymerase I (POLR1) transcripts, 18S and 28S rRNAs and their precursor, 45-47S pre-rRNA, but had no effect on the POLR3 transcribed 5S rRNA levels. To our knowledge, this is the first report of flavivirus-induced decrease of specifically POLR1 rRNA transcripts accompanied by host translational shut-off.

Author summary

Tick-borne encephalitis virus (TBEV) is a causative agent of a severe human neuroinfection that threatens Europe and Asia. Little is known about the interaction of this neurotropic virus with neural cells, even though this may be important to better understand why or how TBEV can cause high pathogenicity in humans, especially following neural cell infection. Here, we showed that TBEV induced host translational shut-off in cells of neural origin. In addition, TBEV interfered also with the expression of host ribosomal RNAs. Interestingly, the transcriptional shut-off was documented for rRNA species transcribed by RNA polymerase I (18S rRNA, 28S rRNA and their precursor 45-47S pre-rRNA), but not for RNA polymerase III rRNA transcripts (5S rRNA). Artificial inhibition

76

of host translation using cycloheximide resulted in the decrease of all rRNA species. Based on these data, TBEV seems to specifically target transcription of RNA polymerase I. These new findings further increase our understanding of TBEV interactions with a key target cell type.

Introduction

The *Flaviviridae* family contains arthropod-borne viruses including medically important pathogens with worldwide distribution and impact, such as dengue virus (DENV), yellow fever virus (YFV), West Nile virus (WNV), Japanese encephalitis virus (JEV), Zika virus (ZIKV), and tick-borne encephalitis virus (TBEV) [1].

TBEV causes a severe neuroinfection known as tick-borne encephalitis, which affects thousands of people across Eurasia annually [2, 3]. In recent years, an increase in TBEV infection rates in affected countries and in its geographical distribution has been observed, involving previously unaffected areas such as Switzerland and northern Germany [4–6]. Although the disease is not always fatal (mortality rate of 1–2%), a high percentage of patients (35–58%) suffer from permanent sequelae, such as cognitive or neuropsychiatric afflictions, balance disorders, headaches, dysphasia, hearing defects, and spinal paralysis after overcoming the main symptoms [2, 7]. Specific antiviral therapy for tick-borne encephalitis does not exist. Neurons are the primary target for TBEV infection in mice and humans, and according to *post mortem* studies of TBEV-infected patients, the cerebellum is one of the main foci affected [8–10]. Understanding the interaction between TBEV and human neural cells is essential as it could lead to possible new treatment targets and a better understanding of why TBEV infection can result in severe neurological symptoms. Like all flaviviruses, TBEV is an enveloped virus with a single-stranded RNA (ssRNA) genome of positive polarity (approx. 11 kb) with a 7-methylguanosine cap at the 5´end. The coding segment is flanked on both ends by untranslated regions (UTR). Viral proteins are encoded in a single open reading frame that is translated in one poly-protein which is then proteolytically processed into three structural (C, prM, E) and seven non-structural proteins (NS1, NS2A, NS2B, NS3, NS4A, NS4B, NS5) [11–13]. While the structural proteins are the main building units of the viral particle, the non-structural proteins are crucial in the TBEV life cycle. They are essential components of viral replication within the host endoplasmic reticulum or Golgi apparatus-derived membrane compartments and the virion assembly processes and are involved in immune response evasion/counteractions [14–16].

Virus replication is reliant on the host protein synthesis apparatus and manipulates it in favour of viral requirements. There are various strategies viruses use to accomplish this goal and generally aim at three levels: host translational shut-off, processing of host mRNA, and host transcriptional shut-off [17, 18]. Translation of eukaryotic and viral proteins is often controlled at the rate-limiting step of initiation and viruses such as Bunyamwera virus, influenza A virus or poliovirus were shown to target initiation factors [19–23]. More specifically for flaviviruses, a recent study [24] documented repression of the host translation initiation step during DENV infection and general translational repression was also recorded for WNV and ZIKV. While inducing host translational shut-off, viral proteins are still synthesised thanks to alternative translation initiation strategies, such as cap-independent translation [20, 25–27].

Transcription in eukaryotic organisms is carried out by three RNA polymerases: RNA polymerase I, II, and III. Each of the RNA polymerase complexes is responsible for the transcription of different genes. RNA polymerase I (POLR1) yields a single transcription unit 45-47S

77

pre-rRNA, which undergoes a complex maturation process that generates 5.8S, 18S, and 28S rRNA [28, 29]. RNA polymerase III (POLR3) produces 5S rRNA, tRNAs, and specific small RNAs [29]. RNA polymerase II (POLR2) transcribes protein-coding genes and certain small RNAs [30]. Out of all the transcripts synthesised in the eukaryotic cell, ribosomal RNA is the most abundant and a key component of ribosomes. Virus-induced interference with transcription and subsequent processing of host rRNA has been described for influenza A virus [31], herpes simplex virus type I [32], human papillomavirus type 8 [33], human cytomegalovirus [34], and human immunodeficiency virus (HIV) [35]. However, this was not described for flaviviruses.

Given the indications for flaviviruses affecting host translation [24], we aimed at exploring this topic further in TBEV infection of naturally permissive host cells of neural origin, that represent a key cell type responsible for tick-borne encephalitis manifestation. We found that TBEV triggered host translational shut-off that involved lowered expression of GAPDH and HPRT1 housekeeping genes as well as the interferon-induced protein viperin. TBEV further specifically impaired the production of POLR1-transcribed rRNAs. Therefore, we postulate that TBEV specifically targets POLR1-mediated transcription of rRNA and rate of host translation thus promoting virus replication.

Methods

Cell lines

The human medulloblastoma (DAOY HTB-186; ATCC), human lung adenocarcinoma (A549; a gift from R. Randall, University of St. Andrews, UK), and Vero (green monkey kidney; Biology Centre, CAS, CZ) cell lines were grown in low glucose DMEM medium supplemented with 10% foetal bovine serum (FBS), 1% antibiotics-antimycotics (amphotericin B 0.25 µg/ml, penicillin G 100 units/ml, streptomycin 100 µg/ml), and 1% L-alanyl-L-glutamine. DAOY HTB-186 cell line is derived from desmoplastic cerebellar medulloblastoma of a 4-year-old Caucasian male [36]. A549s are derived from a lung cancerous tissue (alveolar basal epithelial cells) of a 58-year-old Caucasian male [37]. Vero cells are derived from kidney epithelial cells from African green monkey (*Cercopithecus aethiops*). PS cells (porcine kidney stable) were grown in L15 medium with 3% new-born calf serum (NCS), 1% antibiotics-antimycotics, and 1% L-alanyl-L-glutamine [38]. The human osteosarcoma cell line MG-63 (Sigma-Aldrich) was grown in RPMI 1640 medium supplemented with 10% FBS, 1% antibiotics-antimycotics, 1% L-alanyl-L-glutamine, and 50 nM β-mercaptoethanol. These were explanted from a 14-year-old Caucasian male [39].

For metabolic labelling experiments, all cell lines were grown in RPMI 1640 medium supplemented with 10% FBS, 1% antibiotics-antimycotics, 1% L-alanyl-L-glutamine, and 50 nM β-mercaptoethanol. All cell lines were grown at 37°C and 5% CO_2; with the exception of PS cells (37°C without additional CO_2).

Transfection and plasmids

PolyJet *In Vitro* Transfection Reagent (SignaGen; #SL100688) was used for transfection. The procedure was carried out according to the manufacturer's protocol. For GFP and *Renilla* luciferase expression, the mammalian expression vectors phMGFP (Promega) and pRL-CMV (Promega) were used, respectively. The wt viperin mammalian expression vector was a kind gift from Lisa F.P. Ng (Singapore Immunology Network, Agency for Science, Technology and Research (A* STAR), Singapore), in which the viperin gene with C-terminal c-myc tag is transcribed under the control of the CMV promoter [40].

78

Viruses and infection

Two representatives of the West-European TBEV subtype with different degrees of virulence were used–medium (Neudoerfl) and severe (Hypr). Both strains differ in their coding sequences by only 12 nonconservative amino acid substitutions [41], and in the length and structure of the 3´UTR [42]. When mice were infected peripherally, the Hypr strain exhibited pronounced neuroinvasiveness and caused shorter survival than strain Neudoerfl [41]. The low passage TBEV strain, Neudoerfl (fourth passage in suckling mice brains; GenBank accession no. TEU27495), was provided by Prof. F.X. Heinz (Medical University of Vienna, Austria) [43]. The low passage TBEV strain, Hypr (fourth passage in suckling mice brains; GenBank accession no. TEU39292), is available at the Institute of Parasitology, Biology Centre of CAS, České Budějovice, Czech Republic [44]. Viruses were handled under biosafety level 3 conditions.

TBEV was added to the cells one day post seeding. Cells were then incubated for 2 hours, washed with PBS, and finally fresh pre-warmed medium was added. Brain suspension from uninfected suckling mice was used as a negative control.

Virus titration

Viral titres were determined by plaque assay as described [45], with minor modifications. Briefly, PS cell monolayers ($9x10^4$ cells per well) were grown in 24-well plates and incubated with 10x serial dilutions of infectious samples for 4 hours at 37˚C. The samples were then covered by 1:1 (v/v) overlay mixture (carboxymethyl cellulose and 2x L15 medium including 6% NCS, 2% antibiotics-antimycotics, and 2% L-glutamine). After five days, medium with overlay was removed, cells washed with physiological solution, subsequently fixed and stained (0.1% naphthalene black in 6% acetic acid solution) for 45 minutes. Virus-produced plaques were counted, and titres are stated as PFU/ml.

Antibodies and reagents

The following primary antibodies were used: anti-TBEV C polyclonal antibody (produced in-house), anti-TBEV NS3 polyclonal antibody (a kind gift from Dr. M. Bloom, NIAID, USA), anti-HPRT1 Polyclonal Antibody (Thermo Fisher Scientific; #PA5-22281), anti-GAPDH Antibody [EPR16891] (Abcam; #ab181602), Monoclonal Antibody to Mouse Viperin (Hycult Biotech; #HM1016), anti-NPM1 Monoclonal Antibody FC-61991 (Thermo Fisher Scientific; #MA1-1560), and anti-POLR1A Antibody (Abcam; #ab222065). The following secondary/tertiary antibodies were used: HRP Goat Anti-Guinea Pig (Novex; #A18769), HRP Rabbit Anti-Chicken IgY (H+L) Secondary Antibody (Thermo Fisher Scientific; #A16130), HRP Horse Anti-Mouse IgG Antibody (VectorLabs; #PI-2000), HRP Goat Anti-Rabbit IgG Antibody (VectorLabs; #PI-1000), Biotinylated Anti-Streptavidin Antibody (VectorLabs; #BA-0500), AP-conjugated Streptavidin (VectorLabs; #SA-5100), Streptavidin-DyLight 549 (VectorLabs; Cat#SA-5549), Goat Anti-Rabbit IgG-DyLight 594 (Abcam; #ab96897), Goat Anti-Guinea Pig DyLight 594 (Abcam; #ab150188), and Goat Anti-Chicken IgY H&L-DyLight 488 (Abcam; #ab96947).

L-azidohomoalanine (Click Chemistry Tools; #1066–25) and 5-ethynyl-uridine (Click Chemistry Tools; #1261–25) were used for metabolic labelling of nascent proteins or RNA, respectively. Biotin-PEG4-Alkyne (Click Chemistry Tools; #TA105-25) and Biotin Picolyl Azide (Click Chemistry Tools; #1167–25) were used for subsequent detection of incorporated L-azidohomoalanine or 5-ethynyl-uridine, respectively. Cycloheximide was purchased from Sigma-Aldrich (#01810-1G).

Flow cytometry analysis

DAOY cells were seeded one day prior to infection in the 12-well plate at a density of 2.5×10^5 cells/well. At the indicated time intervals post-TBEV infection, cells were washed with PBS, trypsinized, and fixed by 4% paraformaldehyde in PBS (Roth). After permeabilization (0.1% Triton X-100), cells were stained using guinea pig anti-TBEV C antibodies (1:1500 dilution) and anti-guinea pig DyLight 594 (1:500 dilution) secondary antibodies. Flow cytometry was performed on a FACS Canto II cytometer and data analysed using FACS DIVA software v. 5.0 (BD Biosciences).

RNA isolation

Total cellular RNA was isolated using Trizol-based RNA Blue reagent (Top-Bio; #R013) according to the manufacturer's instructions. RNA pellets were dissolved in DEPC-treated water and directly used for either real-time PCR or analysis on an RNA denaturing gel.

rRNA quantification

The quantity and integrity of rRNA in total RNA samples were analysed on a 2100 Bioanalyzer using Agilent RNA 6000 Nano kit (Agilent Technologies; #5067–1511). The concentration of each sample was determined spectrophotometrically prior the Bioanalyzer measurement and samples were diluted according to the cell number ratio (resulting concentrations were between 10–20 ng/μl). 1 μl of the diluted RNA samples was loaded on the Bioanalyzer chip and the electrophoretic assay was performed according to the manufacturer's instructions. All samples were analysed in technical triplicates. 1.2% agarose MOPS-buffered denaturing gel (with 6.7% formaldehyde) was used for fractionation of isolated total RNA. RNA was visualised by addition of the GelRed dye (Biotium) into the gel. The signal was subsequently quantified using Fiji software.

Sample standardisation

We observed that the viability of TBEV Hypr-infected cells was negatively affected at 36 and 48 hours p.i. (Fig 1D). Therefore, in order to diminish the effect of this phenomenon on our data, we decided to standardise in our experiments to cell counts.

Normalisation to cell numbers was performed for real-time PCR, western blotting, northern blotting, and metabolic labelling analyses. For this, we established a viability-based method using alamarBlue reagent (Thermo Fisher Scientific; #DAL1025). Our data demonstrate that viability measurement is directly proportional to the cell number, and therefore this method is fully suitable for normalisation to the cell number (S1 Fig). The procedure was performed according to the manufacturer's instructions. Briefly, cells were washed with PBS and fresh pre-warmed growth medium with diluted alamarBlue reagent was added (1:10 dilution ratio; v/v). Cells were incubated for 2–2.5 hours and fluorescence of the reduced product was measured on a BioTek plate reader (λ_{ex} = 550 nm; λ_{em} = 590 nm). Growth medium with alamarBlue without cells was used as a blank. All samples were analysed in technical triplicates. Average fluorescence values for TBEV-treated sample were normalized to the respective mock control cells. The viability factor (f) was subsequently used as a normalisation factor for the calculation of RNA/protein input based on the pre-set mock control input.

$$f = \frac{viability_{sample}[a.u.]}{viability_{control}[a.u.]} \qquad\qquad V_{sample}[\mu l] = \frac{V_{control}[\mu l]}{f}$$

80
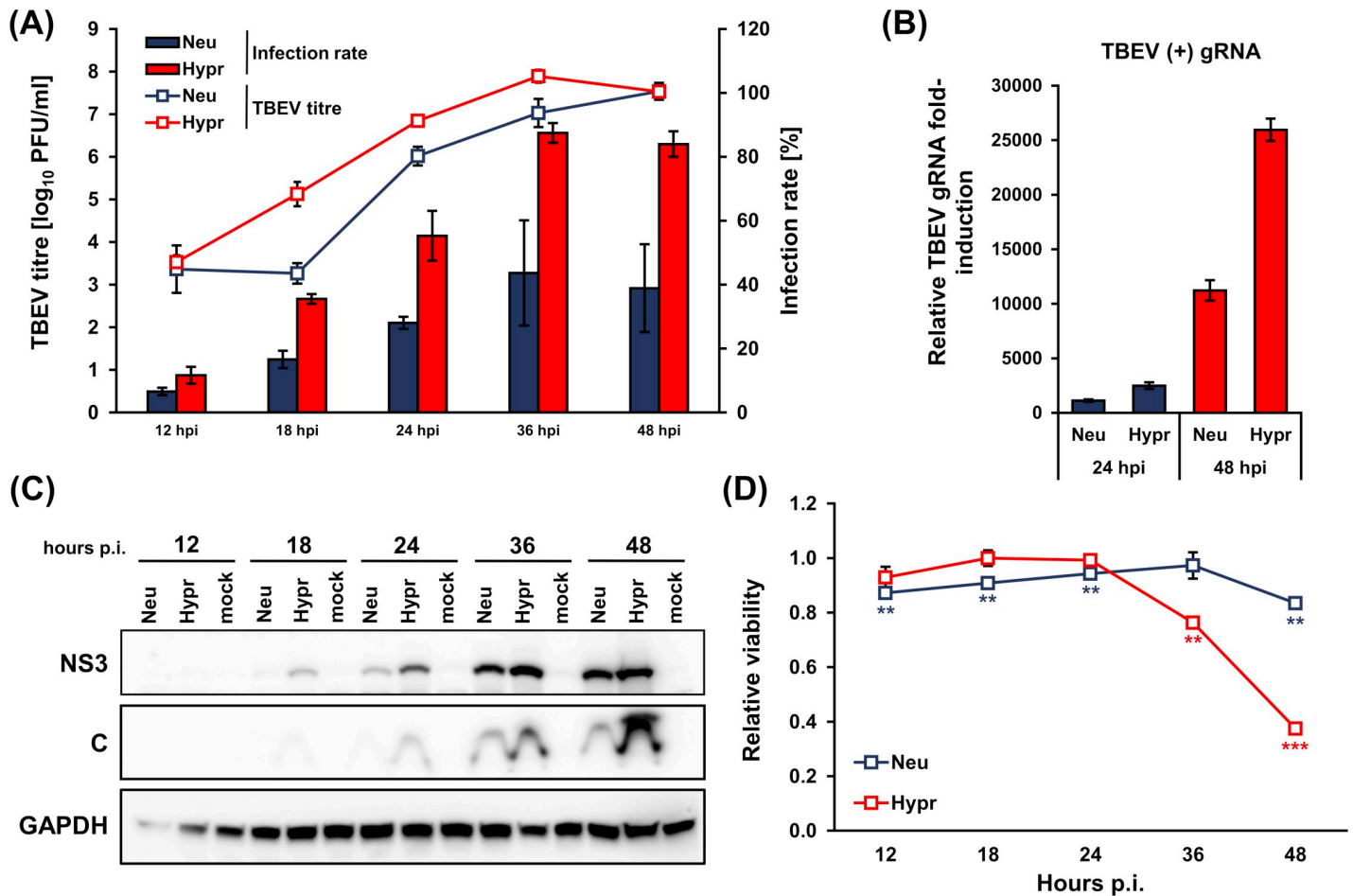
Fig 1. Characterization of TBEV Hypr and Neudoerfl infection kinetics in DAOY cells. DAOY cells were infected with TBEV Neudoerfl or Hypr strain (MOI 5). (A) Viral titres (indicated in trend lines) determined by plaque assay on PS cells and infection rate (indicated in bars) determined by flow-cytometric detection of TBEV C-stained cells were analysed at 12, 18, 24, 36, 48 hours p.i. Graphical summary of three independent experiments is shown with values expressed as mean with SEM. (B) Total RNA was isolated at 24 and 48 hours p.i. and relative qPCR quantification of TBEV gRNA using Δ-c_t method with normalisation to cell number was performed. Data are summary of three independent experiments and values in graphs are expressed as mean with SEM. (C) Levels of TBEV NS3 and C proteins in infected DAOY cells were determined by immunoblotting at 12, 18, 24, 36, 48 hours p.i. Data are summary of three independent experiments. (D) Viability of infected cells was determined using alamarBlue reagent, at the indicated time intervals p.i. Data are summary of three independent experiments and values are expressed as mean with SEM, normalised to mock infected cells; significant difference from control was calculated by unpaired Student's t-test (** $P < 0.01$; *** $P < 0.001$).

https://doi.org/10.1371/journal.pntd.0007745.g001

Real-time qPCR

For real-time qPCR analyses, the KAPA SYBR FAST Universal One-Step qRT-PCR Kit was used according to the manufacturer's protocol. Data obtained were processed via relative quantification using the delta c_t (Δ-c_t) method; the amount of RNA was adjusted to the cell number instead of the c_t values of the housekeeping reference gene. All samples were treated with dsDNase and subsequently 5× diluted in RNAse-free water before the real-time PCR analysis. All samples were analysed in technical triplicates. List of primers used can be found in S1 Table.

Western blotting

Cells were washed with PBS and RIPA buffer (25 mM Tris-HCl pH 7.6, 150 mM NaCl, 1% NP-40, 0.1% SDS, 1% sodium deoxycholate) with protease inhibitors (Thermo Fisher

81

Scientific; #78430) was added. Cell lysis was performed for 15 minutes on ice while gently shaking. Sonicated and cleared protein lysates in RIPA buffer were separated on 12% denaturing polyacrylamide gels and blotted onto PVDF membranes. The quantity of proteins was normalised to the cell number. Membranes were blocked (5% skimmed milk in PBS-T) and incubated with primary, secondary, and alternatively also tertiary antibodies; between each staining step, membranes were washed three times in PBS-T. Primary antibodies used were guinea pig anti-C (produced in-house; 1:1500), chicken anti-NS3 (M. Bloom laboratory; 1:5000), rabbit anti-GAPDH (Abcam; 1:1000), anti-HPRT1 (Thermo Fisher Scientific; 1:500), anti-viperin (Hycult Biotech; 1:500). Secondary/tertiary antibodies used were goat anti-rabbit HRP (VectorLabs; 1:1000), rabbit anti-chicken HRP (Thermo Fisher Scientific; 1:1000), and horse anti-mouse HRP (VectorLabs; 1:1000). Chemiluminescent signal was developed using either Novex CDP-Star kit for alkaline phosphatase (Thermo Fisher Scientific) or Western-nBright Quantum kit for horseradish peroxidase (Advansta; #K-12042-D20). The signal was subsequently quantified using Fiji software [46]. For stripping of antibodies, membranes were incubated with stripping solution (62.5 mM Tris HCl pH 6.8, 2% SDS, 0.8% β-mercaptoethanol) for 45 minutes at 50˚C. Subsequently, membranes were extensively washed six times with PBS. Following this, membranes were blocked, and immunostaining was again performed as described above.

Luciferase assay

For analyses of *Renilla* luciferase activity in CHX-treated cells, *Renilla* Luciferase Assay Kit from Promega (#E2810) was used according to the manufacturer's instructions. Briefly, 5×10^4 DAOY cells per well were seeded on a 96-well plate. Cells were transfected with 100 ng of pRL-CMV vector per well using PolyJet transfection reagent and incubated with cycloheximide (50–300 μg/ml) for 2, 4, 6, 14, and 24 hours. At 24 hours post-transfection, the viability of cells was measured using alamarBlue. Subsequently, cells were lysed and *Renilla* luciferase activity was determined.

Metabolic labelling of *de novo* synthesised proteins

Cells were seeded in 6-well plates at a density of 1×10^6 (Vero, A549) or 5×10^5 (DAOY, MG-63) cells per well. At indicated time intervals p.i., cells were washed with PBS and starved for 1 hour by addition of complete methionine-free RPMI medium (methionine-free RPMI medium containing 10% FBS, 1% L-alanyl-L-glutamine, 1% antibiotics/antimycotics, and 0.27 mM L-cystine). Subsequently, fresh complete methionine-free RPMI medium was added with 50 μM L-azidohomoalanine (AHA) and 1× AlamarBlue reagent. Metabolic labelling with AHA was performed for 2 hours. Afterwards, cell viability was measured as described earlier. Cells were then washed with PBS and lysed on ice for 15 minutes in 200 μl RIPA buffer with protease inhibitors (Halt Protease Inhibitor Single-Use Cocktail; Thermo Fisher Scientific). Lysates were separated on 12% polyacrylamide gels and transferred by electroblotting onto the PVDF membrane. The quantity of proteins loaded onto the gel was normalised to the cell numbers. Subsequently, the modified detection method Click-on-membrane was performed according to Kočová et al. (in preparation). Briefly, membranes were washed in 0.1 M potassium phosphate buffer pH 7.0 and the Click reaction was performed as follows: membranes were incubated in Click reaction buffer (0.1 M potassium phosphate buffer pH 7.0 with 0.25 mM sodium ascorbate, 0.5 mM THPTA, 0.1 mM $CuSO_4$, and 10 μM biotin-alkyne) for 1 hour in the dark at room temperature. Membranes were washed three times with PBS, blocked (5% skimmed milk in PBS-T) and incubated with primary (AP-streptavidin; VectorLabs; 1:500), secondary (biotinylated anti-streptavidin; VectorLabs; 1:1000) and tertiary antibodies (AP-

82

streptavidin; VectorLabs; 1:2000). Between each staining step, membranes were washed three times in PBS-T. Chemiluminescence signal was developed using Novex CDP-Star kit (Invitrogen; #WP20002). Signal was subsequently quantified using Fiji software [46].

Metabolic labelling of *de novo* synthesised RNA

DAOY cells were seeded in 6-well plates at a density of 5×10^5 cells per well. At the indicated time intervals p.i., 5-ethynyl uridine (5-EU) was added to the cells (final concentration of 5-EU was 1 mM) as well as alamarBlue reagent. Metabolic labelling with 5-EU was performed for 2 hours. Cell viability was measured as described earlier. Cells were then washed with PBS and lysed using RNA Blue reagent. Total RNA was isolated according to the manufacturer's instructions. Next, RNA was separated in MOPS-buffered denaturing gel, as described above. The quantity of RNA was normalised to the cell number. Capillary blotting of RNA to the PVDF membrane (GE Healthcare) using 20× SSC buffering system was performed afterwards. Subsequently, the modified detection method Click-on-membrane was performed according to the method described by Kočová et. al. (in preparation). Briefly, the UV-fixed membrane was washed in 0.1 M potassium phosphate buffer pH 7.0 and the Click reaction on membrane was performed as follows: membranes were incubated in Click reaction buffer (0.1 M potassium phosphate buffer pH 7.0 with 0.25 mM sodium ascorbate, 0.5 mM THPTA, 0.1 mM $CuSO_4$, and 10 μM picolyl biotin azide) for 1 hour in the dark at room temperature. Blocking and triple labelling using biotin-streptavidin system was performed as described above. The chemiluminescence signal was developed using Novex CDP-Star kit (Invitrogen; #WP20002), and signal was subsequently quantified using Fiji software [46].

Immunofluorescence

DAOY cells were seeded in chamber slides (0,3 cm^2/well; 5×10^3 cells/well) and at the indicated time intervals p.i. processed as previously described [47]. Rabbit anti-POLR1A (Abcam; 1:200) and chicken anti-NS3 (a kind gift from Dr. M. Bloom, NIAID, NIH; 1:5000) antibodies were used. As the secondary antibodies, anti-rabbit DyLight 594 (Abcam; 1:500) and anti-chicken DyLight 488 (Abcam; 1:500), were used. In the case of metabolic labelling of nascent RNA, the Click reaction was performed *in situ* before the blocking step. 10 μM Picolyl biotin azide was used for the detection of incorporated 5-EU. For subsequent fluorescent labelling, streptavidin conjugated with DyLight 549 was used (VectorLabs; 1:500). Slides were eventually mounted in Vectashield mounting medium (VectorLabs). The Olympus Fluoview FV10i confocal microscope was used for imaging and subsequent export of images was done in FV10-ASW software (v.1.7).

Statistical analyses

All statistical analyses were performed in MS Excel using one-sample two-tailed Student's t-test. Only in case of qPCR analysis of over-expressed viperin and GFP, an unpaired two-tailed Student's t-test was used. In this case, datasets were first tested for the equality of variances by F-test. If the experiment was performed in technical replicates, the statistics was performed using the means of the independent biological replicates.

Results

TBEV infection reduces host protein production

Recent studies have shown that DENV decreases the rate of *de novo* protein synthesis in host cells [24, 48]. In order to establish whether TBEV also affects translation, *de novo* protein

83

synthesis kinetics was measured in TBEV-infected cells using Click chemistry [49]. For this purpose, we utilized a suitable *in vitro* experimental system of the cerebellum-derived human medulloblastoma cell line DAOY HTB-186 to broaden previous findings [47]. Two closely related members of the European subtype of TBEV with different virulence were used for comparative purposes: a medium virulent prototype strain, Neudoerfl, and a highly virulent strain, Hypr [41]. Initially, we characterized the course of infection for both TBEV strains. DAOY cells were infected at an MOI of 5 with either strain and at 12, 18, 24, 36, 48 hours p.i., replication kinetics, infection rate, viral protein (C, NS3) production and viability of infected cells were determined. Both strains successfully replicated in DAOY cells, with the Hypr strain reaching at least one order of magnitude higher titres during the course of infection until 48 hours p.i., when both strains eventually produced equal titres (Fig 1A). The infection rate was also considerably higher for the Hypr strain, culminating at 36 hours p.i. (87.5% of infected cells), whereas the Neudoerfl strain infected only 43.6% of cells (Fig 1A). Relative quantification of genomic RNA at 24 and 48 hours p.i. revealed that Hypr replicated with higher efficiency than Neudoerfl (Fig 1B). TBEV C and TBEV NS3 protein detection corresponded to replication kinetics and for both strains proteins could be detected earliest at 18 hours p.i., increasing thereafter (Fig 1C). While TBEV Neudoerfl affected the viability of the infected cells only mildly (maximal decrease by 16.6% at 36 hours p.i.), TBEV Hypr lowered the viability of the infected cells by 23.8% and 62.5% in comparison to mock-infected control at 36 and 48 hours p.i., respectively (Fig 1D). Therefore, in order to compensate the potential bias originating from cell death, we standardised our experiments to viability which is directly proportional to the number of living cells (S1 Fig). In the following experiments we pursued interaction of TBEV with DAOY cells during the period of productive infection for both TBEV strains, ranging from 24 to 48 hours p.i.

After this detailed characterization of our *in vitro* model, *de novo* protein synthesis and quantification was performed. DAOY cells were infected with either TBEV Hypr or Neudoerfl and metabolic labelling was carried out for 2 hours at 24, 36, and 48 hours p.i. using the methionine analogue L-azidohomoalanine (AHA). At 24 hours p.i., translation levels were comparable in control and infected cells, but infection resulted in a significant decrease of AHA-labelled proteins at 36 and 48 hours p.i. in TBEV Hypr-infected cells and at 48 hours p.i. in TBEV Neudoerfl-infected cells (Fig 2A and 2B; S2A Fig). Interestingly, the viral NS3 protein levels increased over the course of the infection with both strains (Fig 2A, lower panel). Furthermore, TBEV-induced host translational shut-off was also documented for cell lines of non-neural origin (A549 cells, Vero cells, and MG-63 cells) at 48 hours p.i., for both TBEV strains (Fig 2C; S2B Fig). Interestingly, despite the observed host translational shut-off both TBEV strains were able to replicate (Fig 1B) successfully and reached high titres (Fig 1A) in DAOY cells throughout the infection.

Since these experiments revealed a significant decrease in host protein synthesis upon TBEV infection on a global level, we evaluated the specificity of this for particular host proteins. First, the effect of TBEV infection on common housekeeping genes GAPDH and HPRT1 was determined by analysing their mRNA and protein levels. Relative quantification of GAPDH and HPRT1 mRNAs revealed a strong inhibition of expression for both genes and TBEV strains at 48 hours p.i. (Fig 3A and 3B; upper panel). Similar results were observed for their protein levels, although the more virulent strain Hypr elicited a stronger reduction (Fig 3A and 3B; lower panel).

As the subversion of host translation process can be used as an immune evasion strategy by viruses [17], we investigated the effect of translational shut-off on the interferon-inducible gene viperin. Viperin has been described so far as an antiviral protein that interferes with TBEV on multiple levels [50]. A time course of viperin mRNA production in response to
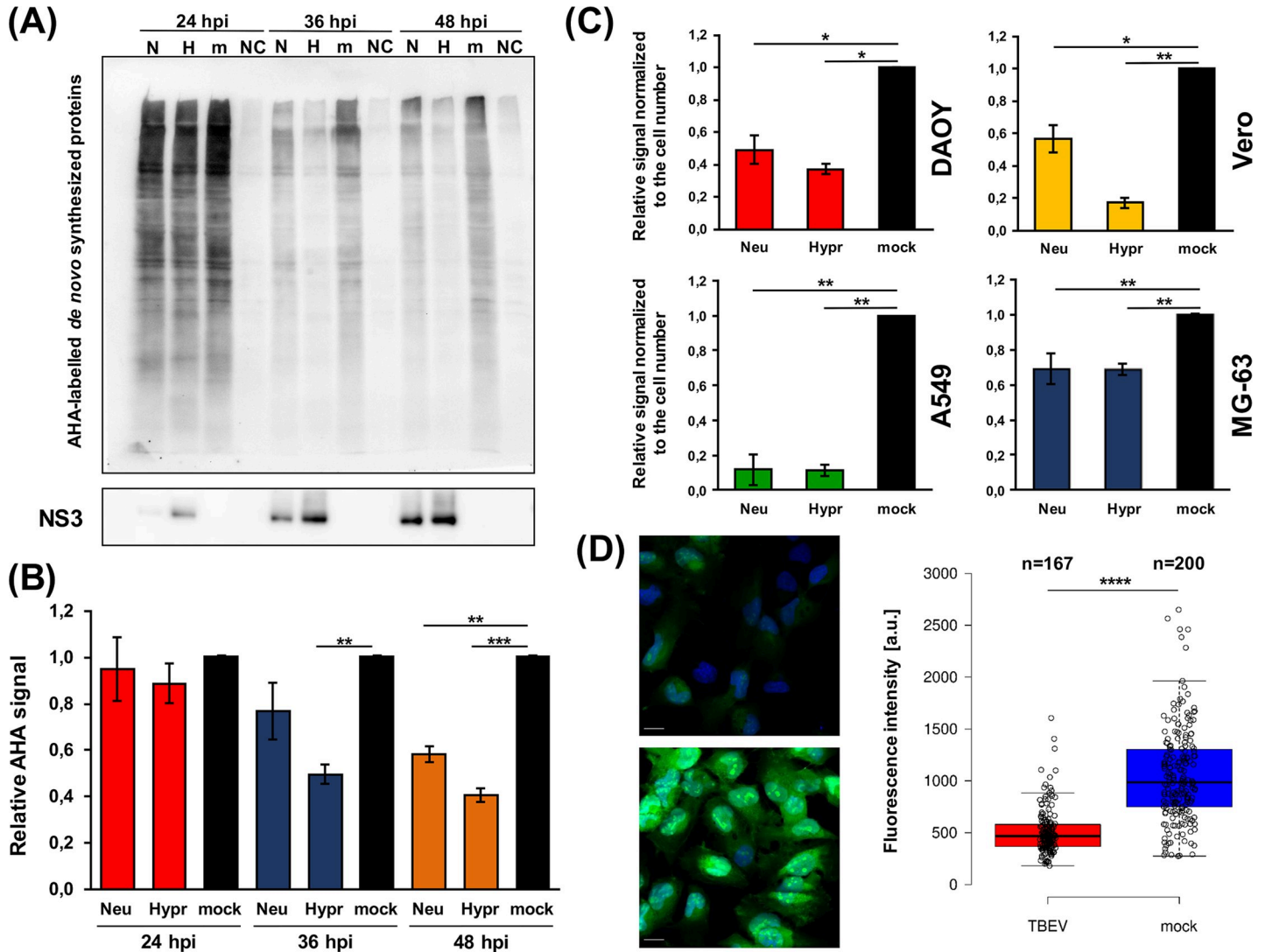
84

Fig 2. TBEV infection induces host translational shut-off. (A) DAOY cells were infected with TBEV Neudoerfl or Hypr strain (MOI 5) and *de novo* protein synthesis was assessed at 24, 36, and 48 hours p.i. by incorporation of methionine analogue L-azidohomoalanine (AHA). AHA-labelled proteins were visualised by immunodetection using HRP-conjugated antibodies; stripped membranes were subsequently used for the immunodetection of viral NS3 protein. Data are representative of three independent experiments; N–TBEV Neudoerfl strain (AHA-labelled), H–TBEV Hypr strain (AHA labelled), m–mock (AHA-labelled), NC–negative control (non-labelled). (B) Summary of *de novo* protein synthesis from (A) including all three performed experiments. Relative chemiluminescent signal was quantified using Fiji software and compared to mock-infected cells. Values were further normalised to the cell number and mock-infected cells were set to 1. Data are representative of three independent experiments and values are expressed as mean with SEM; significant difference from control was calculated by unpaired Student's t-test (** $P<0.01$; *** $P<0.001$). (C) Summary of *de novo* protein synthesis rate in TBEV-infected DAOY, Vero, A549, and MG-63 cells. Cell lines were infected with either Neudoerfl or Hypr strain (MOI 5) and subsequently analysed for *de novo* protein synthesis at 48 hours p.i. Relative chemiluminescent signal was quantified using Fiji software and compared to mock-infected cells. Values were further normalised to the cell number and mock-infected cells were set to 1. Data are summary of three independent experiments and values are expressed as mean with SEM; significant difference from mock-infected cells was calculated by Student's t-test (* $P<0.05$; ** $P<0.01$). (D) DAOY cells were infected with TBEV Hypr strain (MOI 5), and *de novo* protein synthesis was assessed at 36 hours p.i. by incorporation of methionine analogue L-azidohomoalanine (AHA). AHA-labelled proteins were visualised by Click reaction using AlexaFluor 488-conjugated alkyne. Representative images of TBEV-infected and control cells are shown on the left. Scale bar represents 100 μm. On the right, scatter plot is shown illustrating *de novo* protein synthesis rate measured by fluorescence intensity of the AlexaFluor 488 (fluorescence intensity per pixel; a.u.–arbitrary units). Data are representative of two independent experiments and values in graphs are expressed as mean, with whiskers extending to data points that are less than 1.5 x interquartile range away from 1st/3rd quartile (Tukey's boxplot); significant difference from mock-infected cells was calculated by Student's t-test (**** $P<0.0001$).

TBEV infection in DAOY cells was determined. Induction of viperin mRNA expression was detected at 24 hours p.i. and increasing throughout next 24 hours (Fig 3C; upper panel). Despite significantly increased viperin mRNA levels, none or very small amounts of viperin
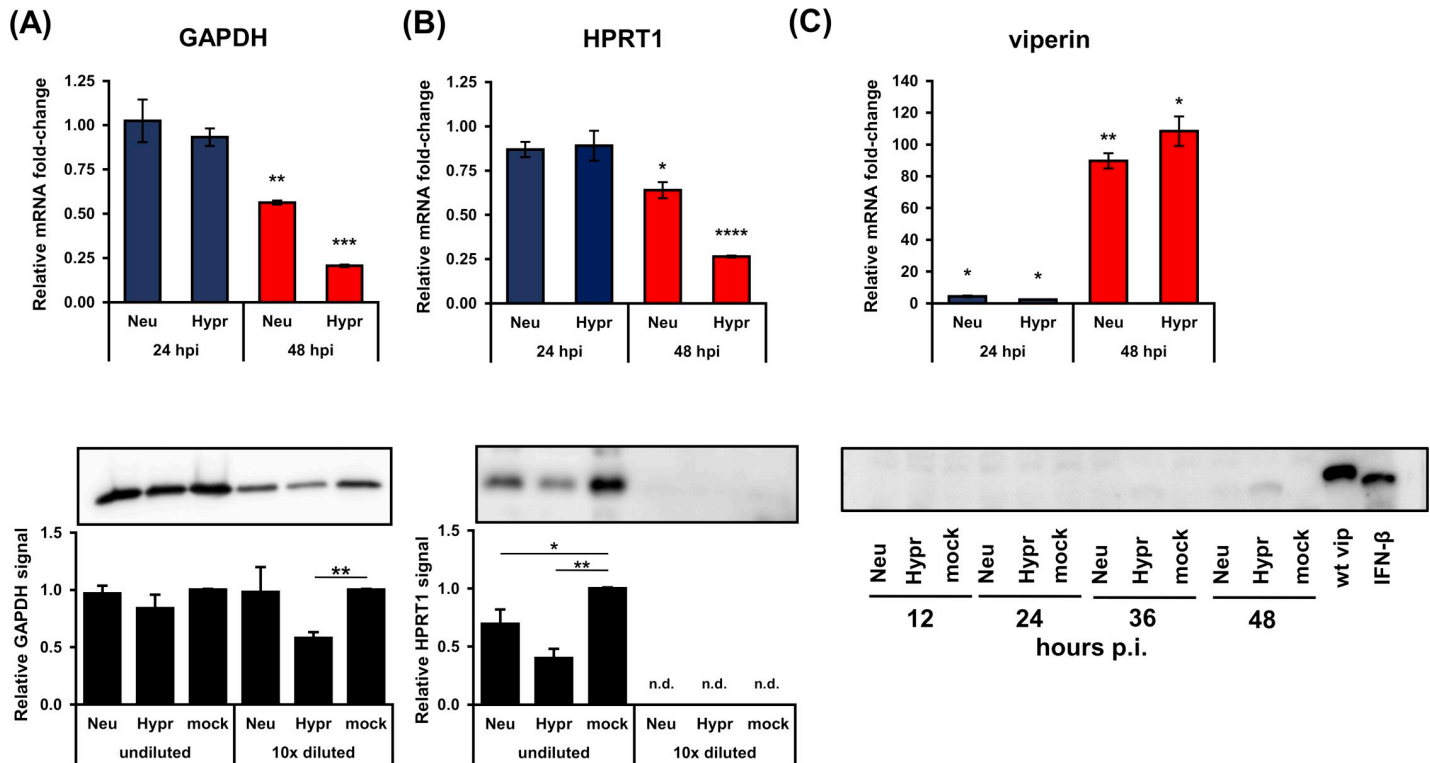
85

Fig 3. TBEV-induced translational arrest results in the decreased protein levels of GAPDH, HPRT1, and viperin. (A) Upper panel: DAOY cells were infected with either TBEV Neudoerfl or Hypr strain (MOI 5) and total RNA was isolated at indicated time intervals. Relative qPCR quantification of GAPDH mRNA using Δ-c$_t$ method with normalisation to the cell number was performed. Lower panel: DAOY cells were infected with either Neudoerfl or Hypr TBEV strain (5 MOI) and lysed at 48 hours p.i. Western blot analysis of GAPDH protein levels was performed using protein-specific antibodies with undiluted and 10-times diluted samples. Relative chemiluminescent signal was quantified using Fiji software and compared to mock-infected cells. Values were further normalised to the cell number. Data are summary of three independent experiments and values in graphs are expressed as mean with SEM. Significant difference from mock-infected cells was calculated using one-sample Student's t-test (** $P<0.01$; *** $P<0,001$). (B) Upper panel: DAOY cells were infected with either TBEV Neudoerfl or Hypr strain (MOI 5) and total RNA was isolated at indicated time intervals. Relative qPCR quantification of HPRT1 mRNA using Δ-c$_t$ method with normalisation to the cell number was performed. Lower panel: DAOY cells were infected with either Neudoerfl or Hypr TBEV strain (5 MOI) and lysed at 48 hours p.i. Western blot analysis of HPRT1 protein levels was performed using protein-specific antibodies with undiluted and 10-times diluted samples. Relative chemiluminescent signal was quantified using Fiji software and compared to mock-infected cells. Values were further normalised to the cell number. Data are summary of three independent experiments and values in graphs are expressed as mean with SEM. Significant difference from mock-infected cells was calculated using one-sample Student's t-test (* $P<0.05$; ** $P<0.01$; **** $P<0.0001$); n.d.–not detected. (C) Upper panel: DAOY cells were infected with either TBEV Neudoerfl or Hypr strain (MOI 5) and total RNA was isolated at the indicated time intervals. Relative qPCR quantification of viperin mRNA using Δ-c$_t$ method with normalisation to the cell number was performed. Data are summary of three independent experiments and values are expressed as mean with standard error of mean (SEM). Lower panel: Immunodetection of viperin protein in TBEV-infected DAOY cells at indicated intervals p.i. (MOI 5). As a positive control, cells transfected with a c-myc-tagged viperin expression plasmid (wt vip) and cells treated with IFN-β (12 hours; 50 ng/ml) were used.

https://doi.org/10.1371/journal.pntd.0007745.g003

protein were detected in cell lysates from TBEV-infected DAOY cells by western blot analysis (Fig 3C; lower panel). As a positive control, DAOY cells treated with INF-β (12 hours; 50 ng/ml) as well as DAOY cells transfected with a human viperin expression vector [40] were used.

To assess whether the effect of TBEV on endogenous viperin production can be overcome by artificial over-expression, DAOY cells were first infected (TBEV Neudoerfl and Hypr; MOI 5) and subsequently transfected with a wt-viperin expression construct at 12 hours p.i. Viperin mRNA, as well as protein levels, were analysed at 12 hours post-transfection (S3A Fig). As a control, GFP expression construct was used. S3B Fig shows that viperin protein was produced; however, the protein levels were significantly reduced in TBEV-infected cells compared to control cells. Hypr strain infection also resulted in a statistically significant decrease in mRNA levels of viperin. As expected, GFP production in TBEV infected cells was negatively affected in case of both TBEV strains (S3C Fig). Again, Hypr strain infection also caused a significant
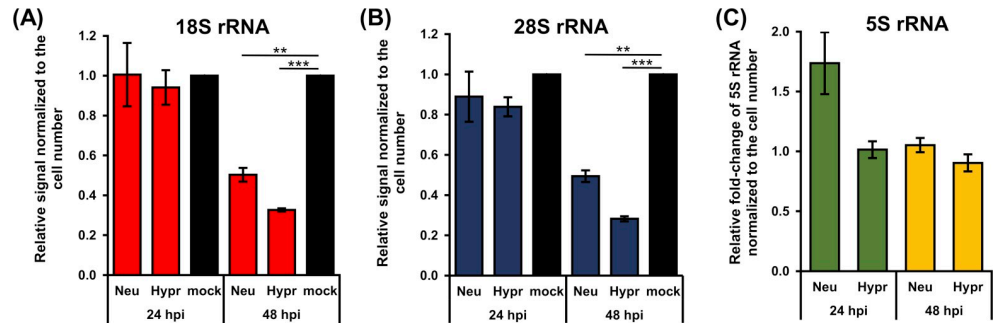
86

Fig 4. TBEV infection decrease levels of 18S and 28S rRNA but not 5S rRNA. (A, B) Total RNA was isolated from TBEV-infected DAOY cells (24 and 48 hours p.i.; MOI 5) and analysed using Bioanalyzer 2100. Graphs represent relative mean of areas for 18S (a) and 28S (b) peaks compared to mock-infected cells. Values were further normalised to the cell number. Data are representative of three independent experiments and values are expressed as mean with SEM. Significant difference from mock-infected cells was calculated using one-sample Student's t-test (** $P<0.01$; *** $P<0,001$). (C) Relative quantification of 5S rRNA in TBEV-infected DAOY cells at 24 and 48 hours p.i. (MOI 5) using the Δ-c_t method. Graph represents relative fold-induction of 5S rRNA levels in comparison to mock-infected cells with normalisation to cell number. Data are representative of three independent experiments and values are expressed as mean with SEM.

https://doi.org/10.1371/journal.pntd.0007745.g004

decrease in GFP mRNA. Consequently, TBEV induces a general translational shut-off, which can negatively affect even the production of overexpressed transcripts. Nevertheless, viral titres were increasing throughout the infection (Fig 1).

TBEV infection downregulates the levels of specific host rRNAs

Previous data revealed a significant decrease in RNA encoding genes including 5.8S rRNA and 7SL RNA following TBEV infection [47]. Here, we verified the link between the TBEV-induced translational shut-off and production of host rRNAs. We quantified the levels of 18S and 28S rRNAs in total cellular RNA from TBEV-infected DAOY cells at 24 and 48 hours p.i. We found that infection by both TBEV strains significantly decreased the 18S and 28S rRNA (S4 Fig). 18S rRNA levels decreased to 50 ± 6% or 33 ± 1% for TBEV Neudoerfl- or Hypr-infected cells compared to controls, respectively (Fig 4A). For 28S rRNA, its transcription levels fell to 49 ± 5% or 28 ± 2% for TBEV Neudoerfl- or Hypr-infected cells, respectively (Fig 4B). Both 18S and 28S rRNAs are transcripts of POLR1. Interestingly, the POLR3 transcript 5S rRNA levels remained unaffected by TBEV infection (Fig 4C). These data imply that the effect of TBEV infection on host cells also involves the transcription of specific ribosomal RNA genes.

TBEV interferes with *de novo* production of 45-47S pre-rRNA transcripts

In order to elucidate at which step TBEV interferes with rRNA production, we first analysed the integrity of mature rRNA molecules. No degradation products were observed following infection with either TBEV strains at 24 or 48 hours p.i. in DAOY cells (Fig 5A and 5B). Next, we investigated the rRNA expression and processing via quantification of *de novo* synthesised RNA in TBEV-infected DAOY cells. We labelled nascent RNA in TBEV-infected DAOY cells at 24, 36 and 48 hours p.i. with 5-ethynyl uridine (EU). Incorporated EU was visualised using Click chemistry and the biotin-streptavidin detection system. The presence of TBEV Hypr strain resulted in a decreased quantity of 45-47S pre-rRNA transcripts at 36 and 48 hours p.i., whereas infection with TBEV Neudoerfl strain reduced *de novo* synthesis of 45-47S pre-rRNA at 48 hours p.i. (Fig 5C).

87
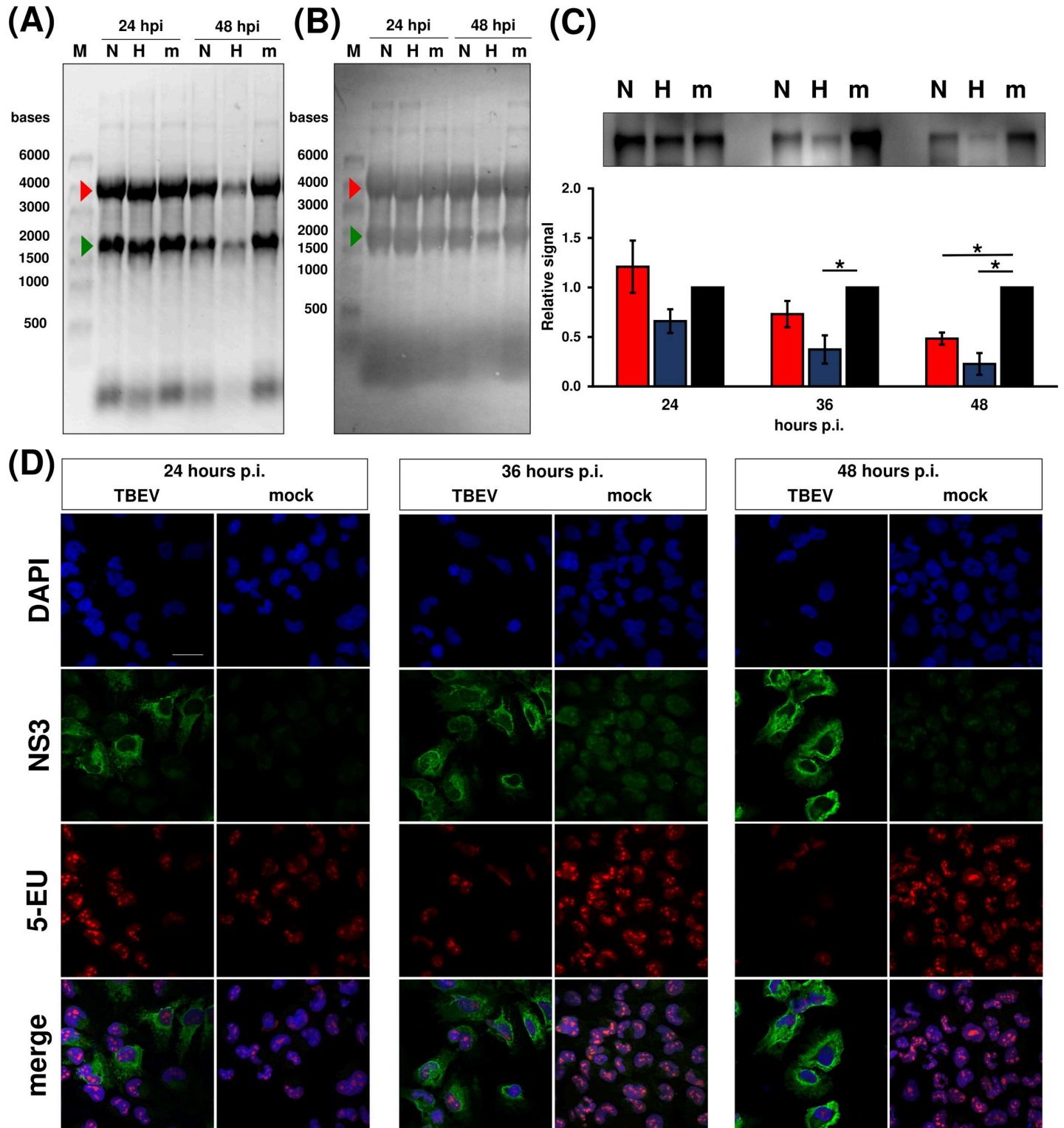
Fig 5. TBEV infection results in decrease of *de novo* synthesised 45-47S pre-rRNA. DAOY cells were either infected with Neudoerfl (N) or Hypr strain (H) at MOI 5 or mock-infected (m). Total RNA was isolated at indicated time post infection; 5-ethynyl uridine (1 mM) was added 2 hours before the collection interval. Data are representative of three independent experiments. (A) Integrity of 28S (red arrow) and 18S rRNA (green arrow), evaluated by using in-gel staining with GelRed. (B) Integrity of 28S (red arrow) and 18S rRNA (green arrow), evaluated by methylene blue staining after capillary transfer on PVDF membrane. (C) Upper panel: metabolic labelling of nascent 45-47S pre-rRNA was carried out using Click chemistry and biotin picolyl azide (10 μM) with subsequent chemiluminescent visualisation via biotin-streptavidin-alkaline phosphatase system. Lower panel: values are expressed as mean of three independent experiments with SEM. Significant difference from mock-

88

infected cells was calculated using one-sample Student's t-test (* P<0.05). (D) *In situ* metabolic labelling revealed TBEV-induced reduction of nascent RNA at 36 hours p.i. without change in RNA localization. DAOY cells were infected with TBEV Hypr strain (MOI 5) and at indicated time intervals incubated for 2 hours with 1 mM 5-ethynyl uridine (5-EU) in order to label nascent RNA. Detection of incorporated 5-EU was performed by Click reaction using 10 μM biotin picolyl azide followed by fluorescent labelling with streptavidin-DyLight549. Cells were co-stained with anti-NS3 antibodies; signal was further visualised using anti-chicken DyLight488 antibodies. Nuclei were stained with DAPI. Scale bar represents 200 μm.

Previously, a link between the inhibition of expression of 45-47S pre-rRNA and nucleolar stress was documented [31]. There are several hallmarks typical for nucleolar stress including disruption of nucleolus structure [51]. We, therefore, characterised the localization and production of nascent RNA at the cellular level and also investigated the structure of the nucleolus. DAOY cells infected with TBEV Hypr strain were analysed at 24, 36, and 48 hours p.i. using *in situ* Click reaction with 10 μM picolyl biotin azide and subsequent visualisation *via* streptavidin conjugated with DyLight-549. As shown in Fig 5D, the overall production of nascent RNA in TBEV-infected cells started to decrease from 36 hours p.i.; *de novo* synthesised RNA was exclusively detected in nuclei with foci of nascent RNA molecules localised in nucleoli. In addition, these nascent RNA foci were not structurally altered upon TBEV infection. The specificity of the labelling reaction was determined using EU-unlabelled cells in the Click reaction (S5A Fig). In order to further verify that TBEV did not induce nucleolar re-arrangement due to nucleolar stress, we analysed the nucleolar structure upon TBEV Hypr infection using nucleophosmin (NPM1; a nucleolar marker). As a positive control, cells were treated with 1 mM H_2O_2 for 45 minutes. No disruption of nucleoli in TBEV-infected cells was observed (S5B Fig). These data imply that TBEV inhibits 45-47S pre-rRNA production without triggering the nucleolar stress pathway.

TBEV infection affects POLR1 levels but not nucleolar localisation

Based on the observed TBEV interference with rRNA production on the transcriptional level, we sought to investigate if the levels and cellular localization of POLR1 changes in infected cells. As shown in Fig 6A and 6B, POLR1 was localised exclusively to the nuclei, and no translocation occurred in infected cells at any time interval tested. Nevertheless, POLR1 protein levels were impaired in TBEV Hypr-infected cells at 48 hours p.i. This may be a result of the previously mentioned translational shut-off since it coincided at 48 hours p.i. Besides, POLR1 mRNA levels were negatively affected by TBEV infection, too (Fig 6C). In particular, POLR1A (the largest subunit of the RNA polymerase I complex) mRNA levels dropped to 60 ± 5% or 25 ± 1% in TBEV Neudoerfl- or Hypr-infected DAOY cells at 48 hours p.i., respectively.

TBEV-induced translational shut-off and the decrease in production of nascent 45-47S pre-rRNA raised the question whether these processes are casually interconnected. We analysed the rate of rRNA production in DAOY cells after treatment with cycloheximide (CHX), an inhibitor of translation elongation. First, we determined the time- and dosage-dependent effect of CHX in DAOY cells using a *Renilla* (RL) luciferase-based reporter system. DAOY cells were first transfected with pRL-CMV and treated with CHX (50, 100, and 300 μg/ml). As shown in S6 Fig, all CHX concentrations tested decreased the production of luciferase. Moreover, the inhibition rate of luciferase production increased with longer exposure to CHX. Next, rRNA production in DAOY cells with decreased translational rate was assessed. Cells were treated with CHX (100 μg/ml) for 6 or 14 hours and *de novo* RNA synthesis in CHX-treated cells was subsequently determined. Fig 7A shows a statistically significant decrease in levels of nascent 45-47S pre-rRNA for both intervals. In particular, the levels decreased to 22 ± 9% or 56 ± 16% during CHX treatment for 14 or 6 hours, respectively. In addition, total levels of mature 18S and 28S rRNAs were quantified in CHX-treated cells. Significant

89
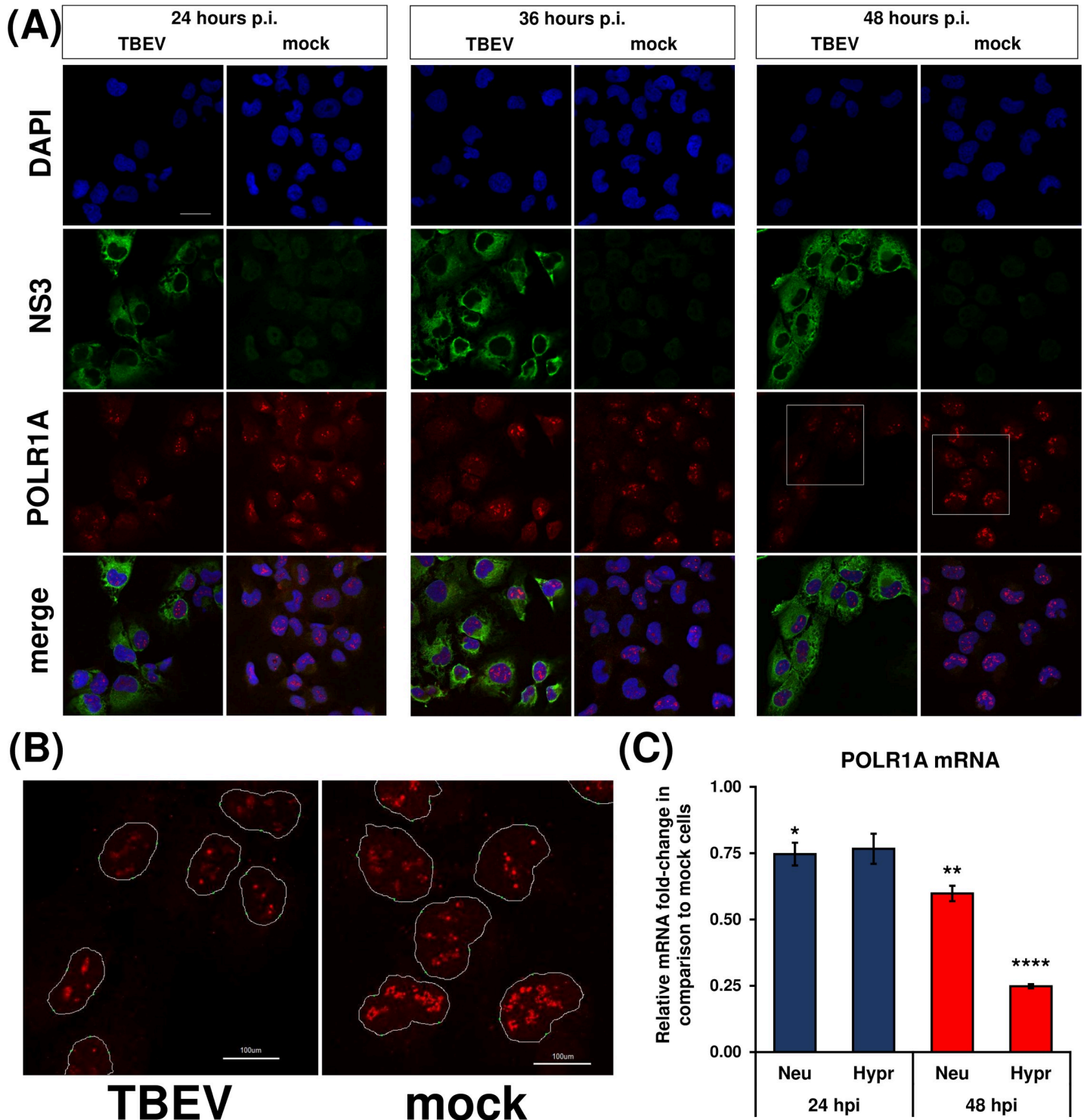
Fig 6. RNA polymerase I is not translocated upon TBEV infection. (A) DAOY cells were infected with TBEV Hypr strain (MOI 5) and at indicated time intervals fixed and POLR1A was detected using rabbit anti-POLR1A and anti-rabbit DyLight594 antibodies. Cells were further co-stained for viral NS3 protein using chicken anti-NS3 and anti-chicken DyLight488 antibodies. Nuclei were stained with DAPI. Scale bar represents 200 μm. (B) Zoomed images from panel (A) at 48 hours p.i. (areas marked by the white squares); POLR1 is localised in distinct foci in host nuclei without any observable virus-induced translocation. Scale bar represents 100 μm. (C) DAOY cells were infected with either TBEV Neudoerfl or Hypr strain (MOI 5) and total RNA was isolated at indicated time intervals. Relative qPCR quantification of POLR1A mRNA using Δ-c_t method with normalisation to the cell number was performed. Data are representative of three independent experiments and values are expressed as mean with SEM. Significant difference from mock-infected cells was calculated using one-sample Student's t-test (* $P<0.05$; ** $P<0.01$; **** $P<0,0001$).

90
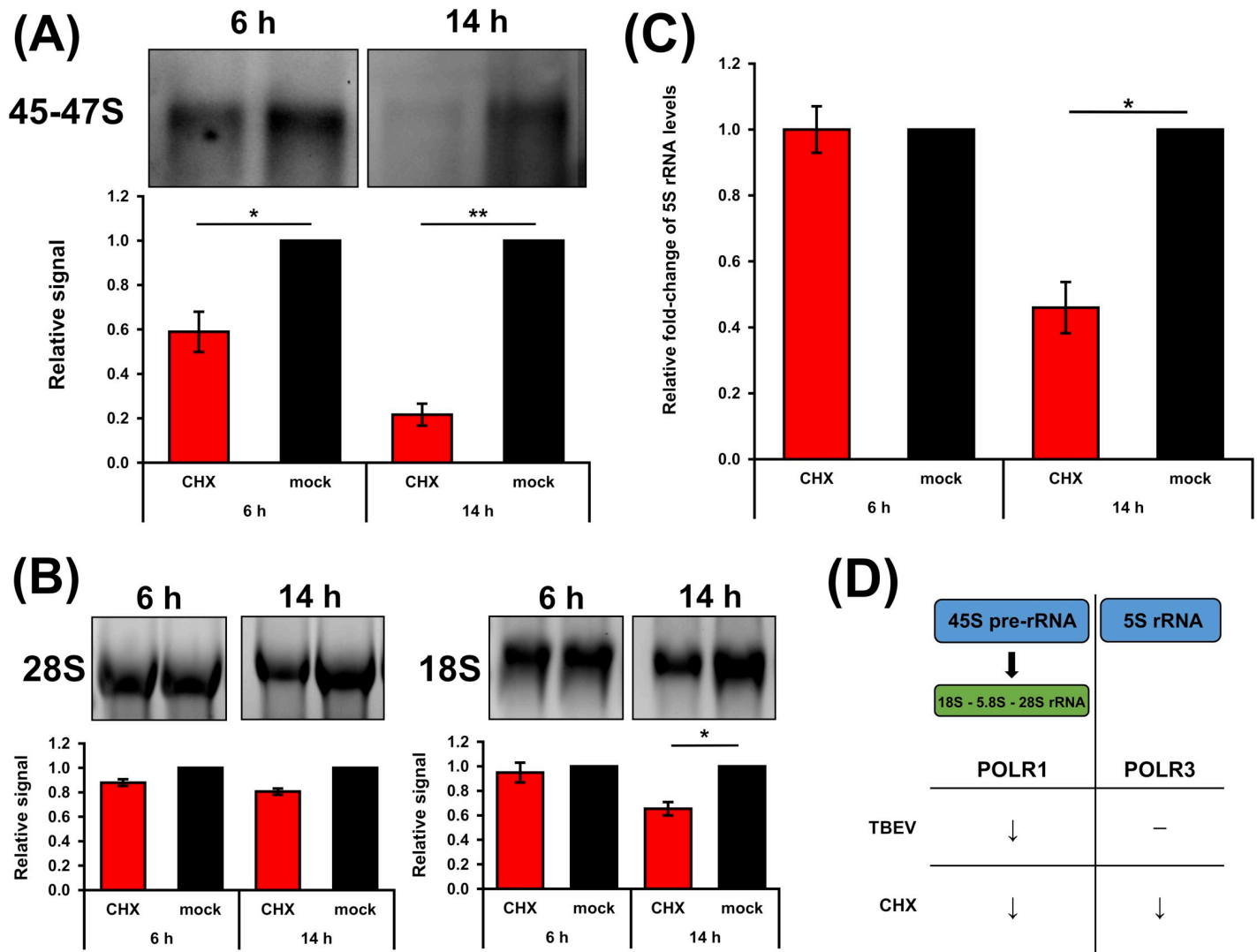
Fig 7. Cycloheximide (CHX) treatment decreases production of rRNA transcripts by POLR1 and POLR3. (A) DAOY cells were treated with CHX (100 µg/ml) for either 6 or 14 hours; for metabolic RNA labelling, 5-EU was added 2 hours before the sample collection. Cell viability was measured before the cell lysis. Isolated total RNA was transferred to a PVDF membrane and nascent RNA quantified using Click chemistry with 10 µM biotin picolyl azide before subsequent chemiluminescent detection. Data are representative of three independent experiments and values in graphs are expressed as mean with SEM, normalised to cell numbers and mock infected cells. Significant difference from the control was calculated using one-sample Student's t-test (* P<0.05; ** P<0.01). (B) Levels of 28S and 18S rRNA were analysed by in-gel RNA staining with GelRed before blotting. Data are representative of three independent experiments and values in graphs are expressed as mean with SEM, normalised to cell number and mock infected samples. Significant difference from the control was calculated using one-sample Student's t-test (* P<0.05). (C) Relative quantification of 5S rRNA in CHX-treated DAOY cells (6 and 14 hours post treatment; 100 µg/ml) using the Δ-c$_t$ method. Graph represents relative fold-induction of 5S rRNA levels in comparison to mock-treated cells, with normalisation to cell number. Data are representative of three independent experiments and values are expressed as mean with SEM. Significant difference from the control was calculated using one-sample Student's t-test (* P<0.05). (D) Schematic summary of CHX versus TBEV effect on the expression of POLR1 and POLR3 transcripts. (↓) indicates observed decrease of the RNA levels and (—) indicates no change in RNA levels.

https://doi.org/10.1371/journal.pntd.0007745.g007

decreases in 18S rRNA levels were observed after a 14-hour incubation (65 ± 9%; Fig 7B). 28S rRNA levels were reduced to 81 ± 4% compared to control cells; however, this effect was not statistically significant (Fig 7B). Quantification of 5S rRNA, a POLR3 transcript, revealed a statistically significant decrease even for this rRNA species after 14 hours of CHX treatment (46 ± 11%; Fig 7C). These data demonstrated that during translation inhibition induced by CHX, the quantity of rRNA transcripts of both RNA polymerases (POLR1 and POLR3) were

91

decreased. In comparison to the general rRNA synthesis shut-down resulting from the action of CHX, TBEV infection induced only a decrease in POLR1 rRNA transcripts (Fig 7D). This suggests that TBEV infection specifically targeted POLR1, which may subsequently result in translational shut-off.

Discussion

TBEV infection is spreading through Europe, resulting in increased numbers of TBEV cases and emergence in previously unaffected areas. TBEV is known to be able to cause neurological symptoms in some infected patients, though little is known about its interplay with neural cells. The molecular basis of damage to the CNS following TBEV infection is still not fully understood. So far, it seems that it is a complex phenomenon combining multiple factors including host immune system [52]. Therefore, understanding the TBEV interaction with target cells and detailed description of processes of viral or host response can help to reveal new targets and ideas on how to treat this disease more successfully. To what extent the outcome of these infection-induced processes is reflected on longer term sequelae remains unrevealed.

Metabolic labelling experiments demonstrated that TBEV infection interferes with the global *de novo* protein synthesis in infected cells. Surprisingly, the effect of translational arrest was so robust that even the protein levels of two commonly used housekeeping genes, GAPDH and HPRT1, were significantly lowered (Fig 3A and 3B). Cell lines of both neural and non-neural origin underwent translational shut-off, demonstrating thus the general nature of this phenomenon upon TBEV infection. However, the rate of reduction varied substantially in individual cell lines suggesting cell-dependent effects. TBEV Hypr strain caused a greater translational shut-off in all cell lines compared to the Neudoerfl strain. This may be due to the increased virulence and neuroinvasiveness of the Hypr strain [53] or due to susceptibility and tropism of the virus strains to specific cell types. Recent studies have demonstrated that some flaviviruses can cause translation suppression via diverse mechanisms [24, 48]. These findings together with our results revise the idea of flaviviruses as "non-host cell protein synthesis influencers" [25, 54, 55]. Indeed, flaviviruses have been thought to avoid the host-cell protein synthesis shut-off as they replicate at a slower rate and global protein synthesis manipulation might have potentially deleterious effects on cell viability and virus yields [56, 57]. However, reduced synthesis of host proteins had no adverse effect on the production of viral NS3 and C proteins (Fig 1C), viral gRNA (Fig 1B) or production of viral progeny (Fig 1A). This suggests that protein synthesis shut-off does not stop TBEV from successful replication.

Viperin is a known interferon-stimulated gene (ISG) and has been described as a potent antiviral protein against members of the *Flaviviridae* family, especially TBEV [50, 58–61]. Thereby it is anticipated to see an increase in viperin mRNA levels upon TBEV infection in DAOY cells. However, the absence of endogenous viperin protein in TBEV-infected cells is surprising. Thus, translational shut-off may yield multiple advantages to TBEV. Apart from gearing the host protein synthesis apparatus to the purposes of the virus, it may also perform as an immune evasion strategy by preventing ISG production. A widely used stable overexpression approach in an ISG/viperin study [59] might therefore mask the real interactions among flaviviruses and host cells during the infection. In general, our data highlight the importance of careful experimental design when studying virus-host interactions and ISG function specifically.

To our knowledge virus-driven reduction in host rRNA levels has not been described before for any flavivirus. Only scarce information is available regarding the virus-induced reduction of rRNA expression, production, and maturation. For example, murine hepatitis virus directly reduces the levels of mature 28S rRNA [62]; *Autographa californica* multiple

92
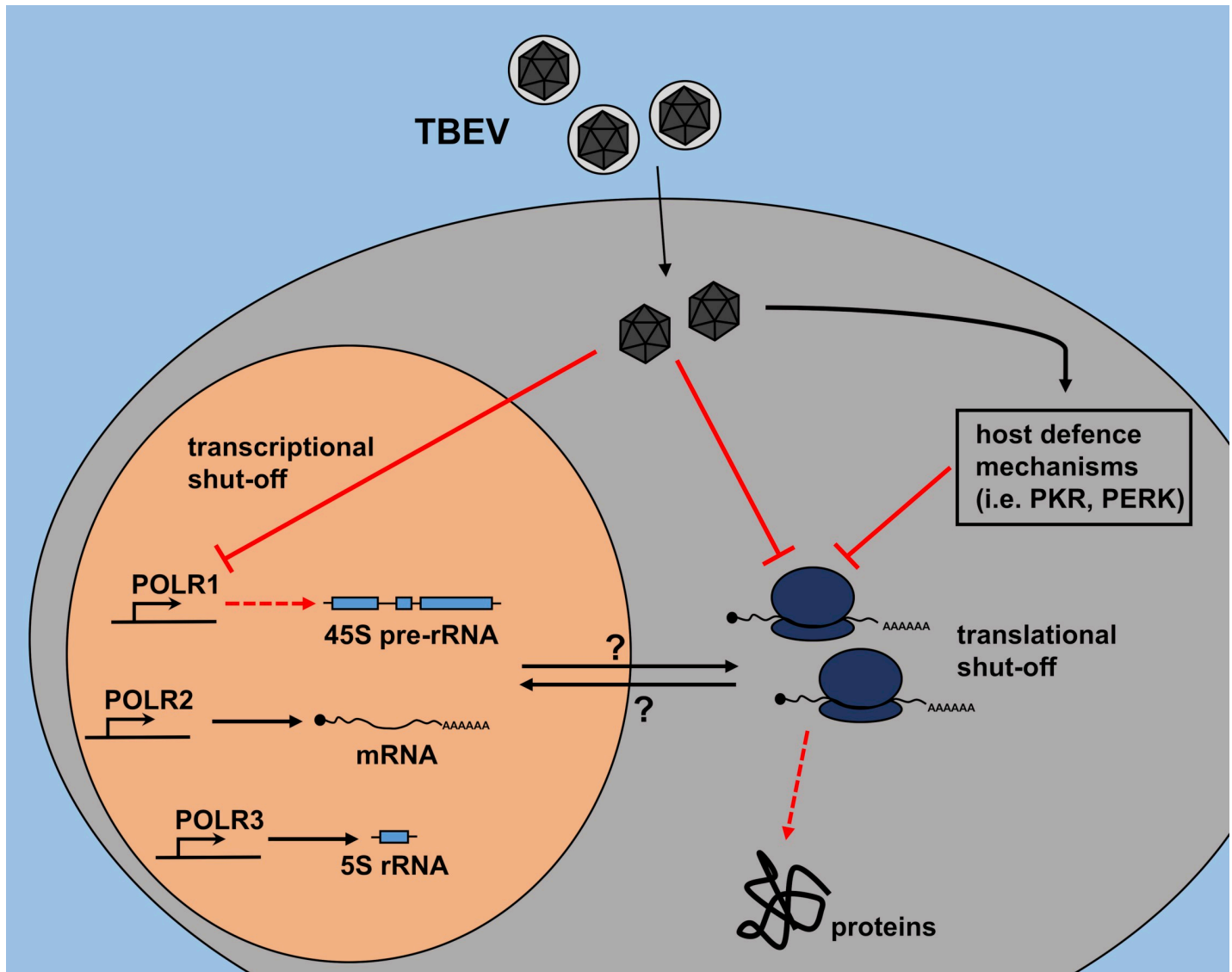
Fig 8. Schematic overview of potential pathways leading to TBEV-driven decrease in synthesis of host rRNA and proteins. TBEV may interfere directly with host translational processes, leading to decreased host protein levels. This decrease could negatively affect pre-rRNA synthesis and eventually rRNA levels. On the other hand, TBEV may also interfere directly with the synthesis of pre-rRNA first, which results in decreased levels of mature rRNAs. Insufficiency of rRNAs subsequently leads to the impairment of ribosome biogenesis and decrease of the translational rate in infected DAOY cells. TBEV infection could also trigger host defence mechanisms leading to the translational arrest. For example, protein kinase R (PKR) activated by dsRNA or PKR-like endoplasmic reticulum kinase (PERK) activated by ER stress could play a significant role in the observed translational shut-off as well.

https://doi.org/10.1371/journal.pntd.0007745.g008

nucleopolyhedrovirus was shown to decrease both, 18S and 28S rRNAs [63]. Additionally, over-expression of HIV Tat protein in *Drosophila melanogaster* led to the impairment of 45S pre-rRNA precursor processing [35]. Similarly, herpes simplex virus 1 decreased the rate of rRNA maturation despite unaltered levels of 45-47S pre-rRNA and unchanged POLR1 activity [32]. The reduction of rRNA levels can be associated with the induction of nucleolar stress, which is characterized by several hallmarks including nucleolar and ribosomal disruption eventually leading to the activation of the p53 signalling pathway. A possible link between flaviviral pathogenesis and nucleolar stress was suggested previously. DENV and ZIKV, but not WNV were shown to induce nucleolar stress in infected cells by disruption of nucleoli, which

93

resulted in an increased rate of apoptosis via the p53 signalling cascade [64]. However, no disruption of nucleoli was observed in the case of TBEV-infected DAOY cells (S5B Fig), possibly not surprising as the TBEV infection specifically affects only the POLR1 activity.

We propose alternative ways by which TBEV could interfere with transcription and/or translation in DAOY cells: 1) TBEV negatively affects the translation of host proteins, including POLR1, transcription factors, and ribosomal proteins; their lower levels subsequently result in a decline in synthesis of all rRNA species; or 2) TBEV directly interferes with *de novo* synthesis of 45-47S pre-rRNA (but not 5S rRNA) via a POLR1 specific mechanism, which reduces the levels of 18S and 28S rRNAs and this leads to the decline of translational rate in host cells; 3) transcription and translation can be modified independently by both viral or cellular factors as a result of infection (summarised in Fig 8). Translational shut-off can otherwise be elicited by host cell defence mechanisms, such as activation of protein kinase R (PKR) or PKR-like endoplasmic reticulum kinase (PERK) [65–67]. To elucidate the exact mechanism of the inhibition of host protein and rRNA production and actual involvement of viral and host factors further experiments will be needed. These may for example assess whether viral proteins can directly inhibit transcription and/or translation. The present study does not elucidate this question and more work will be required to understand the processes; underlying the effects described here.

An overall translational inhibition induced by CHX treatment results in reduced *de novo* synthesis of 45-47S pre-rRNA precursor as well as the levels of 5S rRNA in DAOY cells. In contrast, TBEV infection only affected the 45-47S pre-rRNA precursor (and mature 18S and 28S rRNA levels) and did not affect 5S rRNA. This suggests TBEV-specific inhibition of POLR1 activity, which could result in reduced production of host proteins. Further analyses are needed to characterise the connection between rRNA production arrests and translational shut-off upon TBEV infection.

In summary, our results give new insights into the flavivirus-host interactions at the transcriptional/translational level. Moreover, a virus-induced rRNA decrease was described for flaviviral infection for the first time. The research here can contribute to understanding the mechanisms which determine at least to some extent the subsequent pathological processes. However, the relatively late onset of effects described in this study cannot completely rule out the possibility that our observations are due to cellular responses to TBEV infection rather than virus-mediated, or even combinations of both cellular and viral effects. More work is required to assess these possibilities in detail.

Supporting information

S1 Fig. Cell viability measurement using AlamarBlue in TBEV-infected DAOY cells.
DAOY cells were infected with either TBEV Neudoerfl or Hypr strains (MOI 5) or untreated (mock); at indicated time intervals, cells were counted. A two-fold serial dilution was prepared with range from 50000 to 390 cells/well and cell viability was subsequently analysed by using alamarBlue reagent. Graphs represents fluorescent signal linked to the cell number at 24 hours p.i. (A) and 48 hours p.i. (B). Three independent experiments were performed and values are expressed as mean with SEM.
(TIF)

S2 Fig. TBEV induces host translational shut-off in infected cells. (A) Total protein pattern visualized using Coomassie blue (CBB) staining of the gel used for AHA detection presented in Fig 2A. (N) TBEV Neudoerfl, (H) TBEV Hypr, (m) mock control, (NC) non-labelled mock control. (B) DAOY, MG-63, A549, and Vero cells were infected with either Neudoerfl (N) of Hypr (H) strains of TBEV (MOI 5); as a negative control, mock-infected (m) cells were

94

included. Cells were starved for 1 hour in methionine-free medium and subsequently, nascent proteins were labelled using AHA (incubation for 2 hours; non-labelled negative controls, NC). Cell lysates analysed by SDS-PAGE followed by proteins transfer to PVDF membrane and Click reaction using biotin-alkyne. *De novo* synthesized proteins were further visualized by using biotin-streptavidin detection system along with conjugated alkaline phosphatase. Developed membranes were then stripped and NS3 viral protein detected. Total protein pattern was visualized using CBB staining of the gels after blotting. Representative images out of three independent experiments are shown.
(TIF)

S3 Fig. TBEV inhibits production of over-expressed viperin and GFP. (A) Schematic overview of experimental procedure: DAOY cells were first infected with either Neudoerfl or Hypr strain (MOI 5) and at 24 hours p.i. transfected either with wt-viperin or phMGFP expression constructs. (B) The relative quantification of overexpressed viperin and GFP mRNA in either TBEV Neudoerfl- (Neu) or TBEV Hypr-infected DAOY cells at 24 hours p.t. The Δ-c_t relative quantification method was used, with normalisation to the cell number. Mock-transfected cells (empty vector only) were used as a control. Data are representative of three independent experiments and values are expressed as mean with SEM. Significant difference from the control was calculated using unpaired two-sample Student's t-test (* $P<0.05$, ** $P<0.01$). (C) DAOY cells were first infected with either Neudoerfl or Hypr strain (MOI 5) and at 24 hours p.i. transfected with either viperin or GFP expression plasmids. Analysis of viperin and GFP protein levels was performed at 24 hours p.t. using viperin-specific immunodetection and GFP signal measurement. Relative amounts in comparison to uninfected cells with normalisation to cell numbers are shown for both proteins. Data are representative of three independent experiments and values are expressed as mean with SEM. Significant difference from the control was calculated using a one-sample Student's t-test (* $P<0.05$).
(TIF)

S4 Fig. Raw data of rRNA abundancy in TBEV-infected cells acquired from Bioanalyzer 2100. DAOY cells were infected with either TBEV Neudoerfl or Hypr strains (MOI 5) and total RNA was isolated with RNAblue at the indicated time intervals. Subsequent analysis was performed by using 30 ng of total RNA from mock-infected cells; RNA input of remaining samples was normalised to the cell number. Representative images from three independent experiments are shown.
(TIF)

S5 Fig. Specificity of Click reaction and visualization of nucleoli in DAOY cells. (A) DAOY cells were infected with TBEV Hypr strain (MOI 5) and at indicated time intervals incubated for 2 hours with EU-free cultivation medium. Fixed cells underwent the Click reaction using 10 µM biotin picolyl azide followed by fluorescent labelling with streptavidin-DyLight549. Cells were co-stained with anti-NS3 antibodies; signal was further visualized using anti-chicken DyLight488 antibodies. Scale bar represents 200 µm. (B) DAOY cells were either infected with TBEV Hypr strain (MOI 5) and fixed at 48 hours p.i. or treated with 1 mM hydrogen peroxide for 45 minutes before the fixation. Anti-NPM1 antibodies with the secondary DyLight594-conjugated antibodies were used for the visualization of nucleoli. Scale bar represents 80 µm.
(TIF)

S6 Fig. Cycloheximide (CHX) treatment results in decreased production of Renilla luciferase. DAOY cells were transfected with 100 ng of pRL-CMV reporter vector expressing RL and subsequently treated with CHX (50, 100 or 300 µg/ml) for time periods indicated. At 24 hours

95

p.t. cell viability as well as luciferase activity was analysed. Data are representative of two independent experiments and values are expressed as mean with SEM.
(TIF)

S1 Table. List of used primers.
(PDF)

Acknowledgments

Author Contributions

Conceptualization: Martin Selinger, Hana Tykalová, Ján Štěrba, Alain Kohl, Esther Schnettler.

Funding acquisition: Ján Štěrba, Alain Kohl, Esther Schnettler, Libor Grubhoffer.

Investigation: Martin Selinger, Hana Tykalová, Pavlína Věchtová, Zuzana Vavrušková, Jaroslava Lieskovská.

Methodology: Martin Selinger, Ján Štěrba, Alain Kohl, Esther Schnettler.

Supervision: Alain Kohl, Esther Schnettler, Libor Grubhoffer.

Visualization: Martin Selinger.

Writing – original draft: Martin Selinger, Hana Tykalová.

Writing – review & editing: Martin Selinger, Hana Tykalová, Ján Štěrba, Alain Kohl, Esther Schnettler.

References

1. Simmonds P, Becher P, Bukh J, Gould EA, Meyers G, Monath T, et al. ICTV Virus Taxonomy Profile: Flaviviridae. J Gen Virol. 2017; 98(1):2–3. WOS:000396098700002. https://doi.org/10.1099/jgv.0.000672 PMID: 28218572

2. Dumpis U, Crook D, Oksi J. Tick-borne encephalitis. Clin Infect Dis. 1999; 28(4):882–90. https://doi.org/10.1086/515195 PMID: 10825054.

3. Kunz C, Heinz FX. Tick-borne encephalitis. Vaccine. 2003; 21:S1–S2. ISI:000181967400001.

4. Frimmel S, Krienke A, Riebold D, Loebermann M, Littmann M, Fiedler K, et al. Tick-borne encephalitis virus habitats in North East Germany: reemergence of TBEV in ticks after 15 years of inactivity. Biomed Res Int. 2014. WOS:000339315800001.

5. Boelke M, Bestehorn M, Marchwald B, Kubinski M, Liebig K, Glanz J, et al. First isolation and phylogenetic analyses of tick-borne encephalitis virus in Lower Saxony, Germany. Viruses-Basel. 2019; 11(5). ARTN 462 10.3390/v11050462. WOS:000472676600073.

6. Pagani SC, Malossa SF, Klaus C, Hoffmann D, Beretta O, Bomio-Pacciorini N, et al. First detection of TBE virus in ticks and sero-reactivity in goats in a non-endemic region in the southern part of Switzerland (Canton of Ticino). Ticks Tick-Borne Dis. 2019; 10(4):868–74. WOS:000468379800020. https://doi.org/10.1016/j.ttbdis.2019.04.006 PMID: 31047827

96

7.   Haglund M, Gunther G. Tick-borne encephalitis—pathogenesis, clinical course and long-term follow-up. Vaccine. 2003; 21:S11–S8. ISI:000181967400003. https://doi.org/10.1016/s0264-410x(02)00811-3 PMID: 12628810

8.   Gelpi E, Preusser M, Garzuly F, Holzmann H, Heinz FX, Budka H. Visualization of Central European tick-borne encephalitis infection in fatal human cases. J Neuropathol Exp Neurol. 2005; 64(6):506–12. Epub 2005/06/28. https://doi.org/10.1093/jnen/64.6.506 PMID: 15977642.

9.   Kurhade C, Zegenhagen L, Weber E, Nair S, Michaelsen-Preusse K, Spanier J, et al. Type I Interferon response in olfactory bulb, the site of tick-borne flavivirus accumulation, is primarily regulated by IPS-1. J Neuroinflamm. 2016; 13. WOS:000368886900003.

10. Weber E, Finsterbusch K, Lindquist R, Nair S, Lienenklaus S, Gekara NO, et al. Type I interferon protects mice from fatal neurotropic infection with langat virus by systemic and local antiviral responses. J Virol. 2014; 88(21):12202–12. WOS:000343314900004. https://doi.org/10.1128/JVI.01215-14 PMID: 25122777

11. Gritsun TS, Lashkevich VA, Gould EA. Tick-borne encephalitis. Antiviral Res. 2003; 57(1–2):129–46. https://doi.org/10.1016/s0166-3542(02)00206-1 PMID: 12615309

12. Markoff L. 5'-and 3'-noncoding regions in flavivirus RNA. Adv Virus Res. 2003; 59:177–228. PMID: 14696330

13. Barrows NJ, Campos RK, Liao KC, Prasanth KR, Soto-Acosta R, Yeh SC, et al. Biochemistry and molecular biology of flaviviruses. Chem Rev. 2018; 118(8):4448–82. WOS:000431095200009. https://doi.org/10.1021/acs.chemrev.7b00719 PMID: 29652486

14. Murray CL, Jones CT, Rice CM. Architects of assembly: roles of Flaviviridae non-structural proteins in virion morphogenesis. Nat Rev Microbiol. 2008; 6(9):699–708. ISI:000258413100015. https://doi.org/10.1038/nrmicro1928 PMID: 18587411

15. Lindqvist R, Upadhyay A, Overby AK. Tick-borne flaviviruses and the type I interferon response. Viruses-Basel. 2018; 10(7). Tick-borne flaviviruses and the type I interferon response. WOS:000445153200002.

16. Apte-Sengupta S, Sirohi D, Kuhn RJ. Coupling of replication and assembly in flaviviruses. Curr Opin Virol. 2014; 9:134–42. WOS:000346958700022. https://doi.org/10.1016/j.coviro.2014.09.020 PMID: 25462445

17. Walsh D, Mathews MB, Mohr I. Tinkering with translation: protein synthesis in virus-infected cells. Csh Perspect Biol. 2013; 5(1). WOS:000315983600013.

18. Rivas HG, Schmaling SK, Gaglia MM. Shutoff of host gene expression in influenza A virus and herpesviruses: similar mechanisms and common themes. Viruses-Basel. 2016; 8(4). WOS:000375157800015.

19. Blakqori G, van Knippenberg I, Elliott RM. Bunyamwera orthobunyavirus S-segment untranslated regions mediate poly(A) tail-independent translation. J Virol. 2009; 83(8):3637–46. WOS:000264327300021. https://doi.org/10.1128/JVI.02201-08 PMID: 19193790

20. Walsh D, Mohr I. Viral subversion of the host protein synthesis machinery. Nat Rev Microbiol. 2011; 9 (12):860–75. WOS:000297255800012. https://doi.org/10.1038/nrmicro2655 PMID: 22002165

21. Feigenblum D, Schneider RJ. Modification of eukaryotic initiation factor 4F during infection by influenza virus. J Virol. 1993; 67(6):3027–35. WOS:A1993LB79400008. PMID: 8098776

22. de Breyne S, Bonderoff JM, Chumakov KM, Lloyd RE, Hellen CUT. Cleavage of eukaryotic initiation factor eIF5B by enterovirus 3C proteases. Virology. 2008; 378(1):118–22. WOS:000258316100013. https://doi.org/10.1016/j.virol.2008.05.019 PMID: 18572216

23. Gradi A, Svitkin YV, Imataka H, Sonenberg N. Proteolysis of human eukaryotic translation initiation factor eIF4GII, but not eIF4GI, coincides with the shutoff of host protein synthesis after poliovirus infection. P Natl Acad Sci USA. 1998; 95(19):11089–94. WOS:000075957100017.

24. Roth H, Magg V, Uch F, Mutz P, Klein P, Haneke K, et al. Flavivirus infection uncouples translation suppression from cellular stress responses. Mbio. 2017; 8(1). WOS:000395835000058.

25. Edgil D, Polacek C, Harris E. Dengue virus utilizes a novel strategy for translation initiation when cap-dependent translation is inhibited. J Virol. 2006; 80(6):2976–86. WOS:000236131400039. https://doi.org/10.1128/JVI.80.6.2976-2986.2006 PMID: 16501107

26. Villas-Boas CSA, Conceicao TM, Ramirez J, Santoro ABM, Da Poian AT, Montero-Lomeli M. Dengue virus-induced regulation of the host cell translational machinery. Braz J Med Biol Res. 2009; 42 (11):1020–6. WOS:000271163100001. https://doi.org/10.1590/S0100-879X2009001100004 PMID: 19855901

27. Roberts L, Wieden HJ. Viruses, IRESs, and a universal translation initiation mechanism. Biotechnol Genet Eng Rev. 2018; 34(1):60–75. Epub 2018/05/29. 29804514. https://doi.org/10.1080/02648725.2018.1471567 PMID: 29804514

97

28. Henras AK, Plisson-Chastang C, O'Donohue MF, Chakraborty A, Gleizes PE. An overview of pre-ribosomal RNA processing in eukaryotes. Wiley Interdisciplinary Reviews: RNA. 2015; 6(2):225–42. Epub 2014/10/28. https://doi.org/10.1002/wrna.1269 PMID: 25346433; PubMed Central PMCID: PMC4361047.

29. Khatter H, Vorlander MK, Muller CW. RNA polymerase I and III: similar yet unique. Curr Opin Struc Biol. 2017; 47:88–94. WOS:000419413700013.

30. Chen FX, Smith ER, Shilatifard A. Born to run: control of transcription elongation by RNA polymerase II. Nat Rev Mol Cell Bio. 2018; 19(7):464–78. WOS:000435953700009.

31. Yan Y, Du Y, Wang G, Li K. Non-structural protein 1 of H3N2 influenza A virus induces nucleolar stress via interaction with nucleolin. Sci Rep. 2017; 7(1):17761. Epub 2017/12/21. https://doi.org/10.1038/s41598-017-18087-2 PMID: 29259342; PubMed Central PMCID: PMC5736645.

32. Belin S, Kindbeiter K, Hacot S, Albaret MA, Roca-Martinez JX, Therizols G, et al. Uncoupling ribosome biogenesis regulation from RNA polymerase I activity during herpes simplex virus type 1 infection. RNA. 2010; 16(1):131–40. Epub 2009/11/26. https://doi.org/10.1261/rna.1935610 PMID: 19934231; PubMed Central PMCID: PMC2802023.

33. Oswald E, Reinz E, Voit R, Aubin F, Alonso A, Auvinen E. Human papillomavirus type 8 E7 protein binds nuclear myosin 1c and downregulates the expression of pre-rRNA. Virus Genes. 2017; 53 (6):807–13. Epub 2017/07/25. https://doi.org/10.1007/s11262-017-1491-6 PMID: 28733876.

34. Westdorp KN, Sand A, Moorman NJ, Terhune SS. Cytomegalovirus late protein pUL31 alters pre-rRNA expression and nuclear organization during infection. J Virol. 2017; 91(18). Epub 2017/07/01. https://doi.org/10.1128/JVI.00593-17 PMID: 28659485; PubMed Central PMCID: PMC5571270.

35. Ponti D, Troiano M, Bellenchi GC, Battaglia PA, Gigliani F. The HIV Tat protein affects processing of ribosomal RNA precursor. BMC cell biology. 2008; 9:32. Epub 2008/06/19. https://doi.org/10.1186/1471-2121-9-32 PMID: 18559082; PubMed Central PMCID: PMC2440370.

36. Jacobsen PF, Jenkyn DJ, Papadimitriou JM. Establishment of a human medulloblastoma cell line and its heterotransplantation into nude mice. J Neuropathol Exp Neurol. 1985; 44(5):472–85. Epub 1985/09/01. https://doi.org/10.1097/00005072-198509000-00003 PMID: 2993532.

37. Giard DJ, Aaronson SA, Todaro GJ, Arnstein P, Kersey JH, Dosik H, et al. In vitro cultivation of human tumors: establishment of cell lines derived from a series of solid tumors. J Natl Cancer Inst. 1973; 51 (5):1417–23. Epub 1973/11/01. https://doi.org/10.1093/jnci/51.5.1417 PMID: 4357758.

38. Kozuch O, Mayer V. Pig kidney epithelial (PS) cells: a perfect tool for the study of flaviviruses and some other arboviruses. Acta Virol. 1975; 19(6):498. Epub 1975/11/01. 1999.

39. Billiau A, Edy VG, Heremans H, Van Damme J, Desmyter J, Georgiades JA, et al. Human interferon: mass production in a newly established cell line, MG-63. Antimicrob Agents Chemother. 1977; 12 (1):11–5. Epub 1977/07/01. https://doi.org/10.1128/aac.12.1.11 PMID: 883813; PubMed Central PMCID: PMC352146.

40. Teng TS, Foo SS, Simamarta D, Lum FM, Teo TH, Lulla A, et al. Viperin restricts chikungunya virus replication and pathology. J Clin Invest. 2012; 122(12):4447–60. Epub 2012/11/20. https://doi.org/10.1172/JCI63120 PMID: 23160199; PubMed Central PMCID: PMC3533538.

41. Wallner G, Mandl CW, Ecker M, Holzmann H, Stiasny K, Kunz C, et al. Characterisation and complete genome sequences of high- and low-virulence variants of tick-borne encephalitis virus. J Gen Virol. 1996; 77:1035–42. WOS:A1996UJ08600027. https://doi.org/10.1099/0022-1317-77-5-1035 PMID: 8609469

42. Asghar N, Lindblom P, Melik W, Lindqvist R, Haglund M, Forsberg P, et al. Tick-borne encephalitis virus sequenced directly from questing and blood-feeding ticks reveals quasispecies variance. Plos One. 2014; 9(7). WOS:000341354800074.

43. Heinz FX, Kunz C. Homogeneity of the structural glycoprotein from European isolates of tick-borne encephalitis virus: comparison with other flaviviruses. J Gen Virol. 1981; 57(Pt 2):263–74. Epub 1981/12/01. https://doi.org/10.1099/0022-1317-57-2-263 PMID: 6172553.

44. Pospisil L, Jandasek L. and Pesek J. Isolation of new strains of tick-borne encephalitis virus, Brno region, summer 1953. Lek List. 1954; 9:3–5. PMID: 13131921

45. De Madrid AT, Porterfield JS. A simple micro-culture method for the study of group B arboviruses. Bull World Health Organ. 1969; 40(1):113–21. Epub 1969/01/01. PMID: 4183812; PubMed Central PMCID: PMC2554446.

46. Rueden CT, Schindelin J, Hiner MC, DeZonia BE, Walter AE, Arena ET, et al. ImageJ2: ImageJ for the next generation of scientific image data. BMC bioinformatics. 2017; 18(1):529. Epub 2017/12/01. https://doi.org/10.1186/s12859-017-1934-z PMID: 29187165; PubMed Central PMCID: PMC5708080.

47. Selinger M, Wilkie GS, Tong L, Gu Q, Schnettler E, Grubhoffer L, et al. Analysis of tick-borne encephalitis virus-induced host responses in human cells of neuronal origin and interferon-mediated protection. J

98

Gen Virol. 2017; 98(8):2043–60. Epub 2017/08/09. https://doi.org/10.1099/jgv.0.000853 PMID: 28786780; PubMed Central PMCID: PMC5817271.

48. Reid DW, Campos RK, Child JR, Zheng TL, Chan KWK, Bradrick SS, et al. Dengue virus selectively annexes endoplasmic reticulum-associated translation machinery as a strategy for co-opting host cell protein synthesis. J Virol. 2018; 92(7). WOS:000428409800013.

49. Best MD. Click chemistry and bioorthogonal reactions: unprecedented selectivity in the labeling of biological molecules. Biochemistry. 2009; 48(28):6571–84. Epub 2009/06/03. https://doi.org/10.1021/bi9007726 PMID: 19485420.

50. Lindqvist R, Overby AK. The role of viperin in antiflavivirus responses. DNA Cell Biol. 2018; 37(9):725–30. WOS:000443729600001. https://doi.org/10.1089/dna.2018.4328 PMID: 30059238

51. Yang K, Yang J, Yi J. Nucleolar Stress: hallmarks, sensing mechanism and diseases. Cell Stress. 2018; 2(6):125–40. Epub 10.5. 2018. https://doi.org/10.15698/cst2018.06.139 PMID: 31225478

52. Hayasaka D, Nagata N, Fujii Y, Hasegawa H, Sata T, Suzuki R, et al. Mortality following peripheral infection with Tick-borne encephalitis virus results from a combination of central nervous system pathology, systemic inflammatory and stress responses. Virology. 2009; 390(1):139–50. WOS:000268218200016. https://doi.org/10.1016/j.virol.2009.04.026 PMID: 19467556

53. Mandl CW, Ecker M, Holzmann H, Kunz C, Heinz FX. Infectious cDNA clones of tick-borne encephalitis virus European subtype prototypic strain Neudoerfl and high virulence strain Hypr. J Gen Virol. 1997; 78:1049–57. WOS:A1997WW48500010. https://doi.org/10.1099/0022-1317-78-5-1049 PMID: 9152422

54. Westaway EG. Proteins Specified by Group B Togaviruses in Mammalian-Cells during Productive Infections. Virology. 1973; 51(2):454–65. WOS:A1973P069000019. https://doi.org/10.1016/0042-6822(73)90444-3 PMID: 4632654

55. Heinz FX, Kunz C. Molecular epidemiology of tick-borne encephalitis virus: peptide mapping of large non-structural proteins of European isolates and comparison with other flaviviruses. J Gen Virol. 1982; 62(Oct):271–85. WOS:A1982PL98600008.

56. Emara MM, Brinton MA. Interaction of TIA-1/TIAR with West Nile and dengue virus products in infected cells interferes with stress granule formation and processing body assembly. P Natl Acad Sci USA. 2007; 104(21):9041–6. WOS:000246853700065.

57. Pena J, Harris E. Dengue virus modulates the unfolded protein response in a time-dependent manner. J Biol Chem. 2011; 286(16):14226–36. WOS:000289556200046. https://doi.org/10.1074/jbc.M111.222703 PMID: 21385877

58. Panayiotou C, Lindqvist R, Kurhade C, Vonderstein K, Pasto J, Edlund K, et al. Viperin restricts Zika virus and tick-borne encephalitis virus replication by targeting NS3 for proteasomal degradation. J Virol. 2018; 92(7). WOS:000428409800027.

59. Upadhyay AS, Vonderstein K, Pichlmair A, Stehling O, Bennett KL, Dobler G, et al. Viperin is an iron-sulfur protein that inhibits genome synthesis of tick-borne encephalitis virus via radical SAM domain activity. Cell Microbiol. 2014; 16(6):834–48. Epub 2013/11/20. https://doi.org/10.1111/cmi.12241 PMID: 24245804.

60. Van der Hoek KH, Eyre NS, Shue B, Khantisitthiporn O, Glab-Ampi K, Carr JM, et al. Viperin is an important host restriction factor in control of Zika virus infection. Sci Rep. 2017; 7. WOS:000404451300081.

61. Helbig KJ, Beard MR. The role of viperin in the innate antiviral response. J Mol Biol. 2014; 426(6):1210–9. WOS:000333487600007. https://doi.org/10.1016/j.jmb.2013.10.019 PMID: 24157441

62. Banerjee S, An S, Zhou A, Silverman RH, Makino S. RNase L-independent specific 28S rRNA cleavage in murine coronavirus-infected cells. J Virol. 2000; 74(19):8793–802. Epub 2000/09/12. https://doi.org/10.1128/jvi.74.19.8793-8802.2000 PMID: 10982321; PubMed Central PMCID: PMC102073.

63. Fujita R, Asano S, Sahara K, Bando H. Marked decrease of ribosomal RNA in BmN cells infected with AcMNPV. J Insect Biotechnol Sericol. 2005; 74(3):125–8. https://doi.org/10.11416/jibs.74.125

64. Slomnicki LP, Chung DH, Parker A, Hermann T, Boyd NL, Hetman M. Ribosomal stress and Tp53-mediated neuronal apoptosis in response to capsid protein of the Zika virus. Sci Rep. 2017; 7(1):16652. Epub 2017/12/02. https://doi.org/10.1038/s41598-017-16952-8 PMID: 29192272; PubMed Central PMCID: PMC5709411.

65. Herbert KM, Nag A. A tale of two RNAs during viral infection: how viruses antagonize mRNAs and small non-coding RNAs in the host cell. Viruses-Basel. 2016; 8(6). WOS:000378848600006.

66. Weber F, Kochs G, Haller O. Inverse interference: How viruses fight the interferon system. Viral Immunol. 2004; 17(4):498–515. WOS:000226043900005. https://doi.org/10.1089/vim.2004.17.498 PMID: 15671747

67. Valadao ALC, Aguiar RS, de Arruda LB. Interplay between inflammation and cellular stress triggered by flaviviridae viruses. Front Microbiol. 2016; 7. WOS:000381851000001.

99

Manuscript 4

Selinger M., Věchtová P., **Tykalová H**., Ošlejšková P., Rumlová M., Štěrba J., Grubhoffer L., (2022). Integrative RNA profiling of TBEV-infected neurons and astrocytes reveals potential pathogenic effectors. Computational and Structural Biotechnology Journal, 20: 2759-2777. DOI 10.1016/j.csbj.2022.05.052

Integrative RNA profiling of TBEV-infected neurons and astrocytes reveals potential pathogenic effectors

Martin Selinger [a,b,*], Pavlína Věchtová [a], Hana Tykalová [a,b], Petra Ošlejšková [a], Michaela Rumlová [c], Ján Štěrba [a], Libor Grubhoffer [a,b]

Abbreviations: A3SS, alternative 3′ splice site; A5SS, alternative 5′ splice site; ACACA, Acetyl-CoA Carboxylase Alpha; AKR1C2, Aldo-Keto Reductase Family 1 Member C2; ANKS1A, Ankyrin Repeat And Sterile Alpha Motif Domain Containing 1A; ANOS1, Anosmin 1; AOX1, Aldehyde Oxidase 1; APOBEC3G, Apolipoprotein B MRNA Editing Enzyme Catalytic Subunit 3G; APOL1/6, Apolipoprotein L1/6; ARID2, AT-Rich Interaction Domain 2; AUTS2, Activator Of Transcription And Developmental Regulator AUTS2; BCL11B, BAF Chromatin Remodeling Complex Subunit BCL11B; BCL9L, BCL9 Transcription Coactivator-like; BDKRB2, Bradykinin Receptor B2; BDNF, Brain Derived Neurotrophic Factor; BEND3, BEN Domain Containing 3; BSA, bovine serum albumin; BST2, Bone Marrow Stromal Cell Antigen 2; CALB1, Calbindin 1; CAMK2A, Calcium/Calmodulin Dependent Protein Kinase II Alpha; CD, complement determinant; CDKN1C, Cyclin Dependent Kinase Inhibitor 1C; CFAP61, Cilia And Flagella Associated Protein 61; CHRNA3, Cholinergic Receptor Nicotinic Alpha 3 Subunit; CHRNB4, Cholinergic Receptor Nicotinic Beta 4 Subunit; CLIC5, Chloride Intracellular Channel 5; CMPK2, Cytidine/Uridine Monophosphate Kinase 2; CNS, central nervous system; CNTN2, Contactin 2; CREG2, Cellular Repressor Of E1A Stimulated Genes 2; CXADR, Coxsackievirus B-Adenovirus Receptor; CYYR1, Cysteine And Tyrosine Rich 1; DACH1, Dachshund Family Transcription Factor 1; DAPI, diamidino-2-phenylindole; DCC, Netrin 1 Receptor; DCX, Doublecortin; DDX60, DExD/H-Box Helicase 60; DDX60L, DExD/H-Box 60 Like; DE, differentially expressed; DENV, Dengue virus; DIRAS2, DIRAS Family GTPase 2; DLX1/5/6, Distal-Less Homeobox 1/5/6; DNMT3B, DNA Methyltransferase 3 Beta; DPYSL2, Dihydropyrimidinase Like 2; EBF1, EBF Transcription Factor 1; EGF, Epidermal Growth Factor; ELAVL2/4, ELAV Like RNA Binding Protein 2/4; EPHB1, EPH Receptor B1; EPSTI1, Epithelial Stromal Interaction 1; ERBB4, Erb-B2 Receptor Tyrosine Kinase 4; ES, exon skipping; ESRRG, Estrogen Related Receptor Gamma; FGFb, Fibroblast Growth Factor 2; FPKM, Fragments Per Kilobase of transcript per Million mapped reads; FUT9, Fucosyltransferase 9; G2E3, G2/M−Phase Specific E3 Ubiquitin Protein Ligase; GABRG2, Gamma-Aminobutyric Acid Type A Receptor Subunit Gamma 2; GAPDH, Glyceraldehyde-3-Phosphate Dehydrogenase; GAS2L3, Growth Arrest Specific 2 Like 3; GAS7, Growth Arrest Specific 7; GATAD2B, GATA Zinc Finger Domain Containing 2B; GFAP, Glial Fibrillary Acidic Protein; GIPC2, GIPC PDZ Domain Containing Family Member 2; GLRA2, Glycine Receptor Alpha 2; GNG2, G Protein Subunit Gamma 2; GO, gene ontology; GOLGA4, Golgin A4; GRIN2A, Glutamate Ionotropic Receptor NMDA Type Subunit 2A; gRNA, genomic TBEV RNA; GSEA, gene set enrichment analysis; HERC5/6, HECT And RLD Domain Containing E3 Ubiquitin Protein Ligase 5/6; HEYL, Hes Related Family BHLH Transcription Factor With YRPW Motif Like; hNSC, human neural stem cells; HPRT1, Hypoxanthine Phosphoribosyltransferase 1; HS, hot-spot; HSPA6, Heat Shock Protein Family A (Hsp70) Member 6; HUDD (ELAV4), Hu-Antigen D/ELAV Like Neuron-Specific RNA Binding Protein 4; IFI6, Interferon Alpha Inducible Protein 6; IFIH1 (MDA5), Interferon Induced With Helicase C Domain 1/Melanoma Differentiation-Associated Protein 5; IFIT1-3, Interferon Induced Protein With Tetratricopeptide Repeats 1–3; IFITM1/2, Interferon Induced Transmembrane Protein 1/2; IFN, interferon; IGB, Integrated Genome Browser; IL6, Interleukin 6; IR, intron retention; ISG20, Interferon Stimulated Exonuclease Gene 20; ISGF3, Interferon-Stimulated Gene Factor 3 Gamma; ISGs, interferon-stimulated genes; JEV, Japanese encephalitis virus; KCND2, Potassium Voltage-Gated Channel Subfamily D Member 2; KCNK10, Potassium Two Pore Domain Channel Subfamily K Member 10; KCNS2, Potassium Voltage-Gated Channel Modifier Subfamily S Member 2; KIT, KIT Proto-Oncogene, Receptor Tyrosine Kinase; KLHDC8A, Kelch Domain Containing 8A; KLHL13, Kelch Like Family Member 13; KRR1, KRR1 Small Subunit Processome Component Homolog; LCOR, Ligand Dependent Nuclear Receptor Corepressor; LEKR1, Leucine, Glutamate And Lysine Rich 1; LGI1, Leucine Rich Glioma Inactivated 1; lncRNA, long non-coding RNA; LRRTM3, Leucine Rich Repeat Transmembrane Neuronal 3; LSV, local splicing variation; LUZP2, Leucine Zipper Protein 2; MAN1A1, Mannosidase Alpha Class 1A Member 1; MAP2, Microtubule Associated Protein 2; MBNL2, Muscleblind Like Splicing Regulator 2; MCTP1, Multiple C2 And Transmembrane Domain Containing 1; miRNA, micro RNA; MMP13, Matrix Metallopeptidase 13; MN1, MN1 Proto-Oncogene, Transcriptional Regulator; MOI, multiplicity of infection; mRNA, messenger RNA; MTUS2, Microtubule Associated Scaffold Protein 2; MX2, MX Dynamin Like GTPase 2; MYCN, MYCN Proto-Oncogene, BHLH Transcription Factor; NAV1, Neuron Navigator 1; NCAM1, Neural Cell Adhesion Molecule 1; ncRNA, non-coding RNA; NDRG4, N-Myc Downstream-Regulated Gene 4 Protein; NEK7, NIMA Related Kinase 7; NFASC, Neurofascin; NKAIN1, Sodium/Potassium Transporting ATPase Interacting 1; NMI, N-Myc And STAT Interactor 2; NRAP, Nebulin Related Anchoring Protein; NRARP, NOTCH Regulated Ankyrin Repeat Protein; NREP, Neuronal Regeneration Related Protein; NRN1, Neuritin 1; NS3, flaviviral non-structural protein 3; NXPH2, Neurexophilin 2; NYNRIN, NYN Domain And Retroviral Integrase Containing; OAS, 2′-5′-Oligoadenylate Synthetase; OASL, 2′-5′-Oligoadenylate Synthetase Like; ONECUT2, ONECUT-2 Homeodomain Transcription Factor; OPCML, Opioid Binding Protein/Cell Adhesion Molecule Like; OTX2, Orthodenticle Homeobox 2; PBS, phosphate buffer saline; PBX1, Pre-B-Cell Leukemia Transcription Factor 1; PCDH18/20, Protocadherin 18/20; pc-mRNA, protein-coding mRNA; PFKFB3, 6-Phosphofructo-2-Kinase/Fructose-2,6-Biphosphatase 3; PIK3C2B, Phosphatidylinositol-4-Phosphate 3-Kinase Catalytic Subunit Type 2 Beta; PIP4P2, Phosphatidylinositol-4,5-Bisphosphate 4-Phosphatase 2; PLCH1, Phospholipase C Eta 1; POU3F4, Brain-Specific Homeobox/POU Domain Protein 4; PPM1L, Protein Phosphatase, Mg2+/Mn2+ Dependent 1L; PPP1R17, Protein Phosphatase 1 Regulatory Subunit 17; PRDM12, PR Domain Zinc Finger Protein 12; PSI, percent selective index; PSRC1, Proline And Serine Rich Coiled-Coil 1; PTPN5, Protein Tyrosine Phosphatase Non-Receptor Type 5; PTPRH, Protein Tyrosine Phosphatase Receptor Type H; qRT-PCR, quantitative reverse transcription real-time PCR; RAPGEF5, Rap Guanine Nucleotide Exchange Factor 5; RBFOX1, RNA Binding Fox-1 Homolog 1; RIG-I (DDX58), Retinoic Acid-Inducible Gene 1 Protein; RNF212, Ring Finger Protein 212; RNVU1, RNA, Variant U1 Small Nuclear; RSAD2, Radical S-Adenosyl Methionine Domain Containing 2; RTL8B, Retrotransposon Gag Like 8B; SAMD9, Sterile Alpha Motif Domain Containing 9; SEMA3E, Semaphorin 3E; SH3TC2, SH3 Domain And Tetratricopeptide Repeats 2; SHF, Src Homology 2 Domain Containing F; SHISAL1, Shisa Like 1; SIAH3, Siah E3 Ubiquitin Protein Ligase Family Member 3; SIRPA, Signal Regulatory Protein Alpha; SLITRK5, SLIT And NTRK Like Family Member 5; SNP, single-nucleotide polymorphism; snRNP, small nuclear ribonucleoproteins; SOGA1, Suppressor Of Glucose, Autophagy Associated 1; SPSB4, SplA/Ryanodine Receptor Domain And SOCS Box Containing 4; ST6GAL1, ST6 Beta-Galactoside Alpha-2,6-Sialyltransferase 1; TBC1D30, TBC1 Domain Family Member 30; TBEV, Tick-borne encephalitis virus; TFAP2A, Transcription Factor AP-2 Alpha; TFAP2B, Transcription Factor AP-2 Beta; THSD7A, Thrombospondin Type 1 Domain Containing 7A; THUMPD2, THUMP Domain-Containing Protein 2/SAM-Dependent Methyltransferase; TIPARP, TCDD Inducible Poly(ADP-Ribose) Polymerase; TM4SF18, Transmembrane 4 L Six Family Member 18; TMC8, Transmembrane Channel Like 6; TMEM229B, Transmembrane Protein 229B; TMTC1, Transmembrane O-Mannosyltransferase Targeting Cadherins 1; TNFSF10, TNF Superfamily Member 10; TRHDE, Thyrotropin Releasing Hormone Degrading Enzyme; TRIM38, Tripartite Motif Containing 38; TSHZ1, Teashirt Zinc Finger Homeobox 1; USP18, Ubiquitin Specific Peptidase 18/ISG15-Specific-Processing Protease; UTR, untranslated region; UTS2R, Urotensin 2 Receptor; vd-sRNA, virus-derived small RNA; WNV, West Nile virus; XAF1, XIAP Associated Factor 1; XRN1, 5′-3′ Exoribonuclease 1; ZIKV, Zika virus; ZMAT3, Zinc Finger Matrin-Type 3; ZMYM5, Zinc Finger MYM-Type Containing 5; ZNF124, Zinc Finger Protein 124; ZNF730, Zinc Finger Protein 730.

101

[a] *Faculty of Science, University of South Bohemia in České Budějovice, Branišovská 1760, České Budějovice 370 05, Czech Republic*
[b] *Institute of Parasitology, Biology Centre of the Academy of Sciences of the Czech Republic, Branišovská 31, České Budějovice 370 05, Czech Republic*
[c] *Department of Biotechnology, University of Chemistry and Technology, Prague 166 28, Czech Republic*

ARTICLE INFO

ABSTRACT

Tick-borne encephalitis virus (TBEV), the most medically relevant tick-transmitted flavivirus in Eurasia, targets the host central nervous system and frequently causes severe encephalitis. The severity of TBEV-induced neuropathogenesis is highly cell-type specific and the exact mechanism responsible for such differences has not been fully described yet. Thus, we performed a comprehensive analysis of alterations in host poly-(A)/miRNA/lncRNA expression upon TBEV infection *in vitro* in human primary neurons (high cytopathic effect) and astrocytes (low cytopathic effect). Infection with severe but not mild TBEV strain resulted in a high neuronal death rate. In comparison, infection with either of TBEV strains in human astrocytes did not. Differential expression and splicing analyses with an *in silico* prediction of miRNA/mRNA/lncRNA/vd-sRNA networks found significant changes in inflammatory and immune response pathways, nervous system development and regulation of mitosis in TBEV Hypr-infected neurons. Candidate mechanisms responsible for the aforementioned phenomena include specific regulation of host mRNA levels via differentially expressed miRNAs/lncRNAs or vd-sRNAs mimicking endogenous miRNAs and virus-driven modulation of host pre-mRNA splicing. We suggest that these factors are responsible for the observed differences in the virulence manifestation of both TBEV strains in different cell lines. This work brings the first complex overview of alterations in the transcriptome of human astrocytes and neurons during the infection by two TBEV strains of different virulence. The resulting data could serve as a starting point for further studies dealing with the mechanism of TBEV-host interactions and the related processes of TBEV pathogenesis.

1. Introduction

Tick-borne encephalitis virus (TBEV; genus *Flavivirus*, family *Flaviviridae*) is the most medically important tick-transmitted virus in Eurasia, affecting the lives of 10 000–12 000 diagnosed patients annually [1]. The virus is also gaining attention because of its recent emergence in new localities such as the Netherlands [2]. TBEV, like other flaviviruses, forms spherical virions (50 nm in diameter), and its monopartite genome comprises a ~ 11 kilobases-long single-stranded RNA of positive polarity. The genomic RNA contains one ORF coding for 10 proteins, which is flanked by 5′ and 3′ untranslated regions (UTRs) [3].

Infection dissemination into the central nervous system (CNS) is a final stage in the process of TBEV pathogenesis, where neurons from different brain areas are the predominantly infected cell type and show a high level of death rate [4,5]. TBEV also successfully replicates in astrocytes [6,7], the neuroglial cells that provide all the necessary support for the proper neuronal function. Such as they maintain homeostasis, perform energy metabolism, regulate blood flow, support the synaptic function, and protect neurons from the infection [8]. Unlike in neurons, viability of TBEV-infected astrocytes is not negatively affected, even though similarly high viral titres in both cell types have been described [6,7]. An identical pattern of distinctive pathogenicity in neurons and astrocytes was observed in the case of West Nile virus (WNV) [9,10], but not in Zika virus (ZIKV) [11].

The exact factors responsible for the contrasting outcome of TBEV infection in neurons and astrocytes have not been identified yet; however, it is believed that cell type-specific response on the level of gene expression is one of the key factors involved. Indeed, a recent study by Fares *et al.* have described the neuron/astrocyte-specific response via a distinctive expression profile of specific innate immune response genes [12]. The phenomenon of neuron/ astrocyte-specific immune response to TBEV was confirmed also on the level of cytokine and chemokine production [13]. Both studies point towards the TBEV-induced dysregulation of host gene expression with an outcome strongly dependent on the cell type-specific background.

The regulatory network of non-coding RNAs (ncRNAs) represents one of the most important players in the cell type-specific changes of gene expression upon infection. Among these, expression profiles of specific microRNAs (miRNAs) and long non-coding RNAs (lncRNAs) were shown to be affected by flaviviral infection. miRNAs are a class of short (21–25 nucleotides) ncRNAs regulating gene expression at the post-transcriptional level by sequence-specific binding to mRNA [14]. Several flaviviruses, such as Japanese encephalitis virus (JEV), WNV, and ZIKV, were shown to dysregulate the expression profile of host miRNAs [15–19], of which some were identified to act in a proviral [20] or antiviral manner [16,21,22]. No miRNA-related data are currently available for TBEV [23]. lncRNAs represent another group of ncRNAs that are longer than 200 nucleotides and also contribute to gene expression regulation. In comparison to miRNAs, lncRNAs modulate the gene expression at numerous levels, including chromatin remodelling, cis-/*trans*-regulation of gene transcription, mRNA splicing, and translation [24]. Similarly to miRNAs, the expression pattern of lncRNAs alters upon flaviviral infection [25–29] and particular lncRNAs were identified as proviral [30–32] or antiviral [33] factors. Except for the host-derived ncRNAs, flavivirus-derived small RNAs (vd-sRNAs; 13–36 nt), were identified in mosquito/tick and mammalian cells [34,35]. In arthropod vectors, the generation of vd-sRNAs results from the RNA interference process (RNAi), where vd-sRNAs are used by the host cell to target and cleave viral genomic RNA [36]. However, in the mammalian host, vd-sRNAs may play a different role by mimicking endogenous miRNA and target specific host mRNAs, thus substantially contribute to viral

⁎ Corresponding author at: Faculty of Science, University of South Bohemia in České Budějovice, Branišovská 1760, České Budějovice 370 05, Czech Republic.
E-mail address: selinm01@prf.jcu.cz (M. Selinger).

102

replication and pathogenesis as in the case of influenza A virus and human immunodeficiency virus [37,38].

Despite numerous studies describing TBEV-induced changes in the expression profile of selected genes, no study so far has described a comprehensive transcriptomic analysis of both, ncRNAs and mRNAs in the most affected tissues of CNS. Data from such analysis would extensively broaden our understanding of TBEV-induced pathogenesis mechanism and may identify new target pathways for antiviral drug design. To fill that gap, we performed an integrative analysis describing the changes of host transcriptome on mRNA, miRNA, and lncRNA levels, including the pre-mRNA splicing evaluation, in combination with TBEV-derived vd-sRNA profiling. An *in vitro* model of human primary neurons and astrocytes infected by two TBEV strains of different virulence was utilised to elucidate the key players involved in TBEV-induced neuronal pathogenesis.

2. Methods

2.1. Primary cells cultivation and differentiation

Neural progenitor cells of human origin – Human Neural Stem Cells (hNSCs) purchased from Alstem (#hNSC11, Richmond, USA) were maintained in KnockOut DMEM/F-12 culture medium (#1260012, Gibco), supplemented with FGFb 20 ng/ml (#PHG0021, Thermo Fisher Scientific), EGF 20 ng/ml (#PHG0314, Thermo Fisher Scientific), 2 % StemPro Neural Supplement (#A10508-1, Thermo Fisher Scientific) and 1 % GlutaMAX-1 (2 mM) (#35050061, Gibco, Thermo Fisher Scientific) and grown in a 6-well plate at the basement membrane of Geltrex™ solution (1 % Geltrex™; #A1413302, Thermo Fisher Scientific; in KnockOut DMEM/F-12 culture medium). hNSCs were split after PBS wash by treatment with StemPro Acutase (#A11105-1, Gibco, Thermo Fisher Scientific) when reaching the 80–90 % confluency in a 1:4–1:6 ratio. Cells were cultivated in 5 % CO_2 humidified atmosphere at 37 °C.

hNSCs were seeded at desired density according to the parameters of the specific experiments. Details are summarized in Table S1. After 24 h, differentiation was initiated by a transition to either Astrocyte Medium (#1801; ScienCell Research Labs, Carlsbad, CA, USA) or Neurobasal Plus Medium (#A35829-01, Gibco, Thermo Fisher Scientific), supplemented with 2 % B-27™ supplement (#17504044, Gibco, Thermo Fisher Scientific) and 2 mM GlutaMAX-1 (#35050061, Gibco, Thermo Fisher Scientific) to derive astrocytes or neurons respectively. During the differentiation process, the media were changed twice a week and the differentiation of astrocytes took 21–22 days and neurons 14–18 days before the target experiment was undertaken. For seeding of differentiated or partially differentiated cells, astrocytes or neurons were washed with PBS and detached by CTS™ TrypLE™ Select Enzyme (#A1285901, Thermo Fisher Scientific).

2.2. Viruses and infection

We used two strains of the European TBEV subtype with differing pathogenicity for cell infections. The prototype TBEV strain Neudoerfl originating from infected tick (4th passage in suckling mice brains; GenBank accession no. U27495), was provided by Prof. F.X. Heinz (Medical University of Vienna, Austria) [39]. The highly virulent TBEV strain Hypr (4th passage in suckling mice brains; GenBank accession no. U39292), isolated from a 5-year old child with a multi-tick bite history and suspect tick-borne encephalitis [40], is available at the Institute of Parasitology, Biology Centre of Czech Academy of Sciences, České Budějovice, Czech Republic. Mock-inoculated brain suspensions of suckling mice

brains were used as a control in all experiments. Differentiated astrocytes and neurons were infected with both TBEV strains at the multiplicity of infection of 5 (MOI) for two hours in half volume of cultivation media to favour virus adsorption. Then, the inoculum was removed, and fresh cultivation media was replenished to the normal volume. To determine the appropriate MOI for infection, parallelly differentiated cells were counted prior to the infection in order to determine the cell numbers after differentiation.

2.3. Immunofluorescence assay

The presence of characteristic markers denoting the state of differentiation and development of infection in astrocytes and neurons was analysed by immunofluorescence assay. Cells were seeded on coated chamber slides at concentrations detailed in Table S1 and, when applicable, infected or mock-infected. At 24/72 h post-infection (p.i.), the presence of differentiation and infection markers was assayed. During sample processing, cells were fixed with 4 % paraformaldehyde for 15 min. Cells were washed in PBS and permeabilized by 0.1 % Triton X-100 in PBS, and formaldehyde auto-fluorescence was quenched by 50 mM NH_4Cl in 1 % bovine serum albumin (BSA) in PBS for 10 min twice. After PBS washing, blocking in 3 % BSA in PBS was undertaken for 1 h at room temperature. Target antigens were labelled for 1 h at room temperature or overnight at 4 °C by the following primary and secondary antibodies: dsRNA mAb (#10010200, SCICONS J2 from Scicons, Biocompare), GFAP (GA5) Mouse mAb (#3670S, Cell Signaling Technology), HuC/HuD Monoclonal Antibody (16A11) (#A-21271 Invitrogen, Thermo), MAP2 (#4542S, Cell Signaling Technology), S100B Polyclonal antibody (#bs-2015R Bioss Antibodies), TBEV NS3 Langat Chicken IgY (NS3 antibodies to closely related Langat virus NS3 were kindly provided by Dr M. Bloom, 94 % homology with TBEV), Goat Chicken IgY H&L (DyLight® 488) (#ab96947, Abcam), Goat Guinea pig IgG H&L (Alexa Fluor® 594) (#ab150188, Abcam), Goat Mouse IgG H&L (DyLight® 594) preadsorbed (#ab96881 Abcam), Goat Rabbit IgG H&L (Alexa Fluor® 488) (#ab181448 Abcam). Concurrent nuclei staining and sample mounting were done with VECTASHIELD® Antifade Mounting Medium with DAPI (#H-1200-10, Vector Laboratories). Images were taken with the Olympus Fluoview FV10i confocal microscope equipped with FV10-ASW software (v.1.7).

2.4. Growth curve

To assess the replication rate of TBEV in astrocytes and neurons, cells were either mock-treated or infected with the TBEV strains Hypr and Neudoerfl at the MOI of 5 (see details of differentiation in Table S1). At 2, 12, 24, 48, 72 for both cell lines and at 120 h p.i. (astrocytes only) culture supernatant was sampled and clarified by centrifugation for TBEV titre assessment. TBEV titres were plaque assayed on the human lung adenocarcinoma monolayers (A549; kindly gifted by R. Randall, University of St. Andrews, UK) according to the modified protocol of de Madrid *et al.* [41]. A549 were maintained in low glucose DMEM cultivation medium (#L0064-500, Biowest, VWR) supplemented with 10 % foetal bovine serum (FBS; #S1810-500, Biowest, VWR), 1 % antibiotics (penicillin G 100 units/ml, streptomycin 100 μg/ml; #L0022-020, Biowest), and 1 % L-alanyl-L-glutamine (#X0551-100, VWR) in 5 % CO_2 humidified atmosphere at 37 °C. Briefly, ten-fold dilutions of virus samples were mixed with the A549 cell suspension (1.5×10^5 cells/well of 24-well plate), cells were let to adhere, and virus to adsorb. After 4 h, an overlay mixture (1:1 v/v of carboxymethyl cellulose and 2× concentrated DMEM cultivation medium) was applied dropwise to the cells. After 5 days, cell monolayers were washed with physiologic solution (0.9 % NaCl), and plaques were fixed and stained with naphthalene black solu-

tion (0.1 % naphthalene black in 6 % acetic acid solution) for 45 min.

2.5. Viability assay

To detect the viability rates, neurons and astrocytes were differentiated as specified in Table S1 and infected with 5 MOI of Hypr and Neudoerfl TBEV strain. 2–3 h prior to the sampling interval (12, 24, 48, 72, 120, 168 h p.i.) incubation with AlamarBlue reagent in the cultivation media (1:10 (v/v); #DAL1025, Thermo Fisher Scientific) was performed in a dark. Viability for each cell type was assessed by fluorescence measurement (λ_{Ex} = 550 nm, λ_{Em} = 590 nm) using Tecan infinite 2000Pro, (Tecan i-control, 1.11.1.0) from four biological and two technical replicates and the viability value of the mock-treated cells was set at 1 (100%).

2.6. qRT-PCR

For the analysis of TBEV replication in infected cells, viral RNA was quantified by an assay designed by Achazi et al. [42]. Total RNA (80 ng/reaction) was used for TBEV gRNA quantification with the KAPA PROBE FAST Universal One-Step qRT-PCR Master Mix (2X) (#KK4752, Sigma-Aldrich, MERCK) and relative fold induction of TBEV RNA amount was determined using the delta-delta ct ($\Delta\Delta$-ct) with the comparison to mock. For the verification of poly-(A) transcriptomic data, samples were treated with dsDNase (#EN0771, Thermo Fisher Scientific) and gene expression was analysed with the KAPA SYBR FAST Universal One-Step qRT-PCR Kit (#KK4652, Sigma-Aldrich) according to the manufacturer's protocol. Relative expressions of HSPA-6, OASL, RNVU1, and RSAD2 (viperin) genes were processed via the $\Delta\Delta$-ct method with HPRT1 as a reference gene. All samples were analysed in biological and technical triplicates. A list of primers and probes used can be found in Table S1.

Verification of small RNA transcriptomic data was performed using miRCURY LNA miRNA PCR Assay Kit (#339306, Qiagen) according to the manufacturer's instructions. 200 ng of total RNA was used as an input with subsequent quantification of *hsa-miR-1248* (#YP00204253) and *hsa-miR-145-5p* (#YP00204483) in all samples. Data obtained were processed via relative quantification using the delta-delta c_t ($\Delta\Delta$-c_t) method with *hsa-miR-103a* as a reference miRNA and Sp6 as an internal spike-in control. All samples were analysed in biological and technical triplicates.

2.7. Transcriptomic analysis

2.7.1. Sample preparation

Each sample was prepared and analysed in biological triplicates. Total RNA from TBEV-infected human neurons and astrocytes was isolated at 24 and 72 h p.i. using RNA Blue reagent (Top-Bio, Vestec, Czech Republic) according to the manufacturer's instructions. RNA concentration was measured using NanoPhotometer Pearl (Implen, München, Germany) and the quality of RNA was determined using 2100 Bioanalyzer with RNA 6000 Nano kit (Agilent Technologies, Santa Clara, CA, USA).

2.7.2. Poly-(A)-enriched RNAs

Sequencing library construction, sequencing, raw read quality check and adapter trimming were done by Novogene Co., Ltd (Beijing, China). The 150 PE library was sequenced in HiSeq 4000 sequencer (Illumina, San Diego, CA, USA). Quality filtering was performed using Cutadapt v1.15 [43] and the subsequent clean read quality check was done using FastQC v0.11.5. [44]. The mapping (GRCh38.p13 reference genome), assembly and differential expression analysis were performed using the Tuxedo suite [45].

2.7.3. Small RNAs

Sequencing library construction, sequencing, raw read quality check and adapter trimming were done by Novogene Co., Ltd (Beijing, China). The 50 SE library was sequenced in HiSeq 2500 sequencer (Illumina, San Diego, CA, USA). The clean read quality check was done using FastQC v0.11.5 [44]. Adapter contamination, short and low quality reads were removed using Cutadapt v1.15 [43]. The clean reads were mapped to the reference genome (GRCh38.p13) using miRDeep 2.0.1.2 [46]. The -q option for the mapper.pl script was used to allow 1 mismatch for mapping. The miRDeep2.pl module was run using the human miRBase database (miRBase v.21) [47]. Identification of differentially expressed (DE) miRNAs was based on Benjamini-Hochberg P-value < 0.05 (unpaired Student's *t*-test) and $\log_2$ fold change >1.5 or <−1.5 using the normalized fragments per kilobase of transcript per million mapped reads (FPKMs; cut-off 10 FPKM per miRNA species) ratios between the respective TBEV-infected sample and mock control.

2.7.4. Virus-derived small RNAs

The raw reads from small RNA library were also mapped to the genome of both TBEV strains, Hypr (GenBank accession number U39292) and Neudoerfl (GenBank accession number U27495), using Bowtie [48]. The read depth counts of each sample were retrieved from the corresponding bedgraphs produced using Bedtools v.2.27.1 [49]. Read distribution along the TBEV genome was evaluated and visualised using Geneious Prime v2020.0.5. (Biomatters, Ltd, Auckland, New Zealand). The sense and antisense reads were additionally discriminated by extracting individual read types from their respective bam files using Samtools v1.10 [50] and their counts were compared for each sample.

2.8. In silico miRNA/vd-sRNA target prediction

miRNA *trans* target prediction was performed using miRWalk [51] and LncBase v.2 [52] toolkits. Briefly, DE miRNAs were divided into two groups: (1) up-regulated and (2) down-regulated; these served as an input for the respective prediction toolkit. Generated lists of predicted miRNA targets were subsequently used to identify these targets in DE protein-coding mRNAs (pc-mRNAs)/lncRNA datasets. For up-regulated miRNAs, the datasets of down-regulated pc-mRNAs/lncRNAs were used, and *vice versa*, datasets of up-regulated pc-mRNAs/lncRNAs were used in the case of down-regulated miRNAs. Default settings were used for miRWalk (P-value < 0.05, miRNAs targeting 3′UTR) in combination with the miRDB prediction tool. In the case of LncBase, the prediction module with default settings was used (cut-off score > 0.90). Identification of human miRNAs targeting TBEV Hypr/Neudoerfl genomic RNA or human mRNAs being targeted by 21–23 nt long vd-sRNAs was performed using the miRDB tool with a cut-off score > 0.70 [53].

2.9. Differential splicing analysis

The identification and quantification of differential splicing were computed using MAJIQ v2.2 [54], which employs Local splicing variations (LSV) derived from the provided transcriptome annotation file and RNA-seq data. The differential splicing was considered significant for LSVs with MAJIQ default cut-off values for deltaPSI ($|\Delta\Psi|{\geq}0.2$) supported by P($|\Delta\Psi|{\geq}0.2$) with a 0.05 cut-off (Bonferroni correction).

The raw reads of each sample represented by biological triplicates were mapped to the reference genome (GRCh38.p13) with STAR 2.7.7a [55]. The resulting bam files and an annotation file of the respective human genome were supplied to a MAJIQ builder for splice graph construction using default parameters. The relative abundance of LSVs was calculated using MAJIQ Quantifier with

104

default parameters. The quantifier module computes the abundance of each LSV using marginal percent spliced index (PSI, denoted Ψ). The PSI is calculated for each splice junction (SJ) and expresses the probability of splicing compared to other SJs in a given splicing event. The differential splicing is inferred from relative changes of LSVs among different conditions using delta PSI (dPSI, denoted $\Delta\Psi$). The summary and visualization of differential splicing were done for each sample with the MAJIQ Voila package.

2.10. Immunoblotting

Isolation of proteins was performed from the samples used for RNA isolation using RNA Blue according to the manufacturer's instructions. The resulting protein isolates were separated on 12 % polyacrylamide gels and subsequent immunoblotting detection was performed as described previously [56]. The following anti-

bodies were used: guinea-pig polyclonal serum against TBEV capsid protein (C) (produced in-house), anti-GAPDH antibody [EPR16891] (Abcam; #ab181602), HRP goat anti-guinea pig (Novex; #A18769), HRP goat anti-rabbit IgG antibody (Vector Laboratories; #PI-1000). Sample inputs were standardised by equal protein amounts loaded into each well (10 μg).

2.11. Statistical analyses

If not mentioned otherwise default settings for built-in statistics were used in employed computational packages/tools. Statistical data analysis in the case of TBEV infection dynamics (Fig. 1) was performed in the GraphPad Prism software (version 8.3.0, GraphPad Software, San Diego, CA, USA): cell viability was analysed by Welch's t-test with multiple testing correction by FDR (Benjamini, Krieger, and Yekutieli, q < 0.05) and TBEV titre differences were
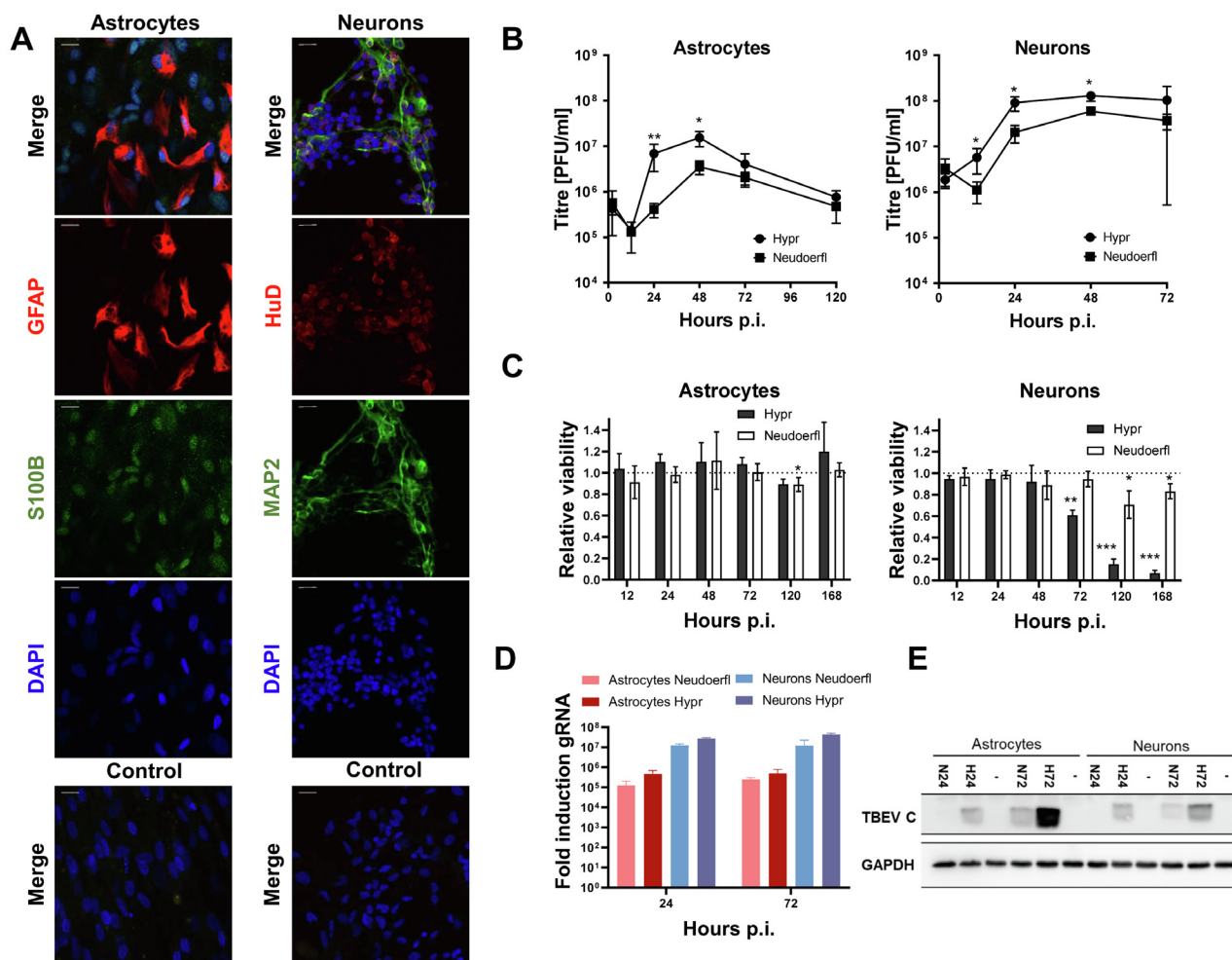
Fig. 1. TBEV infection dynamics assessment in *in vitro* differentiated human neurons and astrocytes reveals higher neuronal susceptibility. Astrocytes were differentiated for 22 days, neurons for 14–17 days prior to infection with TBEV strains Hypr and Neudoerfl at MOI of 5. **(A)** Immunofluorescent labelling of selected differentiation markers in astrocytes (GFAP – red and S100B – green) – left and neurons (HuD – red and MAP2 -green) – right. Nuclei were stained with DAPI. Controls are labelled with secondary antibodies only. The scale bar represents 20 μm. Representative images from two independent experiments are shown. **(B)** TBEV growth curve of strains Hypr and Neudoerfl, virus shedding into cultivation media was quantified by plaque assay using A549 cells. Data summarise three independent experiments and values in graphs are expressed as mean ± SD. Significant difference from control was calculated by unpaired Student's t-test (p < 0.05 (*), p < 0.01(**)). **(C)** Relative viability of neurons and astrocytes upon TBEV infection measured by metabolic conversion of alamarBlue and related to the viability of mock-treated cells (1.0 = 100 %, dotted line). Data summarise four biological and two technical replicates experiments, and values in graphs are expressed as mean ± SD. Welch's t-test showed a significant difference from control with the multiple testing correction by FDR (Benjamini, Krieger, and Yekutieli, q ≤ 0.05), p ≤ 0.05 (*), p ≤ 0.01 (**), p ≤ 0.001 (***). **(D)** TBEV replication in astrocytes and neurons was assessed by the amount of genomic RNA quantified by qRT-PCR and related to mock with the $\Delta\Delta$-ct method. Results are represented as means ± SD of three biological and technical replicates. **(E)** TBEV C (capsid protein) and GAPDH (loading control) levels in infected astrocytes and neurons at 24 and 72 h p.i. were determined by immunoblotting. Representative data from three independent experiments are shown. N – Neudoerfl strain, H – Hypr strain. (For interpretation of the references to colour in this figure legend, the reader is referred to the web version of this article.)

analysed by unpaired Student's *t*-test (α = 0.05). Conformity of sequencing and qRT-PCR data was analysed with the Spearman correlation analysis (α = 0.05).

3. Results

3.1. Infection of in vitro differentiated human neurons and astrocytes by TBEV Hypr or Neudoerfl resulted in a different pathogenic pattern

Initially, we focused on deriving a suitable experimental model to study TBEV infection in the target cells, human neurons and astrocytes. Primary human neurons and astrocytes were derived from neural progenitor cells of human origin – Human Neural Stem Cells (hNSCs). Following the differentiation, the characteristic appearance of astrocyte and neuron morphology was observed and further, the expression of cell-type-specific markers was verified using an immunofluorescence assay. Neuron identity was verified by the presence of markers HUDD and MAP2, and astrocytes identity was assayed by the expression of S100B and GFAP (Fig. 1A). In each cell type, at least 90 % of cells were labelled positively for at least one of the differentiation markers (data not shown).

Further, we intended to characterize the development of infection in neurons and astrocytes. Therefore, both cell types were infected with two European subtype strains of TBEV, the highly pathogenic Hypr and mild Neudoerfl, at the multiplicity of infection (MOI) of 5. The production of the virus in both cell lines was analysed with plaque assay on A549 cells (Fig. 1B). In addition to TBEV titres, the relative levels of TBEV genomic RNA (gRNA) were determined in the course of infection as well (Fig. 1D).

Infection of both cell types with TBEV resulted in the production of relatively high viral titres. In neurons, peak production of the virus was reached at 48 h p.i. ($12.96{\times}10^7 \pm 3.21{\times}10^7$ and $5.93{\times}10^7 \pm 1.16{\times}10^7$ for Hypr and Neudoerfl, respectively) and remained steady further on. In astrocytes, the peak production of the virus was reached at 48 h p.i. ($1.53{\times}10^7 \pm 0.46{\times}10^7$ and $0.35{\times}10^7 \pm 0.09{\times}10^7$ for Hypr and Neudoerfl, respectively), however, a decline in the viral titres was observed hereafter (Fig. 1B).

The viability of infected astrocytes was not significantly affected by TBEV in most of the time periods tested (12–168 h p.i.) regardless of the strain of TBEV used. The only significant reduction in viability by 10 % was seen in astrocytes infected with Neudoerfl after 5 days p.i. Dissimilarly, TBEV Hypr reduced the viability of infected neurons by 40 % at 72 h p.i. and <20 % of cells survived in the later time points. Less virulent strain Neudoerfl affected cell viability the most at 120 h p.i. by killing approximately 30 % of the neurons (Fig. 1C).

To illustrate the infection process entirely, the amount of viral genomic RNA was measured by qRT-PCR (Fig. 1D), and the amount of viral capsid protein reflecting the proteosynthesis was determined by immunoblotting at 24 and 72 h p.i. (Fig. 1E). Alike the progeny production, the amount of viral RNA in neurons exceeded the amount in astrocytes by >10-fold in both intervals examined. The more virulent TBEV strain Hypr exhibited a slightly higher replication rate than the Neudoerfl strain (Fig. 1D). A similar trend of more pronounced viral protein production in the case of TBEV Hypr infection was apparent also in the viral protein production (Fig. 1E).

In situ labelling of viral proteins and dsRNA showed that TBEV replication was concentrated in discrete regions adjacent to nuclei, whereas TBEV non-structural protein NS3 exhibited a more diffuse, whole cytoplasmic pattern of distribution (Fig. S1).

To sum up, both cell types were highly susceptible to TBEV infection, supporting virus replication and progeny production.

However, neural cell types differed in resilience, with astrocytes able to withstand the infection. We wanted to examine further the factors that underlay the difference in response between neurons and astrocytes.

3.2. Differential expression analysis of TBEV-infected human neurons and astrocytes reveals significant differences linked to the cell origin and virus virulence

Higher susceptibility of neurons to TBEV infection accompanied by higher pathogenicity than in astrocytes is a previously described phenomenon [5,7,12]. However, no comprehensive study combines the description of the host response on the mRNA, miRNA, and lncRNA levels. Thus, we performed an integrated differential expression analysis in both human neurons and astrocytes challenged by either TBEV Hypr or Neudoerfl infection. Fig. 2 summarizes the experimental outline for RNA-seq sample preparation (Fig. 2A) and subsequent *in silico* analyses (Fig. 2B). Differentiated cells were infected at MOI of 5 and total RNA was isolated at 24 and 72 h p.i. to describe the transcription dynamics of the host response. In total, 36 samples were prepared; this number includes three biological replicates for each variant (Table 1).

3.2.1. Differential expression analysis of poly-(A) RNAs

Sequencing of poly-(A) selected library of all samples yielded on average in 80 M 150 PE reads. Quality filtering using Cutadapt dropped on average 1.8 % low-quality and/or short reads. The remaining reads were mapped to the human genome assembly (GRCh38.p13) using TopHat with 78.1 % average mapping efficiency [57]. The details of sequencing output, quality filtering, and mapping statistics per sample are given in Table S2.

For poly-(A)-enriched datasets, a total number of 4288 differentially expressed genes (DE genes, Benjamini-Hochberg P-value < 0.05 and $\log_2$ fold change >1.5 or <−1.5) was identified in TBEV-infected cells when compared to mock control (Table S3). Of these, 2975 genes (69.4 %) represented protein-coding mRNAs (pc-mRNAs) and 923 (21.5 %) ncRNAs (Fig. 3A); pseudogenes and unclassified genes (9.1 %) were excluded from further analyses. Infection with TBEV Hypr resulted in a considerably higher number of DE genes in both, astrocytes and neurons, in comparison to TBEV Neudoerfl (Fig. 3B). Moreover, based on the expression profiles of pc-mRNAs and ncRNAs (Fig. 3C and D), a strong cell- and strain-specific response was observed, when only 1287 (33.1 %) and 591 (15.2 %) DE genes were identified in both cell types or both TBEV strains, respectively (Fig. S2). From those, a conserved group of 32 DE pc-mRNAs up-regulated in TBEV-infected datasets was identified (Table 2), which included genes coding for effectors of the innate immune response, such as receptors sensing viral infection RIG-I and MDA5, or proteins with direct antiviral effect (e.g. BST2, IFIT1-3, RSAD2, MX1, OAS1-3, OASL).

The differential expression analysis results were verified using real-time PCR quantification of mRNA levels for selected DE genes (RSAD2, RNVU1, HSPA6, OASL). The correlation between qPCR and NGS data is statistically significant (Spearman correlation r = 0.81, p < 0.001), therefore, the RNA-seq data were successfully validated (Fig. 3E).

To describe the cellular processes affected by the dysregulation of identified DE pc-mRNAs, we performed a gene set enrichment analysis (GSEA) using the DAVID toolkit [58]. A vast majority of significantly enriched GO classes (Benjamini-Hochberg P-value < 0.05) were related to the antiviral immune response (Fig. 3G). In addition, the same analyses of down-regulated gene sets uncovered an interesting phenomenon, where the proper neural development and assembly of the extracellular matrix are negatively affected by TBEV infection (Fig. 3G).

106
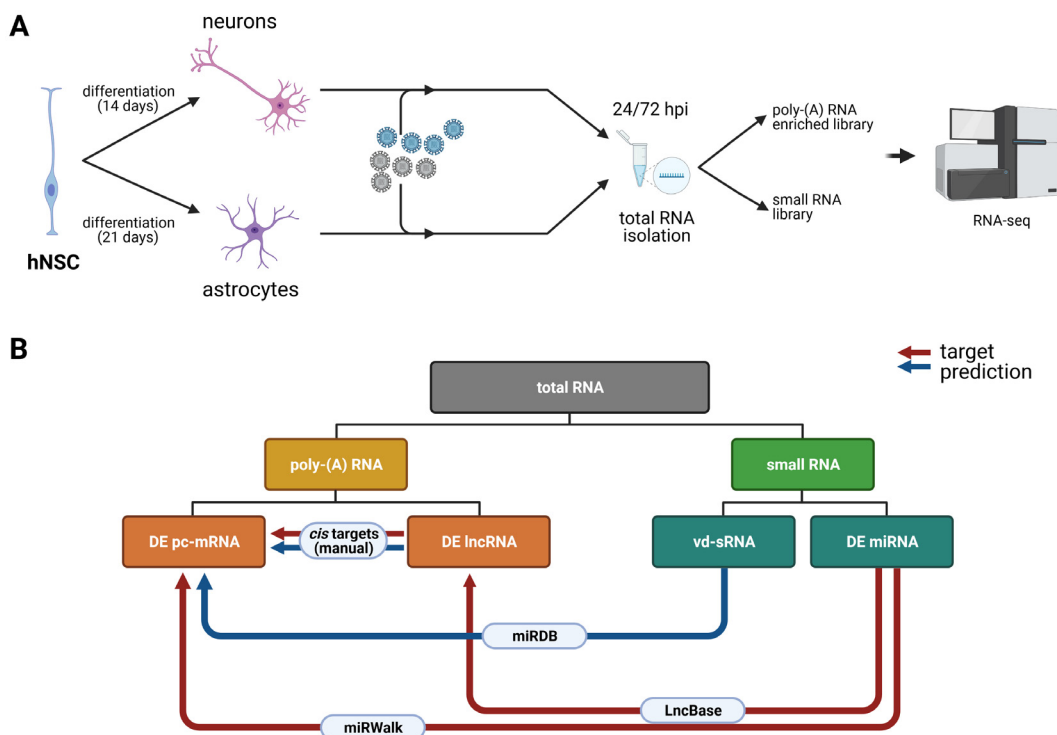
Fig. 2. Schematic representation of an experimental design performed in this study. (A) hNSCs were differentiated into astrocytes and neurons, infected with TBEV strains Hypr and Neudoerfl at the MOI of 5 and total RNA was isolated at 24 and 72 h p.i. with RNA Blue reagent. The quality of RNA was verified using Bioanalyzer 2100 and **(B)** Diagram describing the generation of miRNA/mRNA/lncRNA/vd-sRNA networks. (For interpretation of the references to colour in this figure legend, the reader is referred to the web version of this article.)

Table 1
An overview of samples subjected to RNA-seq analysis.

	Cell type	TBEV strain	Hours p.i.	Number of samples
A24_H	astrocytes	Hypr	24	3
A24_N	astrocytes	Neudoerfl	24	3
A24_M	astrocytes		24	3
A72_H	astrocytes	Neudoerfl	72	3
A72_N	astrocytes	Hypr	72	3
A72_M	astrocytes		72	3
N24_H	neurons	Neudoerfl	24	3
N24_N	neurons	Hypr	24	3
N24_M	neurons		24	3
N72_H	neurons	Neudoerfl	72	3
N72_N	neurons	Hypr	72	3
N72_M	neurons		72	3

3.2.2. Differential expression analysis of small RNAs

Sequencing the small RNA selected library of all samples yielded an average of 41 M 50 SE reads. Quality filtering using Cutadapt dropped on average 1.8 % low-quality and/or short reads. The remaining reads were mapped to the human genome assembly (GRCh38.p13) using miRDeep2 with 58.2 % average mapping efficiency. The details of sequencing output, quality filtering and mapping statistics per sample are given in Table S4.

In small RNA datasets, a total of 145 miRNA species were described as significantly dysregulated upon TBEV infection (Benjamini-Hochberg P-value < 0.05 and $\log_2$ fold change >1.5 or <−1.5) (Fig. 4; Table S5). Interestingly, while infection with severe Hypr strain resulted in higher numbers of dysregulated pc-mRNAs and ncRNAs when compared to mild Neudoerfl strain, the DE miRNA pattern showed an opposite trend (Fig. 4A), that is distinct reduction of significantly affected miRNAs by more virulent TBEV strain. Furthermore, the expression profiles document

a surprisingly high cell-specific response as only one miRNA species (*hsa-miR-592*) was found to be up-regulated in both cell types, astrocytes (A72_H) and neurons (N72_N) (Fig. 4B and D). The phenomenon of high specificity was also observed between TBEV strains, where only 14 (9.7 %) miRNA species followed the same pattern of dysregulation in the case of both, Hypr and Neudoerfl (Fig. 4C and D). The verification of miRNA-seq data was performed using qPCR quantification of *hsa-miR-1248* and *hsa-miR-145-5p; the* positive correlation between both methods was confirmed to be statistically significant (Fig. 4E; Spearman correlation r = 0.64, p = 0.009).

Several studies dealing with small RNA profiling in flavivirus-infected cells have reported the presence of vd-sRNAs [34,35]. We, therefore, assessed whether TBEV infection also resulted in the generation of vd-sRNAs by mapping the small RNA datasets from RNA-seq to TBEV Hypr genomic sequence (GenBank accession no. U39292). The production of

107

Fig. 3. Differential expression analysis of poly-(A) enriched RNAs in TBEV-infected neurons and astrocytes reveals strain-specific and cell-specific responses. **(A)** Graphic summary of poly-(A) classes identified as differentially expressed upon TBEV infection. **(B)** Graphic summary of DE genes (protein-coding mRNAs and non-coding RNAs) in the respective dataset. **(C)** Heatmap visualizing the overall expression pattern of protein-coding mRNAs in analysed samples. **(D)** Heatmap visualizing the overall expression pattern of non-coding RNAs in analysed samples. **(E)** Verification of RNA-seq data by qRT-PCR. Relative expressions of HSPA-6, OASL, RNVU1, and RSAD2 (viperin) genes were processed via the ΔΔ–ct method with HPRT1 as a reference gene. All samples were analysed in biological and technical triplicates. Spearman correlation was evaluated with GraphPad Prism software. **(F)** Gene set enrichment analysis (DAVID tool; GO Biological processes; p < 0.001) of significantly up-regulated genes in analysed samples performed by DAVID tool. **(G)** Gene set enrichment analysis (DAVID tool; GO Biological processes; p < 0.001) of significantly down-regulated genes in analysed samples performed by DAVID tool.

vd-sRNAs was confirmed in all TBEV Hypr-infected samples with small RNA species ranging from 16 to 50 nucleotides in size. As expected, the amounts of mapped reads increased with the infection progress in all specimens. Furthermore, vd-sRNAs were predominantly derived from the sense strand of the TBEV genome (Fig. S3) and reached higher, but not significantly dif-

ferent (unpaired Student's t-test; p < 0.05), levels in neurons $(6.24 \times 10^5 \pm 5.74 \times 10^4)$ than in astrocytes $(4.87 \times 10^5 \pm 6.30 \times 10^4)$ (Fig. 4E). These findings positively correlate with higher viral titres and gRNA observed in neurons (Fig. 1). The pattern of reads distribution throughout the viral genome appears rather mosaic with several specific hot-spots. Besides, the hot-

108

Table 2
Identification of a common set of genes with TBEV-induced expression in human neurons and astrocytes.

gene_id	gene_name	A24_H	A24_N	A72_H	A72_N	N24_H	N24_N	N72_H	N72_N
ENSG00000239713	APOBEC3G	2.39	1.97	2.87	1.85	1.62	1.54	1.70	1.72
ENSG00000100342	APOL1	2.90	2.12	2.98	1.90	3.83	3.32	2.17	2.14
ENSG00000221963	APOL6	3.29	3.03	3.02	1.99	3.02	2.76	2.77	2.42
ENSG00000130303	BST2	7.06	6.40	9.80	8.65	5.46	6.16	7.50	7.60
ENSG00000134326	CMPK2	3.75	3.51	4.46	3.58	1.86	2.23	2.94	2.89
ENSG00000107201	DDX58	3.41	3.23	3.94	2.99	3.23	2.93	4.05	3.05
ENSG00000137628	DDX60	2.60	2.45	3.12	2.45	2.46	2.31	3.23	2.03
ENSG00000181381	DDX60L	2.60	2.45	3.12	2.45	2.46	2.31	3.23	2.03
ENSG00000108771	DHX58	5.10	4.27	5.57	3.83	4.49	4.00	6.17	4.58
ENSG00000133106	EPSTI1	3.80	3.36	4.25	3.48	3.27	3.18	3.89	3.46
ENSG00000138646	HERC5	5.70	4.76	6.51	5.05	5.24	3.95	7.76	5.55
ENSG00000138642	HERC6	4.50	4.08	4.72	3.90	3.34	3.71	5.00	4.14
ENSG00000068079	IFI35	3.95	3.13	4.64	3.47	1.98	2.76	3.44	3.77
ENSG00000137965	IFI44	2.51	2.52	3.53	2.83	2.01	2.72	3.79	3.15
ENSG00000137959	IFI44L	2.51	2.52	3.53	2.83	2.01	2.72	3.79	3.15
ENSG00000126709	IFI6	3.84	3.11	5.45	4.50	1.95	2.93	4.06	4.44
ENSG00000115267	IFIH1	5.47	4.97	6.24	5.02	5.58	4.56	7.48	5.99
ENSG00000185745	IFIT1	6.47	6.04	7.29	6.30	5.84	5.72	7.84	6.79
ENSG00000119922	IFIT2	6.28	5.72	6.98	5.72	6.74	5.23	8.12	5.57
ENSG00000119917	IFIT3	5.51	5.14	6.71	5.65	6.09	5.24	7.61	6.21
ENSG00000187608	ISG15	5.81	4.84	6.83	5.46	4.25	5.14	6.64	5.99
ENSG00000157601	MX1	7.16	6.37	7.12	6.11	5.11	6.60	6.93	7.45
ENSG00000123609	NMI	2.85	2.54	3.87	2.95	2.39	1.81	3.14	2.90
ENSG00000089127	OAS1	6.63	5.84	8.54	7.47	3.87	4.44	5.88	6.44
ENSG00000111335	OAS2	9.00	8.05	12.07	11.03	9.10	9.32	5.68	5.91
ENSG00000111331	OAS3	3.99	3.37	5.85	4.68	2.83	3.31	4.18	4.01
ENSG00000135114	OASL	8.49	7.18	11.16	9.47	8.55	7.59	9.89	8.58
ENSG00000173193	PARP14	2.37	2.51	2.85	2.27	1.73	1.99	2.26	2.01
ENSG00000134321	RSAD2	6.46	6.01	8.50	7.41	4.19	3.87	6.37	6.09
ENSG00000205413	SAMD9	4.06	3.99	5.06	4.10	3.67	3.84	5.47	4.94
ENSG00000184979	USP18	4.11	3.65	4.87	3.77	1.79	2.55	3.26	3.19
ENSG00000132530	XAF1	2.27	2.20	2.81	2.32	2.95	2.69	3.07	2.98

spots identified in all of the analysed samples are strikingly conserved and the main difference was observed on the level of read counts (Fig. S4). The most universal/abundant peak was identified at the end of the 3′ UTR.

3.3. Candidate gene networks responsible for a different outcome of TBEV Hypr infection in neurons vs. Astrocytes

As TBEV Hypr dramatically decreased the number of living neurons but not astrocytes (Fig. 1C), we sought to characterize the differences between N72_H and A72_H datasets to identify potential key factors involved in higher neuronal susceptibility to TBEV Hypr infection. First, we selected DE pc-mRNAs, which were either uniquely up-/down-regulated in N72_H/A72_H datasets or the difference in up-/down-regulation between N72_H/A72_H datasets was higher than 1.5 log2. A total of 1849 DE pc-mRNAs were identified and further divided into four groups according to their expression profile (unique expression in neurons/astrocytes or higher expression in neurons/astrocytes). Subsequently, the GSEA analysis of all groups revealed that the main difference is a more robust immune response elicited in infected astrocytes (Fig. 5A). In more detail, either a triggering of astrocyte-specific antiviral response genes (e.g., *TNFSF10*, *MX2*, *MMP13*, *IFITM1*, or *IFITM2*) or higher up-regulation of immune response genes (e.g., *OAS1-3*, *RSAD2*, *BST2*, *IL6*, or *ISG20*) was observed (Table 2; Fig. S5). These findings correlate with qPCR data, where *RSAD2* (viperin) and *OASL* were significantly more up-regulated in astrocytes than in neurons (Fig. 5B). A specific expression pattern was observed for *IFN-β* and *IFN-λ* genes, when *IFN-β* seems to be responsible for an early immune response to TBEV followed by the expression of *IFN-λ* (Fig. 5C). Interestingly, the late expression of *IFN-λ* (72 h p.i.) appeared in astrocytes only, suggesting its role as a factor associated with the neuronal susceptibility to TBEV infection. Additionally, to put our data in context with previous research, we

compared our comprehensive list of DE immune response-related genes with altered protein levels of selected cytokines [13] and mRNAs [12] retrieved for TBEV by others (Fig. 5D). Our data showed a high level of coherence with these previously published expression patterns and considerably extended the previous ones.

The DE miRNAs and lncRNAs were selected based on the same unique or more pronounced response criteria used to evaluate pc-mRNAs. This way, the miRNA *trans* target prediction was performed for the selected datasets of pc-mRNAs (miRWalk; [51]) and lncRNAs (LncBase v.2; [52]). Prediction results summarized in Table S6 show that 173 genes were identified as possible *trans* targets (133 pc-mRNAs and 40 lncRNAs), including genes involved in immune response (e.g., *OAS1*, *TRIM38*, *SPSB4*), proper neuronal development and function (e.g., *NRARP*, *KCNK10*, *SIRPA*, *CLIC5*, *TMC8*, *KIT*, *CNTN2*, *DCC*) as well as transcription factors (e.g., *TFAP2B*, *HEYL*, *GATAD2B*, *BEND3*). In order to get a complete overview of the possible interactions, potential *cis* targets (100 kb upstream and downstream) were predicted for DE lncRNAs with log2-fold change >4 or <−4 as well as for lncRNAs identified as potential targets of DE miRNAs (Table S7). In total, 45 *cis* targets were predicted, including immune response-related genes (loci *RSAD2*/*CMPK2* and IFNL1-4; *IFI6*), receptors (e.g., *DCC*, *UTS2R*), and transcription factors (e.g., *DLX5*, *OTX2*).

The differences in the vd-sRNA mapping profile between the two cell types may substantially influence the enhanced neuronal sensitivity to Hypr infection. One of the possible scenarios suggests that vd-sRNAs could mimic host miRNAs, leading to a lowered expression of a target gene [37]. Therefore, we extracted the 21–23 nt long vd-sRNAs and selected hotspots HS1-HS12 which were present uniquely or in higher/lower numbers in N72_H and A72_H samples (Table 3; Fig. 5E). Surprisingly, HS3, HS7, HS9, HS10, and HS12 had higher read counts in Hypr-infected astrocytes, and only HS11 had a higher read count in Hypr-infected neurons. Subsequently, the prediction of vd-sRNA targets was performed using
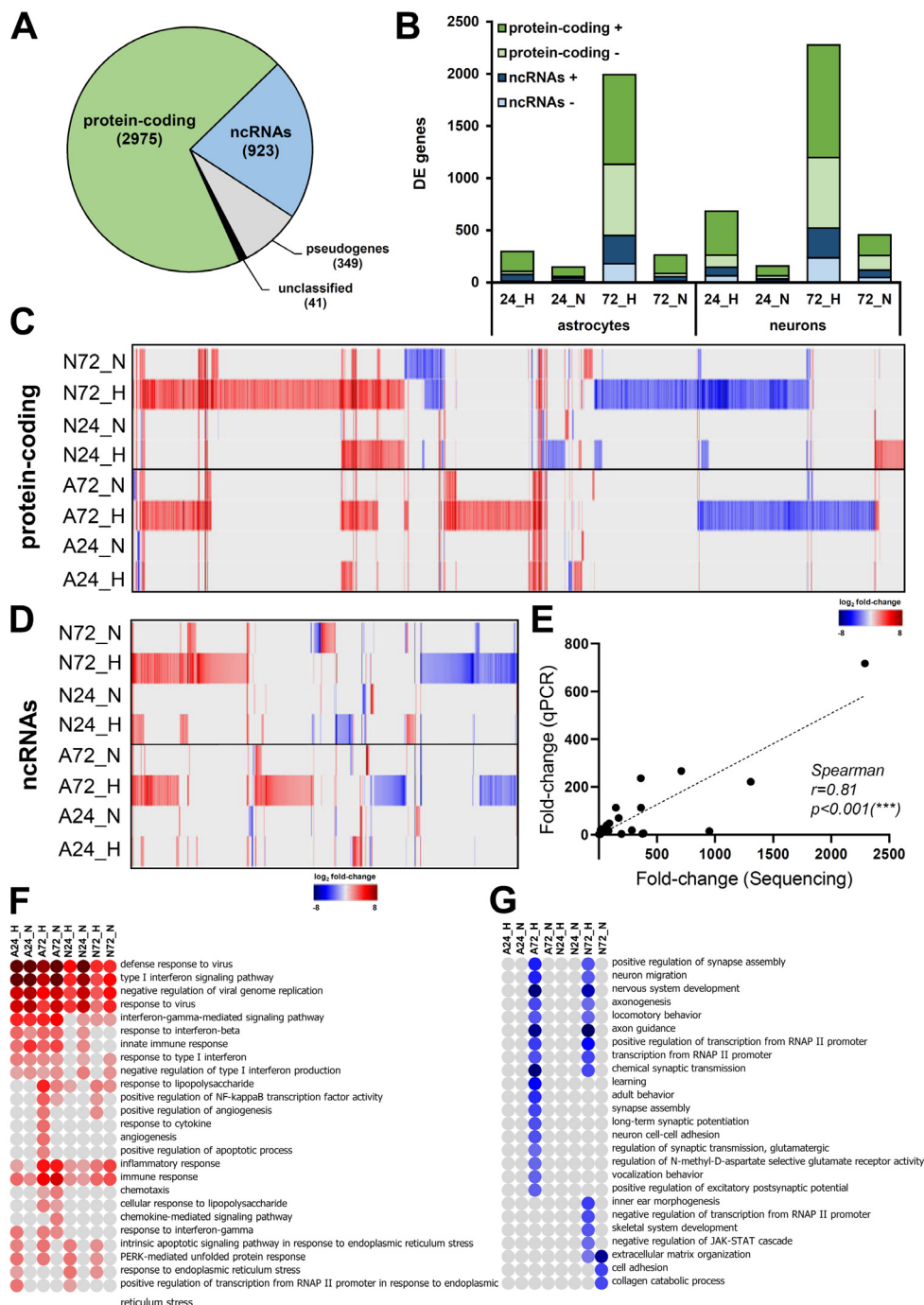
109
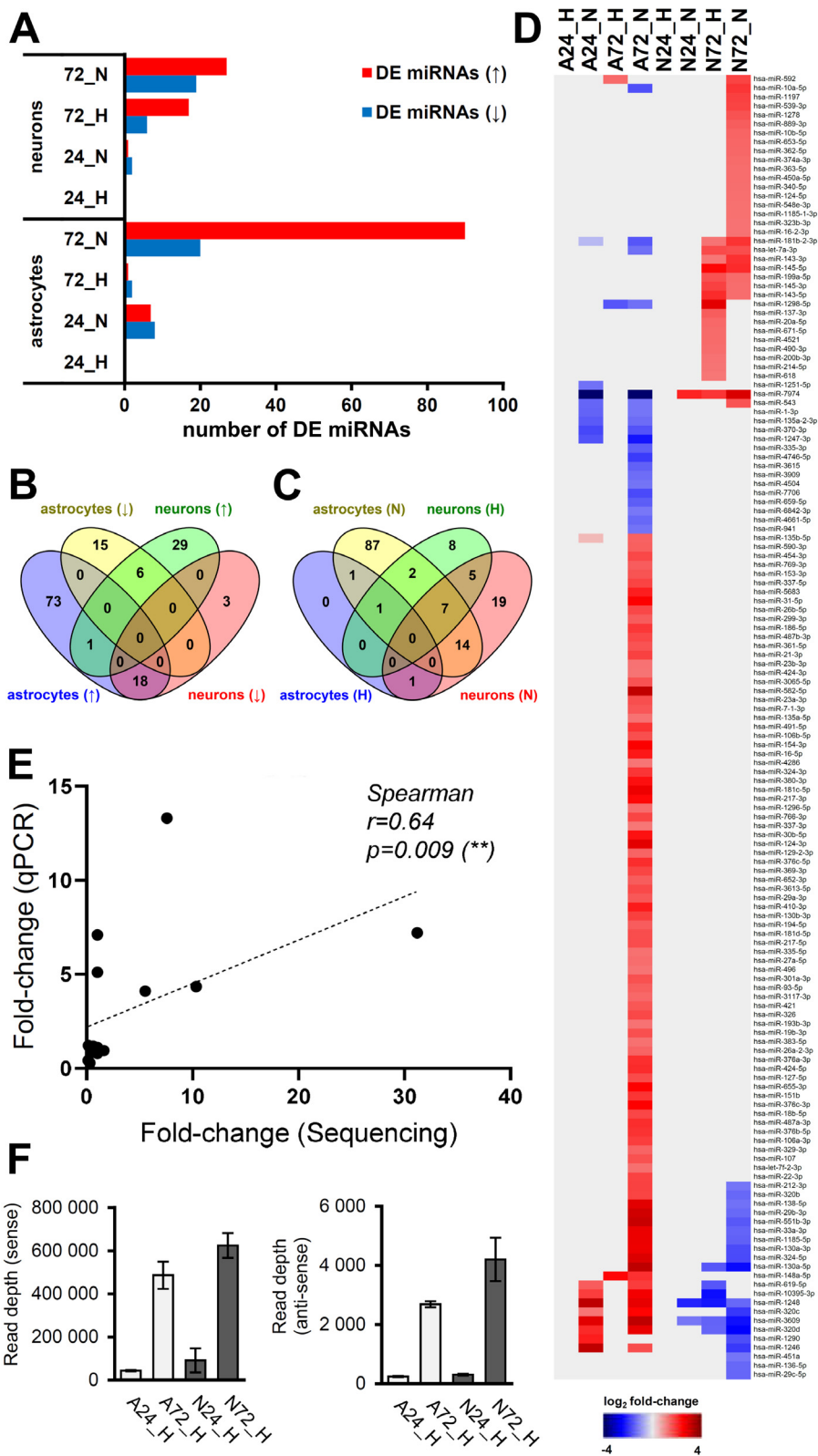
Fig. 4. Differential expression analysis of miRNAs in TBEV-infected neurons and astrocytes revealed strain-specific and cell-specific responses. (A) Graphic summary of DE miRNAs in analysed samples. (↑) up-regulated miRNAs, (↓) down-regulated miRNAs. **(B)** Venn diagram describing the cell specificity of miRNA expression upon TBEV infection. (↑) up-regulated miRNAs, (↓) down-regulated miRNAs. **(C)** Venn diagram describing the strain specificity of miRNA expression upon TBEV infection. (H) – TBEV Hypr strain, (N) – TBEV Neudoerfl strain. **(D)** Heatmap visualizing the overall expression pattern of mi RNAs in analysed samples. **(E)** Verification of RNA-seq data by qRT-PCR. Relative expression of *hsa-miR-1248* and *hsa-miR-145-5p* was calculated using the ΔΔ-ct method with *hsa-miR-103a* as a reference gene and Sp6 as an internal control. All samples were analysed in biological and technical triplicates. Spearman correlation was evaluated with GraphPad Prism software. **(F)** Frequency distribution of 21–23 nt vd-sRNAs mapped to TBEV Hypr genome in N72_H (black) and A72_H (red) samples. HS – hot-spot. (For interpretation of the references to colour in this figure legend, the reader is referred to the web version of this article.)

110
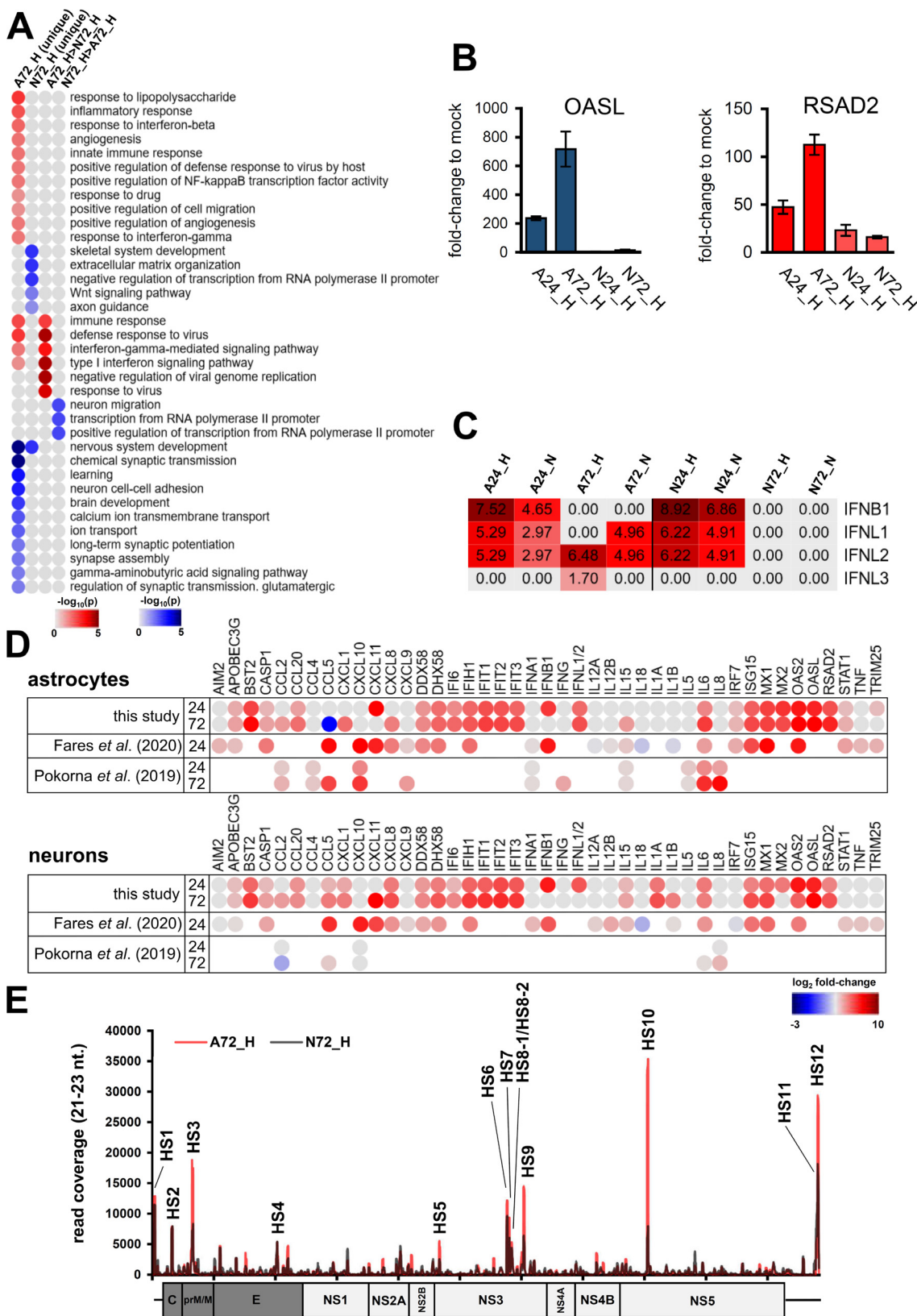
Fig. 5. TBEV Hypr infection in astrocytes results in a stronger innate immune response than in neurons. (A) Heatmap summarizing results from gene set enrichment analysis (DAVID tool; GO Biological processes; p < 0.05) of DE genes 1) uniquely expressed in either A72_H or N72_H, and 2) genes expressed with >1.5 log$_2$ difference in one of the samples. **(B)** Relative expression of OASL and RSAD2 (viperin) genes in TBEV infected cells. Calculations were performed via the ΔΔ-ct method with HPRT1 as a reference gene. All samples were analysed in biologcal and technical triplicates. **(C)** Expression pattern of *IFN-β* and *IFN-λ* in TBEV-infected cells based on RNA-seq data. **(D)** Overview and comparison of the expression pattern of selected immune response-related genes from this study and works of Fares *et al.* [12] and Pokorna *et al.* [13] **(E)** Number of mapped reads for vd-sRNAs (16–50 nt) in the respective sample. Data summarise three independent experiments, and values in graphs are expressed as mean ± SD.

111

the miRDB tool in combination with DE pc-mRNA lists. In total, 51 host DE pc-mRNAs were identified (Table 4). Interestingly, vd-sRNAs derived from HS10 and HS12, the two hot-spots with the highest read count in astrocytes, were both predicted to target RNA splicing factors MBNL2 and RBFOX1, whose mRNA levels were significantly lower in A72_H in comparison to N72_H (Table S3). For HS11-derived vd-sRNA, nine mRNA targets with the corresponding expression pattern (N72_H < A72_H) were predicted (*LEKR1*, *DLX1*, *AOX1*, *MYCN*, *PCDH18*, *DPYSL2*, *TSHZ1*, *PFKFB3*, *BCL9L*). Notably, four out of nine identified target genes were characterized as transcription factors (*DLX1*, *MYCN*, *TSHZ1*, *BCL9L*), with DLX1 and DPYSL2 further considered as factors contributing to proper neural development [59,60].

3.4. Candidate gene networks responsible for distinct TBEV infection outcomes in neurons during infection with strains of varying severity

The comparison of infection dynamics and cell death rate between severe Hypr and mild Neudoerfl strains in infected neurons confirmed a higher pathogenic effect for Hypr (Fig. 1). Therefore, observed differences between Hypr and Neudoerfl infection manifestation in human neuronal cells drove us to search for differences between N72_H and N72_N datasets on the pc-mRNA/miRNA/ncRNA level. Using an *in silico* approach, we employed an analogous pipeline to A72_H and N72_H datasets.

We identified 1935 DE pc-mRNAs either uniquely up-/down-regulated in N72_H/N72_N datasets or differentially expressed (both up and down-regulated) between N72_H/N72_N datasets with a fold change higher than 1.5 log$_2$. The GSEA analysis found significant differences in infection between the two TBEV strains in (i) the extent of the negative impact of Hypr infection on neuronal development, (ii) the level of Hypr-induced dysregulated activity of RNA polymerase II promoters, and (iii) higher activation of host immune response to Hypr infection (Fig. 6A).

We identified 1935 DE pc-mRNAs either uniquely up-/down-regulated in N72_H/N72_N datasets or differentially expressed (both up and down-regulated) between N72_H/N72_N datasets with a fold change higher than 1.5 log$_2$. The GSEA analysis found significant differences in infection between the two TBEV strains in (i) the extent of the negative impact of Hypr infection on neuronal development, (ii) the level of Hypr-induced dysregulated activity of RNA polymerase II promoters, and (iii) higher activation of host immune response to Hypr infection (Fig. 6A).

Identifying the complex regulatory network of small regulatory RNAs also requires the identification of their target sites. Thus, we selected DE expressed miRNAs and lncRNAs under the same conditions as the pc-mRNAs selection. Using the miRWalk and lncBase v.2 databases, the miRNA targets were identified for pc-mRNAs and lncRNAs, respectively. The predicted 268 *trans* targets for both small RNA classes (207 pc-mRNAs and 61 lncRNAs) are listed in Table S8. The complete overview of the possible interactions was predicted by the identification of potential *cis* targets (100 kb upstream and downstream) for DE lncRNAs with log$_2$-fold change >4 or <−4 and lncRNAs identified as potential targets of DE miRNAs (Table S9). In total, 47 cis targets were predicted, including transcription factors (e.g. *DLX5*, *DLX6*, *TFAP2A*) and various receptors (e.g. *CHRNA3*, *CHRNB4*, *DCC*, *PTPRH*).

The assessment of vd-sRNA presence in TBEV Neudoerfl-infected cells revealed a similar pattern to Hypr vd-sRNA data – increasing number of vd-sRNAs through the infection and higher numbers of sense reads (Fig. S4). Comparison between N72_N and N72_H datasets further documented higher numbers of mapped reads during Hypr infection compared to Neudoerfl (Fig. 6B and C), which is in agreement with higher titres and viral gRNA levels (Fig. 1). The distribution pattern of 21–23 nt long vd-sRNAs was identical for 12 hot-spots with higher abundance in N72_H samples (Table 3; Fig. 6D). Prediction of host mRNA targets was performed using the miRDB tool in combination with DE pc-mRNA datasets with 66 identified host mRNA targets (Table 4).

We further focused on HS11, the hot-spot with the highest number of mapped 21–23 nt reads in N72_H samples. The vd-sRNA derived from HS11 was predicted to target 22 mRNAs with the corresponding expression pattern (N72_H < N72_N), out of which seven pc-mRNAs (*DLX1*, *MYCN*, *PCDH18*, *DPYSL2*, *TSHZ1*, *PFKFB3*, *BCL9L*) were also identified as less expressed in A72_H samples compared to N72_H. We suggest that these genes represent a candidate set of markers of increased pathogenicity that Hypr strain confers towards neurons.

3.5. TBEV infection results in altered pre-mRNA splicing

Both, neuron/astrocyte-specific response to infection and pathogenicity-related response to infection, led us to examine the potential impairment of host pre-mRNA splicing events since several lncRNAs and vd-sRNAs were predicted to interact with partners involved in this pathway. The idea was also supported by previous studies describing DENV- and ZIKV-induced alterations in host pre-mRNA splicing [27,61,62]. Thus, RNA-seq data of astrocytes and neurons infected with TBEV were submitted to a differential splicing analysis using MAJIQ v2.2 [54]. The corresponding mock controls were used as a reference for differential splicing calculation. Identified LSVs were further classified by MAJIQ to binary and complex events. Binary LSVs include exon skipping (ES), intron retention (IR), alternative 3′/5′ splice site (A3SS/A5SS) and involve only two exons or two splice sites in the same exon. Complex LSVs combine several binary events originating from or targeting the same site. In total, differential splicing analysis revealed 4009 LSVs in all datasets (Table 10) and the vast majority of detected LSVs (3639; 90.7 %) were documented for N72_H (2390; 59.6 %) and A72_H (1249; 31.2 %) datasets; interest-

Table 3
Identification of hot-spots for 21–23 nucleotides long vd-sRNAs in TBEV Neudoerfl and Hypr genome. SNPs characteristic for either Hypr or Neudoerfl strains are marked in bold.

vd-sRNA	sequence (5′-3′)	start	end
HS1	TGCTTCGGACAGCATTAGCAGC	26	47
HS2	AAGGCGTTCTGGAACTCAGTCCC	310	332
HS3	AGGAGAAGAGCCTGTTGACGTG	645	666
HS4	ATCTCCAGATGTGAACGTGGCC	2016	2037
HS5	TAAGGACGGTGTCTACAGGATT	4659	4680
HS6	AAAGTGTGAT**C**TGTTTGAACAG (Hypr) AAAGTGTGAT**T**TGTTTGAACAG (Neu)	5756	5777
HS7	TGAAAAGGACTACTC**A**AGAGT (Hypr) TGAAAAGGACTACTC**C**AGAGT (Neu)	5787	5807
HS8-1	TGTGGTGACGACTGATATCTC	5829	5849
HS8-2	TGACGACTGATATCTCGGAGATG	5834	5856
HS9	TGGACAGTGTGATGATGATGAC	6030	6051
HS10	ATTT**A**GATCAGGAATGGACGTG (Hypr) ATTT**C**GATCAGGAATGGACGTG (Neu)	8040	8061
HS11	GACACAGA**A**TAGTCTGACAAGGA (Hypr) GACACAGG**G**TAGTCTGACAAGGA (Neu)	10,784 (Hypr), 11,090 (Neu)	10,805 (Hypr), 11,111 (Neu)
HS12	TGATGTGTGACTCGGAAAAAC	10,808 (Hypr), 11,114 (Neu)	10,828 (Hypr), 11,134 (Neu)

112

Table 4

List of miRDB tool-predicted host targets of vd-sRNAs. A/N ratio – mapped read count ratio between astrocytes and neurons.

vd-sRNA	Σ read count		A/N ratio	predicted gene targets (miRDB)
	A72_H	N72_H		
HS1	279 497	243 019	1.15	N/A
HS2	171 548	169 885	1.01	N/A
HS3	373 158	159 523	2.34	OPCML, THUMPD2, LPXN, GAS7, CDH7, ERBB4, ZMAT3, ANKS1A, GIPC2
HS4	92 596	96 652	0.96	N/A
HS5	108 436	50 154	2.16	no targets
HS6	246 963	193 317	1.28	N/A
HS7	193 436	120 863	1.60	TBC1D30, PLCH1, G2E3, PBX1, ESRRG, TIPARP, MAN1A1
HS8-1	91 952	72 746	1.26	N/A
HS8-2	92 748	81 201	1.14	N/A
HS9	309 580	125 640	2.46	BDNF, KCNS2, SHISAL1, GOLGA4, LGI1
HS10	751 154	150 617	4.99	PCHD20, TM4SF18, TMTC1, MCTP1, RBFOX1, TRHDE, ZMYM5, SEMA3E, MBNL2, LCOR, CXADR, CALB1, ARID2, GABRG2, DIRAS2, NEK7, FUT9
HS11	124 140	202 003	0.61	LEKR1, DLX1, AOX1, MYCN, PCDH18, DPYSL2, TSHZ1, PFKFB3, BCL9L
HS12	597 869	338 876	1.76	RBFOX1, RNF212, MBNL2, GRIN2A, CREG2, KRR1
vd-sRNA	Σ read count		N/H ratio	predicted gene targets (miRDB)
	N72_N	N72_H		
HS1	5 594	243 019	0.02	no targets
HS2	26 642	169 885	0.16	no targets
HS3	39 241	159 523	0.25	SIAH3, NKAIN1, EBF1, KLHDC8A, ST6GAL1, DNMT3B, SOGA1, SHF, KLHL13
HS4	25 886	96 652	0.27	PIK3C2B, EPHB1, NYNRIN, ELAVL2, SH3TC2, ZNF124, SLITRK5, SIRPA, ONECUT2, BDKRB2, ACACA, RTL8B, ZNF730
HS5	11 486	50 154	0.23	no targets
HS6	27 970	193 317	0.14	AKR1C2, NCAM1
HS7	22 292	120 863	0.18	TFAP2A, ELAVL4, BCL11B, POU3F4, AUTS2, MN1, SH3TC2, DACH1, ONECUT2, PIP4P2, TMEM229B
HS8-1	20 918	72 746	0.29	NFASC, NCAM1
HS8-2	22 262	81 201	0.27	no targets
HS9	34 893	125 640	0.28	NAV1, GLRA2, GAS2L3
HS10	52 035	150 617	0.35	PRDM12, NRN1, ELAVL4, CDKN1C, ANOS1, NXPH2, PSRC1, PPM1L, CYYR1, LUZP2, LRRTM3
HS11	19 224	202 003	0.10	PTPN5, DCX, MYCN, DLX1, NREP, THSD7A, NXPH2, PIK3C2B, CAMK2A, EPHB1, RAPGEF5, PCDH18, DPYSL2, KCND2, GNG2, TSHZ1, KLHL13, ONECUT2, ISGF3, PFKFB3, BCL9L, PPP1R17
HS12	46 500	338 876	0.14	DACH1, NDRG4

ingly, infection with Neudoerfl strain resulted in a total of only 94 (2.3 %) identified LSVs. The detailed characterization of identified LSVs revealed that exon skipping was the most frequent LSV type (Fig. 7B). The biological pathways affected by TBEV-induced differential splicing were determined using a GSEA analysis for A72_H, N72_H, and N72_N samples using the list of differentially spliced genes. Significantly enriched GO terms (biological process; Benjamini-Hochberg P-value < 0.05) were identified only in the case of A72_H and N72_H samples (Fig. 7C). Only a single GO term "mRNA splicing process" was significantly enriched in both samples. The remaining biological processes were significantly enriched only in the case of N72_H. The most highly ranking terms were found among DNA repair, G2/M transition of mitotic cell cycle, protein transport, and membrane fusion biological processes. *MTUS2* and *CFAP61* were the top-ranked genes recognized in the list of TBEV-induced alterations in host pre-mRNA splicing in A72_H and N72_H samples, respectively. Therefore, we prepared sashimi plots of LSVs identified as significantly spliced in these two genes using the MAJIQ Voila tool (Fig. 7D). As a control, the visualization of bam files used for LSV identification in *MTUS2* and *CFAP61* genes was done using Integrated Genome Browser (IGB) v9.1.8 [71] to support the MAJIQ LSV detection and quantification capacity. Both IGB graphs also support the presence of newly included exons in LSV detection by MAJIQ in these two genes in Hypr-infected cells (Fig. 7E).

4. Discussion

TBEV, a neurotropic flavivirus, targets the host CNS and frequently causes severe encephalitis in infected patients. The exact mechanism responsible for TBEV-induced neuropathogenesis has not been fully understood to date, although several studies suggest

the combination of virus-induced neuronal cell death and the immunopathogenic effect of activated host immune response [10,12]. The complexity of the whole process is further supported by the different outcomes of TBEV infection in neurons and astrocytes [5–7,12]. One of the suggested mechanisms underlying the distinct susceptibility of both cell types to TBEV infection is the neuron-/astrocyte-specific expression pattern of immune response-related genes [12,13]. However, both studies assayed only a limited number of pre-selected genes in a microarray-based analysis. Here, we present a thorough transcriptomic study describing differential expression of both small RNAs as well as poly-(A) RNAs in human neurons and astrocytes infected by mild and severe strains of TBEV in an early and late stage infection. Thus, the combination of all factors (infection time, cell type, TBEV strain) gives a complex overview of host-cell response at the RNA level and provides new significant data for a better understanding of TBEV neuropathogenesis.

4.1. Cell-type specific response in neurons and astrocytes challenged by TBEV

In silico pc-mRNA-miRNA-lncRNA interactome analysis identified major differences in response between TBEV challenged astrocytes and neurons. The key feature was the expression pattern of immune response-related genes (Fig. 5; Table S3; Fig. S3), which is in concordance with studies of Fares *et al.* and Pokorna *et al.* [12,13]. The phenomenon of cell type-specific immune response to flaviviral infection in CNS was also described for WNV [63], which further highlights its relevance for the flaviviral pathogenic effect. Besides, Hypr infection negatively affects extracellular matrix organization and RNAPII promoter activity pathways in

113
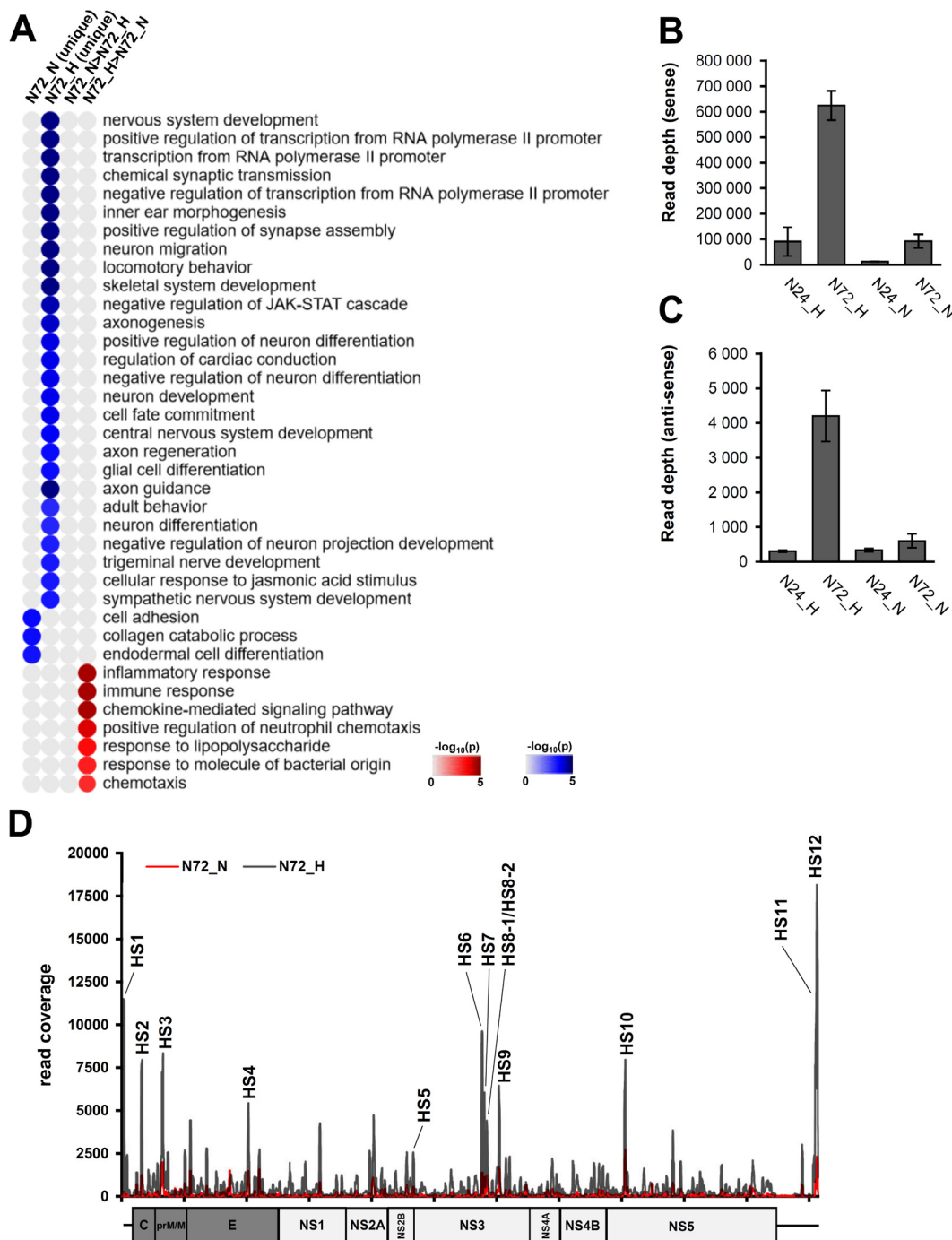
Fig. 6. Comparison of TBEV Hypr/Neudoerfl infection in neurons reveals disruption of proper neural development. (A) Heatmap summarizing results from gene set enrichment analysis (DAVID tool; GO Biological processes; p < 0.05) of DE genes 1) uniquely expressed in either N72_H or N72_N, and 2) genes expressed with >1.5 log₂ difference in one of the samples. **(B)** Number of mapped reads for vd-sRNAs (16–50 nt) in the respective sample. Data summarise three independent experiments and values in graphs are expressed as mean ± SD. **(C)** Frequency distribution of 21–23 nt vd-sRNAs mapped to TBEV Hypr/Neudoerfl genome in N72_H (black) and N72_N (red) samples. HS – hot-spot. (For interpretation of the references to colour in this figure legend, the reader is referred to the web version of this article.)

infected neurons, which may also play a substantial role in the impairment of the neuronal tissue.

The altered expression pattern of pc-mRNAs, which belong to the aforementioned pathways, could result from the miRNA/lncRNA-driven regulation process. Thus, we further focused on the linkage of the DE miRNAs/lncRNAs to their possible targets in the DE pc-mRNA datasets. The *in silico* prediction revealed several networks possibly involved in the differential expression pattern documented in astrocytes and neurons.

Interferon signalling is considered a key regulatory cascade of the innate immune system triggering the expression of a wide panel of ISGs with a direct or indirect antiviral effect [64]. Our data revealed that in addition to IFN-β, IFN-λ1/2 expression is induced in both cell types in an early TBEV infection (24 h p.i.). However, only astrocytes maintained the IFN-λ1/2 expression later during the infection (72 h p.i.). Interestingly, the IFN-λ cluster was predicted to be a *cis* target regulated by AC011445.2 lncRNA (ENSG00000269246), which was highly up-regulated in A72_H,

114
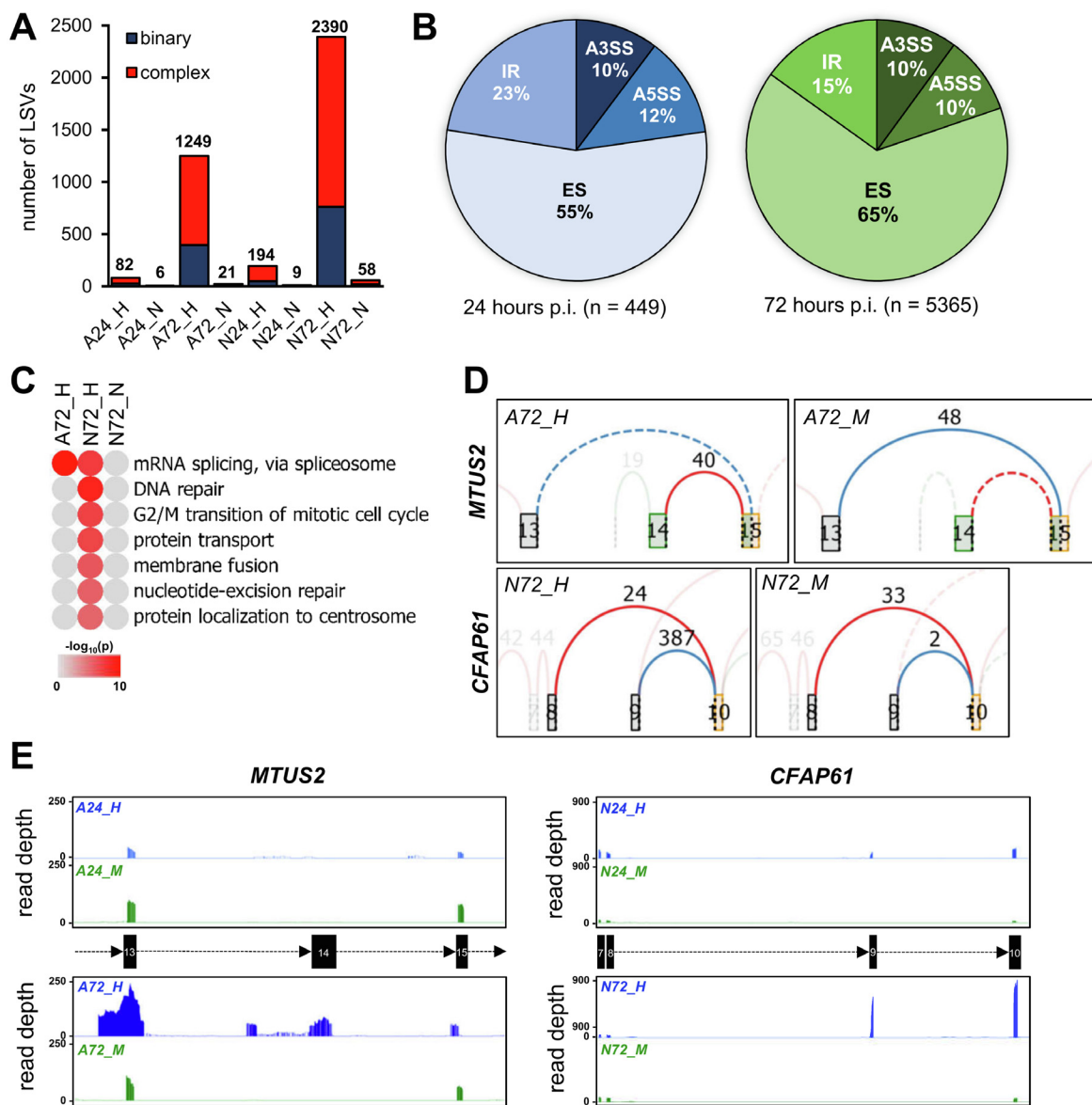
Fig. 7. TBEV infection induces changes in the splicing of host pre-mRNAs. (A) Graphical summary of identified LSVs (local splicing variants) in RNA-seq data using MAJIQ tool. Binary LSVs include exon skipping (ES), intron retention (IR), alternative 3′/5′ splice site (A3SS/A5SS) and involve only two exons or two splice sites in the same exon. Complex LSVs combine several binary splicing events originating from or targeting the same site. **(B)** Classification of binary and complex LSVs identified in TBEV-infected astrocytes and neurons (combined). **(C)** Heatmap summarizing results from gene set enrichment analysis (DAVID tool; GO Biological processes; p < 0.05) of genes in which > 1 LSV was identified (for samples A72_H, N72_H, and N72_N). **(D)** MAJIQ-generated Sashimi plots of top-ranked genes in N72_H (*CFAP61*) and A72_H (*MTUS2*) samples. Numbers above splicing event arcs represent the number of mapped junction reads. For the sake of readability, cropped areas with identified LSVs are shown. **(E)** Analysis of read depth distribution across *CFAP61* and *MTUS2* genes (areas with identified LSVs) in N72_H/M and A72_H/M samples, respectively, using the integrated genome browser.

but not in N72_H samples (Fig. 5, Table S3). Our previous study demonstrates that IFN-λ1 is the predominantly expressed interferon in response to TBEV infection in cells of neuronal origin [28], and its significance was also demonstrated in the case of WNV infection [65]. Thus, the deficiency of IFN-λ1/2 production in neurons is a potential contributor to the decreased expression of specific ISGs, which are necessary for a successful antiviral response to TBEV in astrocytes. Similarly, astrocyte-specific up-regulation of AL445490.1 lncRNA (ENSG00000225886) may contribute to the elevated expression of *IFI6*, a predicted *cis*-target of this lncRNA (Table S7).

When we focused on the neural cell-type-specific response in the case of host miRNAs, the *hsa-miR-1298* is the only miRNA species which was significantly up-regulated in Hypr-infected neu-

rons, while significantly down-regulated in Hypr-infected astrocytes (Fig. 4D). Among the predicted *hsa-miR-1298* mRNA targets with the corresponding DE profile (*LUZP2, SPSB4, VCAN, TFAP2B, MAST3, RSAD2, CMPK2,* and *DLX5*), the *RSAD2* and *CMPK2* we found the most important since both were documented to interfere with flavivirus infection [66]. Additionally, *hsa-miR-7974*, the second most up-regulated miRNA in Hypr-infected neurons, was predicted to target OAS1, whose DE profile also showed a decreasing induction rate in Hypr-infected neurons and which has already been proven to possess strong antiviral activity against flaviviruses [67]. Interestingly, a post mortem analysis of brain tissue from children with congenital ZIKV syndrome revealed elevated levels of *hsa-miR-145* and *hsa-miR-148a* [68]. Similarly, here we documented that *hsa-miR-145-5p* was up-regulated exclusively in

Hypr- and Neudoerfl-infected neurons, whereas *hsa-miR-148a-5p* was up-regulated exclusively in Hypr- and Neudoerfl-infected astrocytes (Fig. 4).

Besides dysregulated host miRNAs, small RNAs derived from the viral genome may also interfere with host mRNA levels [37,38]. Our data document an accumulation of TBEV vd-sRNAs in infected neurons and astrocytes; the distribution pattern of vd-sRNAs across the TBEV genome was remarkably similar among the samples, with coverage rate as the only variable factor. Interestingly, in the case of TBEV Hypr-infected astrocytes, vd-sRNAs (21–23 nt long) derived from the two hot-spots with the highest coverage (HS10, HS12) were both predicted to target *MBNL2* and *RBFOX1*. These genes are involved in pre-mRNA splicing regulation necessary for proper neural development [69–72], and their depletion may thus contribute to the observed dysregulation of the splicing process in astrocytes. This hypothesis is supported by a finding that one of the *RBFOX1* targets, *SNAP25* [69], was identified among differently spliced mRNAs in TBEV Hypr-infected astrocytes. Analogously, vd-sRNA derived from HS11 (hot-spot with the highest coverage in TBEV Hypr-infected neurons) was predicted to target 22 genes in total. However, only seven genes (*DLX1*, *MYCN*, *PCDH18*, *DPYSL2*, *TSHZ1*, *PFKFB3*, *BCL9L*) met the criterion of being expressed at a lower rate in N72_H in comparison to A72_H and N72_N samples. The dysregulation of mRNA levels through HS11-derived vd-sRNA for these genes could be thus responsible for the severe pathogenic effect in Hypr-infected neurons when compared to Hypr-infected astrocytes and Neudoerfl-infected neurons.

4.2. Alternative splicing as an important co-factor of high TBEV Hypr virulence in neurons

Based on the previous studies describing flavivirus-induced changes in the host pre-mRNA splicing process [61,62] in combination with observed dysregulation of various splicing factors upon TBEV infection (e.g., MBNL2, RBFOX1, or CELF3/4/5; Table S3), we hypothesized that TBEV infection alters the splicing of host mRNAs. Indeed, the differential splicing analysis revealed significant alterations in TBEV-infected cells. Since more than half of differently spliced LSVs were identified in Hypr-infected neurons (64.5 %), we contemplate that this phenomenon may also contribute substantially to the high pathogenic effect of Hypr strain in infected neurons. This assumption is further corroborated by the list of affected significantly enriched biological pathways, including DNA repair, G2/M transition during the mitotic cycle, protein transport, and membrane fusion. Malfunction of these processes, especially DNA repair and G2/M checkpoint, results in an elevated apoptotic rate and neuronal dysfunction [73,74].

Earlier, we reported a diverse rate of pathogenesis between TBEV Hypr and Neudoerfl strains in a human cell line of neuronal origin [56]. Similar findings were documented in the human primary neurons in this work, where Hypr infection resulted in a substantially more severe pathogenic effect (Fig. 1C). Therefore, we tried to extrapolate the link between the intensity of pathogenesis, replication rate, and host transcriptional response. Even though both strains reached high titres in neurons, Hypr strain replication and progeny production were more efficient, generating almost 10-times more mature virions (Fig. 1B), gRNA (Fig. 1D), and vd-sRNAs (Fig. 6B-D). Moreover, a lower replication rate of the Neudoerfl strain correlates with low numbers of identified DE poly-(A) RNAs (Fig. 3B) and altered splicing events (Fig. 7A), which suggests a direct dependency on virus replication rate and intensity of the host response. Almost identical findings were described in the study of Överby *et al.*, where the Hypr strain replicated with higher efficiency and induced a stronger immune response than the Neudoerfl strain [75]. On the contrary, the study of Sessions *et al.* described an inverse trend, where an attenuated DENV1 strain caused three-fold more changes in the host transcriptome than the wild-type DENV1 [61].

4.3. Diverse strain virulence in neurons

The lower replication and pathogenesis rates observed for the mild Neudoerfl strain can also be perceived as a consequence of a more successful host response. However, Neudoerfl-infected cells showed a lower rate of immune response activation in the case of pc-mRNAs (Table S3 and Fig. S3). Thus, the dysregulation of miRNA with proviral or antiviral properties may be the factor involved. We, therefore, compared the list of DE miRNAs in N72_H and N72_N samples with the list of experimentally verified proviral and antiviral miRNAs in the case of ZIKV [76] and DENV [77]. However, no corresponding matches were found. We, therefore, searched for novel antiviral miRNAs targeting Hypr or Neudoerfl gRNA using the miRDB tool. The *hsa-miR-592* was identified as the only miRNA species targeting Hypr and Neudoerfl gRNA. At the same time, this miRNA was up-regulated in samples with lower TBEV titres (A72_H and N72_N), but not in samples with higher TBEV titres (N72_H) (Fig. 4). These correlations thus suppose that *hsa-miR-592* may negatively regulate TBEV replication in human neurons and astrocytes. Except for the direct interaction with TBEV gRNA, *hsa-miR-592* may indirectly affect TBEV replication as well. He *et al.* [78] experimentally proved that *hsa-miR-592* targets SPRY2 mRNA, which is a negative regulator of interferon signalling [79], and in our study was shown to be up-regulated only in N72_H samples. We thus identified a new potential circuit of host cell countermeasure against TBEV involving *hsa-miR-592* unique among flaviviruses.

5. Conclusions

Altogether, we have characterized the alterations in poly-(A) RNA and small RNA expression profile of human neurons and astrocytes upon TBEV infection using two TBEV strains of distinctive virulence (mild Neudoerfl and severe Hypr). Subsequent integrative *in silico* analysis of miRNA/mRNA/lncRNA/vd-sRNA networks and pre-mRNA splicing found significant changes in inflammatory and immune response pathways, nervous system development and regulation of mitosis in TBEV Hypr-infected neurons. Candidate mechanisms include specific regulation of host mRNA levels via differentially expressed miRNAs/lncRNAs or vd-sRNAs mimicking endogenous miRNAs and virus-driven modulation of host pre-mRNA splicing. Thus, our data provide a valuable source of information for any research that aims to investigate and further characterise the mechanism of TBEV-host interactions and the related process of TBEV pathogenesis. Moreover, strain-specific expression pattern of selected host genes also represents a list of potential biomarkers, which can be used for improved TBEV diagnostics.

Declaration of Competing Interest

The authors declare that they have no known competing financial interests or personal relationships that could have appeared to influence the work reported in this paper.

Funding

This research was supported by the Ministry of Education, Youth, and Sports of the Czech Republic INTER-ACTION (projects LTARF 18021 and LTAUSA 18040), and the Czech Science Foundation (GA18-27204S).

Appendix A. Supplementary data

Supplementary data to this article can be found online at https://doi.org/10.1016/j.csbj.2022.05.052.

References

[1] Gritsun TS, Lashkevich VA, Gould EA. Tick-borne encephalitis. Antiviral research. 2003;57(1-2):129-46. Epub 2003/03/05. doi: 10.1016/s0166-3542 (02)00206-PubMed PMID: 12615309.

[2] de Graaf JA, Reimerink JH, Voorn GP, Bij de Vaate EA, de Vries A, Rockx B, et al. First human case of tick-borne encephalitis virus infection acquired in the Netherlands, July 2016. Euro surveillance : bulletin Europeen sur les maladies transmissibles = European communicable disease bulletin. 2016;21(33). Epub 2016/08/27. doi: 10.2807/1560-7917.Es .2016.21.33.30318. PubMed PMID: 27562931; PubMed Central PMCID: PMCPMC4998423.

[3] Neufeldt CJ, Cortese M, Acosta EG, Bartenschlager R. Rewiring cellular networks by members of the Flaviviridae family. Nature reviews Microbiology. 2018;16(3):125-42. Epub 2018/02/1doi: 10.1038/nrmicro.2017.170. PubMed PMID: 29430005; PubMed Central PMCID: PMCPMC7097628.

[4] Gelpi E, Preusser M, Garzuly F, Holzmann H, Heinz FX, Budka H. Visualization of Central European tick-borne encephalitis infection in fatal human cases. Journal of neuropathology and experimental neurology. 2005;64(6):506-12. Epub 2005/06/28. doi: 10.1093/jnen/64.6.506. PubMed PMID: 15977642.

[5] Bílý T, Palus M, Eyer L, Elsterová J, Vancová M, Růžek D. Electron Tomography Analysis of Tick-Borne Encephalitis Virus Infection in Human Neurons. Scientific reports. 2015;5:1074Epub 2015/06/16. doi: 10.1038/srep1074PubMed PMID: 26073783; PubMed Central PMCID: PMCPMC4466586.

[6] Potokar M, Korva M, Jorgačevski J, Avšič-Županc T, Zorec R. Tick-borne encephalitis virus infects rat astrocytes but does not affect their viability. PloS one. 2014;9(1):e86219. Epub 2014/01/28. doi: 10.1371/journal.pone.0086219. PubMed PMID: 24465969; PubMed Central PMCID: PMCPMC3896472.

[7] Palus M, Bílý T, Elsterová J, Langhansová H, Salát J, Vancová M, et al. Infection and injury of human astrocytes by tick-borne encephalitis virus. The Journal of general virology. 2014;95(Pt 11):2411-26. Epub 2014/07/09. doi: 10.1099/vir.0.068411-0. PubMed PMID: 25000960.

[8] Sofronew MV, Vinters HV. Astrocytes: biology and pathology. Acta neuropathologica. 2010;119(1):7-35. Epub 2009/12/17. doi: 10.1007/s00401-009-0619-PubMed PMID: 20012068; PubMed Central PMCID: PMCPMC2799634.

[9] Diniz JA, Da Rosa AP, Guzman H, Xu F, Xiao SY, Popov VL, et al. West Nile virus infection of primary mouse neuronal and neuroglial cells: the role of astrocytes in chronic infection. The American journal of tropical medicine and hygiene 2006;75(4):691–6. Epub 2006/10/14 PubMed PMID: 17038696.

[10] van Marle G, Antony J, Ostermann H, Dunham C, Hunt T, Halliday W, et al. West Nile virus-induced neuroinflammation: glial infection and capsid protein-mediated neurovirulence. Journal of virology. 2007;81(20):10933-49. Epub 2007/08/03. doi: 10.1128/jvi.02422-06. PubMed PMID: 17670819; PubMed Central PMCID: PMCPMC2045515.

[11] Jorgačevski J, Korva M, Potokar M, Lisjak M, Avšič-Županc T, Zorec R. ZIKV Strains Differentially Affect Survival of Human Fetal Astrocytes versus Neurons and Traffic of ZIKV-Laden Endocytotic Compartments. Scientific reports. 2019;9(1):8069. Epub 2019/05/31. doi: 10.1038/s41598-019-44559-8. PubMed PMID: 31147629; PubMed Central PMCID: PMCPMC6542792.

[12] Fares M, Cochet-Bernoin M, Gonzalez G, Montero-Menei CN, Blanchet O, Benchoua A, et al. Pathological modeling of TBEV infection reveals differential innate immune responses in human neurons and astrocytes that correlate with their susceptibility to infection. Journal of neuroinflammation. 2020;17 (1):76. Epub 2020/03/05. doi: 10.1186/s12974-020-01756-x. PubMed PMID: 32127025; PubMed Central PMCID: PMCPMC7053149.

[13] Pokorna Formanova P, Palus M, Salat J, Hönig V, Stefanik M, Svoboda P, et al. Changes in cytokine and chemokine profiles in mouse serum and brain, and in human neural cells, upon tick-borne encephalitis virus infection. Journal of neuroinflammation. 2019;16(1):205. Epub 2019/11/09. doi: 10.1186/s12974-019-1596-z. PubMed PMID: 31699097; PubMed Central PMCID: PMCPMC6839073.

[14] O'Brien J, Hayder H, Zayed Y, Peng C. Overview of MicroRNA Biogenesis, Mechanisms of Actions, and Circulation. Frontiers in endocrinology. 2018;9:402. Epub 2018/08/21. doi: 10.3389/fendo.2018.00402. PubMed PMID: 30123182; PubMed Central PMCID: PMCPMC6085463.

[15] Kumar M, Nerurkar VR. Integrated analysis of microRNAs and their disease related targets in the brain of mice infected with West Nile virus. Virology.

[16] Slonchak A, Shannon RP, Pali G, Khromykh AA. Human MicroRNA miR-532-5p Exhibits Antiviral Activity against West Nile Virus via Suppression of Host Genes SESTD1 and TAB3 Required for Virus Replication. Journal of virology. 2015;90(5):2388-402. Epub 2015/12/18. doi: 10.1128/jvi.02608-15. PubMed PMID: 26676784; PubMed Central PMCID: PMCPMC4810706.

[17] Rastogi M, Srivastava N, Singh SK. Exploitation of microRNAs by Japanese Encephalitis virus in human microglial cells. Journal of medical virology. 2018;90(4):648-54. Epub 2017/11/18. doi: 10.1002/jmv.24995. PubMed PMID: 29149532.

[18] Dang JW, Tiwari SK, Qin Y, Rana TM. Genome-wide Integrative Analysis of Zika-Virus-Infected Neuronal Stem Cells Reveals Roles for MicroRNAs in Cell Cycle and Stemness. Cell reports. 2019;27(12):3618-28.e5. Epub 2019/06/20. doi: 10.1016/j.celrep.2019.05.059. PubMed PMID: 31216479; PubMed Central PMCID: PMCPMC6687627.

[19] Seong RK, Lee JK, Cho GJ, Kumar M, Shin OS. mRNA and miRNA profiling of Zika virus-infected human umbilical cord mesenchymal stem cells identifies miR-142-5p as an antiviral factor. Emerging microbes & infections. 2020;9 (1):2061-75. Epub 2020/09/10. doi: 10.1080/22221751.2020.1821581. PubMed PMID: 32902370; PubMed Central PMCID: PMCPMC7534337.

[20] Hazra B, Kumawat KL, Basu A. The host microRNA miR-301a blocks the IRF1-mediated neuronal innate response to Japanese encephalitis virus infection. Sci Signaling 2017;10(466):eaaf5185.;PubMed 2017/02/16. https://doi.org/10.1126/scisignal.aaf5185. PubMed PMID: 28196914.

[21] Wu N, Gao N, Fan D, Wei J, Zhang J, An J. miR-223 inhibits dengue virus replication by negatively regulating the microtubule-destabilizing protein STMN1 in EAhy926 cells. Microbes and infection. 2014;16(11):911-22. Epub 2014/09/03. doi: 10.1016/j.micinf.2014.08.011. PubMed PMID: 25181337; PubMed Central PMCID: PMCPMC7110837.

[22] Diosa-Toro M, Echavarría-Consuegra L, Flipse J, Fernández GJ, Kluiver J, van den Berg A, et al. MicroRNA profiling of human primary macrophages exposed to dengue virus identifies miRNA-3614-5p as antiviral and regulator of ADAR1 expression. PLoS neglected tropical diseases. 2017;11(10):e0005981. Epub 2017/10/19. doi: 10.1371/journal.pntd.0005981. PubMed PMID: 29045406; PubMed Central PMCID: PMCPMC5662241.

[23] Cai W, Pan Y, Cheng A, Wang M, Yin Z, Jia R. Regulatory Role of Host MicroRNAs in Flaviviruses Infection. Frontiers in microbiology. 2022;13:869441. Epub 2022/04/29. doi: 10.3389/fmicb.2022.869441. PubMed PMID: 35479613; PubMed Central PMCID: PMCPMC9036177.

[24] Statello L, Guo CJ, Chen LL, Huarte M. Gene regulation by long non-coding RNAs and its biological functions. Nature reviews Molecular cell biology. 2021;22(2):96-118. Epub 2020/12/doi: 10.1038/s41580-020-00315-9. PubMed PMID: 33353982; PubMed Central PMCID: PMCPMC7754182.

[25] Bhattacharyya S, Vrati S. The Malat1 long non-coding RNA is upregulated by signalling through the PERK axis of unfolded protein response during flavivirus infection. Scientific reports. 2015;5:17794. Epub 2015/12/05. doi: 10.1038/srep17794. PubMed PMID: 26634309; PubMed Central PMCID: PMCPMC4669524.

[26] Wang XJ, Jiang SC, Wei HX, Deng SQ, He C, Peng HJ. The Differential Expression and Possible Function of Long Noncoding RNAs in Liver Cells Infected by Dengue Virus. The American journal of tropical medicine and hygiene. 2017;97(6):1904-12. Epub 2017/10/11. doi: 10.4269/ajtmh.17-0307. PubMed PMID: 29016307; PubMed Central PMCID: PMCPMC5805055.

[27] Hu B, Huo Y, Yang L, Chen G, Luo M, Yang J, et al. ZIKV infection effects changes in gene splicing, isoform composition and lncRNA expression in human neural progenitor cells. Virology journal. 2017;14(1):217. Epub 2017/11/09. doi: 10.1186/s12985-017-0882-6. PubMed PMID: 29116029; PubMed Central PMCID: PMCPMC5688814.

[28] Selinger M, Wilkie GS, Tong L, Gu Q, Schnettler E, Grubhoffer L, et al. Analysis of tick-borne encephalitis virus-induced host responses in human cells of neuronal origin and interferon-mediated protection. The Journal of general virology. 2017;98(8):2043-60. Epub 2017/08/09. doi: 10.1099/jgv.0.000853. PubMed PMID: 28786780; PubMed Central PMCID: PMCPMC5817271.

[29] Zhong XL, Liao XM, Shen F, Yu HJ, Yan WS, Zhang YF, et al. Genome-wide profiling of mRNA and lncRNA expression in dengue fever and dengue hemorrhagic fever. FEBS open bio. 2019;9(3):468-77. Epub 2019/03/15. doi: 10.1002/2211-5463.12576. PubMed PMID: 30868055; PubMed Central PMCID: PMCPMC6396354.

[30] Wang P, Xu J, Wang Y, Cao X. An interferon-independent lncRNA promotes viral replication by modulating cellular metabolism. Science (New York, NY). 2017;358(6366):1051-5. Epub 2017/10/28. doi: 10.1126/science.aao0409. PubMed PMID: 29074580.

[31] Barriocanal M, Carnero E, Segura V, Fortes P. Long Non-Coding RNA BST2/BISPR is Induced by IFN and Regulates the Expression of the Antiviral Factor Tetherin. Frontiers in immunology. 2014;5:655. Epub 2015/01/27. doi: 10.3389/fimmu.2014.00655. PubMed PMID: 25620967; PubMed Central PMCID: PMCPMC4288319.

[32] Kambara H, Niazi F, Kostadinova L, Moonka DK, Siegel CT, Post AB, et al. Negative regulation of the interferon response by an interferon-induced long non-coding RNA. Nucleic acids research. 2014;42(16):10668-80. Epub 2014/08/15. doi: 10.1093/nar/gku713. PubMed PMID: 25122750; PubMed Central PMCID: PMCPMC4176326.

[33] Qian X, Xu C, Zhao P, Qi Z. Long non-coding RNA GAS5 inhibited hepatitis C virus replication by binding viral NS3 protein. Virology 2016;Epub 2016/03/08

117

(492):155–65. https://doi.org/10.1016/j.virol.2016.02.020. PubMed PMID: 26945984.

[34] Schnettler E, Tykalová H, Watson M, Sharma M, Sterken MG, Obbard DJ, et al. Induction and suppression of tick cell antiviral RNAi responses by tick-borne flaviviruses. Nucleic acids research. 2014;42(14):9436–46. Epub 2014/07/24. doi: 10.1093/nar/gku657. PubMed PMID: 25053841; PubMed Central PMCID: PMCPMC4132761.

[35] Schirtzinger EE, Andrade CC, Devitt N, Ramaraj T, Jacobi JL, Schilkey F, et al. Repertoire of virus-derived small RNAs produced by mosquito and mammalian cells in response to dengue virus infection. Virology. 2015;476:54–60. Epub 2014/12/22. doi: 10.1016/j.virol.2014.11.019. PubMed PMID: 25528416; PubMed Central PMCID: PMCPMC4323773.

[36] Schuster S, Miesen P, van Rij RP. Antiviral RNAi in Insects and Mammals: Parallels and Differences. Viruses. 2019;11(5). Epub 2019/05/19. doi: 10.3390/v11050448. PubMed PMID: 31100912; PubMed Central PMCID: PMCPMC6563508.

[37] Li X, Fu Z, Liang H, Wang Y, Qi X, Ding M, et al. H5N1 influenza virus-specific miRNA-like small RNA increases cytokine production and mouse mortality via targeting poly(rC)-binding protein 2. Cell research. 2018;28(2):157–71. Epub 2018/01/13. doi: 10.1038/cr.2018.3. PubMed PMID: 29327729; PubMed Central PMCID: PMCPMC5799819.

[38] Ouellet DL, Vigneault-Edwards J, Létourneau K, Gobeil LA, Plante I, Burnett JC, et al. Regulation of host gene expression by HIV-1 TAR microRNAs. Retrovirology. 2013;10:86. Epub 2013/08/14. doi: 10.1186/1742-4690-10-86. PubMed PMID: 23938024; PubMed Central PMCID: PMCPMC3751525.

[39] Heinz FX, Kunz C. Homogeneity of the structural glycoprotein from European isolates of tick-borne encephalitis virus: comparison with other flaviviruses. The Journal of general virology. 1981;57(Pt 2):263–74. Epub 1981/12/01. doi: 10.1099/0022-1317-57-2-263. PubMed PMID: 6172553.

[40] Pospisil L, Jandasek L, Pesek J. Isolation of new strains of meningoencephalitis virus in the Brno region during the summer of 1953. Lekarske listy 1954;9 (1):3–5. Epub 1954/01/01 PubMed PMID: 13131921.

[41] De Madrid AT, Porterfield JS. A simple micro-culture method for the study of group B arboviruses. Bulletin of the World Health Organization. 1969;40 (1):113–21. Epub 1969/01/01. PubMed PMID: 4183812; PubMed Central PMCID: PMCPMC2554446.

[42] Achazi K, Nitsche A, Patel P, Radonić A, Donoso Mantke O, Niedrig M. Detection and differentiation of tick-borne encephalitis virus subtypes by a reverse transcription quantitative real-time PCR and pyrosequencing. Journal of virological methods. 2011;171(1):34–9. Epub 2010/10/12. doi: 10.1016/j.jviromet.2010.09.026. PubMed PMID: 20933016.

[43] Martin M. Cutadapt removes adapter sequences from high-throughput sequencing reads. 2011. 2011;17(1):3. Epub 2011-08-02. doi: 10.14806/ej.17.1.200.

[44] Andrews S. FastQC: a quality control tool for high throughput sequence data. 2010;Available online at: http://www.bioinformatics.babraham.ac.uk/projects/fastqc.

[45] Ghosh S, Chan CK. Analysis of RNA-Seq Data Using TopHat and Cufflinks. Methods in molecular biology (Clifton, NJ). 2016;1374:339–61. Epub 2015/11/01. doi: 10.1007/978-1-4939-3167-5_18. PubMed PMID: 26519415.

[46] Friedländer MR, Mackowiak SD, Li N, Chen W, Rajewsky N. miRDeep2 accurately identifies known and hundreds of novel microRNA genes in seven animal clades. Nucleic acids research. 2012;40(1):37–52. Epub 2011/09/14. doi: 10.1093/nar/gkr688. PubMed PMID: 21911355; PubMed Central PMCID: PMCPMC3245920.

[47] Griffiths-Jones S, Grocock RJ, van Dongen S, Bateman A, Enright AJ. miRBase: microRNA sequences, targets and gene nomenclature. Nucleic acids research. 2006;34(Database issue):D140–4. Epub 2005/12/31. doi: 10.1093/nar/gkj112. PubMed PMID: 16381832; PubMed Central PMCID: PMCPMC1347474.

[48] Langmead B, Trapnell C, Pop M, Salzberg SL. Ultrafast and memory-efficient alignment of short DNA sequences to the human genome. Genome biology. 2009;10(3):R25. Epub 2009/03/06. doi: 10.1186/gb-2009-10-3-r25. PubMed PMID: 19261174; PubMed Central PMCID: PMCPMC2690996.

[49] Quinlan AR, Hall IM. BEDTools: a flexible suite of utilities for comparing genomic features. Bioinformatics (Oxford, England). 2010;26(6):841–2. Epub 2010/01/30. doi: 10.1093/bioinformatics/btq033. PubMed PMID: 20110278; PubMed Central PMCID: PMCPMC2832824.

[50] Li H, Handsaker B, Wysoker A, Fennell T, Ruan J, Homer N, et al. The Sequence Alignment/Map format and SAMtools. Bioinformatics (Oxford, England). 2009;25(16):2078–9. Epub 2009/06/10. doi: 10.1093/bioinformatics/btp352. PubMed PMID: 19505943; PubMed Central PMCID: PMCPMC2723002.

[51] Sticht C, De La Torre C, Parveen A, Gretz N. miRWalk: An online resource for prediction of microRNA binding sites. PloS one. 2018;13(10):e0206239. Epub 2018/10/20. doi: 10.1371/journal.pone.0206239. PubMed PMID: 30335862; PubMed Central PMCID: PMCPMC6193719.

[52] Paraskevopoulou MD, Vlachos IS, Karagkouni D, Georgakilas G, Kanellos I, Vergoulis T, et al. DIANA-LncBase v2: indexing microRNA targets on non-coding transcripts. Nucleic acids research. 2016;44(D1):D231–8. Epub 2015/11/28. doi: 10.1093/nar/gkv1270. PubMed PMID: 26612864; PubMed Central PMCID: PMCPMC4702897.

[53] Wong N, Wang X. miRDB: an online resource for microRNA target prediction and functional annotations. Nucleic acids research. 2015;43(Database issue): D146–52. Epub 2014/11/08. doi: 10.1093/nar/gku1104. PubMed PMID: 25378301; PubMed Central PMCID: PMCPMC4383922.

[54] Vaquero-Garcia J, Barrera A, Gazzara MR, González-Vallinas J, Lahens NF, Hogenesch JB, et al. A new view of transcriptome complexity and regulation through the lens of local splicing variations. eLife. 2016;5:e11752. Epub 2016/02/02. doi: 10.7554/eLife.11752. PubMed PMID: 26829591; PubMed Central PMCID: PMCPMC4801060.

[55] Dobin A, Davis CA, Schlesinger F, Drenkow J, Zaleski C, Jha S, et al. STAR: ultrafast universal RNA-seq aligner. Bioinformatics (Oxford, England). 2013;29 (1):15–21. Epub 2012/10/30. doi: 10.1093/bioinformatics/bts635. PubMed PMID: 23104886; PubMed Central PMCID: PMCPMC3530905.

[56] Selinger M, Tykalová H, Štěrba J, Věchtová P, Vavrušková Z, Lieskovská J, et al. Tick-borne encephalitis virus inhibits rRNA synthesis and host protein production in human cells of neural origin. PLoS neglected tropical diseases. 2019;13(9):e0007745. Epub 2019/09/29. doi: 10.1371/journal.pntd.0007745. PubMed PMID: 31560682; PubMed Central PMCID: PMCPMC6785130.

[57] Trapnell C, Roberts A, Goff L, Pertea G, Kim D, Kelley DR, et al. Differential gene and transcript expression analysis of RNA-seq experiments with TopHat and Cufflinks. Nature protocols. 2012;7(3):562–78. Epub 2012/03/03. doi: 10.1038/nprot.2012.016. PubMed PMID: 22383036; PubMed Central PMCID: PMCPMC3334321.

[58] Huang da W, Sherman BT, Lempicki RA. Systematic and integrative analysis of large gene lists using DAVID bioinformatics resources. Nature protocols. 2009;4(1):44–57. Epub 2009/01/10. doi: 10.1038/nprot.2008.211. PubMed PMID: 19131956.

[59] Pla R, Stanco A, Howard MA, Rubin AN, Vogt D, Mortimer N, et al. Dlx1 and Dlx2 Promote Interneuron GABA Synthesis, Synaptogenesis, and Dendritogenesis. Cerebral cortex (New York, NY : 1991). 2018;28(11):3797–815. Epub 2017/10/14. doi: 10.1093/cercor/bhx241. PubMed PMID: 29028947; PubMed Central PMCID: PMCPMC6188538.

[60] Ip JP, Fu AK, Ip NY. CRMP2: functional roles in neural development and therapeutic potential in neurological diseases. The Neuroscientist : a review journal bringing neurobiology, neurology and psychiatry. 2014;20(6):589–98. Epub 2014/01/10. doi: 10.1177/1073858413514278. PubMed PMID: 24402611.

[61] Sessions OM, Tan Y, Goh KC, Liu Y, Tan P, Rozen S, et al. Host cell transcriptome profile during wild-type and attenuated dengue virus infection. PLoS neglected tropical diseases. 2013;7(3):e2107. Epub 2013/03/22. doi: 10.1371/journal.pntd.0002107. PubMed PMID: 23516652; PubMed Central PMCID: PMCPMC3597485.

[62] De Maio FA, Risso G, Iglesias NG, Shah P, Pozzi B, Gebhard LG, et al. The Dengue Virus NS5 Protein Intrudes in the Cellular Spliceosome and Modulates Splicing. PLoS pathogens. 2016;12(8):e1005841. Epub 2016/08/31. doi: 10.1371/journal.ppat.1005841. PubMed PMID: 27575636; PubMed Central PMCID: PMCPMC5004807.

[63] Cho H, Proll SC, Szretter KJ, Katze MG, Gale M, Jr., Diamond MS. Differential innate immune response programs in neuronal subtypes determine susceptibility to infection in the brain by positive-stranded RNA viruses. Nature medicine. 2013;19(4):458–64. Epub 2013/03/05. doi: 10.1038/nm.3108. PubMed PMID: 23455712; PubMed Central PMCID: PMCPMC3618596.

[64] Schneider WM, Chevillotte MD, Rice CM. Interferon-stimulated genes: a complex web of host defenses. Annual review of immunology. 2014;32:513–45. Epub 2014/02/22. doi: 10.1146/annurev-immunol-032713-120231. PubMed PMID: 24555472; PubMed Central PMCID: PMCPMC4313732.

[65] Lazear HM, Daniels BP, Pinto AK, Huang AC, Vick SC, Doyle SE, et al. Interferon-lambda restricts West Nile virus neuroinvasion by tightening the blood-brain barrier. Science translational medicine. 2015;7(284):284ra59. Epub 2015/04/24. doi: 10.1126/scitranslmed.aaa4304. PubMed PMID: 25904743; PubMed Central PMCID: PMCPMC4435724.

[66] Rivera-Serrano EE, Gizzi AS, Arnold JJ, Grove TL, Almo SC, Cameron CE. Viperin Reveals Its True Function. Annual review of virology. 2020;7(1):421–46. Epub 2020/07/01. doi: 10.1146/annurev-virology-011720-095930. PubMed PMID: 32603630; PubMed Central PMCID: PMCPMC8191541.

[67] Soveg FW, Schwerk J, Gokhale NS, Cerosaletti K, Smith JR, Pairo-Castineira E, et al. Endomembrane targeting of human OAS1 p46 augments antiviral activity. eLife. 2021;10. Epub 2021/08/04. doi: 10.7554/eLife.71047. PubMed PMID: 34342578; PubMed Central PMCID: PMCPMC8357416.

[68] Castro FL, Geddes VEV, Monteiro FLL, Gonçalves R, Campanati L, Pezzuto P, et al. MicroRNAs 145 and 148a Are Upregulated During Congenital Zika Virus Infection. ASN neuro. 2019;11:1759091419850983. Epub 2019/06/20. doi: 10.1177/1759091419850983. PubMed PMID: 31213064; PubMed Central PMCID: PMCPMC6585135.

[69] Gehman LT, Stoilov P, Maguire J, Damianov A, Lin CH, Shiue L, et al. The splicing regulator Rbfox1 (A2BP1) controls neuronal excitation in the mammalian brain. Nature genetics. 2011;43(7):706–11. Epub 2011/05/31. doi: 10.1038/ng.841. PubMed PMID: 21623373; PubMed Central PMCID: PMCPMC3125461.

[70] Lovci MT, Ghanem D, Marr H, Arnold J, Gee S, Parra M, et al. Rbfox proteins regulate alternative mRNA splicing through evolutionarily conserved RNA bridges. Nature structural & molecular biology. 2013;20(12):1434–42. Epub 2013/11/12. doi: 10.1038/nsmb.2699. PubMed PMID: 24213538; PubMed Central PMCID: PMCPMC3918504.

[71] Wang ET, Ward AJ, Cherone JM, Giudice J, Wang TT, Treacy DJ, et al. Antagonistic regulation of mRNA expression and splicing by CELF and MBNL proteins. Genome research. 2015;25(6):858-Epub 2015/04/18. doi: 10.1101/gr.184390.114. PubMed PMID: 25883322; PubMed Central PMCID: PMCPMC4448682.

[72] Su CH, D D, Tarn WY. Alternative Splicing in Neurogenesis and Brain Development. Frontiers in molecular biosciences. 2018;5:12. Epub 2018/02/

118

28. doi: 10.3389/fmolb.2018.00012. PubMed PMID: 29484299; PubMed Central PMCID: PMCPMC5816070.

[73] Wang Y, Ji P, Liu J, Broaddus RR, Xue F, Zhang W. Centrosome-associated regulators of the G(2)/M checkpoint as targets for cancer therapy. Molecular cancer. 2009;8:8. Epub 2009/02/17. doi: 10.1186/1476-4598-8-8. PubMed PMID: 19216791; PubMed Central PMCID: PMCPMC2657106.

[74] Ciccia A, Elledge SJ. The DNA damage response: making it safe to play with knives. Molecular cell. 2010;40(2):179-204. Epub 2010/10/23. doi: 10.1016/j.molcel.2010.09.019. PubMed PMID: 20965415; PubMed Central PMCID: PMCPMC2988877.

[75] Overby AK, Popov VL, Niedrig M, Weber F. Tick-borne encephalitis virus delays interferon induction and hides its double-stranded RNA in intracellular membrane vesicles. Journal of virology. 2010;84(17):8470-83. Epub 2010/06/18. doi: 10.1128/jvi.00176-10. PubMed PMID: 20554782; PubMed Central PMCID: PMCPMC2919015.

[76] Polonio CM, Peron JPS. ZIKV Infection and miRNA Network in Pathogenesis and Immune Response. Viruses. 2021;13(10). Epub 2021/10/27. doi: 10.3390/v13101992. PubMed PMID: 34696422; PubMed Central PMCID: PMCPMC8541119.

[77] Wong RR, Abd-Aziz N, Affendi S, Poh CL. Role of microRNAs in antiviral responses to dengue infection. Journal of biomedical science. 2020;27(1):4. Epub 2020/01/04. doi: 10.1186/s12929-019-0614-x. PubMed PMID: 31898495; PubMed Central PMCID: PMCPMC6941309.

[78] He Y, Ge Y, Jiang M, Zhou J, Luo D, Fan H, et al. MiR-592 Promotes Gastric Cancer Proliferation, Migration, and Invasion Through the PI3K/AKT and MAPK/ERK Signaling Pathways by Targeting Spry2. Cellular physiology and biochemistry : international journal of experimental cellular physiology, biochemistry, and pharmacology. 2018;47(4):1465-81. Epub 2018/06/28. doi: 10.1159/000490839. PubMed PMID: 29949784.

[79] Sharma B, Joshi S, Sassano A, Majchrzak B, Kaur S, Aggarwal P, et al. Sprouty proteins are negative regulators of interferon (IFN) signaling and IFN-inducible biological responses. The Journal of biological chemistry. 2012;287 (50):42352-60. Epub 2012/10/18. doi: 10.1074/jbc.M112.400721. PubMed PMID: 23074222; PubMed Central PMCID: PMCPMC3516778.

119

MANUSCRIPT 5

Helmová R., Hönig V., **Tykalová H**., Palus M., Bell-Sakyi L., Grubhoffer L. (2020). Tick-borne encephalitis virus adaptation in different host environments and existence of quasispecies. Viruses 12(8):902. DOI: 10.3390/v12080902

Tick-Borne Encephalitis Virus Adaptation in Different Host Environments and Existence of Quasispecies

Renata Helmová [1], Václav Hönig [1,2,3,*], Hana Tykalová [1,2], Martin Palus [2,3], Lesley Bell-Sakyi [4] and Libor Grubhoffer [1,2]

[1] Faculty of Science, University of South Bohemia in České Budějovice,
    37005 České Budějovice, Czech Republic; Darcenka@seznam.cz (R.H.);
    tykalova@paru.cas.cz (H.T.); liborex@paru.cas.cz (L.G.)
[2] Institute of Parasitology, Biology Centre of the Czech Academy of Sciences,
    370 05 České Budějovice, Czech Republic; palus@paru.cas.cz
[3] Department of Virology, Veterinary Research Institute, 62100 Brno, Czech Republic
[4] Institute of Infection, Veterinary and Ecological Sciences, University of Liverpool, Liverpool L3 5RF, UK;
    L.Bell-Sakyi@liverpool.ac.uk
[*] Correspondence: honig@paru.cas.cz; Tel.: +420-387-775-463

Abstract: A highly virulent strain (Hypr) of tick-borne encephalitis virus (TBEV) was serially subcultured in the mammalian porcine kidney stable (PS) and *Ixodes ricinus* tick (IRE/CTVM19) cell lines, producing three viral variants. These variants exhibited distinct plaque sizes and virulence in a mouse model. Comparing the full-genome sequences of all variants, several nucleotide changes were identified in different genomic regions. Furthermore, different sequential variants were revealed to co-exist within one sample as quasispecies. Interestingly, the above-mentioned nucleotide changes found within the whole genome sequences of the new variants were present alongside the nucleotide sequence of the parental strain, which was represented as a minority quasispecies. These observations further imply that TBEV exists as a heterogeneous population that contains virus variants pre-adapted to reproduction in different environments, probably enabling virus survival in ticks and mammals.

Keywords: TBEV; host alternation; neuroinvasiveness; genome mutation; quasispecies; flavivirus adaptation; tick cell line

1. Introduction

Tick-borne encephalitis virus (TBEV), a member of the genus Flavivirus in the family Flaviviridae, is endemic in many parts of Europe and Asia and causes serious, even fatal encephalitis in humans [1]. AS with other flaviviruses, TBEV is an enveloped virus with single-stranded RNA of positive polarity. The RNA genome of TBEV is about 11 kb in length and encodes a single large polyprotein flanked by 5' and 3' untranslated regions (UTR) of variable sizes. Following translation, the viral polyprotein is cleaved by viral and cellular proteases into three structural proteins, namely capsid (C), membrane (M, derived from its precursor prM), and envelope (E) proteins, as well as seven nonstructural proteins, namely NS1, NS2A, NS2B, NS3, NS4A, NS4B, and NS5 [2].

In nature, tick-borne flaviviruses are maintained through a transmission cycle involving an ixodid tick vector and a vertebrate host. The virus can persist in ticks throughout their lifespan, enabling virus transmission for years after the initial infection [3]. Although the majority of the evolutionary life of the virus is spent in the tick vector, transmission to a vertebrate host is required to ensure the survival of the virus in natural foci [4,5]. Since arthropod and vertebrate species are only distantly related, flaviviruses have to be very adaptable to persistently infect the arthropod host, yet also to

replicate quickly in vertebrates upon transmission. Host alternations presumably select for a virus population that is well adapted to both host systems [6,7]. However, the mechanisms that allow efficient replication in the new host after host switch have not yet been elucidated.

One possible explanation for the adaptability of RNA viruses and their rapid evolution is the presence of quasispecies. Quasispecies are dynamic distributions of non-identical but closely related mutant and recombinant viral genomes existing as one population in a single host. Quasispecies result from the high error rates of most RNA virus-encoded RNA-dependent RNA polymerases, as well as from short viral generation times and large population sizes [8]. They are subjected to a continuous process of genetic variation, competition, and selection, and act as a unit of selection [9–11]. The diversity of viral quasispecies has been shown to be both host- and virus-dependent [12,13], and is a critical determinant of virus fitness [14,15]. A genetically diverse virus population would seem to have an adaptive advantage due to the pre-existence of variants that may have a higher rate of reproduction in a novel or changing environment [16]. The existence of quasispecies was previously described for several mosquito-borne flaviviruses [17–19]. There is growing evidence from field studies [16,20] and laboratory experiments [21–23] that the same is true for TBEV.

Serial passage of viruses in cell culture in certain cases produces cell-adapted mutant viruses. Many reports state that virus adaptation to cell lines results in reduced virulence in vivo [24–26]. However, the mechanism by which cell-adapted flaviviruses undergo attenuation in vivo is unclear.

In this study, we serially subcultured the highly virulent TBEV strain Hypr in parallel in mammalian porcine kidney stable (PS) cells [27] and in the tick cell line IRE/CTVM19 [23,28], producing three new viral variants. The biological properties of these new variants were investigated in a mouse model and compared to each other, as well as to the parental virus. In addition, complete nucleotide sequences of all these variants were analyzed and differences were appraised as potential genetic determinants important for replication in either the tick or the mammalian host. The correlation between virulence and observed genome changes is discussed.

2. Materials and Methods

2.1. Cell Lines and Viruses

Porcine kidney stable (PS) cells [27] were cultured at 37 °C in L-15 (Leibovitz) medium (PAA Laboratories, Pasching, Austria) supplemented with 3% newborn calf serum (Sigma-Aldrich, Darmstadt, Germany), 2 mM L-glutamine (Sigma-Aldrich, Darmstadt, Germany) and 100 IU/mL penicillin, 100 μg/mL streptomycin, and 0.25 μg/mL amphotericin B (Sigma-Aldrich, Darmstadt, Germany). The tick cell line IRE/CTVM19 [28] derived from *Ixodes ricinus* embryos was grown at 28 °C in L-15 (Leibovitz) medium supplemented with 10% tryptose phosphate broth, 20% foetal bovine serum, 2 mM L-glutamine and 100 IU/mL penicillin, 100 μg/mL streptomycin, and 0.25 μg/mL amphotericin B (Sigma-Aldrich, Darmstadt, Germany). The Czech prototype TBEV strain Hypr was originally isolated from the blood of a 10-year-old child diagnosed with tick-borne encephalitis in 1953 [29]. Subsequently, the strain was propagated through 4 mouse brain passages and used directly as the parental virus strain in our experiments.

2.2. Passage Series and Plaque Size Measurement

The parental virus (designated as 0 P) was serially passaged in PS or IRE/CTVM19 cells forty times, producing two new viral variants (40 PS and 40 IRE). Since TBEV produces permanent infection of the tick cells, a third variant was derived by long-term propagation without passage in tick cells for one month and designated as LT IRE. For a passage series, PS and IRE/CTVM19 cells were seeded in 24-well plates (10^6 and 10^5 cells/well respectively) and infected with 10^3 PFU of the parental virus. The cells were then grown at the respective appropriate temperatures in an atmosphere of 5% CO_2. After four days of cultivation, the cells were harvested, frozen at −70 °C to release intracellular viral particles, then the suspension was clarified by centrifugation (2500× *g* for 5 min at 4 °C). Subsequently, 100 μL

of the supernatant was used as inoculum for the next passage. Plaque morphology and virus titers were determined by plaque assay on PS cells, as described previously [30]. After washing with saline (0.9% NaCl *w/v*), the cells were fixed and stained using naphthalene black solution (0.1% naphthalene black in 6% acetic acid solution) for 45 min, subsequently washed with water, then air-dried. During propagation in PS cells, titers of the virus at 4 days post infection fell gradually between passages 20 and 30 due to the increased replication rate of the virus, early onset of cytopathic effect, and thus faster depletion of the cells. Thereafter, the passage interval in PS cells was shortened to two days.

To assess the evolution of the plaque size during the passaging history, the plaque sizes in passage numbers 5, 10, 20, 30, 35, and 40 in both cell lines and in LT IRE were measured using ImageJ software (NIH, Bethesda, MD, USA, version 1.52a) [31] and compared to the 0 P plaque size. The diameters of a minimum of 20 randomly chosen discrete plaque samples per viral variant were measured in duplicate and mean value sizes were plotted and compared statistically.

2.3. Virulence Assays

Virulence assays for all viral variants were performed in adult CD1 mice (TBEV-susceptible strain of mice, females, body weight 15–20 g; AnLab Prague, Czech Republic). Groups of 9 mice were inoculated subcutaneously with 100 PFU of the 0 P, 40 PS, 40 IRE, or LT IRE viruses. Survival rates were recorded daily for a period of 30 days post inoculation (p.i.).

Laboratory animals were used in compliance with all relevant national legislation and regulations of the European Union. The experiments were approved by the Committee on the Ethics of Animal Experiments of the Institute of Parasitology of the Biology Centre of the Czech Academy of Sciences of the Czech Republic.

2.4. Virus Replication in the Mouse Model

Groups of 15 adult CD1 mice (females, body weight 15–20 g) were inoculated subcutaneously with 100 PFU of viruses 0 P, 40 PS, or 40 IRE. At different time points p.i., two mice from each group were anesthetized and euthanized. Samples of blood, spleen, and brain were collected. Organs were individually homogenized using a TissueLyser II (Qiagen, Hilden, Germany) and prepared as 20% (spleen) or 33% (brain) (*w/v*) suspensions. The suspensions were clarified by centrifugation at 16,000× *g* for 10 min at 4 °C. Blood samples were allowed to clot for 30 min at room temperature and serum samples were obtained by centrifugation at 1000× *g* for 5 min at 4 °C. Samples were analyzed by quantitative reverse transcription–PCR (qRT-PCR).

2.5. Quantitative RT-PCR

The number of virus genome copies was determined by qRT-PCR (TaqMan, Waltham, MA, USA). Viral RNA was extracted from serum and organs using a QIAamp Viral RNA Mini Kit (Qiagen). The cDNA was synthesized using a First Strand cDNA Synthesis Kit (Fermentas, Vilnius, Lithuania). Real-time PCR quantitative analysis was performed using the absolute quantification method, whereby the sample concentrations were determined using a standard curve derived from measurements of serial dilutions of a TBEV sample with a known titer. All samples and standards were analyzed in triplicate. The following primers and probe were used: E(F), ACA CGG GAG ACT ATG TTG CCG CA (nt 1409-1431); E(R), CCG TTG GAA GGT GTT CCA CT (nt 1606-1587) [32]; and probe, BHQ1-FAM, ACG CCA CTA GCG ACC CTG CAC AAC A. The qRT-PCR was carried out in a Rotor Gene 3000 instrument (Corbett Research, Cambridge, UK) using an amplification protocol consisting of enzyme activation steps at 95 °C, 10 min; followed by 45 cycles of 95 °C, 15 s denaturation; and 60 °C, 30 s annealing–synthesis steps.

2.6. Statistical Analysis

Statistical evaluation of plaque size of TBEV viral variants in comparison to the parental strain Hypr 0 P were tested in GraphPad Prism 8 software using the Kruskal-Wallis test followed by Dunn's

post hoc test corrected for multiple comparisons. Statistical significance of differences in virus growth in sera and organs and the assessment of relative survival rates was evaluated using Statistica (StatSoft CR, Prague, Czech Republic, version 9.). The Fisher's Least Significant Difference (LSD) post hoc test was used. Statistical significance was accepted at $p < 0.05$.

2.7. Genome Analysis

The viral genome was transcribed into cDNA as described above and amplified by PCR using overlapping sets of TBEV-specific primers (Supplementary Table S1) [33]. Sequencing was carried out directly from purified PCR products. Sequencing data were processed using MEGA software, version 4 [34]. The sequences were aligned with ClustalW software in MEGA. Modeling of 3D structures of the modified TBEV E protein was done in GENO3D (http://geno3d-pbil.ibcp.fr) and SwissPdbViewer (Basel, Switzerland, version 4.1.0) [35–37] using the E protein structure obtained by crystallography (PDB: 1SVB) [38]. Different model variants were compared using Swiss Model Structure Assessment (http://swissmodel.expasy.org). The best performing model was used for visualization of the amino acid substitutions by DeepView and Swiss-PdbViewer (Basel, Switzerland, version 4.1.0) [39].

2.8. Viral Genome Variability

To study viral genome variability within individual isolates and the potential presence of quasispecies, PCR products were cloned using a CloneJET PCR Cloning Kit (Fermentas). Plasmid isolation was performed with a GeneJET^{TM} Plasmid Miniprep Kit (Fermentas). Purified plasmid DNA was then sequenced directly using the pair of universal primers surrounding the vector cloning site.

3. Results

3.1. Changes in Growth Characteristics During Passaging

The growth characteristics of TBEV strain Hypr (0 P) were evaluated over 40 serial passages in mammalian (PS) and tick (IRE/CTVM19) cells. Viral titers and plaque sizes of new viral variants were estimated by plaque assay at every 5th passage (except at passage numbers 15 and 25). The titer of the parental virus at the beginning was 3×10^4 PFU/mL (Figure 1). After an initial increase in virus titers in both cell lines, the titer in IRE/CTVM19 cells remained more or less constant, about 10^6–10^7 PFU/mL, while the titer in PS cells was more variable, ranging from 10^5–10^8 PFU/mL. Between passages 20 and 30, virus replication rates in PS cells increased substantially, resulting in a pronounced cytopathic effect and decrease in the virus titer due to depletion of the host cells at the end of the 4-day incubation period. Thereafter, the passage interval in PS cells was shortened to two days to compensate for the replication rate increase, which led to a subsequent titer increase (Figure 1).

While the plaque size of the virus selected in PS cells did not change dramatically (in 40 PS the mean plaque size was 1.1 mm and over 60% of plaque samples had a diameter above 1.0 mm) in comparison to the parental virus (mean plaque size 1.6 mm and over 60% of plaque samples with diameter above 1.0 mm), the plaque size of the virus selected in IRE/CTVM19 cells changed considerably (Figure 2, Supplementary Figure S1). From the 30th passage, the plaque samples were approximately half the size of the plaque samples of the parental strain (in 30 IRE the mean plaque size was 0.8 mm and more than 70% of plaque samples had a diameter below 1.0 mm) (Figure 2A,B; Supplementary Figure S1). The plaque sizes did not change further up to the 40th passage, which was then used for further analysis (Figure 2C). After the final passage, the derived TBEV variants were designated 40 PS and 40 IRE for the mammalian and tick cell lines, respectively.
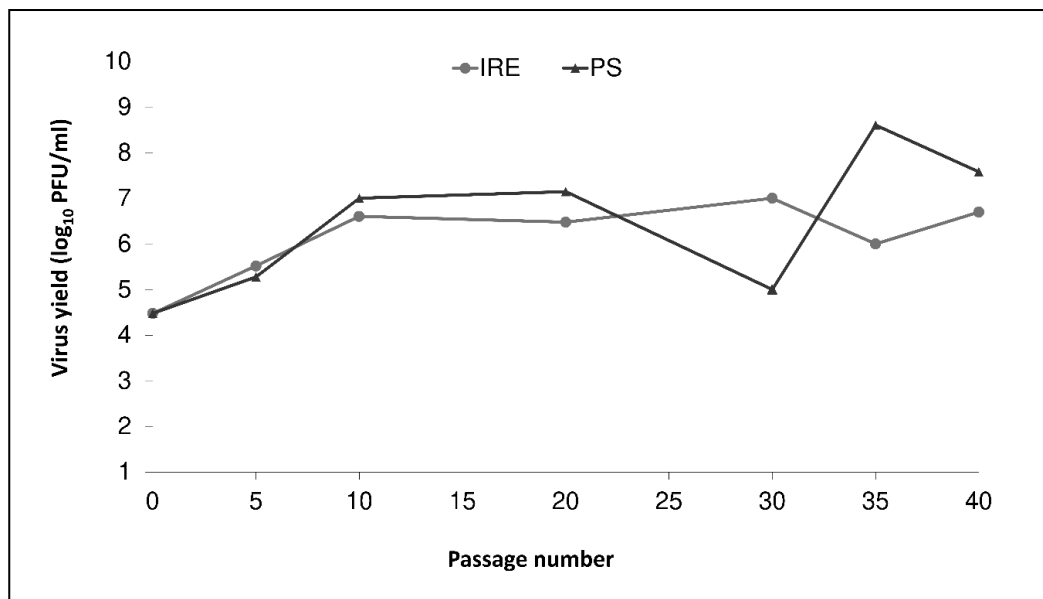
Figure 1. Viral replication kinetics during serial passages of tick-borne encephalitis virus parental strain Hypr in mammalian porcine kidney cells (PS) (dark line with triangles) and in the tick cell line IRE/CTVM19 (light line with circles). The titer was determined using plaque assay and viruses were sampled once at the indicated passage levels per virus variant.
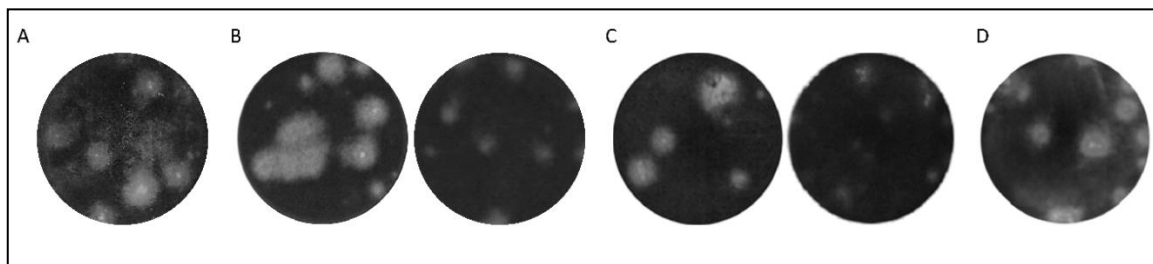
Figure 2. Plaque size and morphology in mammalian porcine kidney (PS) cells during serial passaging of tick-borne encephalitis virus variants in PS and IRE/CTVM19 tick cells. (**A**) Plaque size of the parental strain 0P. (**B**) Difference in plaque size between 30 PS (left) and 30 IRE (right). (**C**) Difference in plaque size between 40 PS (left) and 40 IRE (right). (**D**) Plaque samples of LT IRE after continuous propagation for a month in the IRE/CTVM19 cell line. Well diameter captured in the photographs is 16 mm.

A third experimental TBEV variant (LT IRE) was derived by long term continual propagation in IRE/CTVM19 cells for a period of one month to simulate virus adaptation to permanent infection of tick vectors. From the initial inoculum, the titer of LT IRE increased slightly up to 9×10^4 PFU/mL. In the plaque assay, a mixture of small and large plaque samples was observed (mean plaque size 1.5 mm and 75% of plaque samples had a diameter above 1.0 mm; Figure 2D). The size of the large plaque samples corresponded to the plaque size of the parental virus strain, while small plaque samples corresponded to plaque samples of 30 IRE and 40 IRE variants.

By applying specific cultivation conditions to the TBEV Hypr strain, three virus variants adapted to tick and mammalian cells were derived, exhibiting either altered replication rate in cell culture or altered plaque morphology.

3.2. Virulence Assay in the Mouse Model

Different plaque size of variants obtained under the three different modes of propagation indicated that biological properties of such viruses could vary. To test this hypothesis, we performed a virulence assay in a mouse model. Mice were inoculated subcutaneously with 100 PFU of viral variants or

parental strain. A significantly longer median survival time and lower mortality rate were observed in mice inoculated with 40 PS in comparison to 0 P-, 40 IRE-, and LT IRE-inoculated mice (Fisher's LSD, $p < 0.05$). Moreover, 66% of mice survived the challenge with 40 PS, whereas only 11–33% of mice survived infection with the remaining strains (Figure 3). By challenging laboratory mice with individual TBEV variants, different virulence levels and outcomes of the disease were observed.
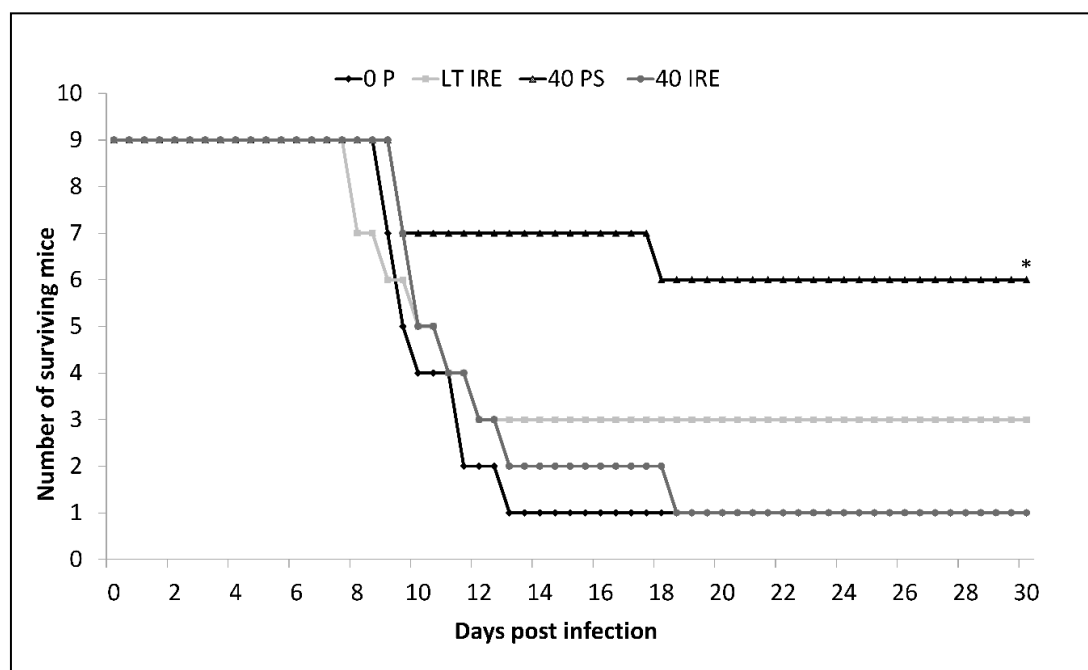
Figure 3. Survival curve of CD1 mice after subcutaneous inoculation with 100 PFU of parental TBEV strain 0 P (dark line with diamonds) or virus variants 40 IRE (light line with circles), 40 PS (dark line with triangles), and LT IRE (light line with squares). Mice infected with 40 PS had significantly prolonged median survival times and lower mortality rates when compared to other viral strains. Statistical significance was tested using Fisher's Least Significant Difference (LSD) post hoc test (* $p < 0.05$).

3.3. Virus Replication in the Mouse Model

To investigate the cause of the differences in the survival rate of mice inoculated with the TBEV variants, the dynamics of virus replication in the mouse model were determined. CD1 mice were challenged with 100 PFU of TBEV parental strain, 40 PS, or 40 IRE variants, then samples were collected daily for eight days from two individuals (except from day 7, when only one individual was sampled). Virus loads in the blood, spleen, and brain were estimated by qRT-PCR (Supplementary Figure S2). In all groups of mice, the virus was first detected in blood 2–3 days p.i., followed by infection of organs (spleen) at days 3–4 p.i. (Supplementary Figure S2A,B). In mice inoculated with 40 PS, a lower level of virus amplification in blood and tissues was observed compared with mice inoculated with 0 P or 40 IRE. However, the viruses differed markedly in their dissemination to the brain. In 0 P- and 40 IRE-infected mice, the virus was present in the brain by the 5th day p.i. and the viral titer increased during the following two days. In mice challenged with 40 PS, the virus was detected for the first time on the 8th day and in one individual only (Supplementary Figure S2C). Due to the limited size of the experimental groups, statistical evaluation of these data was not possible. Results from this experiment are in concordance with the virulence assay results. The viral variant adapted by serial passaging in mammalian cells showed markedly lower neuroinvasiveness than the parental strain or the variant passaged in tick cells.

3.4. Sequence Changes Associated with Adaptation to Mammalian or Tick Cell Lines

To identify genetic changes associated with adaptation to mammalian or tick cell lines and altered neuroinvasiveness in mice, almost the entire viral genome (10,835 bp) was sequenced for the parental virus and for all three new viral variants (40 PS, 40 IRE, and LT IRE). The sequences were submitted to the NCBI GenBank database under the following accession numbers: parental strain: MT228627; 40 PS: MT228628; 40 IRE: MT228625; LT IRE: MT228626. No insertions or deletions were observed in any of the variants. Whole genome sequence analysis revealed 20 single-nucleotide changes, 12 of which were non-conservative at the level of amino acids (Table 1). The highest number of changes compared to the parental virus sequence was recorded in 40 PS (11 nucleotide substitutions, 6 amino acid substitutions). One or more of these substitutions could be responsible for the lower virulence of 40 PS. The 40 IRE variant differed from 0 P in nine nucleotide positions and four amino acids. The least-altered sequence was LT IRE, with only three nucleotide and two amino acid substitutions.

Table 1. Genetic differences between the parental tick-borne encephalitis virus (0 P) and individual new variants (40 PS, 40 IRE, and LT IRE) based on a comparison of full genome sequences. (UTR stands for "untranslated regions")

Genome Region	Nucleotide Substitution		Amino Acid Substitution	
	Substitution	TBEV Variant	Substitution	TBEV Variant
5′ UTR	G (52) → A	40 IRE		
Protein C	A (315) → G	40 IRE		
Protein prM	C (101) → T	40 IRE	Thr (34) → Ile	40 IRE
	A (913) → G	40 PS	Thr (305) → Ala	40 PS
Protein E	C (1078) → T	40 PS	Pro (360) → Ser	40 PS
	A (1411) → T	LT IRE	Met (471) →Leu	LT IRE
Protein NS1	G (169) → A	40 IRE	Val (57) → Ile	40 IRE
	G (237) → A	40 PS		
Protein NS2A	T (605) → C	40 PS	Val (202) → Ala	40 PS
Protein NS2B	G (97) → A	40 IRE	Val (33) → Met	40 IRE
Protein NS3	T (978) → C	40 PS, 40 IRE		
	A (1314) → G	LT IRE		
	C (240) → T	40 PS		
Protein NS4B	G (253) → T	40 IRE	Ala (85) → Ser	40 IRE
	T (262) → A	40 PS	Phe (88) → Ile	40 PS
	G (333) → A	40 PS, 40 IRE		
Protein NS5	A (529) → C	LT IRE	Thr (177) → Pro	LT IRE
	C (2332) → T	40 PS	Leu (778) → Phe	40 PS
	A (2588) → G	40 PS	Asn (863) → Ser	40 PS
3′ UTR	T (282) → C	40 PS, 40 IRE		

To evaluate the potential impacts of nucleotide substitutions on virulence, the locations of the alterations in the least-virulent variant 40 PS was investigated in detail. Amino acid substitutions were found in the NS2A and NS4B proteins (one substitution each) and in the NS5 and E proteins (two substitutions each). Because of several crucial functions of the E protein in the viral life cycle, mutations in this protein were analyzed more closely. The substitution Thr (305) → Ala was situated in the region connecting domain I with domain III (DI–DIII linker). The second substitution Pro (360) → Ser was placed close to the region with a probable function in binding to a cell receptor (Figure 4).

Figure 4. Locations of amino acid substitutions in the TBEV variant 40 PS mapped on the three-dimensional structure of flavivirus E protein (PDB: 1SVB). Domain I—red, domain II—yellow, domain III—green, fusion loop—violet.

3.5. Presence of Quasispecies

Considering the hypothesis of viral adaptation to different environments due to selection from co-existing sequential variants (quasispecies), we tried to identify the sequence variability within our viral variants. Four important parts of the genome were cloned, namely the C protein gene (333 bp), 5' UTR (132 bp), 3' UTR (458 bp), and part of the gene coding E protein (796 bp), then between 5 and 13 individual clones per virus variant were sequenced (Figure 5). Nucleotide sequence variability was observed in both coding sequences and the 5' UTR. On average, the highest nucleotide diversity was observed in the non-coding 5' UTR (0.4–0.9%). Frequencies of nucleotide changes in the remaining genome regions varied from 0.1% to 0.4% and from 0.3% to 0.4% in C and E protein regions, respectively.

Figure 5. Comparison of partial nucleotide sequences of (**A**) 5'UTR, (**B**) C protein, and (**C**) E protein among clones derived from parental tick-borne encephalitis virus (0 P) and virus variants 40 PS, 40 IRE, and LT IRE. Numbers in parentheses represent the frequency of a particular substitution among the sequenced clones. Dots represent conserved nucleotides, letters indicate substitutions.

Most of the nucleotide substitutions were found only in a single clone within one viral variant. However, some of the changes were detected in several colonies independently. In the case of position 52 in the 5' UTR of variant 40 IRE, eight clones carried adenine, while only two carried guanine, as in the parental strain. Interestingly, guanine in this position was observed in all colonies obtained from other viral variants. Consensus nucleotide sequences created from the clone sequences showed

100% identity with the full genome sequence (Figure 5A). Further on in the genome, a synonymous substitution within the C protein sequence of 40 IRE in position 315 was detected. Seven clones had guanine in this position, while in the four remaining colonies adenine was present (Figure 5B). Similarly, variability was found in the E protein sequence of 40 PS in position 913. While this variant had guanine within its consensus genome sequence and sequences of two colonies, a third colony displayed adenine, the same as all colonies of the other viral variants (Figure 5C). To conclude, here we demonstrate the intra-population nucleotide variability contained within individual TBEV variants derived from the parental virus by long-term specific cell line cultivation constraints, which indicates the existence of quasispecies.

4. Discussion

Closely related viral strains may produce a considerably different course of infection in the host [40,41]. Detailed information on particular determinants of virulence at the molecular level would allow a better understanding of the infectious process leading to optimization of disease treatment or development of attenuated vaccines. In the current study, by adapting TBEV to different cell lines in vitro, we have obtained strains of TBEV differing in growth characteristics in cell culture, as well as pathogenicity in a mouse model. We attempted to track back the differences in biological properties among these strains to changes at the genome and amino acid levels.

The first apparent difference between the newly prepared variants was in plaque size. While the variant adapted to tick cells (40 IRE) produced plaque samples of approximately half the size of the parental strain, the variant adapted to mammalian cells (40 PS) produced plaque samples of the same size as the parental strain. Similar observations were reported for strains of Siberian subtype TBEV passaged in ticks and tick cell lines [22]. Nevertheless, the assumption that the production of larger plaque samples in cell culture is associated with increased virulence in vertebrates [42] was not confirmed in our virulence experiments in the mouse model. Similar results were obtained in the case of the mutant TBEV Oshima 5–10 strain [24] and related Langat and dengue viruses [43]. Similarly, the small plaque phenotype is not necessarily associated with reduced virulence (neuroinvasiveness) in a vertebrate animal model, as described for the Siberian subtype of TBEV using small plaque purified clones [22].

Frequently described changes related to reduction in TBEV plaque size and attenuation in vivo are mutations in the E protein resulting in an increase of its positive charge, subsequently leading to an increased affinity to glycosaminoglycans, particularly heparan sulphate [21,22,24,25,44]. A combined effect of multiple amino acid substitutions on the small plaque phenotype was suggested previously [45]. Interestingly, no amino acid substitutions were found in the E protein sequence of the 40 IRE that produced a small plaque phenotype. Apparently, different mechanisms may result in small plaque phenotypes (including innate immune responses) [46].

The course of infection with the individual viral variants corresponded to the results of the virulence assay in laboratory mice. The onset of viraemia from the parental strain and viral variants 40 PS and 40 IRE occurred in the blood on days 2–3 after infection, and in the spleen on days 3–4. However, the titer of the 40 PS variant was lower than that of the other two viruses. We speculate that these differences could have been caused by incapacitation of 40 PS in the preceding steps of pathogenesis, either affecting its ability to replicate in the hypodermis [47], infect dendritic cells, or spread to the draining lymph nodes [2,48]. Following replication in the blood and internal organs, TBEV overcomes the hematoencephalic barrier to reach the brain. If the virus is sufficiently neurovirulent, it causes encephalitis [49]. Both of the more virulent variants (0 P and 40 IRE) were detected in mouse brains soon after their presence in blood (by the 5th day p.i.), then their titers rose steeply to the 7th day p.i. The 40 PS variant was first detected in the brain on the 8th day, the last day of the experiment. By comparing the spread of the virus in the blood and tissues to the virulence assay results, we found out that time of death of the mice correlated with high virus burden in the brain. Differences in the degree of virulence between 0 P, 40 IRE, and the attenuated variant 40 PS can be attributed to the lower

efficiency of viral replication, demonstrated by the lower level of viraemia, prior to entry into the brain (lower neuroinvasiveness). Lower neuroinvasiveness was also described as a cause of lower virulence in previous studies [24,43].

Full genome sequences were acquired for the three variants of the virus, as well as for the parental strain. The frequency of substitutions was higher in the mammalian cell-line-passaged viruses in comparison to tick-cell-derived variants. This might reflect the faster reproduction cycle in mammalian cells in comparison to tick cells. An increased number of replication cycles gives an error-prone TBEV NS5 viral polymerase a higher chance of introducing a mutation into the genome.

Comparing biological properties, the variant most different from the parental virus was 40 PS. Two amino acid substitutions were found in the E protein. Particular attention was paid to these because of important roles that this protein plays in the viral life cycle. The mutation Thr (305) → Ala was located in the region connecting domain I with domain III (DI–DIII linker). During TBEV entry into the host cell and virion uncoating in the endosome, E protein is exposed to acidic pH, and important conformational changes occur in this region, enabling domain III to take a correct position in the E protein trimer [50]. Therefore, we assume that the mutation, even if it did not affect charge distribution, could influence the spatial interactions between E protein monomers, and consequently all the processes of virion fusion with the endosome membrane and release of viral RNA into the cytoplasm.

Virulence could also possibly be influenced by the second E protein mutation (Pro (360) → Ser) in domain III, since it is close to the region that is supposed to have a role in cell receptor binding. The receptor domain has not yet been exactly defined, and therefore some participation of amino acids in proximity to the receptor binding site cannot be completely excluded. Previously, several single-nucleotide changes that influence virulence were identified in domain III. In the TBEV genome, such changes were found at positions 384 [51], 310 [52], and 368 [53]. All these mutations were associated with lower virulence in mice.

Another amino acid change in 40 PS was Val (202) → Ala in the NS2A protein. This protein is a membrane-associated part of the flavivirus replication complex [54]. NS2A participates in virion assembly and release of infectious particles from host cells. A significant effect on virion assembly was proven for mutations within the restriction site [55] and mutations distorting hydrophobic domains [56]. The mutation in 40 PS was located in the N-terminus, and both original and mutated amino acids were hydrophobic, thus both of the two above-mentioned mechanisms are unlikely to be involved in the viral attenuation observed in the present study. Moreover, the NS2A protein is generally one of the least-conserved proteins in the TBEV genome [57]. Another amino acid change in 40 PS was found in the NS4B protein at position Phe (88) → Ile. NS4B is a transmembrane protein with a poorly defined function that colocalizes with TBEV membrane NS proteins and takes part in replication complex formation and ER membrane invagination [43,58,59]. However, this mutation was possibly related to the adaptation of 40 PS to PS cells. The last two amino acid substitutions were found in the region encoding the NS5 protein, in positions Leu (778) → Phe and Asn (863) → Ser. This highly conserved bifunctional protein works as a methyltransferase and RNA-dependent RNA polymerase [60]. The catalytic domain of the RNA-dependent RNA polymerase lies in position 270–900 and includes six highly conserved regions [61]. Both amino acid changes in 40 PS were found in the catalytic domain of the viral RNA polymerase but outside of conserved regions, so they probably had no influence on its function.

The variant 40 IRE showed almost the same virulence for laboratory mice as the parental virus, even though it differed from 0 P in nine nucleotide substitutions and four amino acid changes. This variant also differed from all the others in terms of plaque morphology. One amino acid mutation was found in position Thr (34) → Ile in the prM protein. This mutation destroyed the only potential glycosylation site in the prM protein, Asn-X-Thr. The prM protein plays an important role as a chaperonin of E protein [62]. Goto and co-workers found that mutations in the glycosylation site of prM caused a considerable decrease of secretion of "virus-like particles" in comparison to the glycosylated variant [63]. Thus, the mutation in prM could cause accumulation of virions in cells, slower viral spread

from cell to cell, and consequently smaller plaque samples in PS cell culture. The mutation Ala (85) → Ser found in NS4B could relate to the adaptation of 40 IRE to tick cells. As mentioned before, mutations in this protein possibly participate in adaptation to specific host organisms [43]. The two remaining mutations, Val (57) → Met in the NS1 protein and Val (33) → Met in the NS2B protein, are unlikely to contribute to the phenotype we observed. A mutation in the replication-participating protein NS1 lay neither in any of the 12 conserved cysteines nor in the potential glycosylation site, which is a key region linked to defects of RNA and limited virus production in the case of a related flavivirus [64]. The NS2B protein creates a stable complex with the NS3 protein and serves as a co-factor of NS2B-NS3 serine protease [65]. Position 33 lies outside of the 47 amino acid residues of the central part of the protein involved in this co-factor activity [66].

The variant LT IRE showed a partly attenuated phenotype in comparison with the parental virus. This could have been conferred by two nucleotide substitutions that affected amino acid sequences. The first, Met (471) → Leu, was located in the E protein outside the main ectodomain in a so-called stem–anchor region that participates in binding of E protein to the cell membrane, in interactions with prM protein, and in pH-dependent conformational changes [67]. Position 471 is specifically included in the region serving as protein anchorage to the cell membrane ("anchor"). Some stem–anchor region mutations have been reported previously as a result of TBEV adaptation to tick cells. Mutation at position 426 was responsible for lower virulence for laboratory mice [21]. In another study, mutation at position 496 influenced viral neuroinvasiveness [68]. Thus, it is possible that the mutation at position 471 of E protein conditioned the partial viral attenuation that we observed. The second amino acid change in LT IRE was found in the NS5 protein, in position Thr (177) → Pro, which falls within a functional domain of methyltransferase. Previous studies showed that single-nucleotide mutations in NS5 protein influence viral attenuation, but that these mutations rather participate in the cumulative effect of single mutations, where the biggest influences are from changes in E protein, while mutations in NS5 merely contribute to attenuation [68,69].

Mutations in proteins and in non-coding regions could influence viral pathogenesis [70,71]. In our study, both non-coding regions showed higher nucleotide variability in comparison to coding regions. Untranslated regions participate with their secondary structures in regulation of viral replication, translation, and packaging. Therefore, multibase deletions in particular influence the virulence and viability of the virus [70,71]. However, the extent of attenuation depends on the particular conserved region affected [71]. Previously, single-nucleotide mutations in the 5' UTR related to the production of smaller plaque samples have been described [21,72]. Therefore, it is possible that mutation G (52) → A in 40 IRE resulted in the production of small plaque samples, the only phenotypic trait where this variant differed from all the others.

The T (282) → C mutation in the 3' UTR was shared by 40 PS and 40 IRE variants, which differed in plaque size and virulence in vivo. Involvement of this particular mutation in newly acquired phenotypic traits in these variants is, thus, unclear. This mutation lies in the terminal 190 nucleotide region that forms the conserved 3'stem loop. This secondary structure is required for viral RNA cyclization and replication, and was also identified as an important determinant of virulence [73]. In the related West Nile virus, single-nucleotide mutations in a region responsible for cyclization have impaired the replication efficiency of the virus or plaque size [74]. However, the specific cyclization sequence in TBEV has not yet been defined. Thus, the implications of our findings cannot be confirmed without further investigation.

In summary, both amino acid changes in the E protein of the 40 PS probably contribute to lower virulence in vivo, while the mutation in the NS4B protein most likely arose as a consequence of viral adaptation to PS cells. An underlying role of the structural genes in the pathogenicity for mice was reported previously [75]. Small plaque production by 40 IRE might be the consequence of mutations in the prM protein and 5' UTR, while the mutation in the NS4B protein arose most likely as a consequence of viral adaptation to tick cells. In order to determine the exact contribution of each of these amino acid changes to the virus phenotype, each of the mutations observed in this study should be investigated

individually or in combination using mutated TBEV infectious clones. Results from several studies dealing with attenuated viral strains indicate that viral adaptation to a specific environment does not happen only on the basis of actual random mutations. It is more likely that the adapted variant is selected from an already existing set of sequential variants—quasispecies [16,21–23,76]. To explore the variability within the individual viral variants, we used cloning and sequencing of parts of the 5′ UTR, E protein, and C protein, focusing on nucleotide variability in positions in which we documented changes by whole genome sequencing. Several independent clones were used to minimize the possibility of accidental nucleotide substitutions caused by the error rate of Taq polymerase during PCR amplification [77]. Several mutations were found in more than one colony per viral variant.

The mutation (G (52) → A) in the 5′ UTR and the non-conservative mutation in the E protein (Thr (305) → Ala) may play roles in virus adaptation to different environments. In both cases, the same situation was observed. In the viral variant in which nucleotide variability was detected, the minor base was identical to whole genome sequences of the remaining viral variants, as well as to all their colonies. Very similar results were obtained with the Langat virus [43], West Nile virus [18], and the Siberian subtype of TBEV [22]. Thus, it is possible that after the emergence of a new mutation that is advantageous in a new environment, the original variant is retained by a certain mechanism, albeit at a lower frequency. This assumption corresponds with results of previous experiments, in which new viral variants of TBEV were obtained after serial passaging in ticks or tick cell lines, which produced a mixture of small plaque samples and plaque samples of original size in mammalian cell culture. After plaque purification and sequencing, nucleotide changes unique to the virus producing small plaque samples and to phenotypic revertants were detected [21,22]. Phenotypic variability after serial passaging of TBEV in ticks was also observed in the study by Labuda and co-workers [76]. In another study [78], two virulent variants were obtained from a naturally attenuated TBEV strain after five passages in mice or a single passage in PS cells. These variants had identical nucleotide substitutions in their genomes.

Unfortunately, we cannot be sure which of the mutations found in our study provides a selective advantage within a certain environment and which are just equivalent alternatives without any influence on viral traits. The mutation in the E protein, causing the change of amino acid in the connection of domains I and III, probably influences the protein function, as discussed above. The mutation in the 5′ UTR seems to have some importance because the ratio among the clones (8:2) shows strong dominance of A over G. The direct relationship of a single-nucleotide change in the 5′ UTR to the change in phenotypic traits, specifically to plaque size, is less probable, as other authors emphasize the cumulative effect of single-nucleotide changes and their combinations on viral traits [43,45,79]. The substitutions found in our study confirm some changes from a previously published list of mutations involved in changes in virulence and other biological properties of TBEV and other flaviviruses [73], and even contribute further evidence of such involvement. Such information may be particularly important for genetic comparisons with sequences acquired from newly isolated TBEV field strains and viruses sequenced directly from ticks or clinical samples.

To conclude, serial passaging and long-term persistent infection of tick cell lines do not result in attenuation of TBEV in a vertebrate host. Plaque size in mammalian cells is not directly linked to the virulence of a viral strain. There are mechanisms ensuring maintenance of a certain level of genotypic and phenotypic variability during an adaptation process, which allow rapid selection of adapted variants from a pre-existing pool of viral variants (quasispecies).

Author Contributions: R.H., V.H., and M.P. contributed to the conception and the design of the study. R.H. performed the experiments and wrote the first draft of the manuscript. V.H. and H.T. contributed to manuscript major editing. R.H., V.H., and H.T. contributed to data analysis and visualization. R.H. and M.P. performed the statistical analysis. L.B.-S. and L.G. provided resources and supervision. All authors contributed to manuscript

revision and read and approved the submitted version. All authors have read and agreed to the published version of the manuscript.

References

1. Dumpis, U.; Crook, D.; Oksi, J. Tick-borne encephalitis. *Clin. Infect. Dis.* **1999**, *28*, 882–890. [CrossRef]
2. Lindenbach, B.D.; Thiel, H.J.; Rice, C.M. Flaviviridae: The viruses and their replication. In *Fields Virology*, 5th ed.; Knipe, D.M., Howley, P.M., Eds.; Lippincott-Raven Publishers: Philadelphia, PA, USA, 2007; pp. 1101–1133.
3. Rehacek, J. Cultivation of different viruses in tick tissue cultures. *Acta Virol.* **1965**, *9*, 332–337.
4. Gritsun, T.S.; Lashkevich, V.A.; Gould, E.A. Tick-borne encephalitis. *Antivir. Res.* **2003**, *57*, 129–146. [CrossRef]
5. Nuttall, P.A.; Labuda, M. Dynamics of infection in tick vectors and at the tick-host interface. *Adv. Virus Res.* **2003**, *60*, 233–272. [PubMed]
6. Weaver, S.C.; Brault, A.C.; Kang, W.L.; Holland, J.J. Genetic and fitness changes accompanying adaptation of an arbovirus to vertebrate and invertebrate cells. *J. Virol.* **1999**, *73*, 4316–4326. [CrossRef]
7. Cooper, L.A.; Scott, T.W. Differential evolution of eastern equine encephalitis virus populations in response to host cell type. *Genetics* **2001**, *157*, 1403–1412.
8. Holland, J.; Spindler, K.; Horodyski, F.; Grabau, E.; Nichol, S.; VandePol, S. Rapid evolution of RNA genomes. *Science* **1982**, *215*, 1577–1585. [CrossRef]
9. Domingo, E.; Holland, J.J.; Biebricher, C.; Eigen, M. Quasispecies: The concept and the word. In *Molecular Basis of Virus Evolution*; Gibbs, A., Calisher, C., García-Arenal, F., Eds.; Cambridge University Press: Cambridge, UK, 1995; pp. 171–180.
10. Eigen, M. On the nature of virus quasispecies. *Trends Microbiol.* **1996**, *4*, 216–218. [CrossRef]
11. Domingo, E.; Holland, J.J. RNA virus mutations and fitness for survival. *Annu. Rev. Microbiol.* **1997**, *51*, 151–178. [CrossRef]
12. Schneider, W.L.; Roossinck, M.J. Evolutionarily related Sindbis-like plant viruses maintain different levels of population diversity in a common host. *J. Virol.* **2000**, *74*, 3130–3134. [CrossRef]
13. Schneider, W.L.; Roossinck, M.J. Genetic diversity in RNA virus quasispecies is controlled by host-virus interactions. *J. Virol.* **2001**, *75*, 6566–6571. [CrossRef] [PubMed]
14. Martínez, M.A.; Carrillo, C.; Gonzalezcandelas, F.; Moya, A.; Domingo, E.; Sobrino, F. Fitness alteration of foot-and-mouth disease virus mutants: Measurement of adaptability of viral quasispecies. *J. Virol.* **1991**, *65*, 3954–3957. [CrossRef] [PubMed]
15. Ruiz-Jarabo, C.M.; Arias, A.; Baranowski, E.; Escarmis, C.; Domingo, E. Memory in viral quasispecies. *J. Virol.* **2000**, *74*, 3543–3547. [CrossRef]
16. Asghar, N.; Lindblom, P.; Melik, W.; Lindqvist, R.; Haglund, M.; Forsberg, P.; Overby, A.K.; Andreassen, A.; Lindgren, P.E.; Johansson, M. Tick-borne encephalitis virus sequenced directly from questing and blood-feeding ticks reveals quasispecies variance. *PLoS ONE* **2014**, *9*, e103264. [CrossRef]
17. van Boheemen, S.; Tas, A.; Anvar, S.Y.; van Grootveld, R.; Albulescu, I.C.; Bauer, M.P.; Feltkamp, M.C.; Bredenbeek, P.J.; van Hemert, M.J. Quasispecies composition and evolution of a typical Zika virus clinical isolate from Suriname. *Sci. Rep.* **2017**, *7*, 2368. [CrossRef] [PubMed]
18. Jerzak, G.; Bernard, K.A.; Kramer, L.D.; Ebel, G.D. Genetic variation in West Nile virus from naturally infected mosquitoes and birds suggests quasispecies structure and strong purifying selection. *J. Gen. Virol.* **2005**, *86*, 2175–2183. [CrossRef]

19. Kurosu, T.; Khamlert, C.; Phanthanawiboon, S.; Ikuta, K.; Anantapreecha, S. Highly efficient rescue of dengue virus using a co-culture system with mosquito/mammalian cells. *Biochem. Biophys. Res. Commun.* **2010**, *394*, 398–404. [CrossRef]

20. Asghar, N.; Pettersson, J.H.; Dinnetz, P.; Andreassen, A.; Johansson, M. Deep sequencing analysis of tick-borne encephalitis virus from questing ticks at natural foci reveals similarities between quasispecies pools of the virus. *J. Gen. Virol.* **2017**, *98*, 413–421. [CrossRef]

21. Romanova, L.I.; Gmyl, A.P.; Dzhivanian, T.I.; Bakhmutov, D.V.; Lukashev, A.N.; Gmyl, L.V.; Rumyantsev, A.A.; Burenkova, L.A.; Lashkevich, V.A.; Karganova, G.G. Microevolution of tick-borne encephalitis virus in course of host alternation. *Virology* **2007**, *362*, 75–84. [CrossRef]

22. Belova, O.A.; Litov, A.G.; Kholodilov, I.S.; Kozlovskaya, L.I.; Bell-Sakyi, L.; Romanova, L.I.; Karganova, G.G. Properties of the tick-borne encephalitis virus population during persistent infection of ixodid ticks and tick cell lines. *Ticks Tick Borne Dis.* **2017**, *8*, 895–906. [CrossRef]

23. Růžek, D.; Bell-Sakyi, L.; Kopecký, J.; Grubhoffer, L. Growth of tick-borne encephalitis virus (European subtype) in cell lines from vector and non-vector ticks. *Virus Res.* **2008**, *137*, 142–146. [CrossRef]

24. Goto, A.; Hayasaka, D.; Yoshii, K.; Mizutani, T.; Kariwa, H.; Takashima, I. A BHK-21 cell culture-adapted tick-borne encephalitis virus mutant is attenuated for neuroinvasiveness. *Vaccine* **2003**, *21*, 4043–4051. [CrossRef]

25. Mandl, C.W.; Kroschewski, H.; Allison, S.L.; Kofler, R.; Holzmann, H.; Meixner, T.; Heinz, F.X. Adaptation of tick-borne encephalitis virus to BHK-21 cells results in the formation of multiple heparan sulfate binding sites in the envelope protein and attenuation in vivo. *J. Virol.* **2001**, *75*, 5627–5637. [CrossRef]

26. Nitayaphan, S.; Grant, J.A.; Chang, G.J.J.; Trent, D.W. Nucleotide sequence of the virulent SA-14 strain of Japanese encephalitis virus and its attenuated vaccine derivative, SA-14-14-2. *Virology* **1990**, *177*, 541–552. [CrossRef]

27. Kozuch, O.; Mayer, V. Pig kidney epithelial (PS) cells: A perfect tool for a study of flaviviruses and some other arboviruses. *Acta Virol.* **1975**, *19*, 498.

28. Bell-Sakyi, L.; Zweygarth, E.; Blouin, E.F.; Gould, E.A.; Jongejan, F. Tick cell lines: Tools for tick and tick-borne disease research. *Trends Parasitol.* **2007**, *23*, 450–457. [CrossRef]

29. Pospíšil, L.; Jandásek, L.; Pešek, J. Isolation of new strains of meningoencephalitis virus in the Brno region during the summer of 1953. *Lek List* **1954**, *9*, 3–5.

30. De Madrid, A.T.; Porterfield, J.S. A simple microculture method for the study of group B arboviruses. *Bull. World Health Org.* **1969**, *40*, 113–121.

31. Schneider, C.A.; Rasband, W.S.; Eliceiri, K.W. NIH Image to ImageJ: 25 years of image analysis. *Nat. Methods* **2012**, *9*, 671–675. [CrossRef]

32. Růžek, D.; Šťastná, H.; Kopecký, J.; Golovljová, I.; Grubhoffer, L. Rapid subtyping of tick-borne encephalitis virus isolates using multiplex RT-PCR. *J. Virol. Methods* **2007**, *144*, 133–137. [CrossRef]

33. Kupca, A.M.; Essbauer, S.; Zoeller, G.; de Mendonca, P.G.; Brey, R.; Rinder, M.; Pfister, K.; Spiegel, M.; Doerrbecker, B.; Pfeffer, M.; et al. Isolation and molecular characterization of a tick-borne encephalitis virus strain from a new tick-borne encephalitis focus with severe cases in Bavaria, Germany. *Ticks Tick Borne Dis.* **2010**, *1*, 44–51. [CrossRef] [PubMed]

34. Tamura, K.; Dudley, J.; Nei, M.; Kumar, S. MEGA4: Molecular evolutionary genetics analysis (MEGA) software version 4.0. *Mol. Biol. Evol.* **2007**, *24*, 1596–1599. [CrossRef] [PubMed]

35. Peitsch, M.C. Protein modeling by E-mail. *Nat. Biotechnol.* **1995**, *13*, 658–660. [CrossRef]

36. Arnold, K.; Bordoli, L.; Kopp, J.; Schwede, T. The SWISS-MODEL workspace: A web-based environment for protein structure homology modelling. *Bioinformatics* **2006**, *22*, 195–201. [CrossRef] [PubMed]

37. Kiefer, F.; Arnold, K.; Kunzli, M.; Bordoli, L.; Schwede, T. The SWISS-MODEL Repository and associated resources. *Nucleic Acids Res.* **2009**, *37*, D387–D392. [CrossRef] [PubMed]

38. Rey, F.A.; Heinz, F.X.; Mandl, C.; Kunz, C.; Harrison, S.C. The envelope glycoprotein from tick-borne encephalitis virus at 2 Å resolution. *Nature* **1995**, *375*, 291–298. [CrossRef]

39. Guex, N.; Peitsch, M.C. SWISS-MODEL and the Swiss-PdbViewer: An environment for comparative protein modeling. *Electrophoresis* **1997**, *18*, 2714–2723. [CrossRef]

40. Růžek, D.; Kopecký, J.; Štěrba, J.; Golovchenko, M.; Rudenko, N.; Grubhoffer, L. Non-virulent strains of TBE virus circulating in the Czech Republic. *J. Clin. Virol.* **2006**, *36*, S41. [CrossRef]

41. Wallner, G.; Mandl, C.W.; Ecker, M.; Holzmann, H.; Stiasny, K.; Kunz, C.; Heinz, F.X. Characterisation and complete genome sequences of high- and low-virulence variants of tick-borne encephalitis virus. *J. Gen. Virol.* **1996**, *77*, 1035–1042. [CrossRef]

42. Mayer, V. Study of virulence of tick-borne encephalitis virus. III. Biological evaluation of large-plaque and small-plaque variants of viruses of tick-borne encephalitis complex. *Acta Virol.* **1964**, *8*, 507–520.

43. Mitzel, D.N.; Best, S.M.; Masnick, M.F.; Porcella, S.F.; Wolfinbarger, J.B.; Bloom, M.E. Identification of genetic determinants of a tick-borne flavivirus associated with host-specific adaptation and pathogenicity. *Virology* **2008**, *381*, 268–276. [CrossRef] [PubMed]

44. Kozlovskaya, L.I.; Osolodkin, D.I.; Shevtsova, A.S.; Romanova, L.I.; Rogova, Y.V.; Dzhivanian, T.I.; Lyapustin, V.N.; Pivanova, G.P.; Gmyl, A.P.; Palyulin, V.A.; et al. GAG-binding variants of tick-borne encephalitis virus. *Virology* **2010**, *398*, 262–272. [CrossRef] [PubMed]

45. Khasnatinov, M.A.; Ustanikova, K.; Frolova, T.V.; Pogodina, V.V.; Bochkova, N.G.; Levina, L.S.; Slovak, M.; Kazimirova, M.; Labuda, M.; Klempa, B.; et al. Non-hemagglutinating flaviviruses: Molecular mechanisms for the emergence of new strains via adaptation to European ticks. *PLoS ONE* **2009**, *4*, e7295. [CrossRef] [PubMed]

46. Goh, K.C.; Tang, C.K.; Norton, D.C.; Gan, E.S.; Tan, H.C.; Sun, B.; Syenina, A.; Yousuf, A.; Ong, X.M.; Kamaraj, U.S.; et al. Molecular determinants of plaque size as an indicator of dengue virus attenuation. *Sci. Rep.* **2016**, *6*, 26100. [CrossRef]

47. Labuda, M.; Austyn, J.M.; Zuffova, E.; Kozuch, O.; Fuchsberger, N.; Lysy, J.; Nuttall, P.A. Importance of localized skin infection in tick-borne encephalitis virus transmission. *Virology* **1996**, *219*, 357–366. [CrossRef]

48. Fialova, A.; Cimburek, Z.; Iezzi, G.; Kopecky, J. Ixodes ricinus tick saliva modulates tick-borne encephalitis virus infection of dendritic cells. *Microb. Infect.* **2010**, *12*, 580–585. [CrossRef]

49. McMinn, P.C.; Dalgarno, L.; Weir, R.C. A comparison of the spread of Murray Valley encephalitis viruses of high or low neuroinvasiveness in the tissues of Swiss mice after peripheral inoculation. *Virology* **1996**, *220*, 414–423. [CrossRef]

50. Bressanelli, S.; Stiasny, K.; Allison, S.L.; Stura, E.A.; Duquerroy, S.; Lescar, J.; Heinz, F.X.; Rey, F.A. Structure of a flavivirus envelope glycoprotein in its low-pH-induced membrane fusion conformation. *EMBO J.* **2004**, *23*, 728–738. [CrossRef]

51. Holzmann, H.; Heinz, F.X.; Mandl, C.W.; Guirakhoo, F.; Kunz, C. A single amino acid substitution in envelope protein E of tick-borne encephalitis virus leads to attenuation in the mouse model. *J. Virol.* **1990**, *64*, 5156–5159. [CrossRef]

52. Mandl, C.W.; Allison, S.L.; Holzmann, H.; Meixner, T.; Heinz, F.X. Attenuation of tick-borne encephalitis virus by structure-based site-specific mutagenesis of a putative flavivirus receptor binding site. *J. Virol.* **2000**, *74*, 9601–9609. [CrossRef]

53. Holzmann, H.; Stiasny, K.; Ecker, M.; Kunz, C.; Heinz, F.X. Characterization of monoclonal antibody-escape mutants of tick-borne encephalitis virus with reduced neuroinvasiveness in mice. *J. Gen. Virol.* **1997**, *78*, 31–37. [CrossRef] [PubMed]

54. Mackenzie, J.M.; Khromykh, A.A.; Jones, M.K.; Westaway, E.G. Subcellular localization and some biochemical properties of the flavivirus Kunjin nonstructural proteins NS2A and NS4A. *Virology* **1998**, *245*, 203–215. [CrossRef] [PubMed]

55. Kümmerer, B.M.; Rice, C.M. Mutations in the yellow fever virus nonstructural protein NS2A selectively block production of infectious particles. *J. Virol.* **2002**, *76*, 4773–4784. [CrossRef] [PubMed]

56. Leung, J.Y.; Pijlman, G.P.; Kondratieva, N.; Hyde, J.; Mackenzie, J.M.; Khromykh, A.A. Role of nonstructural protein NS2A in flavivirus assembly. *J. Virol.* **2008**, *82*, 4731–4741. [CrossRef] [PubMed]

57. Chambers, T.J.; Hahn, C.S.; Galler, R.; Rice, C.M. Flavivirus genome organization, expression, and replication. *Annu. Rev. Microbiol.* **1990**, *44*, 649–688. [CrossRef]

58. Miller, S.; Sparacio, S.; Bartenschlager, R. Subcellular localization and membrane topology of the dengue virus type 2 non-structural protein 4B. *J. Biol. Chem.* **2006**, *281*, 8854–8863. [CrossRef]

59. Yau, W.L.; Nguyen-Dinh, V.; Larsson, E.; Lindqvist, R.; Overby, A.K.; Lundmark, R. Model system for the formation of tick-borne encephalitis virus replication compartments without viral RNA replication. *J. Virol.* **2019**, *93*, e00292-19. [CrossRef]

60. Koonin, E.V. Computer-assisted identification of a putative methyltransferase domain in NS5 protein of flaviviruses and lambda 2 protein of reovirus. *J. Gen. Virol.* **1993**, *74*, 733–740. [CrossRef]

61. Yap, T.L.; Xu, T.; Chen, Y.L.; Malet, H.; Egloff, M.P.; Canard, B.; Vasudevan, S.G.; Lescar, J. Crystal structure of the dengue virus RNA-dependent RNA polymerase catalytic domain at 1.85-Angstrom resolution. *J. Virol.* **2007**, *81*, 4753–4765. [CrossRef]

62. Guirakhoo, F.; Heinz, F.X.; Mandl, C.W.; Holzmann, H.; Kunz, C. Fusion activity of flaviviruses: Comparison of mature and immature (prM-containing) tick-borne encephalitis virions. *J. Gen. Virol.* **1991**, *72*, 1323–1329. [CrossRef]

63. Goto, A.; Yoshii, K.; Obara, M.; Ueki, T.; Mizutani, T.; Kariwa, H.; Takashima, I. Role of the N-linked glycans of the prM and E envelope proteins in tick-borne encephalitis virus particle secretion. *Vaccine* **2005**, *23*, 3043–3052. [CrossRef] [PubMed]

64. Muylaert, I.R.; Chambers, T.J.; Galler, R.; Rice, C.M. Mutagenesis of the N-linked glycosylation sites of the yellow fever virus NS1 protein: Effects on virus replication and mouse neurovirulence. *Virology* **1996**, *222*, 159–168. [CrossRef] [PubMed]

65. Falgout, B.; Pethel, M.; Zhang, Y.M.; Lai, C.J. Both nonstructural proteins NS2B and NS3 are required for the proteolytic processing of dengue virus nonstructural proteins. *J. Virol.* **1991**, *65*, 2467–2475. [CrossRef] [PubMed]

66. Erbel, P.; Schiering, N.; D'Arcy, A.; Renatus, M.; Kroemer, M.; Lim, S.P.; Yin, Z.; Keller, T.H.; Vasudevan, S.G.; Hommel, U. Structural basis for the activation of flaviviral NS3 proteases from dengue and West Nile virus. *Nat. Struct. Mol. Biol.* **2006**, *13*, 372–373. [CrossRef]

67. Hurrelbrink, R.J.; McMinn, P.C. Molecular determinants of virulence: The structural and functional basis for flavivirus attenuation. *Adv. Virus Res.* **2003**, *60*, 1–42.

68. Gritsun, T.S.; Desai, A.; Gould, E.A. The degree of attenuation of tick-borne encephalitis virus depends on the cumulative effects of point mutations. *J. Gen. Virol.* **2001**, *82*, 1667–1675. [CrossRef]

69. Hayasaka, D.; Gritsun, T.S.; Yoshii, K.; Ueki, T.; Goto, A.; Mizutani, T.; Kariwa, H.; Iwasaki, T.; Gould, E.A.; Takashima, I. Amino acid changes responsible for attenuation of virus neurovirulence in an infectious cDNA clone of the Oshima strain of tick-borne encephalitis virus. *J. Gen. Virol.* **2004**, *85*, 1007–1018. [CrossRef]

70. Cahour, A.; Pletnev, A.; Vazeillefalcoz, M.; Rosen, L.; Lai, C.J. Growth-restricted dengue virus mutants containing deletions in the 5′ noncoding region of the RNA genome. *Virology* **1995**, *207*, 68–76. [CrossRef]

71. Proutski, V.; Gritsun, T.S.; Gould, E.A.; Holmes, E.C. Biological consequences of deletions within the 3-untranslated region of flaviviruses may be due to rearrangements of RNA secondary structure. *Virus Res.* **1999**, *64*, 107–123. [CrossRef]

72. Butrapet, S.; Huang, C.Y.H.; Pierro, D.J.; Bhamarapravati, N.; Gubler, D.J.; Kinney, R.M. Attenuation markers of a candidate dengue type 2 vaccine virus, strain 16681 (PDK-53), are defined by mutations in the 5′ noncoding region and nonstructural proteins 1 and 3. *J. Virol.* **2000**, *74*, 3011–3019. [CrossRef]

73. Kellman, E.M.; Offerdahl, D.K.; Melik, W.; Bloom, M.E. Viral Determinants of virulence in tick-borne flaviviruses. *Viruses* **2018**, *10*, 329. [CrossRef] [PubMed]

74. Basu, M.; Brinton, M.A. West Nile virus (WNV) genome RNAs with up to three adjacent mutations that disrupt long distance 5′-3′ cyclization sequence basepairs are viable. *Virology* **2011**, *412*, 220–232. [CrossRef] [PubMed]

75. Khasnatinov, M.A.; Tuplin, A.; Gritsun, D.J.; Slovak, M.; Kazimirova, M.; Lickova, M.; Havlikova, S.; Klempa, B.; Labuda, M.; Gould, E.A.; et al. Tick-borne encephalitis virus structural proteins are the primary viral determinants of non-viraemic transmission between ticks whereas non-structural proteins affect cytotoxicity. *PLoS ONE* **2016**, *11*, e0158105. [CrossRef] [PubMed]

76. Labuda, M.; Jiang, W.R.; Kaluzova, M.; Kozuch, O.; Nuttall, P.A.; Weismann, P.; Eleckova, E.; Zuffova, E.; Gould, E.A. Change in phenotype of tick-borne encephalitis virus following passage in Ixodes ricinus ticks and associated amino acid substitution in the envelope protein. *Virus Res.* **1994**, *31*, 305–315. [CrossRef]

77. Malet, I.; Belnard, M.; Agut, H.; Cahour, A. From RNA to quasispecies: A DNA polymerase with proofreading activity is highly recommended for accurate assessment of viral diversity. *J. Virol. Methods* **2003**, *109*, 161–170. [CrossRef]

78. Růžek, D.; Gritsun, T.S.; Forrester, N.L.; Gould, E.A.; Kopecký, J.; Golovchenko, M.; Rudenko, N.; Grubhoffer, L. Mutations in the NS2B and NS3 genes affect mouse neuroinvasiveness of a Western European field strain of tick-borne encephalitis virus. *Virology* **2008**, *374*, 249–255. [CrossRef]

79. Davis, C.T.; Galbraith, S.E.; Zhang, S.L.; Whiteman, M.C.; Li, L.; Kinney, R.M.; Barrett, A.D.T. A combination of naturally occurring mutations in North American West Nile virus nonstructural protein genes and in the 3′ untranslated region alters virus phenotype. *J. Virol.* **2007**, *81*, 6111–6116. [CrossRef]

SUMMARY AND FUTURE PERSPECTIVES

CHARACTERIZATION OF VECTOR CELLS RESPONSE TO TBEV INFECTION

Tick antiviral responses are poorly characterized (207). Findings on more intensively studied MBFVs and their vectors are often extrapolated also on their tick-borne relatives, usually without considering tick specifics. Nevertheless, it does not compromise the need to perform tick-specific studies and describe the real responses elicited in ticks against viral infections. RNAi pathway was the only generally accepted antiviral mechanism described in ticks so far. In Manuscript 1 we have characterized the tick RNAi pathway and determined that the main group of interfering RNAs derived are 22-nt long, which is in striking contrast to mosquito RNAi response and its predominant production of 21-nt-long dsRNA fragments (211). Our data indicate that there might be considerable diversity in the immune responses within arthropods when we compare the more basal Chelicerates (Parasitiformes) and the evolutionary younger Insecta (Hexapoda) (357). Our finding of the length of siRNAs in ticks was later confirmed also *in vivo* (358). Tick siRNAs preferentially targeted 5´and 3´ends of the flaviviral genome. Further, we identified key components of the tick antiviral immune pathway. We have documented genomic expansion of *Ago* and *Dcr* genes and identified their involvement in antiviral immune response (Manuscript 1). Ago16 and Ago30 were universally effective against LGTV infection and LGTV replicon. Further, Ago68 and Dcr90 showed an effect at least against one of the targets (either replicon or virus). The antiviral function of Ago30 and Dcr90 was verified also in our successive study on IDE8 cells (Manuscript 2). The validated antiviral function in the gene Dcr90, that shares homology to insect Dcr1 (miRNA pathway), argues for selective pressure in ticks for evolving a higher diversity of antiviral genes. We cannot however exclude that also other homologous proteins (e.g., Dcr89), for which we did not obtain consistent or complete knockdowns, are parts of the pathway as well. Only the methodological approach (RNAi) was not sufficient to silence the genes to prove their antiviral role. Possibly another methodological approach, such as CRISPR/Cas9-mediated gene editing, which has recently become available for ticks as well, would bring us the answer (359).

With RNAi pathway being the only confirmed antiviral innate immunity pathway in ticks, an additional investigation would be needed to explore the functionality of other tick immune pathways known to be active in insect. Publication of *I. scapularis* genome and *Hyalomma asiaticum* transcriptome allowed the components of other immune signalling pathways known from insect (Toll, Imd, Jak-STAT) to be revealed as well (360,361). In Manuscript 2, we explored the response elicited against TBEV infection on mRNA and protein production level in two tick cell lines. As a general feature, stimulation of immunity and metabolism and repression of cell stress response and protein folding was found. We obtained a list of immunity response activated and cell stress response repressed genes and proteins. New putative candidates for genes with antiviral function were revealed by targeted gene knock-down, such as complement-associated factor H, trypsin protease or heat-shock

proteins (Hsp90, Hsp70, pg96). Several proteins out of those identified by us in TBEV-infected tick cell culture (IRE/CTVM19), were currently identified in infected tick cell lines also by Grabowski et al. (362) or Loginov et al. (363). That opens a question whether these new factors somehow participate in RNAi pathway, or a novel, so far unrecognized immune pathway distinct from insects, might be active in ticks. To get a specific answer, a hunt for the RNA and protein interaction partners of those candidate proteins, e.g., by specific pull-downs followed by modern transcriptomic and proteomic analyses, would reveal a broader context in which those proteins are able to exert their antiviral function. An example of a virus-host protein study is a recently published work from Lemasson et al. (192). They identified new protein-protein interactions between viral (TBEV) and *I. ricinus* proteins by the yeast two-hybrid screening. Putative functions of those proteins were predicted to be associated with response to cytokine (Ir3, Ir9, Ir11), regulation of MAPK cascade, regulation of phosphorus metabolic process or regulation of signalling and cell communication (Ir9, Ir10, Ir11, Ir17), and response to an organic substance (Ir3, Ir8, Ir9, Ir11). Putative factors involved in the protein degradation pathway, NF-κB, and MAPK putatively associated signalling were also revealed, however, whether their role is proviral or antiviral in the viral pathogenesis remains to be elucidated (192).

Finally, when exploring the immune response against LGTV, we described the production of sfRNA in tick as well as mammalian cells. The pattern of sfRNA species lengths differed in the mammalian versus tick cells (Manuscript 1). A similar difference was observed in DENV (59). Additionally, we provided evidence for evasion of tick RNAi pathway by LGTV via its sfRNA proving the importance of sfRNA also for the tick-borne flaviviruses life cycle. More data should be gained on the sfRNA functions in tick-borne flaviviruses and particularly TBEV to understand this phenomenon. Specifically, the structure of sfRNA from tick-borne flavivirus has not been elucidated yet, a detailed fate and function of sfRNA in the host cell should be described, and virus- and host-derived interaction partners need to be identified. Understanding the immune evasion principle exploited by sfRNA can reveal a new strategy for flaviviral infection treatment. Lastly, it will be valuable to define the effect the sfRNA potentially has on the host switch.

Characterization of neural cell response to TBEV infection

Although the TBEV life cycle has been studied, there are still a lot of missing pieces to understanding the processes ongoing in the infected cells, especially in neuronal cells which are terminal TBEV targets. In Manuscript 3 we studied the effect of TBEV infection on host protein production in neural cells. We documented a virus-induced decline in the synthesis of host proteins also termed translational shut-off. Such interference with the host proteosynthetic pathway can be advantageous for the virus in multiple ways. It frees the host cell machinery that the virus needs to its own replication and assembly and more importantly

it promotes the escape from the host immune response (354). Furthermore, this translational shut-off is accompanied by interference with host cell transcription and a decrease of specifically RNA polymerase 1-produced transcripts, 18S and 28S rRNA, and their precursor 45-47S pre-rRNA was noted. This makes our findings the first description of transcriptional and translational shut-off occurring in neuronal cells following flavivirus infection. Until now, only scarce evidence about flaviviruses and translational shut-off has been published (353,356) thus, our data bring new evidence on this so far overlooked phenomenon in flavivirus host cell pathogenesis. It would be intriguing to determine the mechanism which links TBEV infection with transcriptional and translational shut-off. In the future, we would like to define viral factors responsible for the described features. Our preliminary data suggest at least partial involvement of TBEV structural protein (364). Also defining the checkpoint of translation initiation that is targeted by TBEV would be beneficial. For other flaviviruses the canonical pathways that lead to translational arrest have been excluded by Roth et al., as neither phosphorylation of eIF2α was found nor eIF4E cap binding to translation initiation complex was affected. An unconventional strategy that led to activation p38/Mnk1 signalling was found instead (356). It is also important to explore whether manipulation of host transcription and translation machinery happens also during an infection of tick cells. However, some indices are already there, e.g., higher numbers of proteins were identified in mock compared to infected cells in a proteomic survey (Manuscript 2).

Viral derange of host transcriptional and translational machinery surprisingly also affected the production of potent antiviral ISG viperin (Manuscript 3), whose expression was upregulated on the mRNA level, but the protein was missing in infected cells. It is tempting to speculate, that general shut-off helps flaviviruses suppress the antiviral immune response of the host cell. Lately, viral mechanism of specific targeting of viperin function emerged. Degradation of viperin was mediated by the successive action of HAT1 acetyltransferase and UBE4A ubiquitin ligase. The chain of action of these enzymes could be reverted by the administration of an interfering peptide (365). It would be tempting to explore whether this mechanism could answer the lack of viperin protein we observed in TBEV-infected cells. For silencing of production of other ISGs, flaviviruses use yet another way; flaviviral NS5 sequesters the HSP90 chaperone which results in dysregulation of Jak/STAT signalling and lack of production of specific ISG proteins (MX1, IFIT1, OAS1, and ISG15) (338). Restoration of active ISG protein levels could open new potentials for TBEV elimination or treatment.

In TBEV infection, infiltration of the brain is the final step of pathogenesis in humans. We sought to identify the response elicited in human primary neural cells, neurons and astrocytes, by TBEV infection. The benefit of studying viral infections on a primary cell line model is a higher resemblance to *in viv*o conditions, and, more importantly, a more accurate immune response unaffected by the accumulation of mutations as in the case of stable cell lines (366). Even though both, neurons and astrocytes, are highly susceptible to TBEV infection in Manuscript 4, we confirmed that the outcome of the infection differs significantly

140

for individual cell types, with neurons having significantly affected viability. We characterized the complex small RNA and mRNA expression response and identified a common as well as a unique response of neural cells to TBEV infection. In a common set of differentially expressed genes, we identified the immune response factors triggered in neural cells and identified effector antiviral ISGs, such as IFIT1, IFIT2, IFIT3, IFI6, OAS1, OAS2, OAS3, OASL, ISG15, MX1, viperin, and CMPK2. A similar representation of ISGs expressed in primary neural cells was found previously for TBEV (137,148) and related flaviviruses (367). Although signalling preferentially through RIG-I and not MDA-5 has been suggested for TBEV in stable cell lines (251). We found that in both examined neural cell types all RLRs (RIG-I, MDA5 and LGP2) are up-regulated and probably used for the TBEV infection sensing upon TBEV infection. That could mean that the infection recognition sensors and immune signalling cascades leading towards mounting of antiviral response by the host cell can be divergent in different cell types and can also differ between primary and stable cell culture models.

When dissecting the unique response of human astrocytes and neurons, we found that astrocytes elicit a stronger immune response when compared to neurons, especially on the scale of higher expression rate of certain immune-related genes. We recorded higher upregulation of OAS1-3 genes, viperin, BST2, IL6, and ISG2 in astrocytes. Brain region and neural cell type specific expression of viperin was revealed before. Viperin was able to restrict LGTV replication in certain neuronal types, moreover, its effect was also substantial for TBEV, WNV, and ZIKV infection control in distinct brain regions and cell types (323). Also, unique factors, such as TNFSF10, MX2, IFNλ2, MMP-13, IFITM1, and IFITM2 were induced in astrocytes. These factors can be fundamental for the differing outcome of TBEV infection in astrocytes and their differing resilience. Also, this set of genes represents a pallet of potent cell type specific ISGs and in a broader context deciphering contribution of individual of these factors to the outcome of TBEV infection would be important for understanding TBEV pathogenesis.

Interestingly neurons and astrocytes differed also in the duration of IFNλ response. While neurons activated the IFNλ response in early intervals only, astrocytes were able to sustain the IFNλ response to the later time point. Active IFNλ response can be one of the factors conditioning different spectra of ISGs in neurons and astrocytes mentioned earlier. The importance of a stronger and longer-lasting antiviral response to TBEV infection in astrocytes was suggested earlier, but the specific antiviral program contained TLR3, viperin, and TRIM5alpha (137).

Except for different regulation of mRNA transcripts, we also identified the regulation of small RNAs – miRNAs, long non-coding RNAs (lncRNAs), and virus-derived small RNAs (vdRNAs) in TBEV infected neurons and astrocytes. By predicting the targets of those small RNAs and putting them in the context of differentially regulated mRNAs in infected neurons and astrocytes we were able to predict several regulatory pathways that would be of interest

to explore in the future. Such examples are a commonly up-regulated miRNA species hsa-miR-592 induced in astrocytes and neurons with putative targets (among others) viperin and CMPK2 mRNAs. Similarly, the hsa-miR-7974 was predicted to regulate OAS1 mRNA. Also, candidate vdRNAs HS10 and HS12 were proposed to mimic miRNA function and regulate thus host RNA splicing factors RBFOX1 and MTUS2. This predicted chain of regulation is of special interest also due to an affection of host splicing machinery in infected neural cells found by us. Real interactions of small RNAs and their target mRNAs still need to be verified experimentally.

ADAPTATION OF TBEV TO THE VECTOR AND HOST CELL BACKGROUND

One of the white spaces in understanding TBEV biology is what underlays the capacity of the virus to persist on a long-term basis in the vector and at the same time to burst into rapid spread after infecting the mammalian host. By a long-term adaptation to the tick and mammalian cell culture, we intended to identify parts of the genomic sequence important to either of these environments (Manuscript 5).

Several mechanisms have been proposed to contribute to TBEV adaptation to vector and host backgrounds and transition between them. First, specific changes in 3´UTR and deletions in the 3´UTR variable region were described as a sign of host adaptation (52,53,368-370). However, in our study (Manuscript 5) adaptation yielded only one SNP in 3´UTR and no major rearrangements, such as insertions or deletions in the variable region of the 3´UTR were found. Another aspect implicated in the adaptation is the presence of quasispecies, that are well adapted to both host systems (371). For TBEV quasispecies were previously described in the field studies (229,230) as well as laboratory experiments (191,231,232). In our study, we have documented the presence of quasispecies in three different loci of TBEV (Manuscript 5). The original sequence was retained in the pool of viral variants after adaptation and remained thus available in reserve for the potential change of host/cell background. Finally, differences in patterns of sfRNA production have been proposed to play an important role in mosquito-borne arbovirus adaption to mammalian vs. arthropod host cells (372). This aspect was not investigated in our study, however the inspection of sfRNA species production in the vector and host background would bring valuable insight. To conclude, our data speak for the importance of quasispecies in vector-host switch of all the individual aforementioned mechanisms; however, a profound study testing *in vivo* would be needed to validate this hypothesis. Our data contribute to the importance of quasispecies diversity for the pathogenicity of TBEV (223), especially when their importance is more and more obvious from natural tick and patient isolates without previous passage history (230,373). One day the diversity of quasispecies could have also a potential application in diagnosing TBE patients for example in estimating their prognosis (373).

In Manuscript 5, certain mutations in coding, as well as non-coding regions, were identified by TBEV adaptation to the mammalian or tick cells. Although our strains represent only a small-scale sample for a broader evaluation of regions prone to mutation, more than one mutation was found in genomic regions of E, NS3, NS4B, and NS5. Such mutation-prone regions might be virus specific because, for example, for WNV the highest diversity between virus isolates from human and mosquito were documented for the C, NS1, and NS2A genomic regions, and conversely, 5´UTR and E regions were relatively stable (374). For DENV, a few hot spots that might be under selective pressure emerged in E protein in humans and in NS3 and 3´UTR in mosquitoes. In mosquitoes, cold spots in prM and NS5 have been identified that hint at the functionally important loci (227). On the other hand, 3´UTR was found to be highly heterogeneous for TBEV (229).

The defined sequence changes led to altered biological properties of individually selected variants. We show in Manuscript 5 that plaque size produced in the cell culture and virulence in the host are independent variables. For the mammalian cells adapted viral variant (40PS), we documented an unaffected large-plaque phenotype, but the virus was attenuated in the pathogenicity in mice. Conversely, IRE40 exhibited reduced plaque size in the cell culture, and resembled in the pathogenicity to the parental strain. Some mutations in the E protein and in the UTR have been proposed to be involved in the attenuation or plaque size phenotype (179,375). In our case, the mechanism of the small plaque phenotype must be independent of the TBEV E protein, which was not affected by the mutation in the adapted viral variant PS40. An alternative mechanism can include a lost capacity to escape some of the host immune mechanisms, which leads to the impaired spread in the cell culture. An example of such factors is IFITM proteins (274). Regarding the attenuation, an increased affinity to glycosaminoglycans (such as heparan sulphate) due to increased charge on the E protein is believed to be the main factor of attenuation (375). Thus, the mutation in the 40PS variant E protein may play a substantial role in the attenuated phenotype. However, to provide a conclusive answer, targeted mutagenesis would be needed to define which of the specific mutations we found during TBEV adaptation to vertebrate and invertebrate host cells determine the phenotypes we have described.

CURRICULUM VITAE

HANA TYKALOVÁ, MSc. *(née ŠŤASTNÁ)*

Born 22nd of January, 1985 in Chomutov, Czech Republic

E-mail: htykalova@prf.jcu.cz

ORCID: 0000-0002-4132-0372

EDUCATION

2007	BSc. in Biology, Faculty of Science, University of South Bohemia in České Budějovice
2009	MSc. In Parasitology, Faculty of Science, University of South Bohemia in České Budějovice
2009 - present	Ph.D. Studies in Parasitology, Faculty of Science, University of South Bohemia in České Budějovice
8/2013-10/2018	Career break - Maternity leave

WORK EXPERIENCE

2008-2020	R&D Scientist, Institute of Parasitology, Biology Centre, Czech Academy of Sciences, the Laboratory of Molecular Biology of Vectors and Parasites
10-12/2012	Work placement, MRC-University of Glasgow Centre for Virus Research, Laboratory of Arboviruses of Prof Alain Kohl, Glasgow, Great Britain
2/2019 – present	Research Assistant, Faculty of Science, University of South Bohemia in České Budějovice, Laboratory of Applied Biochemistry
4/2022 – present	R&D Scientist, Institute of Parasitology, Biology Centre, Czech Academy of Sciences,

PUBLICATIONS

Růžek D., **Šťastná H.**, Kopecký J., Golovjova I., Grubhoffer L. (2007). Rapid subtyping of tick-borne encephalitis virus-isolates using multiplex RT-PCR. Journal of Virological Methods 144(1-2): 133-7.   DOI: 10.1016/s1386-6532(06)80817-6

Ahantarig, A., Růžek, D., Vancová, M., Janowitz, A., **Šťastná, H.**, Tesařová, M., Grubhoffer, L. (2009). Tick-borne encephalitis virus infection of cultured mouse macrophages. Intervirology 52(5): 283-90. DOI: 10.1159/000235741

Schnettler E., **Tykalová H.**, Watson M., Sharma M., Sterken M.G., Obbard D.J., Lewis S.H., McFarlane M., Bell-Sakyi L., Barry G., Weisheit S., Best S.M., Kuhn R.J., Pijlman G.P., Chase-Topping M.E., Gould E.A., Grubhoffer L., Fazakerley J.K., Kohl A. (2014) Induction and suppression of tick cell antiviral RNAi responses by tick-borne flaviviruses. Nucleic Acids Research 42(14): 9436-46. DOI: 10.1093/nar/gku657

Hönig V., Švec P., Halas P., Vavrušková Z., **Tykalová H.**, Kilian P., Vetišková V., Dorňáková V., Štěrbová J., Šimonová Z., Erhart J., Štěrba J., Golovchenko M., Rudenko N., Grubhoffer L. (2015). Ticks and tick-borne pathogens in South Bohemia (Czech Republic) - Spatial variability in *Ixodes ricinus* abundance, *Borrelia burgdorferi* and tick-borne encephalitis virus prevalence. Ticks and Tick-Borne Diseases 6(5): 559-67. DOI: 10.1016/j.ttbdis.2015.04.010

Weisheit, S., Villar, M., **Tykalová, H.**, Popara, M., Loecherbach, J., Watson, M., Růžek, D., Grubhoffer, L.; de la Fuente, J., Fazakerley, J.K., Bell-Sakyi, L. (2015) *Ixodes scapularis* and *Ixodes ricinus* tick cell lines respond to infection with tick-borne encephalitis virus: transcriptomic and proteomic analysis. Parasites & Vectors 8:599. DOI: 10.1186/s13071-015-1210-x

Černý J., Selinger M., Palus M., Vavrušková Z., **Tykalová H.**, Bell-Sakyi L., Štěrba J., Grubhoffer L., Růžek D. (2016). Expression of a second open reading frame present in the genome of tick-borne encephalitis virus strain Neudoerfl is not detectable in infected cells. Virus Genes 52(3):309-16. DOI: 10.1007/s11262-015-1273-y

Selinger M. et **Tykalová H.**; Štěrba J.; Věchtová P.; Vavrušková Z.; Lieskovská J.; Kohl A.; Schnettler E.; Grubhoffer L. (2019) Tick-borne encephalitis virus inhibits rRNA synthesis and host protein production in human cells of neural origin. PLoS neglected tropical diseases 13(9): e0007745. DOI: 10.1371/journal.pntd.0007745

Helmová R., Hönig V., **Tykalová H.**, Palus M., Bell-Sakyi L., Grubhoffer L. (2020). Tick-borne encephalitis virus adaptation in different host environments and existence of quasispecies. Viruses 12(8):902. DOI: 10.3390/v12080902

Selinger M., Věchtová P., **Tykalová H.**, Ošlejšková P., Rumlová M., Štěrba J., Grubhoffer L., (2022). Integrative RNA profiling of TBEV-infected neurons and astrocytes reveals potential pathogenic effectors. Computational and Structural Biotechnology Journal, 20: 2759-2777. DOI 10.1016/j.csbj.2022.05.052

CONFERENCE ABSTRACTS PUBLISHED IN PEER-REVIEWED JOURNALS

Růžek D., **Šťastná H.**, Kopecký J., Grubhoffer L. (2006). Multiplex RT-PCR for detection and subtyping of tick-borne encephalitis virus. Journal of Clinical Virology 36 (suppl. 2): S32.

Selinger M., **Tykalová H.**, Vavrušková Z., Schnettler E., Kohl A., Štěrba J., Grubhoffer, L., (2018). Tick-borne encephalitis virus induces translational shut-off in human cells of neural origin. FEBS OPEN BIO 8, 8 (suppl. 1): 199-199.

Grubhoffer L., Selinger M., **Tykalová H.**, Schnettler E., Štěrba J. (2019). Tick-borne encephalitis virus inhibits production of ribosomal RNA in human cells of neuronal origin. FEBS OPEN BIO 9, 9 (suppl. 1): 158-159.

CONFERENCE CONTRIBUTIONS

Růžek D., **Šťastná H.**, Kopecký J., Grubhoffer L. (2006). Multiplex RT-PCR for detection and subtyping of tick-borne encephalitis virus. 9th Annual Meeting of the European-Society-for-Clinical-Virology, England, Birmingham.

Šťastná H., Růžek D., Grubhoffer L., Kopecký J. (2007). The influence of tick saliva on the replication of tick-borne encephalitis virus. Third European Congress of Virology, Germany, Norinberk.

Šťastná H., Růžek D., Grubhoffer L., Kopecký J. (2007). Vliv klíštěcích slin na replikaci viru klíšťové encefalitidy v podmínkách *in vitro*. 24. kongres Československé společnosti mikrobiologické. Czech Republic, Liberec.

Šťastná H., Růžek D., Kopecký J., Grubhoffer L. (2008). Molecular interaction of tick-borne encephalitis virus with cells of neural origin. XIV. International Congress of Virology Turkey, Istanbul.

Růžek D., Vancová M., **Šťastná H.**, Štěrba J., Kopecký J., Grubhoffer L. (2008). The neuropathogenesis of tick-borne encephalitis. XIV. International Congress of Virology, Turkey, Istanbul.

Šťastná H., Růžek D., Kopecký J., Grubhoffer L. (2009). Molecular interaction of tick-borne encephalitis virus with cells of neural origin. Labudove dni, Slovakia, Bratislava.

Šťastná H., Růžek D., Grubhoffer L. (2010). Changes in global gene expression in human neural cells following tick-borne encephalitis virus infection. EMBO Workshop: Viruses and innate immunity, Ireland, Dublin, Trinity College.

Šťastná H., Růžek D., Grubhoffer L. 2010. Changes in global gene expression in human neural cells following tick-borne encephalitis virus infection. RNA club, Czech Republic, České Budějovice.

Tykalová H., Vavrušková Z., Černý J., Grubhoffer L. (2013). Interaction of tick-borne encephalitis virus and host cell on protein synthesis level. Eurovirology 2013, France, Lyon.

146

Weisheit S., Villar M., Popara M., **Tykalova H.**, Erhart J., Růžek D., Grubhoffer L., de la Fuente J., Watson M., Bell Sakyi L., Fazakerley J.K. (2013). Novel insights into the defence response in ticks against tick-borne encephalitis virus. Eurovirology 2013, France, Lyon.

Selinger M., **Tykalová H.**, Vavrušková Z., Kohl A., Schnettler E., Grubhoffer L. (2015). Viperin production is attenuated in TBEV-infected human neural cell lines. IMAV 2015, Great Britain, Glasgow.

Selinger M., **Tykalová H.**, Vavrušková Z., Schnettler E., Kohl A., Štěrba J., Grubhoffer L. (2018). Tick-borne encephalitis virus induces translational shut-off in human cells of neural origin. FEBS OPEN BIO 8: P.08-019-Mon. doi.org/10.1002/2211-5463.12453

Grubhoffer L., Selinger M., **Tykalová H.**, Schnettler E., Štěrba J. (2019). Tick-borne encephalitis virus inhibits production of ribosomal RNA in human cells of neuronal origin. FEBS OPEN BIO 9: P-10-008. doi.org/10.1002/2211-5463.12675

Tykalová H., Selinger M., Štěrba J., Věchtová P., Vavrušková Z., Lieskovská J., Kohl A., Schnettler E., Grubhoffer L. (2019). Tick-borne encephalitis virus inhibits rRNA synthesis and host protein production in human cells of neural origin. IMAV 2019 (International Meeting on Arboviruses and their Vectors), Great Britain, Glasgow.

Selinger M., Věchtová P., **Tykalová H.**, Štěrba J., Grubhoffer L. (2019). Transcriptomic analysis of human neurons and astrocytes infected with TBEV strains of different virulence. IMAV 2019 (International Meeting on Arboviruses and their Vectors), Great Britain, Glasgow.

GRANTS

Principal investigator:

2001   043/2011/P   The role of viperin in cells infected with tick-borne encephalitis virus, The Grant Agency of the University of South Bohemia.

Research team member of 6 projects   GAČR (4x), MŠMT (2x)

TEACHING EXPERIENCE

Basic and Advanced Laboratory Courses in Biochemistry, Faculty of Science, University of South Bohemia in České Budějovice, in a sum more than 320 hours.

Co-supervisor of 2 Bc. students, 1 Mgr. student. Supervisor of 1 Bc student.

Since academic year 2021/2022 garant of four courses at the Faculty of Science, University of South Bohemia in České Budějovice (UCH/049 Praktikum z biochemie, UCH/050 Pokročilé praktikum z Biochemie, UCH/758 Biochemistry Laboratory 1, UCH/642 Biochemistry Laboratory 2).

2008   CAE, Grade C, (C1 English level)

2009   TOEFL ITP, 627 points (C1 English level)

2009   "Communication skills in research and development" (Komunikační dovednosti ve vědě a výzkumu) Regionální kontaktní organizace jižní Čechy, Czech Republic

2009   "Use of microarrays in biomedicine" (Využití microarrays v biomedicíně), workshop, KRD, Prague, Czech Republic

2010   Operator training for flow-cytometry (BD FACSCanto IITM a BD FACSDiva 6.1 software)

2011   "Basics of scientific work" (Kurz základů vědecké práce v AV ČR), Academy of Sciences of the Czech Republic, Prague, Czech Republic

2014   "Training course in Laboratory Animal Science" (Osvědčení o odborné způsobilosti k navrhování pokusů a projektů pokusů podle § 15d odst. 3 zákona č. 246/1992 Sb., na ochranu zvířat proti týrání, ve znění pozdějších předpisů), Brno, Czech Republic

NUMBER OF PUBLICATIONS IN WoS: 10

H-INDEX: 6

TOTAL CITATIONS WITHOUT SELF-CITATIONS IN WoS (20.6.2022): 188

LIST OF ABBREVIATIONS

The abbreviations used throughout the text are listed below:

2-5A	2´ - 5´oligoadenylate
45-47S pre-rRNA	45-47S pre-ribosomal RNA, precursor to mature ribosomal RNA
5´dA	5´-deoxyadenosyl radical
7mG	7-methylguanosine cap
ADAR1	double-stranded RNA-specific adenosine deaminase
Ago	Argonaute
AP-1	Activator protein 1
ATF6	Activating transcription factor 6
BiP	immunoglobulin heavy chain-binding protein, also known as HSPA5
BBB	blood-brain barrier
BST2	bone marrow stromal antigen 2, also known as Tetherin
CD4+	cluster of differentiation 4 positive cells
CD8+	cluster of differentiation 8 positive cells
CNS	central nervous system
CMPK2	cytidylate monophosphate kinase 2
COPI	coat protein complex I
CARD	caspase activation recruitment domain
CSF	Cerebrospinal fluid
DC(s)	dendritic cell(s)
DC-SIGN	dendritic cell-specific intercellular adhesion molecule-3-grabbing non-integrin
Dcr	Dicer
ddhCTP	3´-deoxy-3´,4´-didehydro-CTP
DENV	Dengue virus
DNA	deoxyribonucleic acid
DNAJC14	DnaJ homolog subfamily C member 14
dsRNA	double-stranded RNA
eIF2α	eukaryotic translation initiation factor 2 subunit alpha
eIF2A	eukaryotic translation initiation factor 2A
eIF2B	guanine nucleotide exchange factor for the eukaryotic initiation factor 2, protein complex
eIF4E	eukaryotic translation initiation factor 4E
ELISA	enzyme-linked immuno sorbent assay
ER	endoplasmic reticulum
FPPS	farnesyl diphosphate synthase

GA	Golgi apparatus
GAF	gamma-activated factor
gRNA	viral genomic RNA
gp96	heat shock protein gp96, also known as heat shock protein 90kDa beta member 1 (HSP90B1)
GBF1	Golgi-specific brefeldin A-resistance guanine nucleotide exchange factor 1
HAT1	histone acetyltransferase 1
HCV	hepatitis C virus
hsa-miR-592/7974	*Homo sapiens* (human) microRNA-592/7974
HSP90	heat shock protein 90
IDE8	tick cell line of *Ixodes scapularis*
Imd	Immune deficiency
IFN	interferon
IFNL2	interferon lambda receptor 1
IFI6	IFN-α-inducible protein 6
Ifi27	IFN-α-inducible protein 27
IFIT 1/2/3	IFN-induced protein with tetra-tricopeptide repeats 1/2/3
IFITM	Interferon-inducible transmembrane proteins
IFNAR	interferon-alpha/beta receptor
IFNGR	interferon-gamma receptor
IFNLR1	interferon lambda receptor 1
Ig	immunoglobulin
IL	interleukine
IL10R1/2	interleukin-10 receptor 1/2
Irg1	Immunity related guanosine triphosphatase 1
IRAK1	interleukin-1 receptor-associated kinase
IRE1	inositol requiring ring enzyme 1
IRE/CTVM19	tick cell line of *Ixodes ricinus*
IRF1	interferon regulatory factor 1
IRF3	interferon regulatory factor 3
IRF7	interferon regulatory factor 7
ISG/s	interferon-stimulated gene/s
ISG15	interferon-stimulated gene 15
ISG20	Interferon-stimulated gene 20 kDa protein
ISGF3	IFN-stimulated gene factor 3 gene complex
ISRE	interferon-stimulated response element
Jak	Janus kinase
JEV	Japanese encephalitis virus
LGTV	Langat virus

LIV	Louping ill virus
lncRNA	long non-coding RNA
LGP2	Laboratory of Genetics and Physiology 2
MAPK	mitogen-activated protein kinase, also known as MAP kinase
MAVS	mitochondrial antiviral signaling (also known as IPS-1, IFN-β promoter stimulator I)
MDA-5	melanoma differentiation-associated protein 5
miRNA	microRNA
MMP-9/13	matrix metalloproteinase-9/13
Mnk1	MAP kinase-interacting serine/threonine-protein kinase 1
mRNA	messenger RNA
MVEV	Murray Valley encephalitis virus
MX 1/2	MX Dynamin Like GTPase 1/2
MTUS2	Microtubule associated scaffold protein 2
NF-κB	nuclear factor kappa-light-chain-enhancer of activated B cells
OAS 1/2/3	2´-5´ oligoadenylate synthetase 1/2/3
OASL	2'-5'-oligoadenylate synthetase-like protein
OHF	Omsk hemorrhagic fever virus
p38	p38 mitogen-activated protein kinases
PAMPs	pathogen-associated molecular patterns
PERK	protein kinase R (PKR)-like endoplasmic reticulum kinase (also known as EIF2AK3 – eukaryotic translation initiation factor 2-α kinase 3)
piRNA	Piwi-interacting RNA
PKR	protein kinase R (as eukaryotic translation initiation factor 2-alpha kinase 2 [EIF2AK2]
POWV	Powassan virus
prM	precursor of M protein of flaviviruses
PRRs	pattern recognition receptors
R2D2	R2D2
RdRp	RNA dependent RNA polymerase
RIG-I	retinoic acid inducible gene I
RISC	RNA-induced silencing complex
RNA	ribonucleic acid
RNAi	RNA interference
RLR(s)	RIG-I-like receptor(s)
rRNA	ribosomal RNA
RSAD2	radical SAM domain-containing 2 gene, see also Viperin
RTN3A	reticulon 3A protein
RBFOX1	Fox-1 homolog A
SAM	S-adenosyl-l-methionine

siRNA	small interfering RNA
sfRNA	subgenomic flavivirus RNA
SNP	single nucleotide polymorphism
STAT	signal transducer and activator of transcription
TAM	TAM receptor protein tyrosine kinases: TYRO3, AXL and MER
TBE	tick-borne encephalitis
TBEV	tick-borne encephalitis virus
TMEM41B	Transmembrane protein 41B
TNF-α	tumor necrosis factor alpha
TIM	T-cell immunoglobulin and mucin domain
TLRs	Toll-like receptors
TNFSF10	TNF-related apoptosis-inducing ligand, also known as TRAIL
TRAF6	TNF receptor associated factor 6; E3 ubiquitin ligase
TRIM	tripartite motif-containing
TRIM25/79α	tripartite motif-containing protein 25/79α
Tyk2	Tyrosine kinase 2
UBE4A	Ubiquitin conjugation factor E4 A
UPR	unfolded protein response pathway
UPD	unpaired cytokine
UTR	untranslated region
vdRNAs	virus derived small RNAs
Viperin	virus inhibitory protein, endoplasmic reticulum-associated, interferon-inducible (also RSAD2, Vig1, or Cig5)
VP	vesicular packets
VMP1	vacuole membrane protein 1
WNV	West Nile virus
XBP1	X box-binding protein 1
XRN1	5´-3´exonuriboclease 1
xrRNA	exoribonuclease-resistant RNA element
YFV	Yellow fewer virus
ZIKV	Zika virus

REFERENCES

1. Pulkkinen, L. I. A., Butcher, S. J., and Anastasina, M. (2018) Tick-borne encephalitis virus: a structural view. *Viruses* **10**, 350
2. WHO. (2017) Global vector control response 2017-2030. World Health Organization, & UNICEF Geneva, Switzerland
3. Beaute, J., Spiteri, G., Warns-Petit, E., and Zeller, H. (2018) Tick-borne encephalitis in Europe, 2012 to 2016. *Euro Surveill* **23**, 1800201
4. Erber, W., and Schmitt, H. J. (2018) Self-reported tick-borne encephalitis (TBE) vaccination coverage in Europe: Results from a cross-sectional study. *Ticks Tick Borne Dis* **9**, 768-777
5. Süss, J. (2003) Epidemiology and ecology of TBE relevant to the production of effective vaccines. *Vaccine* **21**, S19-S35
6. Süss, J. (2008) Tick-borne encephalitis in Europe and beyond-the epidemiological situation as of 2007. *Euro Surveill* **13**, 18916
7. Pagani, S. C., Malossa, S. F., Klaus, C., Hoffmann, D., Beretta, O., Bomio-Pacciorini, N., Lazzaro, M., Merlani, G., Ackermann, R., and Beuret, C. (2019) First detection of TBE virus in ticks and sero-reactivity in goats in a non-endemic region in the southern part of Switzerland (Canton of Ticino). *Ticks Tick Borne Dis* **10**, 868-874
8. Velay, A., Solis, M., Kack-Kack, W., Gantner, P., Maquart, M., Martinot, M., Augereau, O., De Briel, D., Kieffer, P., Lohmann, C., Poveda, J. D., Cart-Tanneur, E., Argemi, X., Leparc-Goffart, I., de Martino, S., Jaulhac, B., Raguet, S., Wendling, M. J., Hansmann, Y., and Fafi-Kremer, S. (2018) A new hot spot for tick-borne encephalitis (TBE): A marked increase of TBE cases in France in 2016. *Ticks Tick Borne Dis* **9**, 120-125
9. Frimmel, S., Krienke, A., Riebold, D., Loebermann, M., Littmann, M., Fiedler, K., Klaus, C., Süss, J., and Reisinger, E. C. (2014) Tick-borne encephalitis virus habitats in North East Germany: reemergence of TBEV in ticks after 15 years of inactivity. *Biomed Res Int*, 308371
10. Boelke, M., Bestehorn, M., Marchwald, B., Kubinski, M., Liebig, K., Glanz, J., Schulz, C., Dobler, G., Monazahian, M., and Becker, S. C. (2019) First isolation and phylogenetic analyses of tick-borne encephalitis virus in Lower Saxony, Germany. *Viruses-Basel* **11**, 462
11. Holding, M., Dowall, S. D., Medlock, J. M., Carter, D. P., Pullan, S. T., Lewis, J., Vipond, R., Rocchi, M. S., Baylis, M., and Hewson, R. (2020) Tick-borne encephalitis virus, United Kingdom. *Emerg Infect Dis* **26**, 90-96
12. Kreusch, T. M., Holding, M., Hewson, R., Harder, T., Medlock, J. M., Hansford, K. M., Dowall, S., Semper, A., Brooks, T., Walsh, A., Russell, K., and Wichmann, O. (2019) A probable case of tick-borne encephalitis (TBE) acquired in England, July 2019. *Euro Surveill* **24**, 1900679
13. Daniel, M., Danielova, V., Kriz, B., Jirsa, A., and Nozicka, J. (2003) Shift of the tick Ixodes ricinus and tick-borne encephalitis to higher altitudes in central Europe. *Eur J Clin Microbiol* **22**, 327-328
14. Solomon, T., Ooi, M. H., and Mallewa, M. (2007) Viral infections of lower motor neurons. in *Motor Neuron Disorders and Related Diseases, Handbook of Clinical Neurology* (Eisen, A. A., and Shaw, P. J. eds.), Elsevier B.V. pp 179-206
15. Simmonds, P., Becher, P., Bukh, J., Gould, E. A., Meyers, G., Monath, T., Muerhoff, S., Pletnev, A., Rico-Hesse, R., Smith, D. B., Stapleton, J. T., and Consortium, I. R. (2017) ICTV Virus Taxonomy Profile: Flaviviridae. *J Gen Virol* **98**, 2-3
16. Zilber, L. A. (1939) Spring-summer tick-borne encephalitis. *Arkhiv Biol Nauk* **56**, 255-261
17. Izbický, A. (1954) *Současný stav výzkumu epidemiologie československé klíšťové encefalitidy [in Czech].* PhD Dissertation Thesis, Prof. Raška Institute of Epidemiology and Microbiology
18. Gallia, F., Rampas, J., and Hollender, L. (1949) Laboratorní infekce způsobené virem klíšťové encefalitidy. *Cas Lek Cesk* **88**, 1171-1190
19. Krejčí, J. (1949) Isolement d´un virus nouveau en course d´une épidémie de meningo-encephalite dans la region de Vyškov (Moraviae) [In French]. *Presse Med* **57**, 1084
20. Rampas, J., and Gallia, F. (1949) Isolace virusu encefalitidy z klíšťat *Ixodes ricinus* [Isolation of encephalitis virus from *Ixodes ricinus* ticks][in Czech]. *Cas Lek Cesk* **88**, 1179-1181
21. Dumpis, U., Crook, D., and Oksi, J. (1999) Tick-borne encephalitis. *Clin Infect Dis* **28**, 882-890
22. Health, T. N. I. o. P. (2021) ISIN, database of The National Institute of Public Health. The National Institute of Public Health, Accessed 15.11.2021, http://www.szu.cz/publikace/data/infekce-v-cr
23. Ecker, M., Allison, S. L., Meixner, T., and Heinz, F. X. (1999) Sequence analysis and genetic classification of tick-borne encephalitis viruses from Europe and Asia. *J Gen Virol* **80 (Pt 1)**, 179-185
24. Heinz, F. X., Collett, M. S., Purcell, R. H., Gould, E. A., Howard, C. R., Houghton, M., Moormann, R. J. M., Rice, C. M., and Thiel, H. J. (2000) Family Flaviviridae. in *Virus Taxonomy* (van Regenmortel, M. H. V., Fauquet, C. M., Bishop, D. H. L., Carstens, E., Estes, M. K., Lemon, S., Maniloff, J., Mayo, M. A., McGeogch, D., Pringle, C. R., and Wickner, R. B. eds.), Academic Press, San Diego, California. pp 859-878
25. Kovalev, S. Y., and Mukhacheva, T. A. (2017) Reconsidering the classification of tick-borne encephalitis virus within the Siberian subtype gives new insights into its evolutionary history. *Infect Genet Evol* **55**, 159-165
26. Dai, X., Shang, G., Lu, S., Yang, J., and Xu, J. (2018) A new subtype of eastern tick-borne encephalitis virus discovered in Qinghai-Tibet Plateau, China. *Emerg Microbes Infect* **7**, 74
27. Grešíková, M., and Kaluzová, M. (1997) Biology of tick-borne encephalitis. *Acta Virol* **41**, 115-124

28. Gritsun, T. S., Lashkevich, V. A., and Gould, E. A. (2003) Tick-borne encephalitis. *Antiviral Res* **57**, 129-146
29. Jones, L. D., Davies, C. R., Steele, G. M., and Nuttall, P. A. (1987) A novel mode of arbovirus transmission involving a nonviraemic host. *Science* **237**, 775-777
30. Labuda, M., Jones, L. D., Williams, T., Danielova, V., and Nuttall, P. A. (1993) Efficient transmission of tick-borne encephalitis virus between cofeeding ticks. *J Med Entomol* **30**, 295-299
31. Labuda, M., Nuttall, P. A., Kozuch, O., Eleckova, E., Williams, T., Zuffova, E., and Sabo, A. (1993) Non-viraemic transmission of tick-borne encephalitis virus: a mechanism for arbovirus survival in nature. *Experientia* **49**, 802-805
32. Labuda, M., Austyn, J. M., Zuffova, E., Kozuch, O., Fuchsberger, N., Lysy, J., and Nuttall, P. A. (1996) Importance of localized skin infection in tick-borne encephalitis virus transmission. *Virology* **219**, 357-366
33. Labuda, M., Kozuch, O., Zuffova, E., Eleckova, E., Hails, R. S., and Nuttall, P. A. (1997) Tick-borne encephalitis virus transmission between ticks cofeeding on specific immune natural rodent hosts. *Virology* **235**, 138-143
34. Suss, J., and Schrader, C. (2004) Durch Zecken ubertragene humanpathogene und bisher als apathogen geltende Mikroorganismen in Europa. Teil I: Zecken und Viren [Tick-borne human pathogenic microorganisms found in Europe and those considered nonpathogenic. Part I: Ticks and Viruses]. *Bundesgesundheitsblatt Gesundheitsforschung Gesundheitsschutz* **47**, 392-404
35. Daneš. (2000) Nákaza člověka virem klíšťové encefalitidy [Human infection with the tick-borne encephalitis virus] [in Czech]. *Medicína* **3**, 16
36. Blaškovič, D. (1954) *Epidémia encefalitídy v Rožňavskom prírodnom ohnisku nákaz [in Slovak]*, SAV, Bratislava
37. Maximova, O. A., Ward, J. M., Asher, D. M., St Claire, M., Finneyfrock, B. W., Speicher, J. M., Murphy, B. R., and Pletnev, A. G. (2008) Comparative neuropathogenesis and neurovirulence of attenuated flaviviruses in nonhuman primates. *J Virol* **82**, 5255-5268
38. Smith, C. E. (1956) A virus resembling Russian spring-summer encephalitis virus from an ixodid tick in Malaya. *Nature* **178**, 581-582
39. Price, W. H., Thind, I. S., Teasdall, R. D., and O'Leary, W. (1970) Vaccination of human volunteers against Russian spring-summer (RSS) virus complex with attenuated Langat E5 virus *Bull World Health Organ* **42**, 89-94
40. Shapoval, A. N., Kamalov, II, Denisova, E., Sokolova, E. D., Luzin, P. M., Shamarina, A. G., Gusmanova, A. G., and Pinaeva, N. I. (1989) [Study of the distant consequences of immunizing people with a live vaccine against tick-borne encephalitis] [in Russian] *Trudi Instituta Imeni Pastera* **65**, 133-135
41. Heinz, F. X., and Kunz, C. (2004) Tick-borne encephalitis and the impact of vaccination. *Archives of virology. Supplementum*, 201-205
42. Lindquist, L., and Vapalahti, O. (2008) Tick-borne encephalitis. *Lancet* **371**, 1861-1871
43. Füzik, T., Formanová, P., Růžek, D., Yoshii, K., Niedrig, M., and Plevka, P. (2018) Structure of tick-borne encephalitis virus and its neutralization by a monoclonal antibody. *Nat Commun* **9**, 436
44. Therkelsen, M. D., Klose, T., Vago, F., Jiang, W., Rossmann, M. G., and Kuhn, R. J. (2018) Flaviviruses have imperfect icosahedral symmetry. *Proc Natl Acad Sci U S A* **115**, 11608-11612
45. Dowd, K. A., and Pierson, T. C. (2018) The many faces of a dynamic virion: Implications of viral breathing on flavivirus biology and immunogenicity. *Annu Rev Virol* **5**, 185-207
46. Wengler, G., Wengler, G., and Gross, H. J. (1978) Studies on virus-specific nucleic acids synthesized in vertebrate and mosquito cells infected with flaviviruses. *Virology* **89**, 423-437
47. Filomatori, C. V., Lodeiro, M. F., Alvarez, D. E., Samsa, M. M., Pietrasanta, L., and Gamarnik, A. V. (2006) A 5' RNA element promotes dengue virus RNA synthesis on a circular genome. *Gene Dev* **20**, 2238-2249
48. Rouha, H., Hoenninger, V. M., Thurner, C., and Mandl, C. W. (2011) Mutational analysis of three predicted 5'-proximal stem-loop structures in the genome of tick-borne encephalitis virus indicates different roles in RNA replication and translation. *Virology* **417**, 79-86
49. Ng, W. C., Soto-Acosta, R., Bradrick, S. S., Garcia-Blanco, M. A., and Ooi, E. E. (2017) The 5' and 3' untranslated regions of the flaviviral genome. *Viruses* **9**, 137
50. Kofler, R. M., Hoenninger, V. M., Thurner, C., and Mandl, C. W. (2006) Functional analysis of the tick-borne encephalitis virus cyclization elements indicates major differences between mosquito-borne and tick-borne flaviviruses. *J Virol* **80**, 4099-4113
51. Ochsenreiter, R., Hofacker, I. L., and Wolfinger, M. T. (2019) Functional RNA structures in the 3'UTR of tick-borne, insect-specific and no-known-vector flaviviruses. *Viruses* **11**, 298
52. Mandl, C. W., Kunz, C., and Heinz, F. X. (1991) Presence of poly (A) in a flavivirus: significant differences between the 3'noncoding regions of the genomic RNAs of tick-borne encephalitis virus strains. *J Virol* **65**, 4070-4077
53. Sakai, M., Muto, M., Hirano, M., Kariwa, H., and Yoshii, K. (2015) Virulence of tick-borne encephalitis virus is associated with intact conformational viral RNA structures in the variable region of the 3'-UTR. *Virus Res* **203**, 36-40
54. Markoff, L. (2003) 5'-and 3'-noncoding regions in flavivirus RNA. *Adv Virus Res* **59**, 177-228
55. Murray, C. L., Jones, C. T., and Rice, C. M. (2008) Architects of assembly: roles of *Flaviviridae* non-structural proteins in virion morphogenesis. *Nat Rev Microbiol* **6**, 699-708
56. Neufeldt, C. J., Cortese, M., Acosta, E. G., and Bartenschlager, R. (2018) Rewiring cellular networks by members of the Flaviviridae family. *Nat Rev Microbiol* **16**, 125-142

57. Pijlman, G. P., Funk, A., Kondratieva, N., Leung, J., Torres, S., van der Aa, L., Liu, W. J., Palmenberg, A. C., Shi, P.-Y., Hall, R. A., and Khromykh, A. A. (2008) A highly structured, nuclease-resistant, noncoding RNA produced by flaviviruses is required for pathogenicity. *Cell Host Microbe* **4**, 579-591

58. Schnettler, E., Sterken, M. G., Leung, J. Y., Metz, S. W., Geertsema, C., Goldbach, R. W., Vlak, J. M., Kohl, A., Khromykh, A. A., and Pijlman, G. P. (2012) Noncoding flavivirus RNA displays RNA interference suppressor activity in insect and Mammalian cells. *J Virol* **86**, 13486-13500

59. Filomatori, C. V., Carballeda, J. M., Villordo, S. M., Aguirre, S., Pallares, H. M., Maestre, A. M., Sanchez-Vargas, I., Blair, C. D., Fabri, C., Morales, M. A., Fernandez-Sesma, A., and Gamarnik, A. V. (2017) Dengue virus genomic variation associated with mosquito adaptation defines the pattern of viral non-coding RNAs and fitness in human cells. *PLoS Pathog* **13**, e1006265

60. Chapman, E. G., Costantino, D. A., Rabe, J. L., Moon, S. L., Wilusz, J., Nix, J. C., and Kieft, J. S. (2014) The structural basis of pathogenic subgenomic flavivirus RNA (sfRNA) production. *Science* **344**, 307-310

61. Akiyama, B. M., Laurence, H. M., Massey, A. R., Costantino, D. A., Xie, X., Yang, Y., Shi, P. Y., Nix, J. C., Beckham, J. D., and Kieft, J. S. (2016) Zika virus produces noncoding RNAs using a multi-pseudoknot structure that confounds a cellular exonuclease. *Science* **354**, 1148-1152

62. Chapman, E. G., Moon, S. L., Wilusz, J., and Kieft, J. S. (2014) RNA structures that resist degradation by Xrn1 produce a pathogenic Dengue virus RNA. *Elife* **3**, e01892

63. MacFadden, A., O'Donoghue, Z., Silva, P., Chapman, E. G., Olsthoorn, R. C., Sterken, M. G., Pijlman, G. P., Bredenbeek, P. J., and Kieft, J. S. (2018) Mechanism and structural diversity of exoribonuclease-resistant RNA structures in flaviviral RNAs. *Nat Commun* **9**, 119

64. Dilweg, I. W., Bouabda, A., Dalebout, T., Gultyaev, A. P., Bredenbeek, P. J., and Olsthoorn, R. C. L. (2021) Xrn1-resistant RNA structures are well-conserved within the genus flavivirus. *RNA Biol* **18**, 709-717

65. Lindenbach, B. D., Thiel, H. J., and Rice, C. M. (2007) Flaviviridae: the viruses and their replication. in *Fields Virology* (Knipe, D. M., and Howley, P. M. eds.), 5th Ed., Lippincott-Raven Publishers, Philadelphia. pp 1101-1133

66. Leung, J. Y., Pijlman, G. P., Kondratieva, N., Hyde, J., Mackenzie, J. M., and Khromykh, A. A. (2008) Role of nonstructural protein NS2A in flavivirus assembly. *J Virol* **82**, 4731-4741

67. Diosa-Toro, M., Echavarria-Consuegra, L., Flipse, J., Fernandez, G. J., Kluiver, J., van den Berg, A., Urcuqui-Inchima, S., and Smit, J. M. (2017) MicroRNA profiling of human primary macrophages exposed to dengue virus identifies miRNA-3614-5p as antiviral and regulator of ADAR1 expression. *PLoS Negl Trop Dis* **11**, e0005981

68. Rastogi, M., Sharma, N., and Singh, S. K. (2016) Flavivirus NS1: a multifaceted enigmatic viral protein. *Virology J* **13**, 131

69. Morita, E., and Suzuki, Y. (2021) Membrane-associated flavivirus replication complex-its organization and regulation. *Viruses* **13**, 1060

70. Goto, A., Yoshii, K., Obara, M., Ueki, T., Mizutani, T., Kariwa, H., and Takashima, I. (2005) Role of the N-linked glycans of the prM and E envelope proteins in tick-borne encephalitis virus particle secretion. *Vaccine* **23**, 3043-3052

71. Kopecký, J., Grubhoffer, L., Kovář, V., Jindrák, L., and Vokurková, D. (1999) A putative host cell receptor for tick-borne encephalitis virus identified by anti-idiotypic antibodies and virus affinoblotting. *Intervirology* **42**, 9-16

72. Martinez-Barragan, J. D., and del Angel, R. M. (2001) Identification of a putative coreceptor on vero cells that participates in dengue 4 virus infection. *J Virol* **75**, 7818-7827

73. Ramos-Castaneda, J., Imbert, J. L., Barron, B. L., and Ramos, C. (1997) A 65-kDa trypsin-sensible membrane cell protein as a possible receptor for dengue virus in cultured neuroblastoma cells. *J Neurovirol* **3**, 435-440

74. Kroschewski, H., Allison, S. L., Heinz, F. X., and Mandl, C. W. (2003) Role of heparan sulfate for attachment and entry of tick-borne encephalitis virus. *Virology* **308**, 92-100

75. Mandl, C. W., Kroschewski, H., Allison, S. L., Kofler, R., Holzmann, H., Meixner, T., and Heinz, F. X. (2001) Adaptation of tick-borne encephalitis virus to BHK-21 cells results in the formation of multiple heparan sulfate binding sites in the envelope protein and attenuation in vivo. *J Virol* **75**, 5627-5637

76. Mandl, C. W. (2005) Steps of the tick-borne encephalitis virus replication cycle that affect neuropathogenesis. *Virus Res* **111**, 161-174

77. Perera-Lecoin, M., Meertens, L., Carnec, X., and Amara, A. (2013) Flavivirus entry receptors: an update. *Viruses* **6**, 69-88

78. Tassaneetrithep, B., Burgess, T. H., Granelli-Piperno, A., Trumpfheller, C., Finke, J., Sun, W., Eller, M. A., Pattanapanyasat, K., Sarasombath, S., and Birx, D. L. (2003) DC-SIGN (CD209) mediates dengue virus infection of human dendritic cells. *The Journal of experimental medicine* **197**, 823-829

79. King, N. J. C., Getts, D. R., Getts, M. T., Rana, S., Shrestha, B., and Kesson, A. M. (2007) Immunopathology of flavivirus infections. *Immunology and Cell Biology* **85**, 33-42

80. Chu, J. J. H., and Ng, M. L. (2004) Infectious entry of West Nile virus occurs through a clathrin-mediated endocytic pathway. *J Virol* **78**, 10543-10555

81. Potokar, M., Korva, M., Jorgacevski, J., Avsic-Zupanc, T., and Zorec, R. (2014) Tick-borne encephalitis virus infects rat astrocytes but does not affect their viability. *PLoS One* **9**, e86219

82. Chambers, T. J., and Diamond, M. S. (2003) Pathogenesis of flavivirus encephalitis. *Adv Virus Res* **60**, 273-342

83. Miorin, L., Romero-Brey, I., Maiuri, P., Hoppe, S., Krijnse-Locker, J., Bartenschlager, R., and Marcello, A. (2013) Three-dimensional architecture of tick-borne encephalitis virus replication sites and trafficking of the replicated RNA. *J Virol* **87**, 6469-6481

84. MacKenzie, J. M., and Westaway, E. G. (2001) Assembly and maturation of the flavivirus Kunjin virus appear to occur in the rough endoplasmic reticulum and along the secretory pathway, respectively. *J Virol* **75**, 10787-10799

85. Mackenzie, J. M., Khromykh, A. A., Jones, M. K., and Westaway, E. G. (1998) Subcellular localization and some biochemical properties of the flavivirus Kunjin nonstructural proteins NS2A and NS4A. *Virology* **245**, 203-215

86. Westaway, E. G., Khromykh, A. A., and Mackenzie, J. M. (1999) Nascent flavivirus RNA colocalized in situ with double-stranded RNA in stable replication complexes. *Virology* **258**, 108-117

87. Miorin, L., Maiuri, P., Hoenninger, V. M., Mandl, C. W., and Marcello, A. (2008) Spatial and temporal organization of tick-borne encephalitis flavivirus replicated RNA in living cells. *Virology* **379**, 64-77

88. Liu, W. J., Chen, H. B., and Khromykh, A. A. (2003) Molecular and functional analyses of Kunjin virus infectious cDNA clones demonstrate the essential roles for NS2A in virus assembly and for a nonconservative residue in NS3 in RNA replication. *J Virol* **77**, 7804-7813

89. Mackenzie, J. (2005) Wrapping things up about virus RNA replication. *Traffic* **6**, 967-977

90. Aktepe, T. E., and Mackenzie, J. M. (2018) Shaping the flavivirus replication complex: It is curvaceous! *Cell Microbiol* **20**, e12884

91. Mazeaud, C., Freppel, W., and Chatel-Chaix, L. (2018) The multiples fates of the flavivirus RNA genome during pathogenesis. *Front Genet* **9**, 595

92. Aktepe, T. E., Liebscher, S., Prier, J. E., Simmons, C. P., and Mackenzie, J. M. (2017) The host protein reticulon 3.1A is utilized by flaviviruses to facilitate membrane remodelling. *Cell Rep* **21**, 1639-1654

93. Mackenzie, J. M., Khromykh, A. A., and Parton, R. G. (2007) Cholesterol manipulation by West Nile virus perturbs the cellular immune response. *Cell Host Microbe* **2**, 229-239

94. Yi, Z., Sperzel, L., Nurnberger, C., Bredenbeek, P. J., Lubick, K. J., Best, S. M., Stoyanov, C. T., Law, L. M., Yuan, Z., Rice, C. M., and MacDonald, M. R. (2011) Identification and characterization of the host protein DNAJC14 as a broadly active flavivirus replication modulator. *PLoS Pathog* **7**, e1001255

95. Bartenschlager, R., and Miller, S. (2008) Molecular aspects of Dengue virus replication. *Future Microbiol* **3**, 155-165

96. Khromykh, A. A., Meka, H., Guyatt, K. J., and Westaway, E. G. (2001) Essential role of cyclization sequences in Flavivirus RNA replication. *J Virol* **75**, 6719-6728

97. Apte-Sengupta, S., Sirohi, D., and Kuhn, R. J. (2014) Coupling of replication and assembly in flaviviruses. *Curr Opin Virol* **9**, 134-142

98. Khromykh, A. A., Varnavski, A. N., Sedlak, P. L., and Westaway, E. G. (2001) Coupling between replication and packaging of flavivirus RNA: evidence derived from the use of DNA-based full-length cDNA clones of Kunjin virus. *J Virol* **75**, 4633-4640

99. Welsch, S., Miller, S., Romero-Brey, I., Merz, A., Bleck, C. K., Walther, P., Fuller, S. D., Antony, C., Krijnse-Locker, J., and Bartenschlager, R. (2009) Composition and three-dimensional architecture of the dengue virus replication and assembly sites. *Cell Host Microbe* **5**, 365-375

100. Barrows, N. J., Campos, R. K., Liao, K. C., Prasanth, K. R., Soto-Acosta, R., Yeh, S. C., Schott-Lerner, G., Pompon, J., Sessions, O. M., Bradrick, S. S., and Garcia-Blanco, M. A. (2018) Biochemistry and molecular biology of flaviviruses. *Chem Rev* **118**, 4448-4482

101. Lobigs, M., Mullbacher, A., and Lee, E. (2004) Evidence that a mechanism for efficient flavivirus budding upregulates MHC class I. *Immunology and Cell Biology* **82**, 184-188

102. Garoff, H., Hewson, R., and Opstelten, D. J. (1998) Virus maturation by budding. *Microbiol Mol Biol Rev* **62**, 1171-1190

103. Stadler, K., Allison, S. L., Schalich, J., and Heinz, F. X. (1997) Proteolytic activation of tick-borne encephalitis virus by furin. *J Virol* **71**, 8475-8481

104. Lattová, E., Straková, P., Pokorná-Formanová, P., Grubhoffer, L., Bell-Sakyi, L., Zdráhal, Z., Palus, M., and Růžek, D. (2020) Comprehensive N-glycosylation mapping of envelope glycoprotein from tick-borne encephalitis virus grown in human and tick cells. *Sci Rep* **10**, 13204

105. Nuttall, P. A., and Labuda, M. (2003) Dynamics of infection in tick vectors and at the tick-host interface. *Adv Virus Res* **60**, 233-272

106. Mejri, N., Rutti, B., and Brossard, M. (2002) Immunosuppressive effects of ixodes ricinus tick saliva or salivary gland extracts on innate and acquired immune response of BALB/c mice. *Parasitol Res* **88**, 192-197

107. Wang, H., Kaufman, W. R., and Nuttall, P. A. (1999) Molecular individuality: polymorphism of salivary gland proteins in three species of ixodid tick. *Exp Appl Acarol* **23**, 969-975

108. Sanders, M. L., Scott, A. L., Glass, G. E., and Schwartz, B. S. (1996) Salivary gland changes and host antibody responses associated with feeding of male lone star ticks (Acari:Ixodidae). *J Med Entomol* **33**, 628-634

109. Kotál, J., Langhansová, H., Lieskovská, J., Andersen, J. F., Francischetti, I. M., Chavakis, T., Kopecký, J., Pedra, J. H., Kotsyfakis, M., and Chmelař, J. (2015) Modulation of host immunity by tick saliva. *J Proteomics* **128**, 58-68

110. Ribeiro, J. M., Alarcon-Chaidez, F., Francischetti, I. M., Mans, B. J., Mather, T. N., Valenzuela, J. G., and Wikel, S. K. (2006) An annotated catalog of salivary gland transcripts from Ixodes scapularis ticks. *Insect Biochem Mol Biol* **36**, 111-129

111. Jones, L. D., Hodgson, E., and Nuttall, P. A. (1989) Enhancement of virus transmission by tick salivary glands. *J Gen Virol* **70**, 1895-1898

112. Thangamani, S., Hermance, M. E., Santos, R. I., Slovak, M., Heinze, D., Widen, S. G., and Kazimirova, M. (2017) Transcriptional immunoprofiling at the tick-virus-host interface during early stages of tick-borne encephalitis virus transmission. *Front Cell Infect Microbiol* **7**, 494

113. Albrecht, P. (1968) Pathogenesis of neurotropic arbovirus infections. *Curr Top Microbiol Immunol* **43**, 44-91

114. Byrne, S. N., Halliday, G. M., Johnston, L. J., and King, N. J. (2001) Interleukin-1beta but not tumor necrosis factor is involved in West Nile virus-induced Langerhans cell migration from the skin in C57BL/6 mice. *The Journal of Investigative Dermatology* **117**, 702-709

115. Hermance, M. E., Santos, R. I., Kelly, B. C., Valbuena, G., and Thangamani, S. (2016) Immune cell targets of infection at the tick-skin interface during Powassan virus transmission. *PLoS One* **11**, e0155889

116. Fialová, A., Cimburek, Z., Iezzi, G., and Kopecký, J. (2010) Ixodes ricinus tick saliva modulates tick-borne encephalitis virus infection of dendritic cells. *Microbes Infect* **12**, 580-585

117. Skallová, A., Iezzi, G., Ampenberger, F., Kopf, M., and Kopecký, J. (2008) Tick saliva inhibits dendritic cell migration, maturation, and function while promoting development of Th2 responses. *J Immunol* **180**, 6186-6192

118. Málková, D. (1968) The significance of the skin and the regional lymph nodes in the penetration and multiplication of tickborne encephalitis virus after subcutaneous infection of mice. *Acta Virol* **12**, 222-228

119. Málková, D., and Filip, O. (1968) Histological picture in the place of inoculation and in lymph nodes of mice after subcutaneous infection with tick-borne encephalitis virus. *Acta Virol* **12**, 355-360

120. Málková, D., and Fraňková, V. (1959) The lymphatic system in the development of experimental tick-borne encephalitis in mice. *Acta Virol* **3**, 210-214

121. Hermance, M. E., and Thangamani, S. (2015) Tick saliva enhances Powassan virus transmission to the host, influencing its dissemination and the course of disease. *J Virol* **89**, 7852-7860

122. Monath, T. P. (1986) Pathobiology of the flaviviruses. in *The Togaviridae and Flaviviridae* (Schlesinger, S., and Schlesinger, M. J. eds.), Plenum Press, New York. pp 375-440

123. Wang, T., Town, T., Alexopoulou, L., Anderson, J. F., Fikrig, E., and Flavell, R. A. (2004) Toll-like receptor 3 mediates West Nile virus entry into the brain causing lethal encephalitis. *Nat Med* **10**, 1366-1373

124. Shrestha, B., Gottlieb, D., and Diamond, M. S. (2003) Infection and injury of neurons by West Nile encephalitis virus. *J Virol* **77**, 13203-13213

125. Sitati, E., McCandless, E. E., Klein, R. S., and Diamond, M. S. (2007) CD40-CD40 ligand interactions promote trafficking of CD8+ T cells into the brain and protection against West Nile virus encephalitis. *J Virol* **81**, 9801-9811

126. Růžek, D., Salát, J., Singh, S. K., and Kopecký, J. (2011) Breakdown of the blood-brain barrier during tick-borne encephalitis in mice is not dependent on CD8+ T-cells. *PLoS One* **6**, e20472

127. Palus, M., Žampachová, E., Elsterová, J., and Růžek, D. (2014) Serum matrix metalloproteinase-9 and tissue inhibitor of metalloproteinase-1 levels in patients with tick-borne encephalitis. *J Infect* **68**, 165-169

128. Palus, M., Bílý, T., Elsterová, J., Langhansová, H., Salát, J., Vancová, M., and Růžek, D. (2014) Infection and injury of human astrocytes by tick-borne encephalitis virus. *J Gen Virol* **95**, 2411-2426

129. Gelpi, E., Preusser, M., Garzuly, F., Holzmann, H., Heinz, F. X., and Budka, H. (2005) Visualization of central European tick-borne encephalitis infection in fatal human cases. *Journal of Neuropathology and Experimental Neurology* **64**, 506-512

130. Verma, S., Lo, Y., Chapagain, M., Lum, S., Kumar, M., Gurjav, U., Luo, H., Nakatsuka, A., and Nerurkar, V. R. (2009) West Nile virus infection modulates human brain microvascular endothelial cells tight junction proteins and cell adhesion molecules: Transmigration across the in vitro blood-brain barrier. *Virology* **385**, 425-433

131. Palus, M., Vancová, M., Širmarová, J., Elsterová, J., Perner, J., and Růžek, D. (2017) Tick-borne encephalitis virus infects human brain microvascular endothelial cells without compromising blood-brain barrier integrity. *Virology* **507**, 110-122

132. Zhou, W., Woodson, M., Neupane, B., Bai, F., Sherman, M. B., Choi, K. H., Neelakanta, G., and Sultana, H. (2018) Exosomes serve as novel modes of tick-borne flavivirus transmission from arthropod to human cells and facilitates dissemination of viral RNA and proteins to the vertebrate neuronal cells. *PLoS Pathog* **14**, e1006764

133. Maximova, O. A., and Pletnev, A. G. (2018) Flaviviruses and the central nervous system: revisiting neuropathological concepts. *Annu Rev Virol* **5**, 255-272

134. Samuel, M. A., and Diamond, M. S. (2006) Pathogenesis of West Nile virus infection: a balance between virulence, innate and adaptive immunity, and viral evasion. *J Virol* **80**, 9349-9360

135. Petry, M., Palus, M., Leitzen, E., Mitterreiter, J. G., Huang, B., Kroger, A., Verjans, G., Baumgartner, W., Rimmelzwaan, G. F., Růžek, D., Osterhaus, A., and Prajeeth, C. K. (2021) Immunity to TBEV related flaviviruses with reduced pathogenicity protects mice from disease but not from TBEV entry into the CNS. *Vaccines (Basel)* **9**, 196

136. Mázló, M., and Szántó, J. (1978) Morphological demonstration of the virus of tick-borne encephalitis in the human brain. *Acta Neuropathol* **43**, 251-253

137. Fares, M., Cochet-Bernoin, M., Gonzalez, G., Montero-Menei, C. N., Blanchet, O., Benchoua, A., Boissart, C., Lecollinet, S., Richardson, J., Haddad, N., and Coulpier, M. (2020) Pathological modeling of TBEV infection reveals differential innate immune responses in human neurons and astrocytes that correlate with their susceptibility to infection. *J Neuroinflamm* **17**, 76

138. Hayasaka, D., Nagata, N., Fujii, Y., Hasegawa, H., Sata, T., Suzuki, R., Gould, E. A., Takashima, I., and Koike, S. (2009) Mortality following peripheral infection with Tick-borne encephalitis virus results from a combination of central nervous system pathology, systemic inflammatory and stress responses. *Virology* **390**, 139-150

139. Růžek, D., Vancová, M., Tesařová, M., Ahantarig, A., Kopecký, J., and Grubhoffer, L. (2009) Morphological changes in human neural cells following tick-borne encephalitis virus infection. *J Gen Virol* **90**, 1649-1658

140. Růžek, D., Salát, J., Palus, M., Gritsun, T. S., Gould, E. A., Dyková, I., Skallová, A., Jelínek, J., Kopecký, J., and Grubhoffer, L. (2009) CD8+ T-cells mediate immunopathology in tick-borne encephalitis. *Virology* **384**, 1-6

141. Wang, Y., Lobigs, M., Lee, E., and Müllbacher, A. (2003) CD8(+) T cells mediate recovery and immunopathology in West Nile virus encephalitis. *J Virol* **77**, 13323-13334

142. Bílý, T., Palus, M., Eyer, L., Elsterová, J., Vancová, M., and Růžek, D. (2015) Electron tomography analysis of tick-borne encephalitis virus infection in human neurons. *Sci Rep* **5**, 10745

143. Hirano, M., Yoshii, K., Sakai, M., Hasebe, R., Ichii, O., and Kariwa, H. (2014) Tick-borne flaviviruses alter membrane structure and replicate in dendrites of primary mouse neuronal cultures. *J Gen Virol* **95**, 849-861

144. Hirano, M., Muto, M., Sakai, M., Kondo, H., Kobayashi, S., Kariwa, H., and Yoshii, K. (2017) Dendritic transport of tick-borne flavivirus RNA by neuronal granules affects development of neurological disease. *Proc Natl Acad Sci U S A* **114**, 9960-9965

145. Maximova, O. A., Bernbaum, J. G., and Pletnev, A. G. (2016) West Nile virus spreads transsynaptically within the pathways of motor control: anatomical and ultrastructural mapping of neuronal virus infection in the primate central nervous system. *PLoS Negl Trop Dis* **10**, e0004980

146. Jurga, A. M., Paleczna, M., Kadluczka, J., and Kuter, K. Z. (2021) Beyond the GFAP-astrocyte protein markers in the brain. *Biomolecules* **11**, 1361

147. Volterra, A., and Meldolesi, J. (2005) Astrocytes, from brain glue to communication elements: the revolution continues. *Nat Rev Neurosci* **6**, 626-640

148. Pokorná Formanová, P., Palus, M., Salát, J., Hönig, V., Stefanik, M., Svoboda, P., and Růžek, D. (2019) Changes in cytokine and chemokine profiles in mouse serum and brain, and in human neural cells, upon tick-borne encephalitis virus infection. *J Neuroinflammation* **16**, 205

149. Delhaye, S., Paul, S., Blakqori, G., Minet, M., Weber, F., Staeheli, P., and Michiels, T. (2006) Neurons produce type I interferon during viral encephalitis. *Proc Natl Acad Sci U S A* **103**, 7835-7840

150. Ghita, L., Breitkopf, V., Mulenge, F., Pavlou, A., Gern, O. L., Duran, V., Prajeeth, C. K., Kohls, M., Jung, K., Stangel, M., Steffen, I., and Kalinke, U. (2021) Sequential MAVS and MyD88/TRIF signaling triggers anti-viral responses of tick-borne encephalitis virus-infected murine astrocytes. *J Neurosci Res* **99**, 2478-2492

151. Cho, H., Proll, S. C., Szretter, K. J., Katze, M. G., Gale, M., Jr., and Diamond, M. S. (2013) Differential innate immune response programs in neuronal subtypes determine susceptibility to infection in the brain by positive-stranded RNA viruses. *Nat Med* **19**, 458-464

152. Brault, J. B., Khou, C., Basset, J., Coquand, L., Fraisier, V., Frenkiel, M. P., Goud, B., Manuguerra, J. C., Pardigon, N., and Baffet, A. D. (2016) Comparative analysis between flaviviruses reveals specific neural stem cell tropism for Zika virus in the mouse developing neocortex. *EBioMedicine* **10**, 71-76

153. Kaiser, R. (1999) The clinical and epidemiological profile of tick-borne encephalitis in southern Germany 1994-98 - A prospective study of 656 patients. *Brain* **122**, 2067-2078

154. Haglund, M., and Gunther, G. (2003) Tick-borne encephalitis-pathogenesis, clinical course and long-term follow-up. *Vaccine* **21**, S11-S18

155. Gustafson, R., Svenungsson, B., Forsgren, M., Gardulf, A., and Granstrom, M. (1992) Two-year survey of the incidence of Lyme borreliosis and tick-borne encephalitis in a high-risk population in Sweden. *Eur J Clin Microbiol* **11**, 894-900

156. Holzmann, H. (2003) Diagnosis of tick-borne encephalitis. *Vaccine* **21**, S36-S40

157. Senel, M., Rapp, D., Mayer, B., Jesse, S., Sussmuth, S. D., Otto, M., Lewerenz, J., and Tumani, H. (2020) Tick-borne encephalitis: a differential pattern of intrathecal humoral immune response and inflammatory cell composition compared with other viral CNS infections. *Cells* **9**, 2169

158. Barrett, P. N., Schober-Bendixen, S., and Ehrlich, H. J. (2003) History of TBE vaccines. *Vaccine* **21 Suppl 1**, S41-49

159. Taba, P., Schmutzhard, E., Forsberg, P., Lutsar, I., Ljostad, U., Mygland, A., Levchenko, I., Strle, F., and Steiner, I. (2017) EAN consensus review on prevention, diagnosis and management of tick-borne encephalitis. *Eur J Neurol* **24**, 1214-e1261

160. Růžek, D., Avšič Županc, T., Borde, J., Chrdle, A., Eyer, L., Karganova, G., Kholodilov, I., Knap, N., Kozlovskaya, L., Matveev, A., Miller, A. D., Osolodkin, D. I., Överby, A. K., Tikunova, N., Tkachev, S., and Zajkowska, J. (2019) Tick-borne encephalitis in Europe and Russia: Review of pathogenesis, clinical features, therapy, and vaccines. *Antiviral Res* **164**, 23-51

161. Guglielmone, A. A., Robbins, R. G., Apanaskevich, D. A., Petney, T. N., Estrada-Peña, A., Horak, I. G., Shao, R., and Barker, S. C. (2010) The *Argasidae*, *Ixodidae* and *Nuttalliellidae* (Acari: Ixodida) of the world: a list of valid species names. *Experimental and Applied Acarology* **28**, 27-54

162. Kožuch, O., Labuda, M., Lysy, J., Weismann, P., and Krippel, E. (1990) Longitudinal study of natural foci of Central European encephalitis virus in West Slovakia. *Acta Virol* **34**, 537-544

163. Grešíková, M., Weidnerová, K., Nosek, J., and Rajčáni, J. (1972) Experimental pathogenicity of tick-borne encephalitis virus for dogs. *Acta Virol* **16**, 336-340

164. Labuda, M., Jones, L. D., Williams, T., and Nuttall, P. A. (1993) Enhancement of tick-borne encephalitis virus transmission by tick salivary gland extracts. *Med Vet Entomol* **7**, 193-196

165. Karbowiak, G., and Biernat, B. (2016) The role of particular tick developmental stages in the circulation of tick-borne pathogens affecting humans in Central Europe. 2. Tick-borne encephalitis virus. *Ann Parasitol* **62**, 3-9

166. Mannelli, A., Bertolotti, L., Gern, L., and Gray, J. (2012) Ecology of *Borrelia burgdorferi* sensu lato in Europe: transmission dynamics in multi-host systems, influence of molecular processes and effects of climate change. *FEMS Microbiol Rev* **36**, 837-861

167. Rosický, B., Černý, V., Daniel, M., Dusbábek, F., Palička, P., Samšiňák, K., and Hájková, Z. (1979) *Roztoči a klíšťata škodící zdraví člověka*, Academia, Praha

168. Hardy, J. L., Houk, E. J., Kramer, L. D., and Reeves, W. C. (1983) Intrinsic factors affecting vector competence of mosquitoes for arboviruses. *Annu Rev Entomol* **28**, 229-262

169. Alekseev, A. N., and Chunikhin, S. P. (1990) [The exchange of the tick-borne encephalitis virus between ixodid ticks feeding jointly on animals with a subthreshold level of viremia] [in Russian] *Meditsinskaya Parazitologiya i Parazitarnye Bolezni* **2**, 48-50

170. Hartemink, N. A., Randolph, S. E., Davis, S. A., and Heesterbeek, J. A. (2008) The basic reproduction number for complex disease systems: defining R(0) for tick-borne infections. *Am Nat* **171**, 743-754

171. Harrison, A., and Bennett, N. C. (2012) The importance of the aggregation of ticks on small mammal hosts for the establishment and persistence of tick-borne pathogens: an investigation using the R(0) model. *Parasitology* **139**, 1605-1613

172. Danielova, V., Holubova, J., Pejcoch, M., and Daniel, M. (2002) Potential significance of transovarial transmission in the circulation of tick-borne encephalitis virus. *Folia Parasitol (Praha)* **49**, 323-325

173. Süss, J., Fingerle, V., Hunfeld, K.-P., Schrader, C., and Wilske, B. (2004) Durch Zecken übertragene humanpathogene und bisher als apathogen geltende Mikroorganismen in Europa. *Bundesgesundheitsblatt Gesundheitsforschung Gesundheitsschutz* **47**, 470-486

174. Danielova, V., and Holubova, J. (1991) Transovarial transmission rate of tick-borne encephalitis virus in *Ixodes ricinus* ticks. in *Modern acarology* (Bukva, V. ed.), Academia, Prague. pp 7-10

175. Slovák, M., Kazimírová, M., Siebenstichová, M., Ustaníková, K., Klempa, B., Gritsun, T., Gould, E. A., and Nuttall, P. A. (2014) Survival dynamics of tick-borne encephalitis virus in *Ixodes ricinus* ticks. *Ticks Tick Borne Dis* **5**, 962-969

176. Estrada-Pena, A., and de la Fuente, J. (2014) The ecology of ticks and epidemiology of tick-borne viral diseases. *Antiviral Res* **108**, 104-128

177. Hönig, V., Švec, P., Halas, P., Vavrušková, Z., Tykalová, H., Kilian, P., Vetišková, V., Dorňáková, V., Štěrbová, T., Simonova, Z., Erhart, J., Štěrba, J., Golovchenko, M., Rudenko, N., and Grubhoffer, L. (2015) Ticks and tick-borne pathogens in South Bohemia (Czech Republic) - Spatial variability in Ixodes ricinus abundance, Borrelia burgdorferi and tick-borne encephalitis virus prevalence. *Ticks Tick Borne Dis* **6**, 559-567

178. Carpi, G., Bertolotti, L., Rosati, S., and Rizzoli, A. (2009) Prevalence and genetic variability of tick-borne encephalitis virus in host-seeking Ixodes ricinus in northern Italy. *J Gen Virol* **90**, 2877-2883

179. Khasnatinov, M. A., Ustanikova, K., Frolova, T. V., Pogodina, V. V., Bochkova, N. G., Levina, L. S., Slovak, M., Kazimirova, M., Labuda, M., Klempa, B., Eleckova, E., Gould, E. A., and Gritsun, T. S. (2009) Non-hemagglutinating flaviviruses: molecular mechanisms for the emergence of new strains via adaptation to European ticks. *PLoS One* **4**, e7295

180. Belova, O. A., Burenkova, L. A., and Karganova, G. G. (2012) Different tick-borne encephalitis virus (TBEV) prevalences in unfed versus partially engorged ixodid ticks--evidence of virus replication and changes in tick behavior. *Ticks Tick Borne Dis* **3**, 240-246

181. Alekseev, A. N., and Chunikhin, S. P. (1990) [The experimental transmission of the tick-borne encephalitis virus by ixodid ticks (the mechanisms, time periods, species and sex differences)] [in Russian] *Parazitologiia* **24**, 177-185

182. Korenberg, E. I. (2000) Seasonal population dynamics of ixodes ticks and tick-borne encephalitis virus. *Exp Appl Acarol* **24**, 665-681

183. Cortinas, R. M., Guerra, M. A., Jones, C. J., and Kitron, U. (2002) Detection, characterization, and prediction of tick-borne disease foci. *Int J Med Microbiol* **291**, 11-20

184. Rajčáni, J., Nosek, J., Kožuch, O., and Waltinger, H. (1976) Reaction of the host to the tick-bite. II. Distribution of tick borne encephalitis virus in sucking ticks. *Zentralbl Bakteriol Orig A* **236**, 1-9

185. Grešíková, M., and Nosek, J. (1981) Kliešte ako vektory arbovírusov [Virus (TBEV) survival in ticks] [in Slovak]. in *Arbovírusy v Československu* (Blaškovič, D. ed.), 1 Ed., Veda, Bratislava. pp 18

186. Nosek, J., Rajčáni, J., and Kožuch, O. (1978) Reaction of the host to the tick bite III. The bite of viruliferous *Ixodes ricinus* female. *Zentralbl Bakteriol Orig A* **242**, 141-147

187. Kožuch, O., Mayer, V., and Nosek, J. (1970) Quantitative study on TBEV in *Ixodes ricinus* ticks. *Acta Virol* **14**, 53-58

188. Süss, J., Schrader, C., Falk, U., and Wohanka, N. (2004) Tick-borne encephalitis (TBE) in Germany — Epidemiological data, development of risk areas and virus prevalence in field-collected ticks and in ticks removed from humans. *Int J Med Microbiol* **293**, 69-79

189. Kožuch, O., and Nosek, J. (1985) Replication of tick-borne encephalitis (TBE) virus in *Ixodes ricinus* ticks. *Folia Parasitol (Praha)* **32**, 373-375

190. Offerdahl, D. K., Dorward, D. W., Hansen, B. T., and Bloom, M. E. (2012) A three-dimensional comparison of tick-borne flavivirus infection in mammalian and tick cell lines. *PLoS One* **7**, e47912

191. Růžek, D., Bell-Sakyi, L., Kopecký, J., and Grubhoffer, L. (2008) Growth of tick-borne encephalitis virus (European subtype) in cell lines from vector and non-vector ticks. *Virus Res* **137**, 142-146

192. Lemasson, M., Caignard, G., Unterfinger, Y., Attoui, H., Bell-Sakyi, L., Hirchaud, E., Moutailler, S., Johnson, N., Vitour, D., Richardson, J., and Lacour, S. A. (2021) Exploration of binary protein-protein interactions between tick-borne flaviviruses and *Ixodes ricinus*. *Parasit Vectors* **14**, 144

193. Hynes, W. L. (2014) How ticks control microbes: innate immune responses. in *Biology of Ticks* (Sonnenshine, D., and Roe, R. M. eds.), Oxford University Press, New York, NY. pp 129-146

194. Hajdušek, O., Šíma, R., Ayllón, N., Jalovecká, M., Perner, J., de la Fuente, J., and Kopáček, P. (2013) Interaction of the tick immune system with transmitted pathogens. *Front Cell Infect Microbiol* **3**, 26

195. Kopáček, P., Hajdušek, O., Burešová, V., and Daffre, S. (2010) Tick Innate Immunity. in *Invertebrate Immunity* (Söderhäll, K. ed.), Springer, New York, NY. pp 137-162

196. Zhioua, E., Yeh, M. T., and LeBrun, R. A. (1997) Assay for phenoloxidase activity in *Amblyomma americanum*, *Dermacentor variabilis*, and *Ixodes scapularis*. *J Parasitol* **83**, 3864-3870

197. Sonenshine, D. E., Hynes, W. L., Ceraul, S. M., Mitchell, R., and Benzine, T. (2005) Host blood proteins and peptides in the midgut of the tick Dermacentor variabilis contribute to bacterial control. *Experimental and Applied Acarology* **36**, 207-223

198. Sonenshine, D. E., and Hynes, W. L. (2008) Molecular characterization and related aspects of the innate immune response in ticks. *Front Biosci* **13**, 7046-7063

199. Kopáček, P., Hajdušek, O., and Burešová, V. (2012) Tick as a model for the study of a primitive complement system. in *Recent advances on model hosts*, 2011/12/01 Ed., Springer, New York, NY. pp 83-93

200. Steele, G. M., and Nuttall, P. A. (1989) Difference in vector competence of two species of sympatric ticks, Amblyomma variegatum and Rhipicephalus appendiculatus, for Dugbe virus (Nairovirus, Bunyaviridae). *Virus Res* **14**, 73-84

201. Nuttall, P. A. (2009) Molecular characterization of tick-virus interactions. *Frontiers in Bioscience (Landmark edition)* **14**, 2466-2483

202. Ruckert, C., Bell-Sakyi, L., Fazakerley, J. K., and Fragkoudis, R. (2014) Antiviral responses of arthropod vectors: an update on recent advances. *Virusdisease* **25**, 249-260

203. Pinheiro, V. B., and Ellar, D. J. (2006) How to kill a mocking bug? *Cell Microbiol* **8**, 545-557

204. Marmaras, V. J., and Lampropoulou, M. (2009) Regulators and signalling in insect haemocyte immunity. *Cell Signal* **21**, 186-195

205. Palmer, W. H., Varghese, F. S., and van Rij, R. P. (2018) Natural variation in resistance to virus infection in dipteran insects. *Viruses* **10**, 118

206. Capelli-Peixoto, J., Carvalho, D. D., Johnson, W. C., Scoles, G. A., Fogaca, A. C., Daffre, S., and Ueti, M. W. (2017) The transcription factor Relish controls Anaplasma marginale infection in the bovine tick Rhipicephalus microplus. *Dev Comp Immunol* **74**, 32-39

207. Fogaca, A. C., Sousa, G., Pavanelo, D. B., Esteves, E., Martins, L. A., Urbanova, V., Kopacek, P., and Daffre, S. (2021) Tick immune system: what is known, the interconnections, the gaps, and the challenges. *Front Immunol* **12**, 628054

208. Merkling, S. H., and van Rij, R. P. (2013) Beyond RNAi: antiviral defense strategies in *Drosophila* and mosquito. *J Insect Physiol* **59**, 159-170

209. Blair, C. D. (2011) Mosquito RNAi is the major innate immune pathway controlling arbovirus infection and transmission. *Future Microbiol* **6**, 265-277

210. Talactac, M. R., Hernandez, E. P., Hatta, T., Yoshii, K., Kusakisako, K., Tsuji, N., and Tanaka, T. (2021) The antiviral immunity of ticks against transmitted viral pathogens. *Developmental and Comparative Immunology* **119**, 104012

211. Tikhe, C. V., and Dimopoulos, G. (2021) Mosquito antiviral immune pathways. *Dev Comp Immunol* **116**, 103964

212. Rozhkov, N. V., Hammell, M., and Hannon, G. J. (2013) Multiple roles for Piwi in silencing *Drosophila* transposons. *Gene Dev* **27**, 400-412

213. Ghildiyal, M., and Zamore, P. D. (2009) Small silencing RNAs: an expanding universe. *Nat Rev Genet* **10**, 94-108

214. Deddouche, S., Matt, N., Budd, A., Mueller, S., Kemp, C., Galiana-Arnoux, D., Dostert, C., Antoniewski, C., Hoffmann, J. A., and Imler, J. L. (2008) The DExD/H-box helicase Dicer-2 mediates the induction of antiviral activity in drosophila. *Nat Immunol* **9**, 1425-1432

215. Donald, C. L., Kohl, A., and Schnettler, E. (2012) New insights into control of arbovirus replication and spread by insect RNA interference pathways. *Insects* **3**, 511-531

216. Hammond, S. M., Bernstein, E., Beach, D., and Hannon, G. J. (2000) An RNA-directed nuclease mediates post-transcriptional gene silencing in Drosophila cells. *Nature* **404**, 293-296

217. Elbashir, S. M., Harborth, J., Lendeckel, W., Yalcin, A., Weber, K., and Tuschl, T. (2001) Duplexes of 21-nucleotide RNAs mediate RNA interference in cultured mammalian cells. *Nature* **411**, 494-498

218. Liu, X., Jiang, F., Kalidas, S., Smith, D., and Liu, Q. (2006) Dicer-2 and R2D2 coordinately bind siRNA to promote assembly of the siRISC complexes. *RNA* **12**, 1514-1520

219. Kemp, C., Mueller, S., Goto, A., Barbier, V., Paro, S., Bonnay, F., Dostert, C., Troxler, L., Hetru, C., Meignin, C., Pfeffer, S., Hoffmann, J. A., and Imler, J. L. (2013) Broad RNA interference-mediated antiviral immunity and virus-specific inducible responses in Drosophila. *J Immunol* **190**, 650-658

220. Grabowski, J. M., Offerdahl, D. K., and Bloom, M. E. (2018) The use of ex vivo organ cultures in tick-borne virus research. *ACS Infect Dis* **4**, 247-256

221. Lauring, A. S., and Andino, R. (2010) Quasispecies theory and the behavior of RNA viruses. *PLoS Pathog* **6**, e1001005

222. Domingo, E., Sheldon, J., and Perales, C. (2012) Viral quasispecies evolution. *Microbiol Mol Biol Rev* **76**, 159-216

223. Vignuzzi, M., Stone, J. K., Arnold, J. J., Cameron, C. E., and Andino, R. (2006) Quasispecies diversity determines pathogenesis through cooperative interactions in a viral population. *Nature* **439**, 344-348

224. Sanjuan, R., Nebot, M. R., Chirico, N., Mansky, L. M., and Belshaw, R. (2010) Viral mutation rates. *J Virol* **84**, 9733-9748

225. Uzcategui, N. Y., Sironen, T., Golovljova, I., Jaaskelainen, A. E., Valimaa, H., Lundkvist, A., Plyusnin, A., Vaheri, A., and Vapalahti, O. (2012) Rate of evolution and molecular epidemiology of tick-borne encephalitis virus in Europe, including two isolations from the same focus 44 years apart. *J Gen Virol* **93**, 786-796

226. Peck, K. M., and Lauring, A. S. (2018) Complexities of viral mutation rates. *J Virol* **92**, e01031-01017

227. Sim, S., Aw, P. P., Wilm, A., Teoh, G., Hue, K. D., Nguyen, N. M., Nagarajan, N., Simmons, C. P., and Hibberd, M. L. (2015) Tracking dengue virus intra-host genetic diversity during human-to-mosquito transmission. *PLoS Negl Trop Dis* **9**, e0004052

228. Jerzak, G., Bernard, K. A., Kramer, L. D., and Ebel, G. D. (2005) Genetic variation in West Nile virus from naturally infected mosquitoes and birds suggests quasispecies structure and strong purifying selection. *J Gen Virol* **86**, 2175-2183

229. Asghar, N., Pettersson, J. H., Dinnetz, P., Andreassen, A., and Johansson, M. (2017) Deep sequencing analysis of tick-borne encephalitis virus from questing ticks at natural foci reveals similarities between quasispecies pools of the virus. *J Gen Virol* **98**, 413-421

230. Asghar, N., Lindblom, P., Melik, W., Lindqvist, R., Haglund, M., Forsberg, P., Överby, A. K., Andreassen, A., Lindgren, P. E., and Johansson, M. (2014) Tick-borne encephalitis virus sequenced directly from questing and blood-feeding ticks reveals quasispecies variance. *PLoS One* **9**, e103264

231. Romanova, L. I., Gmyl, A. P., Dzhivanian, T. I., Bakhmutov, D. V., Lukashev, A. N., Gmyl, L. V., Rumyantsev, A. A., Burenkova, L. A., Lashkevich, V. A., and Karganova, G. G. (2007) Microevolution of tick-borne encephalitis virus in course of host alternation. *Virology* **362**, 75-84

232. Belova, O. A., Litov, A. G., Kholodilov, I. S., Kozlovskaya, L. I., Bell-Sakyi, L., Romanova, L. I., and Karganova, G. G. (2017) Properties of the tick-borne encephalitis virus population during persistent infection of ixodid ticks and tick cell lines. *Ticks Tick Borne Dis* **8**, 895-906

233. Litov, A. G., Deviatkin, A. A., Goptar, I. A., Dedkov, V. G., Gmyl, A. P., Markelov, M. L., Shipulin, G. A., and Karganova, G. G. (2018) Evaluation of the population heterogeneity of TBEV laboratory variants using high-throughput sequencing. *J Gen Virol* **99**, 240-245

234. Robertson, S. J., Mitzel, D. N., Taylor, R. T., Best, S. M., and Bloom, M. E. (2009) Tick-borne flaviviruses: dissecting host immune responses and virus countermeasures. *Immunol Res* **43**, 172-186

235. Lobigs, M., Mullbacher, A., and Regner, M. (2003) MHC class I up-regulation by flaviviruses: Immune interaction with unknown advantage to host or pathogen. *Immunology and Cell Biology* **81**, 217-223

236. Suthar, M. S., Gale, M., and Owen, D. M. (2009) Evasion and disruption of innate immune signalling by hepatitis C and West Nile viruses. *Cell Microbiol* **11**, 880-888

237. Medzhitov, R., and Janeway, C. A. (2002) Decoding the patterns of self and nonself by the innate immune system. *Science* **296**, 298-300

238. Akira, S., and Takeda, K. (2004) Toll-like receptor signalling. *Nat Rev Immunol* **4**, 499-511

239. Seth, R. B., Sun, L. J., and Chen, Z. J. J. (2006) Antiviral innate immunity pathways. *Cell Res* **16**, 141-147

240. Akira, S., Uematsu, S., and Takeuchi, O. (2006) Pathogen recognition and innate immunity. *Cell* **124**, 783-801

241. Yoneyama, M., Kikuchi, M., Natsukawa, T., Shinobu, N., Imaizumi, T., Miyagishi, M., Taira, K., Akira, S., and Fujita, T. (2004) The RNA helicase RIG-I has an essential function in double-stranded RNA-induced innate antiviral responses. *Nat Immunol* **5**, 730-737

242. Venkataraman, T., Valdes, M., Elsby, R., Kakuta, S., Caceres, G., Saijo, S., Iwakura, Y., and Barber, G. N. (2007) Loss of DExD/H box RNA helicase LGP2 manifests disparate antiviral responses. *J Immunol* **178**, 6444-6455

243. Kato, H., Takeuchi, O., Mikamo-Satoh, E., Hirai, R., Kawai, T., Matsushita, K., Hiiragi, A., Dermody, T. S., Fujita, T., and Akira, S. (2008) Length-dependent recognition of double-stranded ribonucleic acids by retinoic acid-inducible gene-I and melanoma differentiation-associated gene 5. *J Exp Med* **205**, 1601-1610

244. Saito, T., Owen, D. M., Jiang, F. G., Marcotrigiano, J., and Gale, M. (2008) Innate immunity induced by composition-dependent RIG-I recognition of hepatitis C virus RNA. *Nature* **454**, 523-527

245. Hornung, V., Ellegast, J., Kim, S., Brzozka, K., Jung, A., Kato, H., Poeck, H., Akira, S., Conzelmann, K. K., Schlee, M., Endres, S., and Hartmann, G. (2006) 5 '-triphosphate RNA is the ligand for RIG-I. *Science* **314**, 994-997

246. Saito, T., and Gale, M. (2008) Differential recognition of double-stranded RNA by RIG-I-like receptors in antiviral immunity. *The Journal of Experimental Medicine* **205**, 1523-1527

247. Takahasi, K., Yoneyama, M., Nishihori, T., Hirai, R., Kumeta, H., Narita, R., Gale, M., Inagaki, F., and Fujita, T. (2008) Nonself RNA-sensing mechanism of RIG-I helicase and activation of antiviral immune responses. *Mol Cell* **29**, 428-440

248. Marques, J. T., Devosse, T., Wang, D., Zamanian-Daryoush, M., Serbinowski, P., Hartmann, R., Fujita, T., Behlke, M. A., and Williams, B. R. G. (2006) A structural basis for discriminating between self and nonself double-stranded RNAs in mammalian cells. *Nat Biotechnol* **24**, 559-565

249. Vazquez, C., and Horner, S. M. (2015) MAVS coordination of antiviral innate immunity. *J Virol* **89**, 6974-6977

250. Best, S. M. (2017) The many faces of the flavivirus NS5 protein in antagonism of type I interferon signaling. *J Virol* **91**, e01970-01916

251. Miorin, L., Albornoz, A., Baba, M. M., D'Agaro, P., and Marcello, A. (2012) Formation of membrane-defined compartments by tick-borne encephalitis virus contributes to the early delay in interferon signaling. *Virus Res* **163**, 660-666

252. Monastyrskaya, G. S., Kostina, M. B., Filyukova, O. B., Protopopova, E. V., Konovalova, S. N., Kachko, A. V., Nikolaev, L. G., Loktev, V. B., and Sverdlov, E. D. (2004) The transcription activation of the RIG-I gene encoding the DEXH/D protein in RH cells infected with tick-borne encephalitis virus. *Russ J Bioorg Chem+* **30**, 129-132

253. Kurhade, C., Zegenhagen, L., Weber, E., Nair, S., Michaelsen-Preusse, K., Spanier, J., Gekara, N. O., Kroger, A., and Överby, A. K. (2016) Type I Interferon response in olfactory bulb, the site of tick-borne flavivirus accumulation, is primarily regulated by IPS-1. *J Neuroinflamm* **13**, DOI 10.1186/s12974-12016-10487-12979

254. Goodbourn, S., Didcock, L., and Randall, R. E. (2000) Interferons: cell signalling, immune modulation, antiviral responses and virus countermeasures. *J Gen Virol* **81**, 2341-2364

255. Sadler, A. J., and Williams, B. R. G. (2008) Interferon-inducible antiviral effectors. *Nat Rev Immunol* **8**, 559-568

256. Muller, U., Steinhoff, U., Reis, L. F. L., Hemmi, S., Pavlovic, J., Zinkernagel, R. M., and Aguet, M. (1994) Functional role of type I and type II interferons in antiviral defense. *Science* **264**, 1918-1921

257. Der, S. D., Zhou, A., Williams, B. R., and Silverman, R. H. (1998) Identification of genes differentially regulated by interferon alpha, beta, or gamma using oligonucleotide arrays. *Proc Natl Acad Sci U S A* **95**, 15623-15628

258. Lazear, H. M., Schoggins, J. W., and Diamond, M. S. (2019) Shared and distinct functions of type I and type III interferons. *Immunity* **50**, 907-923

259. Alspach, E., Lussier, D. M., and Schreiber, R. D. (2019) Interferon γ and its important roles in promoting and inhibiting spontaneous and therapeutic cancer immunity. *Csh Perspect Biol* **11**, a028480

260. Vilcek, J. (2003) Novel interferons. *Nat Immunol* **4**, 8-9

261. Kotenko, S. V., Gallagher, G., Baurin, V. V., Lewis-Antes, A., Shen, M., Shah, N. K., Langer, J. A., Sheikh, F., Dickensheets, H., and Donnelly, R. P. (2003) IFN-lambdas mediate antiviral protection through a distinct class II cytokine receptor complex. *Nat Immunol* **4**, 69-77

262. Ank, N., Iversen, M. B., Bartholdy, C., Staeheli, P., Hartmann, R., Jensen, U. B., Dagnaes-Hansen, F., Thomsen, A. R., Chen, Z., Haugen, H., Klucher, K., and Paludan, S. R. (2008) An important role for type III interferon (IFN-lambda/IL-28) in TLR-induced antiviral activity. *J Immunol* **180**, 2474-2485

263. Randall, R. E., and Goodbourn, S. (2008) Interferons and viruses: an interplay between induction, signalling, antiviral responses and virus countermeasures. *J Gen Virol* **89**, 1-47

264. Schoggins, J. W. (2019) Interferon-stimulated genes: what do they all do? *Annu Rev Virol* **6**, 567-584

265. Berthoux, L. (2020) The restrictome of flaviviruses. *Virol Sin* **35**, 363-377

266. Chiramel, A. I., Meyerson, N. R., McNally, K. L., Broeckel, R. M., Montoya, V. R., Mendez-Solis, O., Robertson, S. J., Sturdevant, G. L., Lubick, K. J., Nair, V., Youseff, B. H., Ireland, R. M., Bosio, C. M., Kim, K., Luban, J., Hirsch, V. M., Taylor, R. T., Bouamr, F., Sawyer, S. L., and Best, S. M. (2019) TRIM5α restricts flavivirus replication by targeting the viral protease for proteasomal degradation. *Cell Rep* **27**, 3269-3283 e3266

267. Taylor, R. T., Lubick, K. J., Robertson, S. J., Broughton, J. P., Bloom, M. E., Bresnahan, W. A., and Best, S. M. (2011) TRIM79alpha, an interferon-stimulated gene product, restricts tick-borne encephalitis virus replication by degrading the viral RNA polymerase. *Cell Host Microbe* **10**, 185-196

268. Wang, K., Zou, C., Wang, X., Huang, C., Feng, T., Pan, W., Wu, Q., Wang, P., and Dai, J. (2018) Interferon-stimulated TRIM69 interrupts dengue virus replication by ubiquitinating viral nonstructural protein 3. *PLoS Pathog* **14**, e1007287

269. Liu, B., Li, N. L., Wang, J., Shi, P. Y., Wang, T., Miller, M. A., and Li, K. (2014) Overlapping and distinct molecular determinants dictating the antiviral activities of TRIM56 against flaviviruses and coronavirus. *J Virol* **88**, 13821-13835

270. Yang, D., Li, N. L., Wei, D., Liu, B., Guo, F., Elbahesh, H., Zhang, Y., Zhou, Z., Chen, G. Y., and Li, K. (2019) The E3 ligase TRIM56 is a host restriction factor of Zika virus and depends on its RNA-binding activity but not miRNA regulation, for antiviral function. *PLoS Negl Trop Dis* **13**, e0007537

271. Yanez, D. C., Ross, S., and Crompton, T. (2020) The IFITM protein family in adaptive immunity. *Immunology* **159**, 365-372

272. Bailey, C. C., Zhong, G., Huang, I. C., and Farzan, M. (2014) IFITM-family proteins: the cell's first line of antiviral defense. *Annu Rev Virol* **1**, 261-283

273. Spence, J. S., He, R., Hoffmann, H. H., Das, T., Thinon, E., Rice, C. M., Peng, T., Chandran, K., and Hang, H. C. (2019) IFITM3 directly engages and shuttles incoming virus particles to lysosomes. *Nat Chem Biol* **15**, 259-268

274. Chmielewska, A. M., Gomez-Herranz, M., Gach, P., Nekulova, M., Bagnucka, M. A., Lipinska, A. D., Rychlowski, M., Hoffmann, W., Krol, E., Vojtesek, B., Sloan, R. D., Bienkowska-Szewczyk, K., Hupp, T., and Ball, K. (2022) The role of IFITM proteins in tick-borne encephalitis virus infection. *J Virol* **96**, e0113021

275. Gorman, M. J., Poddar, S., Farzan, M., and Diamond, M. S. (2016) The interferon-stimulated gene Ifitm3 restricts West Nile virus infection and pathogenesis. *J Virol* **90**, 8212-8225

276. Dukhovny, A., Lamkiewicz, K., Chen, Q., Fricke, M., Jabrane-Ferrat, N., Marz, M., Jung, J. U., and Sklan, E. H. (2019) A CRISPR activation screen identifies genes that protect against Zika virus infection. *J Virol* **93**, e00211-00219

277. Richardson, R. B., Ohlson, M. B., Eitson, J. L., Kumar, A., McDougal, M. B., Boys, I. N., Mar, K. B., De La Cruz-Rivera, P. C., Douglas, C., Konopka, G., Xing, C., and Schoggins, J. W. (2018) A CRISPR screen identifies IFI6 as an ER-resident interferon effector that blocks flavivirus replication. *Nat Microbiol* **3**, 1214-1223

278. Pfaller, C. K., Li, Z., George, C. X., and Samuel, C. E. (2011) Protein kinase PKR and RNA adenosine deaminase ADAR1: new roles for old players as modulators of the interferon response. *Curr Opin Immunol* **23**, 573-582

279. Clemens, M. J., and Elia, A. (1997) The double-stranded RNA-dependent protein kinase PKR: structure and function. *J Interferon Cytokine Res* **17**, 503-524

280. Short, J. A. L. (2009) Viral evasion of interferon stimulated genes. *Biosci Horiz* **2**, 212-224

281. Överby, A. K., Popov, V. L., Niedrig, M., and Weber, F. (2010) Tick-borne encephalitis virus delays interferon induction and hides its double-stranded RNA in intracellular membrane vesicles. *J Virol* **84**, 8470-8483

282. Deo, S., Patel, T. R., Dzananovic, E., Booy, E. P., Zeid, K., McEleney, K., Harding, S. E., and McKenna, S. A. (2014) Activation of 2' 5'-oligoadenylate synthetase by stem loops at the 5'-end of the West Nile virus genome. *PLoS One* **9**, e92545

283. Gusho, E., Baskar, D., and Banerjee, S. (2020) New advances in our understanding of the "unique" RNase L in host pathogen interaction and immune signaling. *Cytokine* **133**, 153847

284. Verheijen, J. C., van der Marel, G. A., van Boom, J. H., Bayly, S. F., Player, M. R., and Torrence, P. F. (1999) 2 ',5 '-oligoadenylate-peptide nucleic acids (2-5A-PNAs) activate RNase L. *Bioorgan Med Chem* **7**, 449-455

285. Perelygin, A. A., Scherbik, S. V., Zhulin, I. B., Stockman, B. M., Li, Y., and Brinton, M. A. (2002) Positional cloning of the murine flavivirus resistance gene. *Proc Natl Acad Sci U S A* **99**, 9322-9327

286. Brinton, M. A., and Perelygin, A. A. (2003) Genetic resistance to flaviviruses. *Adv Virus Res* **60**, 43-85

287. Mashimo, T., Lucas, M., Simon-Chazottes, D., Frenkiel, M. P., Montagutelli, X., Ceccaldi, P. E., Deubel, V., Guenet, J. L., and Depres, P. (2002) A nonsense mutation in the gene encoding 2 '-5 '-oligoadenylate synthetase/L1 isoform is associated with West Nile virus susceptibility in laboratory mice. *Proc Natl Acad Sci U S A* **99**, 11311-11316

288. Diamond, M. S. (2003) Evasion of innate and adaptive immunity by flaviviruses. *Immunology and Cell Biology* **81**, 196-206

289. Yakub, I., Lillibridge, K. M., Moran, A., Gonzalez, O. Y., Belmont, J., Gibbs, R. A., and Tweardy, D. J. (2005) Single nucleotide polymorphisms in genes for 2 '-5 '-Oligoadenylate synthetase and RNase L in patients hospitalized with West Nile virus infection. *J Infect Dis* **192**, 1741-1748

290. Hartmann, R., Justesen, J., Sarkar, S. N., Sen, G. C., and Yee, V. C. (2003) Crystal structure of the 2 '-specific and double-stranded RNA-activated interferon-induced antiviral protein 2 '-5 '-oligoadenylate synthetase. *Mol Cell* **12**, 1173-1185

291. Marques, J., Anwar, J., Eskildsen-Larsen, S., Rebouillat, D., Paludan, S. R., Sen, G., Williams, B. R. G., and Hartmann, R. (2008) The p59 oligoadenylate synthetase-like protein possesses antiviral activity that requires the C-terminal ubiquitin-like domain. *J Gen Virol* **89**, 2767-2772

292. Ibsen, M. S., Gad, H. H., Andersen, L. L., Hornung, V., Julkunen, I., Sarkar, S. N., and Hartmann, R. (2015) Structural and functional analysis reveals that human OASL binds dsRNA to enhance RIG-I signaling. *Nucleic Acids Res* **43**, 5236-5248

293. Choi, U. Y., Kang, J. S., Hwang, Y. S., and Kim, Y. J. (2015) Oligoadenylate synthase-like (OASL) proteins: dual functions and associations with diseases. *Exp Mol Med* **47**, e144

294. Ishibashi, M., Wakita, T., and Esumi, M. (2010) 2 ',5 '-Oligoadenylate synthetase-like gene highly induced by hepatitis C virus infection in human liver is inhibitory to viral replication in vitro. *Biochem Biophys Res Commun* **392**, 397-402

295. Zhu, H., Cong, J. P., and Shenk, T. (1997) Use of differential display analysis to assess the effect of human cytomegalovirus infection on the accumulation of cellular RNAs: Induction of interferon-responsive RNAs. *Proc Natl Acad Sci U S A* **94**, 13985-13990

296. Rivera-Serrano, E. E., Gizzi, A. S., Arnold, J. J., Grove, T. L., Almo, S. C., and Cameron, C. E. (2020) Viperin reveals its true function. *Annu Rev Virol* **7**, 421-446

297. Boudinot, P., Massin, P., Blanco, M., Riffault, S., and Benmansour, A. (1999) vig-1, a new fish gene induced by the rhabdovirus glycoprotein, has a virus-induced homologue in humans and shares conserved motifs with the MoaA family. *J Virol* **73**, 1846-1852

298. Grewal, T. S., Genever, P. G., Brabbs, A. C., Birch, M., and Skerry, T. M. (2000) Best5: a novel interferon-inducible gene expressed during bone formation. *FASEB J* **14**, 523-531

299. Chin, K. C., and Cresswell, P. (2001) Viperin (cig5), an IFN-inducible antiviral protein directly induced by human cytomegalovirus. *Proc Natl Acad Sci U S A* **98**, 15125-15130

300. Fenwick, M. K., Li, Y., Cresswell, P., Modis, Y., and Ealick, S. E. (2017) Structural studies of viperin, an antiviral radical SAM enzyme. *Proc Natl Acad Sci U S A* **114**, 6806-6811

301. Sofia, H. J., Chen, G., Hetzler, B. G., Reyes-Spindola, J. F., and Miller, N. E. (2001) Radical SAM, a novel protein superfamily linking unresolved steps in familiar biosynthetic pathways with radical mechanisms: functional characterization using new analysis and information visualization methods. *Nucleic Acids Res* **29**, 1097-1106

302. Mikulecky, P., Andreeva, E., Amara, P., Weissenhorn, W., Nicolet, Y., and Macheboeuf, P. (2018) Human viperin catalyzes the modification of GPP and FPP potentially affecting cholesterol synthesis. *Febs Lett* **592**, 199-208

303. Hinson, E. R., and Cresswell, P. (2009) The antiviral protein, viperin, localizes to lipid droplets via its N-terminal amphipathic alpha-helix. *Proc Natl Acad Sci U S A* **106**, 20452-20457

304. Hinson, E. R., and Cresswell, P. (2009) The N-terminal amphipathic α-helix of viperin mediates localization to the cytosolic face of the endoplasmic reticulum and inhibits protein secretion. *J Biol Chem* **284**, 4705-4712

305. Jiang, D., Guo, H. T., Xu, C. X., Chang, J. H., Gu, B. H., Wang, L. J., Block, T. M., and Guo, J. T. (2008) Identification of three interferon-inducible cellular enzymes that inhibit the replication of hepatitis C virus. *J Virol* **82**, 1665-1678

306. Upadhyay, A. S., Vonderstein, K., Pichlmair, A., Stehling, O., Bennett, K. L., Dobler, G., Guo, J. T., Superti-Furga, G., Lill, R., Överby, A. K., and Weber, F. (2014) Viperin is an iron-sulfur protein that inhibits genome synthesis of tick-borne encephalitis virus via radical SAM domain activity. *Cell Microbiol* **16**, 834-848

307. Chan, Y. L., Chang, T. H., Liao, C. L., and Lin, Y. L. (2008) The cellular antiviral protein viperin is attenuated by proteasome-mediated protein degradation in Japanese encephalitis virus-infected cells. *J Virol* **82**, 10455-10464

308. Severa, M., Coccia, E. M., and Fitzgerald, K. A. (2006) Toll-like receptor-dependent and -independent viperin gene expression and counter-regulation by PRDI-binding factor-1/BLIMP1. *J Biol Chem* **281**, 26188-26195

309. Duschene, K. S., and Broderick, J. B. (2010) The antiviral protein viperin is a radical SAM enzyme. *Febs Lett* **584**, 1263-1267

310. White, L. K., Sali, T., Alvarado, D., Gatti, E., Pierre, P., Streblow, D., and Defilippis, V. R. (2011) Chikungunya virus induces IPS-1-dependent innate immune activation and protein kinase R-independent translational shutoff. *J Virol* **85**, 606-620

311. Gizzi, A. S., Grove, T. L., Arnold, J. J., Jose, J., Jangra, R. K., Garforth, S. J., Du, Q., Cahill, S. M., Dulyaninova, N. G., Love, J. D., Chandran, K., Bresnick, A. R., Cameron, C. E., and Almo, S. C. (2018) A naturally occurring antiviral ribonucleotide encoded by the human genome. *Nature* **558**, 610-614

312. Kambara, H., Niazi, F., Kostadinova, L., Moonka, D. K., Siegel, C. T., Post, A. B., Carnero, E., Barriocanal, M., Fortes, P., Anthony, D. D., and Valadkhan, S. (2014) Negative regulation of the interferon response by an interferon-induced long non-coding RNA. *Nucleic Acids Res* **42**, 10668-10680

313. Dumbrepatil, A. B., Ghosh, S., Zegalia, K. A., Malec, P. A., Hoff, J. D., Kennedy, R. T., and Marsh, E. N. G. (2019) Viperin interacts with the kinase IRAK1 and the E3 ubiquitin ligase TRAF6, coupling innate immune signaling to antiviral ribonucleotide synthesis. *J Biol Chem* **294**, 6888-6898

314. Saitoh, T., Satoh, T., Yamamoto, N., Uematsu, S., Takeuchi, O., Kawai, T., and Akira, S. (2011) Antiviral protein Viperin promotes Toll-like receptor 7- and Toll-like receptor 9-mediated type I interferon production in plasmacytoid dendritic cells. *Immunity* **34**, 352-363

315. Wang, X. Y., Hinson, E. R., and Cresswell, P. (2007) The interferon-inducible protein viperin inhibits influenza virus release by perturbing lipid rafts. *Cell Host Microbe* **2**, 96-105

316. Waheed, A. A., and Freed, E. O. (2007) Influenza virus not cRAFTy enough to dodge viperin. *Cell Host Microbe* **2**, 71-72

317. Šťastná, H. (2009) *Změny globální genové exprese vlidských neuráĺních buňkách po infekci virem klíšťové encefalitidy [Changes in global gene expression in human neural cells followingtick-borne encephalitis virus infection] [in Czech]*MSc Thesis, University of South Bohemia in České Budějovice

318. Helbig, K. J., Carr, J. M., Calvert, J. K., Wati, S., Clarke, J. N., Eyre, N. S., Narayana, S. K., Fiches, G. N., McCartney, E. M., and Beard, M. R. (2013) Viperin is induced following dengue virus type-2 (DENV-2) infection and has anti-viral actions requiring the C-terminal end of viperin. *PLoS Negl Trop Dis* **7**, e2178

319. Jiang, D., Weidner, J. M., Qing, M., Pan, X. B., Guo, H. T., Xu, C. X., Zhang, X. C., Birk, A., Chang, J. H., Shi, P. Y., Block, T. M., and Guo, J. T. (2010) Identification of five interferon-induced cellular proteins that inhibit west nile virus and dengue virus infections. *J Virol* **84**, 8332-8341

320. Panayiotou, C., Lindqvist, R., Kurhade, C., Vonderstein, K., Pasto, J., Edlund, K., Upadhyay, A. S., and Överby, A. K. (2018) Viperin restricts Zika virus and tick-borne encephalitis virus replication by targeting NS3 for proteasomal degradation. *J Virol* **92**, e02054-02017

321. Vonderstein, K., Nilsson, E., Hubel, P., Nygard Skalman, L., Upadhyay, A., Pasto, J., Pichlmair, A., Lundmark, R., and Överby, A. K. (2018) Viperin targets flavivirus virulence by inducing assembly of non-infectious capsid particles. *J Virol* **92**, e011751-011717

322. Lindqvist, R., and Överby, A. K. (2018) The role of viperin in antiflavivirus responses. *DNA Cell Biol* **37**, 725-730

323. Lindqvist, R., Kurhade, C., Gilthorpe, J. D., and Överby, A. K. (2018) Cell-type- and region-specific restriction of neurotropic flavivirus infection by viperin. *J Neuroinflamm* **15**, 80

324. Youseff, B. H., Brewer, T. G., McNally, K. L., Izuogu, A. O., Lubick, K. J., Presloid, J. B., Alqahtani, S., Chattopadhyay, S., Best, S. M., Hu, X., and Taylor, R. T. (2019) TRAF6 plays a proviral role in tick-borne flavivirus infection through interaction with the NS3 protease. *iScience* **15**, 489-501

325. Hoffmann, H. H., Schneider, W. M., Rozen-Gagnon, K., Miles, L. A., Schuster, F., Razooky, B., Jacobson, E., Wu, X., Yi, S., Rudin, C. M., MacDonald, M. R., McMullan, L. K., Poirier, J. T., and Rice, C. M. (2021) TMEM41B is a pan-flavivirus host factor. *Cell* **184**, 133-148 e120

326. Överby, A. K., and Weber, F. (2011) Hiding from intracellular pattern recognition receptors, a passive strategy of flavivirus immune evasion. *Virulence* **2**, 238-240

327. Daffis, S., Szretter, K. J., Schriewer, J., Li, J., Youn, S., Errett, J., Lin, T. Y., Schneller, S., Zust, R., Dong, H., Thiel, V., Sen, G. C., Fensterl, V., Klimstra, W. B., Pierson, T. C., Buller, R. M., Gale, M., Jr., Shi, P. Y., and Diamond, M. S. (2010) 2'-O methylation of the viral mRNA cap evades host restriction by IFIT family members. *Nature* **468**, 452-456

328. Werme, K., Wigerius, M., and Johansson, M. (2008) Tick-borne encephalitis virus NS5 associates with membrane protein scribble and impairs interferon-stimulated JAK-STAT signalling. *Cell Microbiol* **10**, 696-712

329. Laurent-Rolle, M., Boer, E. F., Lubick, K. J., Wolfinbarger, J. B., Carmody, A. B., Rockx, B., Liu, W. J., Ashour, J., Shupert, W. L., Holbrook, M. R., Barrett, A. D., Mason, P. W., Bloom, M. E., Garcia-Sastre, A., Khromykh, A. A., and

Best, S. M. (2010) The NS5 protein of the virulent West Nile virus NY99 strain is a potent antagonist of type I interferon-mediated JAK-STAT signaling *J Virol* **84**, 3503-3515

330. Best, S. M., Morris, K. L., Shannon, J. G., Robertson, S. J., Mitzel, D. N., Park, G. S., Boer, E., Wolfinbarger, J. B., and Bloom, M. E. (2005) Inhibition of interferon-stimulated JAK-STAT signaling by a tick-borne flavivirus and identification of NS5 as an interferon antagonist. *J Virol* **79**, 12828-12839

331. Lubick, K. J., Robertson, S. J., McNally, K. L., Freedman, B. A., Rasmussen, A. L., Taylor, R. T., Walts, A. D., Tsuruda, S., Sakai, M., Ishizuka, M., Boer, E. F., Foster, E. C., Chiramel, A. I., Addison, C. B., Green, R., Kastner, D. L., Katze, M. G., Holland, S. M., Forlino, A., Freeman, A. F., Boehm, M., Yoshii, K., and Best, S. M. (2015) Flavivirus antagonism of type I interferon signaling reveals prolidase as a regulator of IFNAR1 surface expression. *Cell Host Microbe* **18**, 61-74

332. Guo, J. T., Hayashi, J., and Seeger, C. (2005) West Nile virus inhibits the signal transduction pathway of alpha interferon. *J Virol* **79**, 1343-1350

333. Munoz-Jordan, J. L., Sanchez-Burgos, G. G., Laurent-Rolle, M., and Garcia-Sastre, A. (2003) Inhibition of interferon signaling by dengue virus. *Proc Natl Acad Sci U S A* **100**, 14333-14338

334. Munoz-Jordan, J. L., Laurent-Rolle, M., Ashour, J., Martinez-Sobrido, L., Ashok, M., Lipkin, W. I., and Garcia-Sastre, A. (2005) Inhibition of alpha/beta interferon signaling by the NS4B protein of flaviviruses. *J Virol* **79**, 8004-8013

335. Liu, W. J., Wang, X. J., Mokhonov, V. V., Shi, P. Y., Randall, R., and Khromykh, A. A. (2005) Inhibition of interferon signaling by the New York 99 strain and Kunjin subtype of West Nile virus involves blockage of STAT1 and STAT2 activation by nonstructural proteins. *J Virol* **79**, 1934-1942

336. Liu, W. J., Chen, H. B., Wang, X. J., Huang, H., and Khromykh, A. A. (2004) Analysis of adaptive mutations in Kunjin virus replicon RNA reveals a novel role for the flavivirus nonstructural protein NS2A in inhibition of beta interferon promoter-driven transcription. *J Virol* **78**, 12225-12235

337. Liu, W. J., Wang, X. J., Clark, D. C., Lobigs, M., Hall, R. A., and Khromykh, A. A. (2006) A single amino acid substitution in the west nile virus nonstructural protein NS2A disables its ability to inhibit alpha/beta interferon induction and attenuates virus virulence in mice. *J Virol* **80**, 2396-2404

338. Roby, J. A., Esser-Nobis, K., Dewey-Verstelle, E. C., Fairgrieve, M. R., Schwerk, J., Lu, A. Y., Soveg, F. W., Hemann, E. A., Hatfield, L. D., Keller, B. C., Shapiro, A., Forero, A., Stencel-Baerenwald, J. E., Savan, R., and Gale, M., Jr. (2020) Flavivirus nonstructural protein NS5 dysregulates HSP90 to broadly inhibit JAK/STAT signaling. *Cells* **9**, 899

339. Schuessler, A., Funk, A., Lazear, H. M., Cooper, D. A., Torres, S., Daffis, S., Jha, B. K., Kumagai, Y., Takeuchi, O., Hertzog, P., Silverman, R., Akira, S., Barton, D. J., Diamond, M. S., and Khromykh, A. A. (2012) West Nile virus noncoding subgenomic RNA contributes to viral evasion of the type I interferon-mediated antiviral response. *J Virol* **86**, 5708-5718

340. Bidet, K., Dadlani, D., and Garcia-Blanco, M. A. (2014) G3BP1, G3BP2 and CAPRIN1 are required for translation of interferon stimulated mRNAs and are targeted by a dengue virus non-coding RNA. *PLoS Pathog* **10**, e1004242

341. Donald, C. L., Brennan, B., Cumberworth, S. L., Rezelj, V. V., Clark, J. J., Cordeiro, M. T., Freitas de Oliveira França, R., Pena, L. J., Wilkie, G. S., Da Silva Filipe, A., Davis, C., Hughes, J., Varjak, M., Selinger, M., Zuvanov, L., Owsianka, A. M., Patel, A. H., McLauchlan, J., Lindenbach, B. D., Fall, G., Sall, A. A., Biek, R., Rehwinkel, J., Schnettler, E., and Kohl, A. (2016) Full genome sequence and sfRNA interferon antagonist activity of Zika virus from Recife, Brazil. *PLoS Negl Trop Dis* **10**, e0005048

342. Manokaran, G., Finol, E., Wang, C., Gunaratne, J., Bahl, J., Ong, E. Z., Tan, H. C., Sessions, O. M., Ward, A. M., Gubler, D. J., Harris, E., Garcia-Blanco, M. A., and Ooi, E. E. (2015) Dengue subgenomic RNA binds TRIM25 to inhibit interferon expression for epidemiological fitness. *Science* **350**, 217-221

343. Chang, R. Y., Hsu, T. W., Chen, Y. L., Liu, S. F., Tsai, Y. J., Lin, Y. T., Chen, Y. S., and Fan, Y. H. (2013) Japanese encephalitis virus non-coding RNA inhibits activation of interferon by blocking nuclear translocation of interferon regulatory factor 3. *Vet Microbiol* **166**, 11-21

344. Michalski, D., Ontiveros, J. G., Russo, J., Charley, P. A., Anderson, J. R., Heck, A. M., Geiss, B. J., and Wilusz, J. (2019) Zika virus noncoding sfRNAs sequester multiple host-derived RNA-binding proteins and modulate mRNA decay and splicing during infection. *J Biol Chem* **294**, 16282-16296

345. Moon, S. L., Anderson, J. R., Kumagai, Y., Wilusz, C. J., Akira, S., Khromykh, A. A., and Wilusz, J. (2012) A noncoding RNA produced by arthropod-borne flaviviruses inhibits the cellular exoribonuclease XRN1 and alters host mRNA stability. *RNA* **18**, 2029-2040

346. Pompon, J., Manuel, M., Ng, G. K., Wong, B., Shan, C., Manokaran, G., Soto-Acosta, R., Bradrick, S. S., Ooi, E. E., Misse, D., Shi, P. Y., and Garcia-Blanco, M. A. (2017) Dengue subgenomic flaviviral RNA disrupts immunity in mosquito salivary glands to increase virus transmission. *PLoS Pathog* **13**, e1006535

347. Göertz, G. P., Fros, J. J., Miesen, P., Vogels, C. B. F., van der Bent, M. L., Geertsema, C., Koenraadt, C. J. M., van Rij, R. P., van Oers, M. M., and Pijlman, G. P. (2016) Noncoding subgenomic flavivirus RNA is processed by the mosquito RNA interference machinery and determines West Nile virus transmission by Culex pipiens mosquitoes. *J Virol* **90**, 10145-10159

348. Göertz, G. P., van Bree, J. W. M., Hiralal, A., Fernhout, B. M., Steffens, C., Boeren, S., Visser, T. M., Vogels, C. B. F., Abbo, S. R., Fros, J. J., Koenraadt, C. J. M., van Oers, M. M., and Pijlman, G. P. (2019) Subgenomic flavivirus RNA binds the mosquito DEAD/H-box helicase ME31B and determines Zika virus transmission byAedes aegypti. *Proc Natl Acad Sci U S A* **116**, 19136-19144

349. Villordo, S. M., Carballeda, J. M., Filomatori, C. V., and Gamarnik, A. V. (2016) RNA structure duplications and flavivirus host adaptation. *Trends Microbiol* **24**, 270-283

350. Hetz, C. (2012) The unfolded protein response: controlling cell fate decisions under ER stress and beyond. *Nat Rev Mol Cell Biol* **13**, 89-102

351. Yu, C., Achazi, K., and Niedrig, M. (2013) Tick-borne encephalitis virus triggers inositol-requiring enzyme 1 (IRE1) and transcription factor 6 (ATF6) pathways of unfolded protein response. *Virus Res* **178**, 471-477

352. Breitkopf, V. J. M., Dobler, G., Claus, P., Naim, H. Y., and Steffen, I. (2021) IRE1-mediated unfolded protein response promotes the replication of tick-borne flaviviruses in a virus and cell-type dependent manner. *Viruses* **13**, 2164

353. Carletti, T., Zakaria, M. K., Faoro, V., Reale, L., Kazungu, Y., Licastro, D., and Marcello, A. (2019) Viral priming of cell intrinsic innate antiviral signaling by the unfolded protein response. *Nat Commun* **10**, 3889

354. Walsh, D., Mathews, M. B., and Mohr, I. (2013) Tinkering with translation: protein synthesis in virus-infected cells. *Csh Perspect Biol* **5**, a012351

355. Slomnicki, L. P., Chung, D. H., Parker, A., Hermann, T., Boyd, N. L., and Hetman, M. (2017) Ribosomal stress and Tp53-mediated neuronal apoptosis in response to capsid protein of the Zika virus. *Sci Rep* **7**, 16652

356. Roth, H., Magg, V., Uch, F., Mutz, P., Klein, P., Haneke, K., Lohmann, V., Bartenschlager, R., Fackler, O. T., Locker, N., Stoecklin, G., and Ruggieri, A. (2017) Flavivirus infection uncouples translation suppression from cellular stress responses. *Mbio* **8**, e02150-02116

357. Giribet, G., and Edgecombe, G. D. (2019) The phylogeny and evolutionary history of Arthropods. *Curr Biol* **29**, R592-R602

358. Grubaugh, N. D., Ruckert, C., Armstrong, P. M., Bransfield, A., Anderson, J. F., Ebel, G. D., and Brackney, D. E. (2016) Transmission bottlenecks and RNAi collectively influence tick-borne flavivirus evolution. *Virus Evol* **2**, vew033

359. Sharma, A., Pham, M. N., Reyes, J. B., Chana, R., Yim, W. C., Heu, C. C., Kim, D., Chaverra-Rodriguez, D., Rasgon, J. L., Harrell, R. A., 2nd, Nuss, A. B., and Gulia-Nuss, M. (2022) Cas9-mediated gene editing in the black-legged tick, *Ixodes scapularis*, by embryo injection and ReMOT Control. *iScience* **25**, 103781

360. Gulia-Nuss, M., Nuss, A. B., Meyer, J. M., Sonenshine, D. E., Roe, R. M., Waterhouse, R. M., Sattelle, D. B., de la Fuente, J., Ribeiro, J. M., Megy, K., Thimmapuram, J., Miller, J. R., Walenz, B. P., Koren, S., Hostetler, J. B., Thiagarajan, M., Joardar, V. S., Hannick, L. I., Bidwell, S., Hammond, M. P., Young, S., Zeng, Q., Abrudan, J. L., Almeida, F. C., Ayllon, N., Bhide, K., Bissinger, B. W., Bonzon-Kulichenko, E., Buckingham, S. D., Caffrey, D. R., Caimano, M. J., Croset, V., Driscoll, T., Gilbert, D., Gillespie, J. J., Giraldo-Calderon, G. I., Grabowski, J. M., Jiang, D., Khalil, S. M. S., Kim, D., Kocan, K. M., Koci, J., Kuhn, R. J., Kurtti, T. J., Lees, K., Lang, E. G., Kennedy, R. C., Kwon, H., Perera, R., Qi, Y., Radolf, J. D., Sakamoto, J. M., Sanchez-Gracia, A., Severo, M. S., Silverman, N., Simo, L., Tojo, M., Tornador, C., Van Zee, J. P., Vazquez, J., Vieira, F. G., Villar, M., Wespiser, A. R., Yang, Y., Zhu, J., Arensburger, P., Pietrantonio, P. V., Barker, S. C., Shao, R., Zdobnov, E. M., Hauser, F., Grimmelikhuijzen, C. J. P., Park, Y., Rozas, J., Benton, R., Pedra, J. H. F., Nelson, D. R., Unger, M. F., Tubio, J. M. C., Tu, Z., Robertson, H. M., Shumway, M., Sutton, G., Wortman, J. R., Lawson, D., Wikel, S. K., Nene, V. M., Fraser, C. M., Collins, F. H., Birren, B., Nelson, K. E., Caler, E., and Hill, C. A. (2016) Genomic insights into the Ixodes scapularis tick vector of Lyme disease. *Nat Commun* **7**, 10507

361. Yuan, C., Wu, J., Peng, Y., Li, Y., Shen, S., Deng, F., Hu, Z., Zhou, J., Wang, M., and Zou, Z. (2020) Transcriptome analysis of the innate immune system of *Hyalomma asiaticum*. *Journal of Invertebrate Pathology* **177**, 107481

362. Grabowski, J. M., Perera, R., Roumani, A. M., Hedrick, V. E., Inerowicz, H. D., Hill, C. A., and Kuhn, R. J. (2016) Changes in the proteome of Langat-infected *Ixodes scapularis* ISE6 cells: Metabolic pathways associated with flavivirus infection. *PLoS Negl Trop Dis* **10**, e0004180

363. Loginov, D. S., Bottinger, K., Loginova, Y. F., Dyčka, F., Věchtová, P., and Štěrba, J. (2020) Biotyping of IRE/CTVM19 tick cell line infected by tick-borne encephalitis virus. *Ticks Tick Borne Dis* **11**, 101420

364. Selinger, M., Novotný, R., Sýs, J., Roby, J. A., Tykalová, H., Ranjani, G. S., Vancová, M., Jaklová, K., Kaufman, F., Bloom, M. E., Zdráhal, Z., Grubhoffer, L., Forwood, J. K., Hrabal, R., Rumlová, M., and Štěrba, J. (2022) Structure and biological functions of TBEV Capsid protein. *Unpublished manuscript*

365. Yuan, Y., Miao, Y., Qian, L., Zhang, Y., Liu, C., Liu, J., Zuo, Y., Feng, Q., Guo, T., Zhang, L., Chen, X., Jin, L., Huang, F., Zhang, H., Zhang, W., Li, W., Xu, G., and Zheng, H. (2020) Targeting UBE4A revives viperin protein in epithelium to enhance host antiviral defense. *Mol Cell* **77**, 734-747 e737

366. Hare, D., Collins, S., Cuddington, B., and Mossman, K. (2016) The importance of physiologically relevant cell lines for studying virus–host interactions. *Viruses* **8**, 297

367. Desole, G., Sinigaglia, A., Riccetti, S., Masi, G., Pacenti, M., Trevisan, M., and Barzon, L. (2019) Modelling neurotropic flavivirus infection in human induced pluripotent stem cell-derived systems. *Int J Mol Sci* **20**, 5404

368. Mandl, C. W., Holzmann, H., Meixner, T., Rauscher, S., Stadler, P. F., Allison, S. L., and Heinz, F. X. (1998) Spontaneous and engineered deletions in the 3' noncoding region of tick-borne encephalitis virus: construction of highly attenuated mutants of a flavivirus. *J Virol* **72**, 2132-2140

369. Belikov, S. I., Kondratov, I. G., Potapova, U. V., and Leonova, G. N. (2014) The relationship between the structure of the tick-borne encephalitis virus strains and their pathogenic properties. *PLoS One* **9**, e94946

370. Formanova, P., Cerny, J., Bolfikova, B. C., Valdes, J. J., Kozlova, I., Dzhioev, Y., and Růžek, D. (2015) Full genome sequences and molecular characterization of tick-borne encephalitis virus strains isolated from human patients. *Ticks Tick Borne Dis* **6**, 38-46

371. Weaver, S. C., Brault, A. C., Kang, W. L., and Holland, J. J. (1999) Genetic and fitness changes accompanying adaptation of an arbovirus to vertebrate and invertebrate cells. *J Virol* **73**, 4316-4326

372. Filomatori, C. V., Carballeda, J. M., Villordo, S. M., Aguirre, S., Pallares, H. M., Maestre, A. M., Sanchez-Vargas, I., Blair, C. D., Fabri, C., Morales, M. A., Fernandez-Sesma, A., and Gamarnik, A. V. (2017) Dengue virus genomic variation associated with mosquito adaptation defines the pattern of viral non-coding RNAs and fitness in human cells. *PLoS pathogens* **13**, e1006265

373. Zakotnik, S., Knap, N., Bogovič, P., Zorec, T. M., Poljak, M., Strle, F., Avšič-Županc, T., and Korva, M. (2022) Complete genome sequencing of tick-borne encephalitis virus directly from clinical samples: Comparison of shotgun metagenomic and targeted amplicon-based sequencing. *Viruses* **14**, 1267

374. Ehrbar, D. J., Ngo, K. A., Campbell, S. R., Kramer, L. D., and Ciota, A. T. (2017) High levels of local inter- and intra-host genetic variation of West Nile virus and evidence of fine-scale evolutionary pressures. *Infect Genet Evol* **51**, 219-226

375. Kellman, E. M., Offerdahl, D. K., Melik, W., and Bloom, M. E. (2018) Viral determinants of virulence in tick-borne flaviviruses. *Viruses* **10**, 329